The structure of sensor organic/polymeric solids deposited on surfaces of interest for sensing devices.

LEMON, Paul.

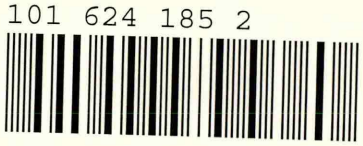

ProQuest LLC.
789 East Eisenhower Parkway
P.O. Box 1346
Ann Arbor, MI 48106 – 1346

Sheffield Hallam University

The Structure of Sensor Organic/Polymeric Solids Deposited on Surfaces of Interest for Sensing Devices

Paul Lemon BSc (Hons) CPhys MInstP

A thesis submitted in partial fulfilment of the requirements of Sheffield Hallam University for the degree of Doctor of Philosophy

August, 2001

In collaboration with: Neotronics Scientific

In collaboration with:

with kind assistance from:

and with thanks to:

Institute *of* **Physics**

"The chess-board is the world; the pieces are the phenomena of the universe; the rules of the game are what we call the laws of nature. The player on the other side is hidden from us. We know that his play is always fair, and patient. But also we know, to our cost, that he never overlooks a mistake, or makes the smallest allowance for ignorance."

Thomas Huxley (1825 - 1895)

Declaration

The production of this thesis was the sole work of the author. The research presented was carried out at the Materials Research Institute at Sheffield Hallam University and is the authors work unless explicitly stated otherwise. See "Acknowledgements" for details of work carried out on the author's behalf.

Paul W. Lemon BSc (Hons) CPhys MInstP
Health and Safety Laboratory
Broad Lane
Sheffield
S3 7HQ
Tel: (0114) 289 2495
Fax: (0114) 289 2526
e-mail: paul.lemon@hsl.gov.uk
pk.lemon@virgin.net
lemononline@talk21.com

Publications

A selection of the work described has been presented in the following ways:

- ***"Electrolytic Dopant Recrystallisation in Polypyrrole Gas-Sensing Thin-Films."***
  P.W. Lemon and J. Haigh, in "*Sensors and their Applications X*", ed. N.M. White and A.T. Augousti, I.O.P. Publishing, Philadelphia, 1999, pp.179-184.

- ***"The Evolution of Nodular Polypyrrole Morphology During Aqueous Electrolytic Deposition: Influence of Electrolytic Gas Discharge."***
  P.W. Lemon and J. Haigh, *Materials Research Bulletin*, Vol. 34, No. 5, (1999), pp. 665-672.

- ***"On a Novel Polypyrrole Morphology."***
  P.W. Lemon, N. Szczur and J. Haigh, *Materials Research Bulletin*, Vol. 33, No. 6, (1998), pp. 909-914.

- ***"The Effects of Monomer Purity on the Morphology of Polypyrrole Thin-Film Gas-Sensing Layers."***
  P.W. Lemon, N. Szczur and J. Haigh, in "*Sensors and their Applications VIII*", ed. A.T. Augousti and N.M. White, I.O.P. Publishing, Philadelphia, 1997, pp. 189-193.

- ***"The Effects of Preparation Conditions on the Structures of Electrochemically Polymerised Polypyrrole Thin Films Doped with Benzenesulfonic Acid Sodium Salt."***
  P.W. Lemon and J. Haigh - Poster Presentation to the Royal Society of Chemistry (Analytical Division) Conference, "*Research & Development Topics in Analytical Chemistry*", Nottingham Trent University, U.K., July 1996.

- ***"The Structure of Polypyrrole Gas-Sensors."***
  P.W. Lemon and J. Haigh - Poster Presentation to the Institute of Physics Conference, "*Condensed Matter and Materials Physics*", University of York, U.K., December 1996.

- ***"The Macrostructure of Polypyrrole Gas-Sensors."***
  P.W. Lemon and J. Haigh - Poster Presentation to the Royal Society of Chemistry (Analytical Division) Conference, "*Advances in Analytical Chemistry - Miniaturisation and Sensors*", University of Huddersfield, U.K., February 1997.

Reprints of the above are included at the end of this thesis.
(See 'Publication Reprints').

Acknowledgements

The work reported forms the basis of the recent polypyrrole gas sensor research by the Materials Research Institute (MRI)/Sheffield Hallam University (SHU) and Neotronics Scientific PLC. The research was kindly sponsored by the MRI.

It is a pleasure to thank Dr. John Haigh and Prof. Jack Yarwood, not only for their expertise, but also for their considerable patience! Many thanks also to Dr. Andrew Hinton and Dr. Natalka Szczur for their invaluable help and encouragement and to colleagues at the MRI and SHU for technical assistance. Thanks to Dr. John Warburton (EEV), Dr. Steve Collins (Neotronics Scientific Ltd.) and Dr. Julian Iredale (Neotronics Ltd.) for advice and the provision of gold microelectrodes and to Dr. Steve Thorpe (Health and Safety Laboratory) for the kind donation of interdigitated 'Yoshi' substrates.

Many thanks to Dr. David Douce and Dr. Malcom Ives for valuable assistance with experimental work (G.C. and G.D.O.E.S. respectively). Thanks also to Belinda Hopley (I.O.P.) and Christina Pyle (Elsevier) for their patience.

My warm thanks to Nick Vaughan, Norman West and Richard Broughton of the Health and Safety Executive for support and advice above and beyond the call of duty.

Thanks Dad for giving me the enthusiasm and fascination to find out the reasons why nature behaves the way it does; thanks Mam for giving me the determination and astuteness to see through a difficult job worth doing well.
Deep thanks to you both for your love and support through the years.

Above all, I am profoundly grateful to my wife for her long-lasting patience and for her ungrudging support throughout, especially when writing has frequently overrun into time which should have been spent with her.

Abstract

For many years, electrochemically deposited polypyrrole has found application in a host of technologically significant areas. Popular applications include use in rechargeable batteries, electrochromic displays and artificial muscles. However, perhaps the most significant application of polypyrrole is as a gas sensing material. The relatively low selectivity of polypyrrole has led to it seldom being used as a 'stand alone' sensor; the ease by which the properties of polypyrrole may be subtly modified during electrochemical deposition (resulting in subtly different sensor responses) makes it ideally suited for incorporation into sensing 'arrays'.

The level of understanding concerning the growth dynamics and structural characteristics of electrochemically deposited polypyrrole was poor prior to the commencement of the work presented; this thesis describes research undertaken in order to elucidate the properties of this material. As variation of the dopant group used during electrochemical deposition has been shown to result in significant structural and operational variations, the work presented focuses on polypyrrole doped with sodium benzene sulfonate (benzene sulfonic acid, sodium salt). The effects of deposition parameter variation have been studied (such as deposition potential and dopant concentration); repeatable relationships were found between deposition parameters and [a] sensor electrical conductivity, and [b] the surface morphology of the films formed. The influence of sensor substrate design is also considered; dissimilarities were found between the consistency and resistance temporal stability of elements deposited on simple 'boot' electrodes and interdigital microelectrodes.

A significant proportion of the work presented concerns the study of the macrostructure of electrochemically deposited polypyrrole films. Several novel structural features have been presented, all of which have been documented in the scientific press. These include:

- The formation of 'tendrillar' morphology (as opposed to the commonly observed polypyrrole 'nodular' morphology) during electrochemical deposition from aqueous electrolyte. Tendril formation has been shown to be the result of the accumulation of impurities at the advancing growth face; a model has been presented which relates impurity accumulation to tendrillar polymer morphology,
- Demonstration of the evolution of gas at the polymer/substrate interface during aqueous electrolytic deposition. It is suggested that gas evolution is the result of the catalysed disassociation of the (aqueous) supporting electrolyte, and shown that the production of gas at the substrate/polymer interface results in the formation of discrete pockets, the positions of which relate strongly to the positions of nodules on the upper film surface.
- Demonstration of the recrystallisation of ionic dopant trapped within the polymer films during maturation. Dopant recrystallisation has been verified by SEM and EDAX; crystal growth has been demonstrated by XRD.

Finally, the microstructures of a range of subtly different polypyrrole films have been considered. Repeatable relationships were observed between deposition potential, electrolyte solution concentration and microstructure. Characteristic features of X-Ray diffractograms have been related to the theoretical spacing between adjacent pyrrole rings (≈3.6Å), we believe for the first time.

1. Introduction

The requirement for reliable methods for the indication or measurement of smell and taste in industrial situations has long been appreciated. Human taste and smell "panels" (known as 'organoleptic panels', which consist of groups of highly trained and carefully selected individuals) are often used to analyse complex odours in areas involving the production of foodstuffs, beverages and perfumes, thus affording manufacturers a measure of product consistency and quality control. Although organoleptic panels benefit from the use of an extremely advanced gas sensing device array (the mammalian nose), combined with the world's most advanced neural processor capable of the identification and classification of an unparalleled range of odours, they are prohibitively expensive to operate, susceptible to environmental changes and are inherently subjective. Such panels therefore often yield results of low repeatability / reproducibility. Further, although organoleptic panels may allow *indications* of odour concentration via routines such as the standard triangular test (where the sample under study is compared with two known samples of dissimilar properties) (AlphaMOS, '98), and indeed, may yield subjective assessments of individual components of a complex odour, accurate data regarding concentration and physiochemical properties of analyte substances are traditionally carried out by well established but time consuming and expensive laboratory based analytical techniques, such as gas chromatography (Bartlett, Blair and Gardner, '93). However, the use of such traditional analytical techniques to study aroma is also fraught with difficulty, as the relationship between physiochemical properties and aroma is known to be obscure.

In other industrial areas, such as environmental monitoring, industrial process control and medicine (Semancik and Cavicchi, '93), where the use of organoleptic panels is rarely practical due to the requirement for high accuracy and reliability (or may not be at all practicable due to the presence of harmful components in the complex odour to be analysed), the demand for reliable alternative methods to measure the concentrations of gaseous analytes is becoming increasingly evident. Alternative techniques are clearly required.

This requirement has, over the last decade or so, resulted in the development of a new breed of alternative analytical technique; one which is not only time and labour non-

intensive, but which is based on technology which allows the discrimination of a sufficiently broad range of odours to permit its use in many industrial areas; the electronic nose (Fig. 1.1).

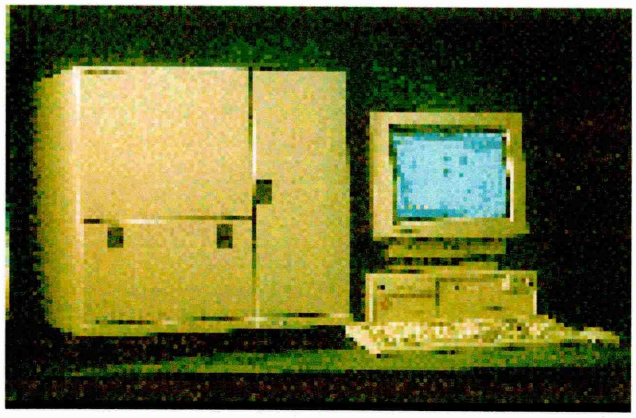

Figure 1.1: *The Neotronics N.O.S.E. (Neotronics Olfactory Sensing Equipment).*

The genesis of the electronic nose, the acceptance of which is growing rapidly, lay in a hybridisation of existing knowledge in the gas sensing arena and research into the operating principles of the mammalian olfactory process. The origins of the sensing technology utilised in the electronic nose may be traced back to the historical development of traditional gas sensing technology.

1.1 The Development of Gas Sensing Technology

Research and development into the design and operation of electronic gas sensing devices has been active for over 40 years, and yet a steady increase in the attention devoted to the subject in the scientific press has been observed over the last two decades, despite the longevity of the subject material. Research has been by both evolution *and* revolution, with refinement of existing technologies attracting more attention in the scientific press than the development of new technology. Many developments in the field have also been the result of particular requirements in specialised fields, such as the measurement of harmful workplace gases in accordance with occupational exposure limits (OEL's) specified by the Health and Safety Executive's Control of Substances Hazardous to Health (COSHH) Regulations (HMSO, '99 a&b). As a result, traditional technology may remain in active use for some decades.

The growth in coal mining activity in the mid 16th century is thought to be responsible for the development of many of the first practical, workplace gas sensing devices. The risks presented to miners by the presence of noxious or explosive gases were appreciated from the early 17th century (Griffin, '71), the most common of these being 'firedamp', a methane-based gas produced from decaying vegetation during the formation of coal seams which is often trapped in a seam and released (either gradually or violently via a 'blower') during mining activity (Griffin, '77). Other noxious gases often present in mines around this period* due to poor ventilation included 'blackdamp' (also known as 'chokedamp'), an inert mixture of nitrogen and carbon dioxide formed by the oxidation of coal and timber, and 'afterdamp', based on carbon monoxide, the presence of which routinely followed an underground fire or explosion.

As a result of increasing knowledge of the risk presented by the presence of the gases mentioned above, many methods were quickly devised and adopted to warn of their presence. In situations where the presence of firedamp was to be expected, such as in the first *deep* mines of the 1700's (Threlkeld, '89), a 'pit fireman' was often employed to search for pockets of trapped explosive gas, wearing rags soaked in water to protect himself against the frequent firedamp 'flashes' (Fig. 1.2). Gas pockets were identified by patrolling the mine with a naked flame mounted on a long cane; changes in the properties of the naked flame (the generation of a blue 'cap') indicated the presence of methane; pockets of which were then purposefully ignited.

Variations in the appearance of naked flames were also commonly used to warn of the presence of firedamp and blackdamp by individual miners at the coal face, who routinely worked by candlelight throughout the late sixteenth and early seventeenth century (although candles were still used in many 'naked light' coalmines until as late as 1947 (Griffin, '71)). The reduction in size of a candle flame was understood to indicate the presence of blackdamp (and therefore a potentially hazardous reduction in oxygen concentration), and the appearance of the aforementioned blue 'gas cap' indicated the presence of methane. The use of the gas cap method to sense firedamp was often less

**** Although the risks posed to miners are now low, and fatalities are extremely rare, Barnsley Council were recently prosecuted and fined £43,500 following the death (by 'blackdamp' asphyxiation) of two contractors working in a trench in close proximity to a former mine (Health & Safety Court Report, 01).***

than successful, as failure to notice the blue cap or the sudden release of a firedamp 'blower' often resulted in underground explosions (Senior, '98).

Figure 1.2: *A 'pit-fireman' successfully searches for trapped 'firedamp' (an explosive gas based on methane (CH_4)) in a northern coalmine in the early eighteenth century (Threlkeld, '89).*

Another common practice throughout the British coal mining industry was the use of caged birds or white mice to indicate the presence of noxious gas (Fig. 1.3). The responses of small birds to firedamp, but especially to blackdamp and afterdamp, were known to closely match those of humans, but symptoms of over exposure occurred at a greater rate than, and at far lower concentrations than those required to endanger humans. An obvious drawback of the use of caged birds (usually canaries) to sense blackdamp and afterdamp was that of their death following over-exposure, analogous to the 'poisoning' of modern day gas sensing materials. This problem was only fairly recently overcome by the addition of small oxygen cylinders to the bird's cage, which allowed the cage to be flooded with oxygen in order to revive the bird if it lost consciousness.

A particularly severe firedamp explosion at the Brandling Main (Felling) Colliery in early 1812 spurred the formation of the *Sunderland Society for the Prevention of Accidents in Coalmines*, who prompted research into the combustion of methane by Sir Humphry Davy, directly leading to the development of the Davy Lamp (Davy, 1815) (Fig. 1.4 [a]).

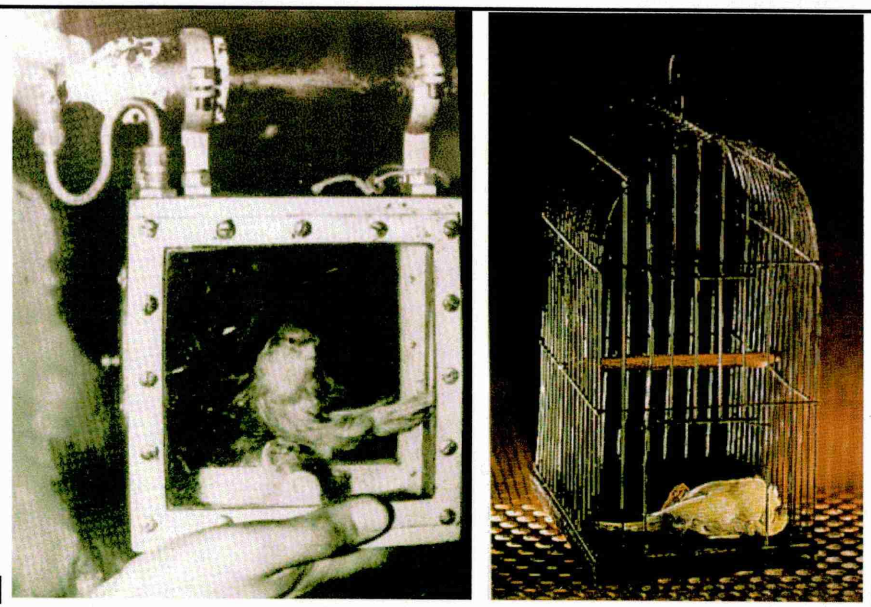

[a] [b]

Figure 1.3: *Traditional Gas-sensing technology; the use of caged birds was popular throughout the 17th century to warn of the presence of 'firedamp' and 'chokedamp' in coalmines. [a] A canary in 'active service' - note the small oxygen cylinder attached, used to revive birds after over exposure (Threlkeld, '89), and [b] a current advertisement for noxious gas alarms.*

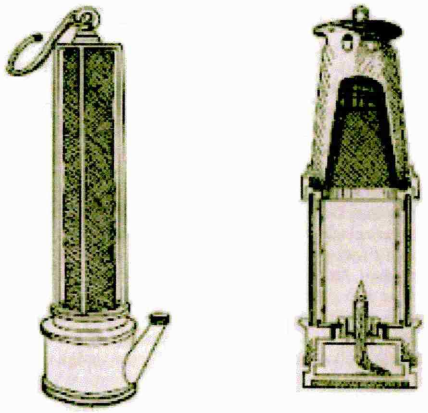

[a] [b]

Figure 1.4: *[a] The original 1816 Davy Lamp, and [b] the Mersaut Safety lamp, a more recent incarnation of Davy's prototype.*

The Davy lamp again relied on the use of a naked flame, the characteristics of which were used to warn of the presence of firedamp. The flame used was, however, encapsulated by a wire mesh, the mesh cooling the flame sufficiently so as not to allow the combustion of surrounding firedamp, which has a high flash point.

Shortly afterwards, George Stephenson made several attempts to produce a rival safety lamp without success, his final attempt, known as the 'Geordie', was received well, but was heavily influenced by Davy's 1812 version. Many improved lamps have emerged since then, with the most notable being that of J.B. Mersaut (Fig. 1.4 [b]), who incorporated a second gauze surrounding the flame. References have suggested that Mersaut-type lamps were still in use in some coalmines until the late 1970's (Griffin, '77), although their use has been greatly reduced, primarily due to the use of electric lamps with the ability to indicate the presence of firedamp, such as the Ringrose* Alarm (Fig. 1.5 [a]), which was itself generally superceded by the methanometer (Fig. 1.5 [b]).

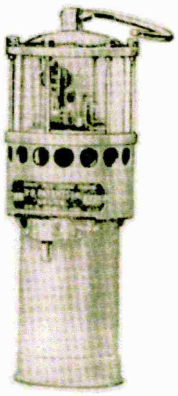

[a]

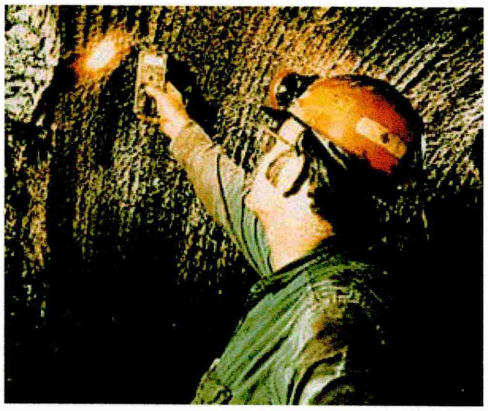

[b]

Figure 1.5: *[a] The Ringrose Lamp, essentially an electric version of the Davy Lamp, used a strong electric light to warn of the presence of firedamp (Threlkeld, '89). The Ringrose has been widely replaced by the methanometer [b].*

Other attempts to develop reliable sensing methods to warn of dangerous levels of combustible gas in air were undertaken in parallel with the evolution of the *gas lamps* described, again driven by mining activity. Novel research was documented in the early 1880's, when Liveing pioneered the measurement of the concentration of flammable gas in air by measuring the heat generated by the combustion of a flammable analyte gas on the surface of a heated filament; the technology developed represented the foundation of today's catalytic pellistor sensors (Liveing, 1880).

* ***The Ringrose detected methane via its combustion within a porous chamber by an electrically heated filament (Statham, '58; Walsh, '01).***

The development of the pellistor, the first popular *electronic* gas-sensing device, (also known as the catalytic gas detector, Fig. 1.6) by the Safety in Mines Research Establishment (now consolidated within the Health and Safety Executive) in the late 1950's again resulted from public concern connected with the safety of coal mining activity. The pellistor was responsible for the earliest attempts to utilise electronic gas sensing devices as environmental monitors, and its use was dominant in the mining, offshore and petrochemical industries for many years.

The detection of flammable gases such as hydrogen and methane is, under normal circumstances, only necessary at quite high levels, but sensors used for these applications must be very reliable. This requirement soon resulted in fears regarding the pellistor's relatively short lifetime and 'fail-unsafe' operation (due to the similarity of the output signals produced before and after 'poisoning' of the catalysed bead), and eventually led to their widespread (but relatively recent) replacement by infrared techniques (McGeehin, '93; CSL, '01).

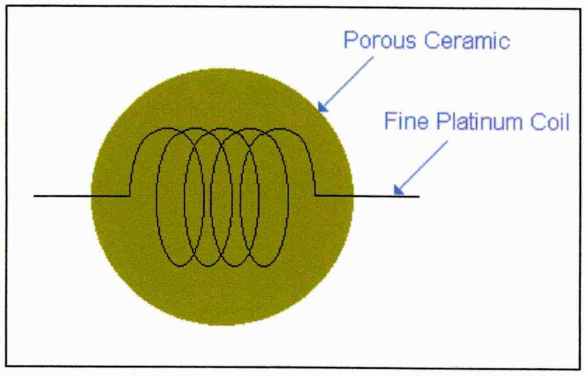

Figure 1.6: *The Catalytic Pellistor.*

Similar concerns regarding the safety on coal mining activity also led to research in the U.S. in the late 1910's, Lamb and Hoover (Lamb *et.al.*, '19) first reported the development of a crude 'colourimetric gas detector tube' for the measurement of carbon monoxide. The technology was based on the development of green pigment on the exposure of an indicator (iodine pentoxide and 'fuming' sulfuric acid on pumice) to carbon monoxide. No further progress was made until Littlefield (1935) reported the development of a similar sensor for hydrogen sulfide, exploiting the visual colour change on exposure of preparations containing lead to hydrogen sulfide (a modern version of which is shown in Fig 1.7).

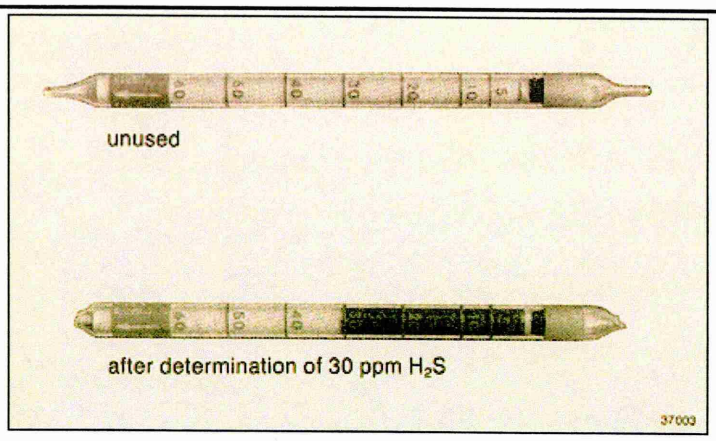

Figure 1.7: *A modern Colourimetric Gas Detector Tube before and after the analysis of 30 ppm hydrogen sulfide (Dräger model 5/b).*

Over a decade after the development of the pellistor, Japanese research led to the development of the Taguchi sensor (Taguchi, '70), a crude but inexpensive (tin dioxide based) device designed for the detection of carbon monoxide and natural gas. These devices were (and are) prone to poisoning during use, and are sensitive to variations in temperature and humidity, as well as being relatively non-specific. Further, their use is only practical after a 'running in' period [stabilisation] of several days. Despite their inherent disadvantages, Taguchi sensors are still in widespread use today.

Subsequent gas sensor research carried out in the 1970's (funded by the National Coal Board and the MoD) resulted in the development of electrochemical sensing equipment for oxygen and carbon monoxide, a technique which has since secured a commanding market share in the area of portable toxic gas detection, despite a routinely short lifetime (as cell life is directly related to analyte concentration).

More recently, the requirement for reliable automotive engine management gas detectors has stimulated much sensor research (McGeehin, '93). Sensing technology based on zirconia, which was traditionally utilised to monitor the content of combustion products (via O_2 concentration) in commercial situations has, after much simplification, found application in the automotive industry as Lambda sensors over the last decade or so, again monitoring the content of combustion products in vehicle exhausts.

The level of interest in the use of gas sensing elements for the monitoring of workplace environments has also increased greatly in recent years. As a result of high demand and

rapid progress in the development of suitable sensitive materials, gas sensors are increasingly becoming an integral part of the workplace as a practical means of environmental monitoring, a role which complements their widespread use as process control devices. Gas sensitive elements are often designed to quantitatively acknowledge the individual presence of a wide range of (discrete) hazardous gases; their base materials, structures and processing optimised to allow high levels of selectivity to 'target' analytes.

The Health and Safety Executive played a key role in the development of such 'optimised' sensitive and selective portable workplace gas detectors [i.e. gas sensors targeted at particular hazardous analytes], as shown in Fig. 1.8, throughout the 1980's and early 1990's. Substituted and unsubstituted phthalocyanines were refined and used extensively as workplace detectors for NO_2 (see for example Jones, Bott and Thorpe, '89; Wilson, Rigby *et.al.*, '92). This work was complicated by the very high sensitivity required by workplace NOx 'monitors'; sensors for water vapour and CO_2 as used in environmental comfort measurement techniques need only respond to gas concentrations in the parts per hundred range, but many atmospheric pollutants must be detectable to below the parts per million (ppm) level in many cases, as is the case for many noxious workplace pollutants including NO_X (see, for example Miasik, Hooper and Tofield, '86).

A significant development in the application of existing gas sensing technology took place in the early 1990's, with the introduction of multi-gas-sensor arrays to the gas analysis arena (for a more detailed account of the development of such arrays, see §1.4). Of the many materials utilised for traditional gas sensing devices (such as metallic oxides, phthalocyanines etc.), the majority of multi-gas-sensor array research in the last 20 years or so has concerned the use of conducting polymer chemoresistors.

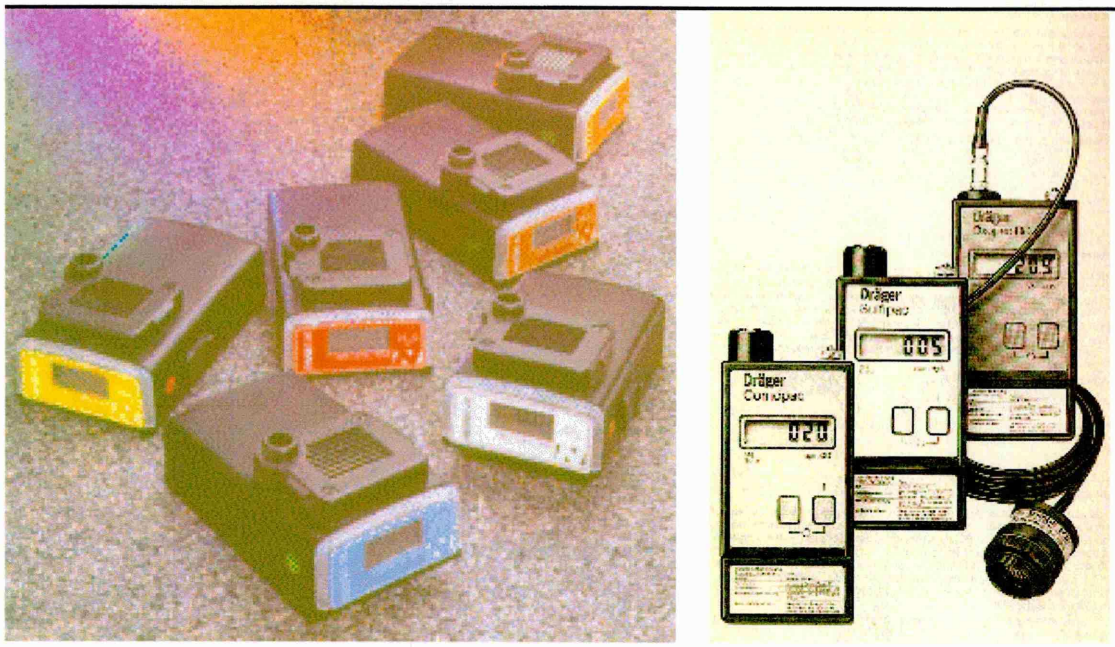

Figure 1.8: *Modern Portable Workplace Gas Monitors.*

1.2 Conducting Polymers

Conducting organic polymers (COP's) have a history of over twenty years, although electrical conductivity had been observed in inorganic polymers and molecular crystals before this time. It is believed that the first organic polymer with the ability to freely conduct electricity was produced by Chiang in 1977, who reported that the addition of appropriate molecules to polyacetylene would result in this ability.

Much research into the development of alternative organic polymers with electrical conductivity soon followed and it was found that several aromatic and heterocyclic polymers could also be rendered electrically conductive. It was, however, soon reported that these polymers were difficult to process (typically not dissolving or melting) once they were polymerised and made conductive, and some were identified as being unstable on exposure to ambient oxygen (see Stubb *et.al.*, '93). New or modified conducting polymers (generally obtained by the incorporation of novel doping groups into known polymer matrices during or subsequent to polymerisation) were developed in attempts to overcome the inherent instability of the original aromatic and heterocyclic species, and reasonably stable polymers were produced.

Materials such as polypyrrole, polythiophene, polyaniline and polyindole were quickly shown to exhibit controllable electrical conductivity by careful selection of dopant and deposition conditions; this has resulted in the commercial exploitation of each of these materials due to their interesting electrical and, in some cases, optical properties. Many of these properties make the use of conducting organic polymers feasible in situations where inorganic materials could not be used (Sukeerthi and Contractor, '94). The new-found family of conducting polymers were, for a time, thought of as potential *replacements* for traditional materials such as semiconductors and metals. It was soon realised, however, that existing materials were highly developed and cost effective, so the original aim of replacement was soon overtaken by the suggestion that the unique properties of conductive polymers should be exploited. An example of the failure of conducting organic polymers to displace 'traditional' and significantly less technologically advanced materials was given by Stubb and co-workers (Stubb *et.al.*, '93), who reported on unsuccessful attempts to replace copper wiring with an electrically conductive polymeric equivalent in a weight saving exercise. The polymer 'equivalent' failed to supplant the original copper wiring due to the inadequate conductivity and stability of the polymers used.

The last twenty years have seen the emergence of polypyrrole (Fig. 1.9) as one of the most technologically important of all the conducting polymers (Scrosati, '88). This is borne out by the enormous volume of scientific literature which is regularly published concerning its properties, synthesis and applications (Wang *et.al.*, '01). The semiconducting* properties of polypyrrole (the material concentrated on in the work presented) were first identified by McNeill *et.al.* in 1963.

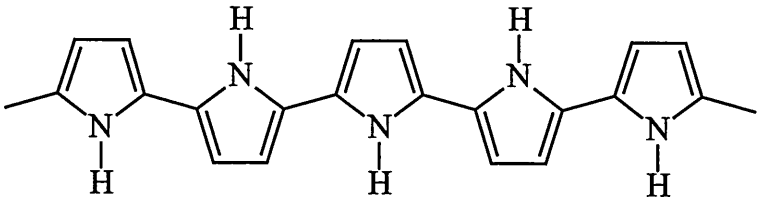

Figure 1.9: *Polypyrrole.*

* ***The term "semiconducting" is used to describe electrical conductivity in the range between full metallic conductivity (ρ = 10E-8 to 10E0 Ω.cm) and insulating behavior (ρ = 10E12 to 10E20 Ω.cm).***

The first reported *electrochemical* preparation of polypyrrole was carried out by Dall'Olio *et.al.* in 1968, who deposited "pyrrole black" (a term used to describe polypyrrole for several years), as a black, powdery precipitate onto a platinum electrode. The benefits of the electrochemical deposition of good quality, free standing *films* of polypyrrole were not subsequently reported until over a decade later (Kanazawa *et.al.*, '79; Diaz *et.al.*, '80). Since then, polypyrrole's novel electrical, optical and mechanical properties have led to its use in many electronic devices. The inherent reversibility of polypyrrole's anion doping reactions (Hanawa and Yoneyama, '89) have led to its widespread utilisation in the production of rechargeable batteries (Kaneto *et.al.*, '82; Torrez-Gómez *et.al.*, '00), electrochromic displays (Kuwabata *et.al.*, '84), artificial muscles (Sansiñena *et.al.*, '97; Coglan, '97; Madden *et.al.*, '99; Okamoto, *et.al.*, '00), and perhaps most importantly as a sensing material.

The application of polypyrrole as a sensing material currently receives much attention from the scientific community; this has been the case for many years. Recent applications have included the use of pH sensitive polypyrrole as a micro-array electrode for the liquid phase detection of penicillin; the use of polypyrrole as the active element in novel potentiometric sensors for chloride ions and perchlorate ions; the use of polypyrrole as a redox potentiometric sensor (Hulkanicki *et.al.*, '94); the use of polypyrrole as a biological glucose sensor (Becerik, '98) and the use of polypyrroles as DNA sensors (Garnier *et.al.*, '99). Other significant applications include the use of polypyrrole as an anti-corrosion coating on steel (Su and Iroh, '00; Herrasti and Ocón, '01), the formation of highly conductive polypyrrole / alumina 'filler' composites (Cho *et.al.*, '00), the use of polypyrrole films as pH sensors (de Marcos and Wolfbeis, '96), use of polypyrrole powders to absorb microwaves (Truong *et.al.*, '98), and the successful use of polypyrrole tubes to aid nerve regeneration (Chen *et.al.*, '00). The use of polypyrrole as a sensing material is, however, dominated by its popularity as a gas sensor.

1.2.1 The Use of Conducting Polymers as Gas Sensors

The operation of a polymer gas sensor relies on the interaction of a 'target analyte' with a conducting organic polymer sensing element. This interaction produces a measurable change in the properties of the element, the most common parameter being d.c.

electrical conductivity. The magnitude of the property change observed is generally related to the concentration of the analyte species; this allows the use of fixed calibration relationships between response and gas concentration (see Semancik and Cavicchi, '93). Under normal circumstances, the adsorption of vapour-phase analyte onto the surface of the sensing element is largely reversible, therefore producing largely reversible changes in the properties of the sensing element. This reversibility is generally aided by the use of relatively thin film polymer layers as active elements.

Gas detection by the measurement of the electrical conductivity changes of a gas sensitive conducting organic polymeric element on adsorption of a vapour-phase analyte gas has been the subject of widespread investigation. The use of conducting organic polymers as sensing elements often results in very large conductivity fluctuations (i.e. large measurable responses); the use of these materials therefore allows the detection of many target gases at quite low concentrations, often in the parts per billion (ppb) range (1 part in 10^9).

A further advantage of the use of conducting polymers as gas sensing elements is the general 'tailorability' of organic molecules. This inherent flexibility allows the production of subtly different derivative molecules which can be tailored to produce new, desirable characteristics yet still maintain valuable characteristics of the 'parent' molecule. Similar subtle modifications may be achieved by variations in the doping and deposition conditions used during polymerisation in order to produce a reasonable ability to respond preferentially (selectively) to specific analytes. This gives conducting polymer gas sensors a great advantage over rival metal oxide sensors, which show a marked lack of selectivity, resulting in a major hindrance to their use for *quantitative* measurement.

The use of conducting polymer gas sensors in preference to other gas sensitive materials, such as semiconductor oxides or phthalocyanines, is advantageous in several other ways; they are simple to miniaturise, are generally very inexpensive to produce, both in terms of the raw materials used and the ease of the preparation techniques involved (compared to other miniaturised sensing devices such as the FET) and their primary measurand is electrical, which means that they can be easily integrated without the need for complicated signal conditioning circuitry. The combination of these factors

has resulted in the widespread, enormous technological importance and popularity of the conducting polymer sensor.

The use of many conducting polymers as gas sensing elements has been reported in the literature; it is generally observed that aromatic and heterocyclic polymeric molecules (such as polypyrrole, polyaniline and polythiophene) are among the most heavily studied due to the presence of alternating single and double bonds along the polymer chain. This results in a high level of π-bond conjugation and so a high degree of π-electron delocalisation which gives rise to the ability of such materials to [a] conduct electricity, and [b] interact with gaseous species in such a way as to allow the level of observed electrical conductivity to change.

Of these materials, the use of polypyrrole as a gas sensing material has been the subject of by far the most research activity. Workers in the field have reported on the use of polypyrrole for the detection of ammonia (Nylander *et.al.*, '83; Gustafsson and Lundström, '87; Kriván *et.al.*, '00; Yadong *et.al.*, '00), dihydrogen sulfide (Kriván *et.al.*, '00), alcohols (Josowicz and Janata, '86) and nitrogen dioxide (Miasik *et.al.*, '86); the sensing properties and sensing mechanisms of PPy films to NO_2 have also been investigated by Hanawa *et.al.*, ('88). Despite the large amount of research into the mechanisms of the gas sensitivity of these polymers, the interactions leading to the observed conductivity fluctuations on exposure to vapour-phase analytes are not yet fully understood.

The large volume of literature published regularly on the subject of conducting organic polymer gas sensing has resulted in several attempts to rationalise the widespread use of these materials as sensing elements. Several handbooks and reviews have been published (see for example, Skothiem, '86) which aim to collate and review the information available. A critical bibliography of research into the use of polypyrrole and other conducting organic polymers as gas sensing elements has also been produced by the author (Lemon and Haigh, '96), reference to which is made throughout the thesis.

Traditional gas sensing devices typically utilise a single sensitive element, carefully designed/chosen to produce 'premium' sensitivity to a single gas type. However, the use of a single element often results in a major lack of selectivity, as the sensor will

normally respond to gases that are chemically similar to the intended analyte. Conducting organic polymers are a family of materials which are often considered as relatively poor materials for the detection of single, known gases (i.e. for use as sensors at the heart of simple gas alarms) due to their *relatively* poor selectivity (their inability to react differently to discrete analytes). However, many recent developments in the field of conducting organic polymer gas sensing have arisen not from attempts to produce highly selective and sensitive 'stand-alone' sensors, but from the use of COP's as members of 'multi-sensor arrays'. Of the many conducting organic polymeric materials used as gas sensing devices, polypyrrole has emerged as a popular base material for use as an array gas sensor, primarily because of the propensity of its gas sensing properties to subtly change with deposition parameters and doping characteristics. The relatively low selectivity* exhibited by polypyrrole was also of fundamental importance in its application in multi-sensor arrays; the use of a selection of similarly non-specific materials is an essential part of multi-sensor array design. The ease by which the gas sensing properties of polypyrrole may be subtly modified allows the use (and simple preparation) of arrays of polypyrrole sensing elements with subtly yet reproducibly different response characteristics; the responses of individual sensors therefore combining to produce highly sensitive and selective arrays.

The use of sensor arrays comprising of many similar active elements employed in parallel as a single device has led to the successful production of highly selective gas sensing instruments from materials from which high levels of selectivity would not normally be expected. The initial and subsequent development of gas sensing arrays was clearly inspired by the processes employed by the mammalian olfactory process (and particularly the human nose, which also operates as a single instrument, but which relies upon information from up to 100 million separate gas sensing devices, as described in § 1.3.1). Indeed, early work involving laboratory-based odour detection was closely related to the operation of the olfactory epithelium (see §1.3.1) (Moncrieff, '61).

More recent research has resulted in the analysis of the information given by arrays of poorly selective materials by powerful processors, some of which incorporate banks of

* ***although still superior to that of many other gas sensing materials, such as metallic oxides.***

data with which to compare newly acquired response profiles. This also mirrors the operation of the mammalian olfactory process, which will now be described.

1.3 Sensory Perception

Sensory reception is the mechanism by which living organisms are able to react to external (or internal) environmental changes. It is common belief that only five senses exist: sight, hearing, smell, taste, and touch, (as distinguished by Aristotle), but accurate categorisation of the many means of sensory perception known to date is far more complicated than first contact would suggest.

One way in which to classify sensory structures is by the stimuli to which they respond. A receptor (a sense cell) is a specialized structure of the sensory nerve that is excited by a certain external stimulus. The stimulus may be electromagnetic (light, electricity, magnetism); mechanical (touch, pressure); thermal (heat, cold); or chemical (taste, smell).

Means of perception may be more correctly classified into the following groups;

- **Photoreception**, the perception of light; the basis of the sense of sight. Photoreception involves the absorption of light energy by photoreceptor cells in the retina; this energy is then transformed into electrical impulses. The diversity of photoreceptor cell pigments in the retina determines the types of light radiation that can be distinguished. The range of detectable light radiation is not, however, limited to those detectable by humans. The diversity of photoreceptor cells allows sensitivity to ultraviolet radiation in insects; some insects also utilise an ability to detect polarized light for navigation. Photoreceptor cells sensitive to infrared radiation are found in snakes, allowing them to locate warm-blooded prey from a distance.

- **Mechanoreception**, the perception of mechanical stimulus. Mechanoreception is responsible for sensitivity to touch, pain (via noniceptors), sound, gravity, and vibration, with sound detection perhaps being the most significant of these (CIE, '98).

Sound reception involves the mechanical detection of sound waves vibrating at frequencies and intensities within the detection range of a particular organism. The sense of hearing is, surprisingly, only found in two groups of animals: arthropods (insects) and vertebrates (amphibians, birds, and mammals).

In vertebrates, sound reception is achieved by two cavities adjacent to the brain that contain sensory receptors (papillae). Reptiles such as snakes are sensitive to sound via a mechanism consisting of a thin plate of bone, which lies beneath the surface of the face, covered by skin and muscle.

One of the most sophisticated mechanisms for sound reception to be found among mammals is that utilised by bats. Mechanoreception is utilised by bats as their primary sense of their surroundings (echolocation, which is used as a substitute for vision) and is applied by bouncing sound pressure waves off nearby objects and detecting and processing reflected sound waves.

Mechanoreception is also responsible for the human body's ability to maintain position and balance (Vestibular sense). This is accomplished by proprioceptors found in muscles, tendons and the inner ear; proprioceptors in muscle tissue detect the motion or position of parts of the body, and so allow 'orchestration' of the expansion and contraction of muscle fibers, therefore allowing posture to be maintained. This ability is aided by kinesthetic sense, the ability to feel motion through receptors found in muscles, tendons, and joints.

- **Thermoreception**, the perception of heat. Thermoreceptor structures in mammals are found in the skin, in the deep tissues of the body, and in the hypothalamus and spinal cord (Gray, '98). Thermoreceptors, which are positioned within mammals to allow sensitivity to external and internal environmental changes, stimulate behavioural responses such as sweating, panting, and shivering. These responses help mammals maintain a constant body temperature.

Reptiles have practically no internal neural or metabolic mechanisms for maintaining their body temperatures (CIE, '98). Thermoreceptors are therefore used to sense the temperature of the surrounding areas in order to locate a basking area of suitable

thermal conditions to maintain a steady body temperature. Birds have thermosensors both in the lower part of the brain and in the skin that allow them to maintain body temperature within a range that varies less than 1°C. Many amphibians and reptiles have sensitive thermoreceptors found in cavities below the eyes. These receptors are adequately sensitive to allow the detection of warm prey at short range. (Note: many thermoreceptors allow the perception of heat by the detection of infrared light radiation, and so are more accurately classified as photoreceptors).

- **Chemoreception**, the perception of smell and taste. In humans, three distinct classes of chemoreceptors are found: taste (gustatory) receptors, smell (olfactory) receptors and trigeminal receptors. Gustatory receptors respond to direct contact with water-soluble materials, (such as sugar and salt), whereas olfactory receptors respond to vapor molecules in the air. Receptors for the trigeminal sense respond to irritants or chemically reactive species (Dodd *et.al.*, '92; Gardner and Bartlett, '94), and are found in mucous membranes. The responses of all three chemoreceptor types are combined in the sensation of 'flavour'. However, the failure of any one of these responses may lead to a partial loss or deterioration of flavour sensation; in humans a loss of smell (often during illness) is generally accompanied by a loss of taste because olfactory and gustatory receptors are excited by similar stimuli. As flavour is perceived as a combination of the responses of the three chemoreceptor types, the loss of any one (especially smell) may result in incorrect interpretation of the information gathered by the remaining two, so leading to deterioration of the overall sensation of flavour. Further, the olfactory sense can often be used in isolation to assess flavour, as sensation of flavour is dominated by the olfactory sense (Gardner and Bartlett, '94).

More recently, it has been shown that the human nose contains a discrete organ which is responsible for the detection of pheromones. This organ, known as the vomeronasal organ was thought to be nonexistent in humans until recently; its role in the animal kingdom has long been known to govern social and reproductive behavior by unconscious detection of pheromones (the vomeronasal organ is therefore often termed the 'sexual nose'). Unlike the sensory receptors in the olfactory epithelium, the results of the signals produced by the vomeronasal organ are not processed via cortical consciousness (Sherwood, '97); response to pheromones is therefore subconscious.

1.3.1 The Human Olfactory System

The human nose is part of the respiratory tract, and is home to the olfactory epithelium, which contains the millions of gas-sensitive nerve ending responsible for the olfactory sense. Externally, the nose is formed by the two 'nose bones' (Figures 1.10 [a] and [b]), which are situated side by side and join to form the bridge of the nose. These bones are covered by the compressor nasi and pyramidalis muscles (Gray, '98), which are attached both to the nasal bones and to soft cartilage, which extends to the tip of the nose and gives the nose its shape.

Internally, the two nose bones articulate with the Superior Maxillary bone (the upper jaw) to form the floor and outer walls of the nose. The Superior Maxillary is divided internally by the palate, the upper face of which forms the lower surface of the nasal cavity and the lower face of which forms the roof of the mouth (Gray, '98).

The nasal cavity is split into two distinct areas by the nasal septum, a wall of cartilage which extends from between the nares (the openings of the nostrils) back through the nasal cavity to the pharyngeal area. Each of the two nostrils therefore leads to a separate cavity, each of which perform identical functions. Each cavity is divided into four 'meatuses' (passages) by three near-horizontal bones; the superior, middle and inferior concha. The primary application of the three concha is to increase the surface area within the nasal cavity. This allows the concha to radiate heat more effectively (so that inhaled air enters the lungs at a more comfortable temperature). The concha also humidify inhaled air by evaporating warm fluids deposited upon them by various glands, including the tear glands. This ensures that inhaled air enters the lungs at a comfortable humidity level.

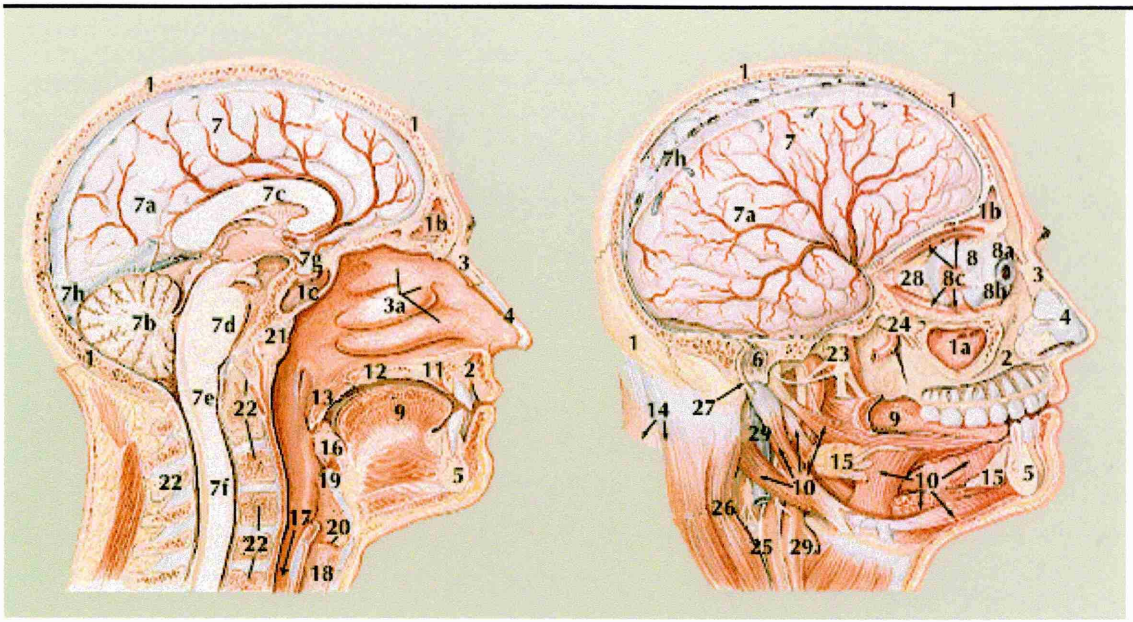

Figure 1.10 [a]: *Internal views of the head, illustrating the complexity of the upper respiratory tract and nasal cavity. (CIE, '98).*

Key:
1a. Maxillary sinus
1b. Frontal sinus
1c. Sphenoid sinus
2. Upper jawbone (maxilla)
3. Nose bone
3a. (Top to bottom) Superior, Middle and Inferior Conchas
4. Nose cartilages
7g. Pituitary gland
11. Hard palate
12. Soft palate
21. Adenoid

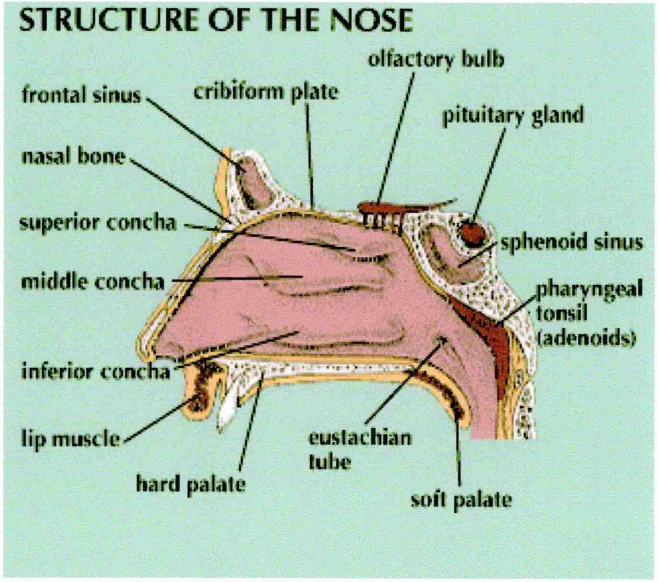

Figure 1.10 [b]: *Detailed cross section of the nasal cavity, showing the olfactory bulb. (CIE, '98).*

An additional task of the three concha is to protect the olfactory epithelium, which contains many of the nerve endings leading to the olfactory bulb. The concha are positioned in such a way as to allow air inhaled through the nostrils to pass over the olfactory bulb, so allowing analysis of odour in inhaled air. Exhaled air however, is diverted so as not to pass over the superior concha. This results in very little or no contact between exhaled air and the olfactory bulb, meaning that a person cannot detect odours in his own exhaled breath (CIE, '98).

Although it is known that the olfactory epithelium contains the vast majority of olfactory receptors (which have a lifetime of around 22 days (Gardner and Bartlett, '94), but are replaced regularly, unlike other neurons), dissection of the anterior lobes of the cerebrum (Gray, '98) show the presence of two olfactory bulbs (which lie on the upper surface of the cribriform plate, either side of the longitudinal fissure, each the size of a small grape (Sherwood, '97)). The olfactory bulbs are thought to be responsible for processing much of the information derived from the receptors in the olfactory epithelium, and are each served by around 20 filaments which pass through the cribriform plate and terminate in the mucous membranes in the nares (nasal cavities). The majority of the filaments terminate in the olfactory epithelia (which lie directly below the two olfactory bulbs, separated only by the cribriform plate and arachnoid membrane), yet some of these have been shown to terminate in the mucous membranes of the superior and middle concha. The mode of termination and, more importantly, the functions of these nerves are as yet unknown.

The nerve filaments which terminate in the olfactory epithelium are known, however, to directly serve the sense of smell. The epithelium is formed of a supporting cellular structure (essentially a mucosa, a mucous membrane) through which the majority of the olfactory nerve endings pass. The nerves terminate with olfactory receptor cells (up to 50 million per cavity) (Bartlett and Gardner, '92; Sherwood, '97) which are covered by a layer of continuously secreted mucous. Up to 20 cilia per receptor cell penetrate this mucous layer. Each cilium is coated with 'G-receptor' proteins (such as gustducin (Sherwood, '97)), which are responsive to interactions with odourant molecules, resulting in a cascade of intracellular reactions through the neural path leading to the olfactory bulbs. It is thought that around 1000 types of receptor proteins are found on

the cilia (Sherwood, '97). The individual selectivity of each protein is relatively low, but all have partially overlapping selectivities to odourants (Schultens and Schild, '92; Gardner and Bartlett '94). This overlapping sensitivity is thought to be responsible for the highly developed discriminatory ability of the human nose, which is reported to allow the discrimination of several thousand odours (Hinton, '96; Gardner and Bartlett, '94).

1.4 *Electronic Analogues of the Human Nose*

The inspiration behind the design of artificial olfactory sensing instruments utilising multi-sensor gas sensor arrays has clearly been heavily influenced by the architecture of the human nose. Indeed, the fundamental methods of operation of commercially available artificial olfactory sensing equipment are essentially equivalent to those of the mammalian olfactory process. Both rely on the use of a collection of relatively non-specific sensing elements, and yet attain high selectivity by manipulation of the sensor responses by a powerful processor. A 'holistic' view of the individual responses of the olfactory receptors is then taken to allow an olfactory 'fingerprint' of the odourant under analysis.

As described in §1.3.1, the human olfactory process allows classification and categorisation of odourants through the use of a huge number of non-selective olfactory receptors. On detection of a complex odourant, the responses of the individual sensors in the olfactory epithelium are processed by the olfactory bulbs (which contain "a considerable amount of cerebral matter in their substance" (Gray, '98)), information is then exchanged with other sections of the brain (the anterior lobe, corpus striatum and the middle lobe of the cerebrum) via the three pairs of olfactory nerves (a "long root", a "grey root" and a "short root" per olfactory bulb). The receptor response pattern is then compared to other established (memorised) patterns, thus allowing rapid classification of the odour. Correct classification relies, of course, on the presence of a suitable response pattern in memory; a collection of such "fingerprints" is constantly built upon (and modified as the response of olfactory receptors changes) throughout one's life.

Similarly, the operation of most electronic analogues of the human olfactory process in response to an analyte odourant may be broken down into the following steps:

- generation of a response to an analyte from a collection of non-selective gas-sensitive elements *(c.f. response of olfactory receptors in the olfactory epithelium)*,
- processing of the signals generated (amplification, smoothing etc),
- generation of a response 'fingerprint' from the responses of individual sensing elements,

• comparison between the fingerprint obtained and known fingerprints stored in memory, via an artificial neural system.

Although several commercial electronic analogues of the human nose (electronic noses) currently exist (see § 1.4.1), it may be shown that their individual evolutions were heavily influenced by early pioneering research. The majority of the systems currently available therefore share many common features as a result of the strength and novelty of the original work.

The historical development of the technology employed by today's artificial olfactory systems will now be discussed. Particular emphasis will be given to the development of the techniques utilised by the Neotronics Olfactory Sensing Equipment (D-type and E-type) used at Sheffield Hallam University. The technology employed by rival instruments will also be discussed.

1.4.1 The Historical Development of the Neotronics Olfactory Sensing Equipment (N.O.S.E.)

Pioneering work involving the laboratory-based detection of odours was carried out by Moncrieff in the early 1960's (see § 1.2.1); research involved the use of a thermistor within a Wheatstone Bridge coated with an 'adsorbent material'; exposure to odourants resulted in a measurable change in the temperature of the thermistor coating. Shortly afterwards, in 1965, Buck *et.al.* reported on the detection of odourants (and other chemical species) by monitoring variations in the electrical conductivity of semiconducting materials on odourant interaction. At the same time, Dravinicks and Trotter (1965) illustrated the propensity of odourant molecules to modify the contact potentials of coated materials on interaction.

Although the development of gas sensitive materials was an area of rapid growth, further work specific to the use of these materials for *odour analysis* was not reported until 1982, when Persaud and Dodd published details of the first fully operational electronic nose. The instrument, developed by a team at Warwick University, utilised an array of "off the shelf" doped tin dioxide gas sensitive elements and was shown to be able to discriminate well between the aromas of commercial products within the

fragrance and food industries. The success of this "Warwick nose" soon resulted in ripples of similar research activity (Ikegami *et.al.*, '85; Kaneyasu *et.al.*, '87), and eventually led to the first conference dedicated to the subject being held in 1990 (Gardner *et.al.*, '90). Papers presented concerned the application of fully developed artificial noses to odour analysis problems, the development and application of both traditional and novel materials to artificial olfactory sensing and developments in neural processing and pattern recognition techniques to allow improved discrimination.

By 1990, the Warwick nose was not only fully operational, but had been the subject of many years of development, well reported in the literature. The original version of the Warwick nose was built around a simple array of three Taguchi gas sensors (see §1.1); changes in the resistances of each sensor were monitored on exposure to odourants in order to solve simple discrimination problems (Persaud and Dodd, '82). Synchronous analysis of the responses of the three elements resulted in a far more powerful analysis tool than previously offered by single element techniques, due to the overlapping sensitivities of the elements used; the individual sensors used in the array were chosen so as to play an active role in the analysis of the analyte vapours. Such array 'optimisation' ensures that each sensor makes an effective, individual contribution to the analysis, and discourages the production of colinear responses (Patrash and Zellers, '93).

Modifications to the equipment soon followed, including the replacement of the original potential divider used to monitor fluctuations in sensor resistance (utilising the sensor in one arm and a fixed resistor in the other) with an a.c. bridge circuit, so increasing sensitivity (Hatfield *et.al.*, '94; Shurmer *et.al.*, '93). This work also resulted in the adoption of digital control. This was achieved by the replacement of the resistor in one arm of a Wheatstone bridge with a d/a converter and allowed simple, digital balancing of the bridges used by the application of a suitable digital code. Noise limitation was also introduced (via narrow-band filtering) in order to enhance sensitivity.

Areas of further development included the optimisation of the neural processing techniques used (see § 1.4.2 for details), the replacement of the Figaro (SnO_2) sensors used with planar SiO_2 based SnO_2 sensing elements (Gardner *et.al.*, '91), and (perhaps most importantly), an increase in the number of elements used in the sensing array from

three to twelve (Shurmer *et.al.*, '90; Shurmer and Gardner, '92). This increase led directly to a fundamental improvement in the operation of the Warwick nose. The ability to incorporate responses from a greater number of sensitive elements into a final response pattern not only resulted in a marked improvement in discriminatory ability, but also led to completion of pilot studies into the suitability of conducting polymers for use as sensing array elements (Gardner and Bartlett, '91; Shurmer and Gardner, '92). Many of the materials developed and used during this work, such as polypyrrole, poly-*n*-methylpyrrole and polyaniline are still used widely in today's electronic noses.

Early organic polymer sensing electrodes for use in electronic nose applications were fabricated by the sputter-coating of gold onto *both* sides of a thin (12μm) mylar* film (see Bartlett *et.al.*, '89). The sensing elements produced were shown to react rapidly, reversibly and reproducibly on exposure to methanol vapour, a novelty for 'room temperature' devices. Further studies into the performance of polypyrrole soon led to criticism however, as baseline resistances were soon shown to drift markedly during a 17-day storage period (Bartlett and Ling-Chung, '89 (a)). Subsequent research concentrated on the identification of suitable polymers for use as array members (Bartlett and Ling-Chung, '89 (b)), and compared the operation of polypyrrole with poly-*n*-methylpyrrole, poly-5-carboxyindole and polyaniline. It was shown that none of the polymers investigated responded suitably to the entire range of vapours tested (methanol, ethanol, acetone, ether and toluene), although the authors stressed that a single deposition regime was used for each polymer type, and performance may be significantly improved by optimisation of deposition conditions. Further research at Warwick (Shurmer *et.al.*, '91) attempted to improve the selectivity of polypyrrole sensing elements by post-deposition overcoating with ultra-thin Langmuir-Blodgett (L-B) films of materials with 'physical holes of molecular dimensions'. It was intended that the use of such 'skeletonised' layers would inhibit the interaction of large molecules with the sensor film, therefore biasing the selectivity of the films produced towards lighter odourants. It was found that the use of L-B films in this way did not result in molecular sieve action, but complex modifications to the operation of the sensor materials were observed.

* ***A commercially available polyester material which adheres well to gold.***

Commercial exploitation of the technology developed was initiated through collaboration between Warwick University, Bass brewery and Neotronics Ltd. through a "Link" project part-funded by the former Department of Trade and Industry and the Ministry of Agriculture, Fisheries and Food (Pearce *et.al.*, '94). Initial development of the technology led to the successful use of the Warwick Nose to discriminate between taints in lager beer samples (Gardner *et.al.*, '94) exclusively using doped, electrochemically deposited, conducting polymer sensors based on polypyrrole. Discrimination was simplified by the use of artificial neural pattern recognition techniques (see § 1.4.2), which were previously the subject of several patent applications (Shurmer, '88; (Gardner and Bartlett, '93)). The success of the Link project led to the commercial release of the Warwick nose (coupled with neural network pattern recognition software), which was marketed as the "**N**eotronics **O**lfactory **S**ensing **E**quipment" (the N.O.S.E.) (Neotronics, '94 a&b; Hodgins, '94). Further development of the sensing materials used was undertaken by the Department of Chemistry and the Materials Research Institute of Sheffield Hallam University (SHU) and led directly to the creation of Neotronics Scientific Ltd., a subsidiary of Neotronics Ltd. (Simmonds and Hodgins, '95; Hodgins, '95). Early work at SHU involved the application of a 'D-type' Neotronics N.O.S.E. (see § 1.4.2) to problems involving the analysis of toothpaste flavour (Webster, '95). Parallel research at SHU resulted in the development of novel conducting organic polymeric materials for use as sensing elements, including polypyrrole and polythiophene derivatives (Hinton, '96). These materials found use in the 'E-type' Neotronics olfactory sensing equipment (the e-NOSE^{TM} 4000), and have been used in all versions since then. Sensor doping regimes using chiral dopant molecules were also developed in order to allow discrimination between positive and negative chiral odourants, resulting in further patent applications, although the materials developed are not yet in commercial use.

The recent takeover of Neotronics (including Neotronics Scientific) by EEV Chemical Sensor Systems (a G.E.C. Company) has resulted in several modifications to the operation of the NOSE (EEV, 1999; Warburton, 1998). These include the use of three individual sensing 'modules' (arrays) based on conducting polymer, metal oxide semiconductor and bulk acoustic wave sensing elements. The use of 'hybrid' sensing arrays in this manner allows the exploitation of existing EEV expertise in MOS and

BAW technology, but was pioneered by AlphaMOS (see §1.4.3). The modified system is currently marketed by EEV as the "EEV Chemical Sensor Systems eNOSE 5000". As the brief of the research programme presented here was biased towards the study of the structure of the sensing materials used in earlier models of the eNOSE (the Neotronics D-type and E-type), the work presented considers only the conducting organic polymeric sensing materials used by these instruments. Details of the operating principles of the E-type Neotronics NOSE (Fig. 1.1) are now given.

1.4.2 The Neotronics Olfactory Sensing Equipment (N.O.S.E.)

The first Neotronics NOSE, commercially released in 1994, adhered closely to the operating principles utilised by the Warwick NOSE, which was not only well developed, but had a proven and well reported ability to discriminate between the characteristics of headspace odours (Fig. 1.11 [a]).

[a] 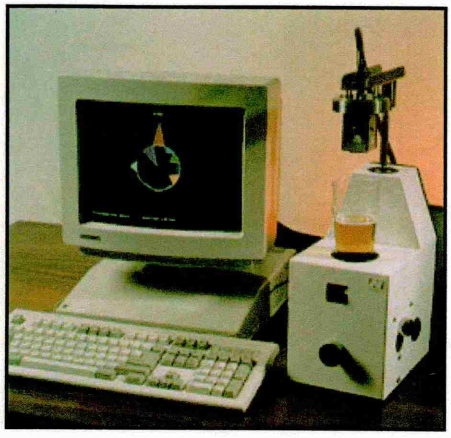 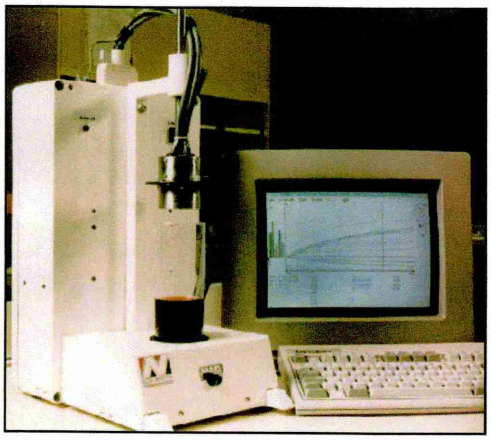 [b]

Figure 1.11: *Prototype versions of the Neotronics NOSE: [a] the original 'A-type', and [b] the 'C-type'. (Note, the latest 'E-type Neotronics e-Nose™ 4000' is illustrated in Figure 1.1).*

The conducting-polymer-based sensing array technology refined during the development of the Warwick NOSE was fully incorporated into the commercial prototype Neotronics NOSE. Since the release of the first commercial version, the internal architecture of the equipment has changed very little. Developments have primarily involved cosmetic improvement (see Fig. 1.11 [b]), modification of the headspace sampling and purging mechanisms, and further design and optimisation of the conducting polymer sensors used.

The heart of all NOSE versions since the commercial prototype is the array of polymeric sensing devices used. Sensing elements (primarily based on polypyrrole, but also including polyaniline, polythiophene, polyindole, and derivatives of each) are electrochemically deposited onto a $\approx 1mm^2$ gold substrate (Fig. 1.12 [a]). Twelve discrete sensing devices are used, the characteristics of which are individually optimised so as to allow maximum discriminatory ability (through the use of broadly overlapping sensitivities). The elements are housed in a circular array, with the polymeric sensing elements facing inwards (Fig. 1.12 [b]). Each sensing 'chip' is held in the array by 'push-fit' connectors. This allows simple replacement of individual sensors after failure (typical lifespans can be as low as 12 months, depending upon the sensing material used), so minimising down-time. Sensor 'types' (i.e. sensors grown under specific conditions, using particular monomers, dopants, electrolytes etc.) are recorded, so allowing 'like-for-like' sensor replacement.

[a] 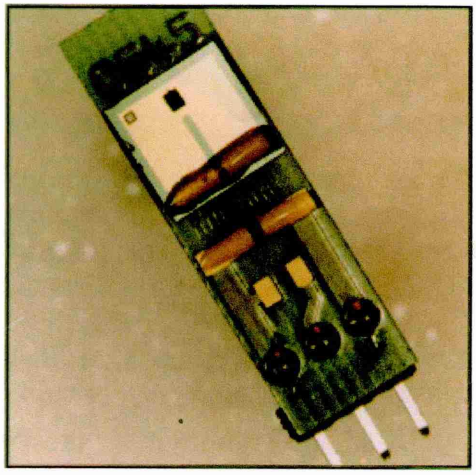 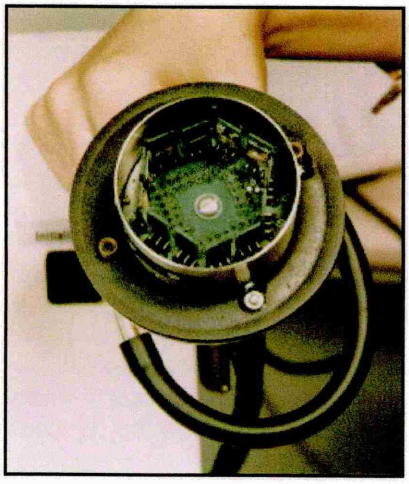 [b]

Figure 1.12: *The fundamentals of the Neotronics NOSE: [a] a standard sensing electrode, and [b] the sensing electrode array.*

Prior to testing, the sensing array is stored in a sealed, environmentally controlled compartment, which is purged with a reference gas (usually dry air, obtained by passing compressed air through silica gel). This allows the user to measure the 'baseline' resistance of the individual sensing devices, and allows the polymeric sensors to refresh subsequent to prior tests. The sample under study is placed in a glass sample vessel (as shown in Fig. 1.11 [b]), which is capped with an airtight seal. The sample headspace (the ambient gas above the solid/liquid sample in the sample vessel) is then purged with

reference gas, and the sample may be stirred and / or heated to increase its volatility. The headspace is then allowed to equilibrate for between 15 seconds and 10 minutes before the sensor head (containing the sensing array) is lowered through the airtight seal.

Equilibration allows the release of volatile odourants into the headspace. Odourants are then free to interact with the polymeric sensing elements immediately once the seal between the sample compartment and the array chamber is breached. Interaction with the odourants present in the headspace results in reversible modifications to the electrical conductivity of each of the sensing elements. Resistance changes are monitored continually from t=0 (the time at which the headspace / array seal is breached); this is achieved by the measurement of the voltage drop across the sensing elements, which are held at constant current. Analogue outputs are amplified, digitised, and fed to a p.c. running dedicated Microsoft Windows™ based software. A real-time graphical representation of the individual sensor resistance changes is then displayed and automatically scaled, as shown in Fig. 1.13. If required, further analyses may be carried out under identical conditions and stored in an 'acquisition set'. The results of three or more analyses can be averaged (giving an *average response vs time* response curve for each sensor). Standard deviations and percentage relative deviations are also calculated.

On completion of the analysis, results may be viewed in *response vs time* format, as shown in Fig. 1.13). The response of each sensor type is assigned an individual colour in order to allow response comparisons. A single measure of resistance change is taken for each sensor in order to facilitate interpretation; the temporal position of this measurement is dictated by the positioning of the vertical cursor by the user, known as the analysis point. The analysis point is typically set at one minute, in order to allow sensor responses to approach plateau. The responses of each array member at the analysis point specified are combined to form a 'response fingerprint' of the material under study. This may be viewed as a bar chart (as shown to the left hand side of Fig. 1.13), or as an offset 'polar plot', as shown in Fig. 1.14.

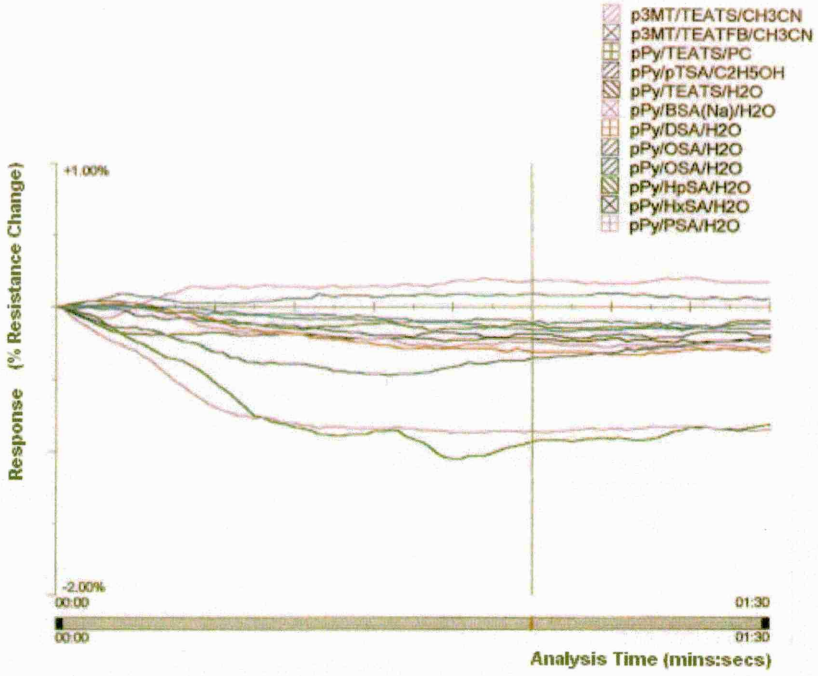

Figure 1.13: *Graphical output illustrating the responses of an array of twelve conducting polymer sensors during exposure to a Cabernet Sauvignon cork.*

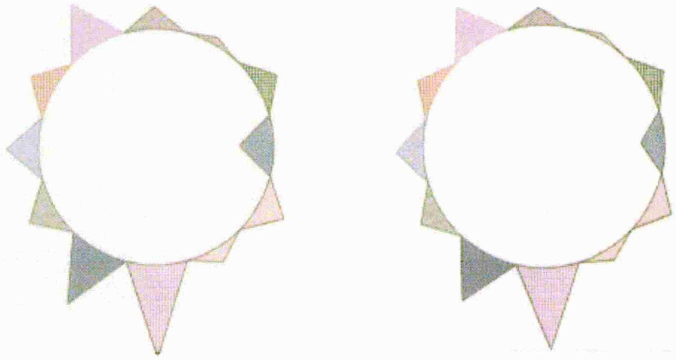

[a] [b]

Figure 1.14: *'Offset polar fingerprints' of the responses of identical twelve sensor arrays to the headspace of two red wine corks: [a] non-tainted, and [b] tainted.*

The polar fingerprint plot is formed by splitting the circumference of a circle into 12 equal parts (producing 12 segments of 30°). The response of each sensing element at the analysis point is represented as a scaled vector; positive responses are represented as vectors outside of the circle, negative responses as vectors inside. User trials have shown that the use of offset polar plots greatly facilitate the interpretation of array responses (Szczur, '97; Hinton, '95). This is aided by the consistent use of individual colours for each sensor throughout the analysis procedure.

Offset polar plots can be compared to previously stored reference plots, or to each other, in order to further simplify the analysis of *differences* between products. Fig. 1.15 shows the results of two such comparisons, one between two red wine corks, and one between two similar malt whiskies.

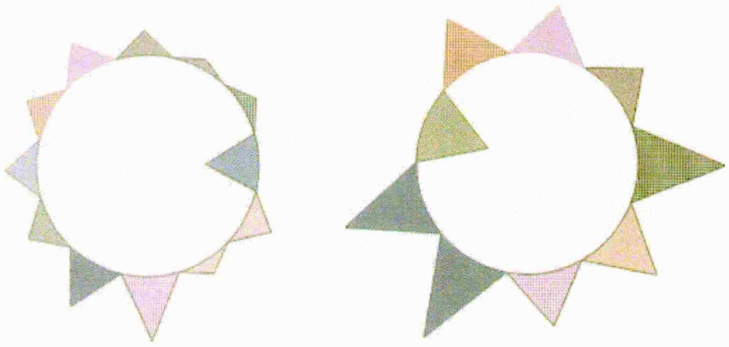

[a] [b]

Figure 1.15: *'Offset polar difference plots' showing differences between the headspaces of [a] two dissimilar red wine corks, and [b] two distinctive malt whiskies.*

This method can be used to discriminate small differences in material odours in a diverse range of applications. Offset polar difference plots have been used within SHU to study the differences in odour between commercially available brands of coffee, beers, tobacco and perfumes. Blind samples of genuine and counterfeit French perfume have also been successfully identified.

The Neotronics e-NOSE 4000 also incorporates pattern recognition and neural processing technology. This allows the system the facility to model human intelligence and so to solve complex classification problems with little human involvement by revealing trends within a data set. Such techniques will now be discussed.

Array Response Processing Techniques

The application of gas sensing arrays to the *identification* of odour types (or simply to the *discrimination* between odour types) may be accomplished by one of two methods, unsupervised and supervised processing (Gardner and Bartlett, '99).

[A] Unsupervised Processing Techniques operate by enhancing the differences in array response (input vectors) produced by the analysis of two or more odours. Some

techniques directly attempt to simplify the interpretation of *n* array outputs (as traditional interpretation becomes increasingly difficult as *n* exceeds 3). One such method is the formation of *polar plots*, as used by Neotronics (described previously). Such plots not only allow visual interpretation of the array response, but also allow the dimensionality of the array response to be reduced; this is achieved by the identification and selection of the sensor outputs which vary by the greatest degree between odour types. When the dimensionality of the sensor response is reduced sufficiently, response vectors may be plotted in mulitdimensional space. Array response may then be displayed in '3-D sensor space', using the responses of three select sensors as coordinates within a 3-D Cartesian system. ***Multivariate Distance Analysis*** involves the calculation of the separation of response points within this system (known as *distance measures,* d_{ij}). This allows a high degree of discrimination between odour types; a popular distance measure is the Euclidean (linear) distance between 'pre-' and 'post-exposure' points in 3-D sensor space (although response routinely strays from the straight line joining these points). This simple technique has been successfully applied to the study of beer aroma by Pearce *et.al.* (1993).

Cluster Analysis is another popular unsupervised processing technique, which allows discrimination between odour types via the natural grouping of reduced dimensionality array responses. This technique has been used extensively to study alcohols (Gardner, '91), coffee (Aishima, '91 (a)), whisky (Aishima, '91 (b)) and pig slurry (Byun *et.al.*, '97), and involves the use of simple pattern recognition algorithms. Cluster analysis allows the visual representation of multi-analysis sample sets as 'clusters' in a reduced dimensionality 'feature space'. The vast majority of cluster analyses reported in the literature use the Hierarchic technique, which operates by the calculation of multivariate distance between an individual response and all other responses. Clusters are then formed by the agglomerative technique, which operates by forming small groups, and progressively merging nearest neighbour groups.

[B] Supervised Processing Techniques such as principal component analysis and neural network techniques operate by the generation of an odour knowledge base, known as the 'training set' or 'calibration set'. The information contained within this knowledge base is collected during exposure of the sensing array to known odour types; the response patterns (or characteristics of the response patterns) produced during

analysis are then stored and archived. Responses produced by unknown odours may then be processed and compared to those contained in the knowledge base, allowing the classification of the unknown odour, provided that the system has previously encountered similar odours. Supervised techniques are also able to continually verify the contents of their knowledge base by a method known as cross-validation, where responses to a known odour (not included in the 'training set') are monitored.

Principal Component Analysis is a popular technique (employed in the Neotronics NOSE) which actively reduces the number of variables which are considered during odour classification. Information from the individual responses from each array sensor is combined linearly into several *principal components* (X_p). The first principal component (X_1) is calculated in such a way as to display the greatest amount of variance, the second (X_2) is calculated similarly, but cannot contain information which correlates with X_1 and so on. This technique essentially removes any colinearity between the sensor responses in the array and so (as many responses are reasonably collinear when a conducting polymer array is used) concentrates the salient information into a small number of variables. It has been shown (Gardner, '91) that principal component analysis is able to 'compress' 85% of the salient information from an array of 12 gas sensors into the first two principal components. This allows very simple diagrammatic representations of array response on a simple X-Y plot. Examples of the use of the PCA technique in odour analysis may be found in Schweizer-Berberich *et.al.* ('94), Holmberg *et.al.* ('95) and Hong *et.al.* ('96). The PCA technique has, more recently, been used for taste analysis using an 'artificial tongue' (Legin *et.al.*, '00; Vlasov *et.al.*, '00), for the identification of the CO and HC content of exhaust gasses (Hong *et.al.*, '00) and for the identification of toxic and combustible gasses (Brudzewski and Osowski, '99).

Artificial Neural Networks

Artificial neural networks (ANNs) are currently in widespread use in many fields, such as image analysis and speech recognition (Gardner and Bartlett, '99); their use in

artificial olfactory techniques is also extensive. The operating principles of ANNs were inspired by the architecture of the mammalian nervous system; their use within artificial olfactory techniques was similarly inspired by the architecture of the mammalian olfactory process.

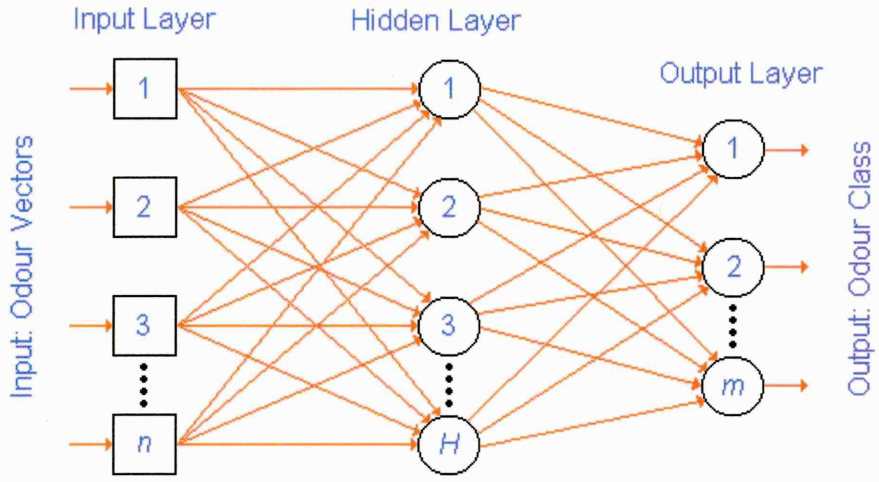

Figure 1.16: *A typical 'multilayer perceptron' artificial neural network. Individual sensor outputs are fed directly to the* n *input layer connections. Signals are then fed to a single hidden neural layer before reduced dimensionality output.*

Although there are several types of ANNs, by far the most popular for use with artificial olfactory techniques are the 'multilayer perceptrons' (see Fig. 1.16), which are based on multilayer neural networks. A typical multilayer perceptron ANN consists of a lattice of artificial neurones, each of which is capable of processing a number of input signals. Processing generally involves the multiplication of each neuron's input by a weighting factor (known as the *synaptic strength* of the neuron), summing, and 'squashing' by an activation function in order to give a single output. The ANN utilised in the Neotronics NOSE (and previously in the Warwick NOSE) operates via the Rumelhart back-propagation method (Rumelhart and McClelland, '86; Gardner and Bartlett, '92; Hinton, '96, Nakamoto *et.al.*, '93). This technique operates by feeding the individual outputs from each sensing array element to individual 'input layer' neurones, which do not process the information *per se* but feed the information forward to the neural 'hidden layer'. The neurons in this layer actively process the signals in the manner described and feed their outputs to the neural 'outer layer'. The number of elements (neurones) in the outer layer is predetermined to match the number of odour types to be classified. This allows the ANN to be trained to produce a 'target output' for each odour

type (i.e. 00001, 00010, 00100 etc. for an outer layer of five neurones) in the initial supervised learning stage. The training process involves the iterative modification of the synaptic strengths of each neurone using the difference between actual and target outputs, which is propagated back through the neural network. Iteration continues until the difference between actual output and target output is small and constant (often over several thousand times). The use of artificial neural networks with the back-propagation technique has proved to be very popular with researchers in the electronic nose arena (see references cited in Gardner and Bartlett, '99). This technique has been shown to be capable of 'learning' array response patterns which are not only subject to noise and drift (Gardner and Bartlett, '94), but which are also non-linear. ANN outputs using the back-propagation technique have also been reported to appear to do far more than simply learn the characteristics of principal component data; a genuine ability to generalise has been reported (Gardner and Bartlett, '92).

1.4.3 Commercial Variants of the N.O.S.E. System

As would be expected, the ongoing development of artificial olfactory equipment was not unique to Neotronics; several rival instruments have been developed, many of which utilise similar operating principles to those employed in the Neotronics NOSE. The development of these instruments will now be discussed.

Early research at the University of Warwick was used as a basis for further development by ***Alpha MOS*** in conjunction with workers at the Universities of Warwick, Southampton and Toulouse. This work led to the production of a range of electronic noses known as the Alpha-MOS FOXes (Alpha MOS, 1997) (Fig. 1.17). The FOX range consists of three models, the FOX 2000, 3000 and 4000, which contain sensor arrays with 6, 12 and 18 members respectively. As with the Neotronics NOSE, the FOX range uses neural network techniques to process sensor array output in order to classify headspace odours. However, unlike the D-type and E-type Neotronics NOSE, the FOX range allows the use of combinations of sensor technologies to achieve optimum discriminatory ability. Conducting polymers, piezoelectric devices and doped / undoped metal oxide semiconductors (including ZnO, SnO_2 and WO_3, all of which may run at one of two temperatures) (Glazier, '99) may be used simultaneously in up to three separate arrays, each containing six sensing elements of equivalent type. Literature

suggests that the use of such 'hybrid' sensor arrays has resulted in the satisfactory classification of tobaccos, plastics odours and cheeses, although attempts to classify wines have been rather less successful (Moy, '95). Parallel research (Hashimoto and Yamida, '94) illustrated that advances in micromachining made possible the production of hybrid (or 'many-principle') gas sensing arrays on a single substrate. This technology was dubbed 'sensor data fusion'.

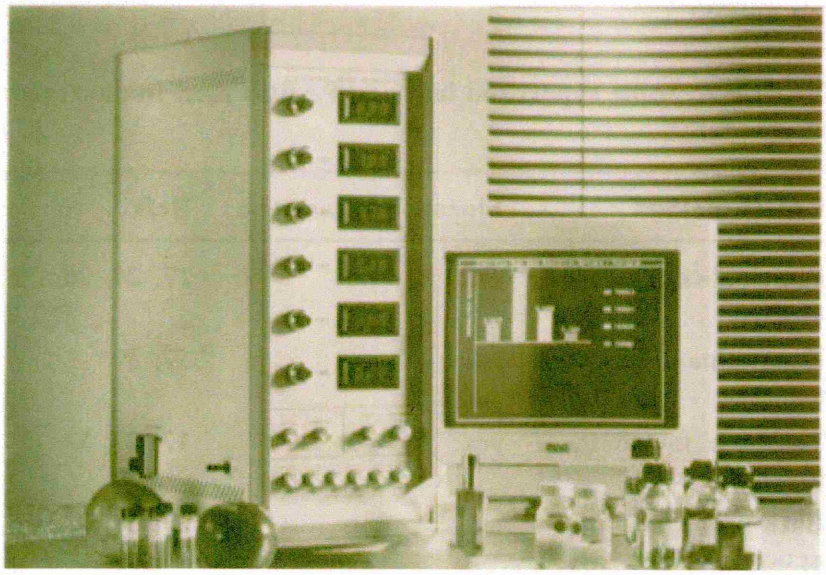

Figure 1.17: *The original Alpha MOS "Fox 2000 Intelligent Nose". Similar operating principles and sensing materials are used in the current Alpha MOS range, although aesthetics have improved significantly.*

More recently, Alpha M.O.S. have produced a novel olfactory sensing system (dubbed "α-Prometheus"), the first of its kind, which combines a gas-sensor array (the FOX 4000) with a mass spectrometer to allow analysis of headspace odourants (Alpha MOS, '99). The responses of *both* techniques are digitised and stored, and may be compared to 'fingerprints' of standard materials via chemometric techniques (predominantly principal component analysis).

The University of Manchester Institute of Science and Technology (UMIST) have also been involved in the development of odour analysis equipment for many years. Research at UMIST, headed by Peter Payne and Krishna Persaud (a former graduate student of Julian Gardner at Warwick University) led to the development of the "OdourMapper" (Fig. 1.18). This apparatus utilises an array of 20 conducting polymer

sensing elements. Commercial exploitation of the system was achieved by the formation of "UMIST Ventures, UK" (Gardner and Bartlett, '94), and "Aromascan PLC".

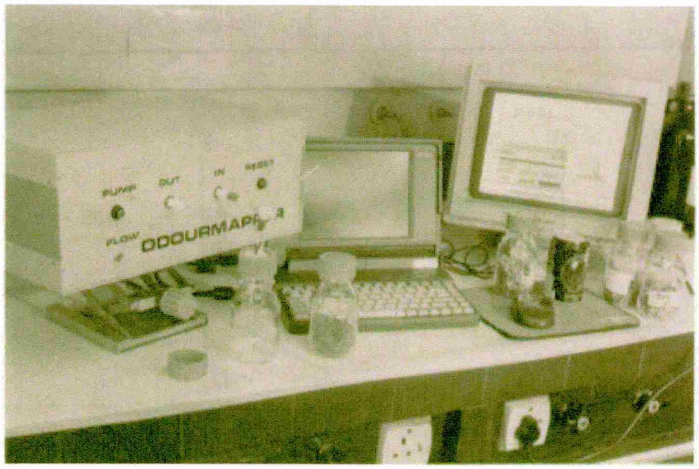

Figure 1.18: *The UMIST Odourmapper.*

More recent incarnations of the UMIST electronic nose, now known as the "Aromascanner" utilise a highly developed, fully integrated array of 32 doped polypyrrole sensing elements *on the same chip* (Fig. 1.19). This is achieved by the deposition of polypyrrole over the entire surface of the chip, which contains 32 pairs of exposed gold electrodes. The polymer layer is patterned via photolithography and plasma etching to leave 32 discrete polypyrrole sections, each bridging the insulating gap between two gold electrodes (Hatfield *et.al.*, '94).

Information from each sensor is fed to an on-chip ASIC (application specific integrated circuit), which forms the first stage of the signal processing required. Initial concerns regarding the impracticality of multi-sensor fabrication on a single chip (due to the short lifetimes of the polypyrrole elements used) were found to be unnecessary (Payne, '97). The technology described has recently been applied to the development of a miniaturised, portable device (the A20S "Smart Gas Sensor"), funded by the European Space Agency. This device has recently been successfully applied to olfaction problems including food quality monitoring (the deterioration of rancid biscuits) and testing of agricultural malodours (pig slurry, Persaud *et.al.*, '96).

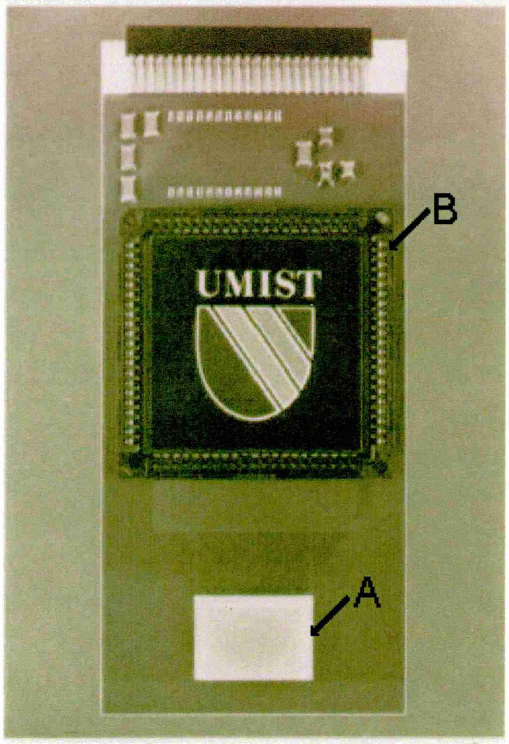

Figure 1.19: *The heart of the UMIST Nose, showing [a] the 32 sensor array, and [b] the on-board A.S.I.C.*

Further research at UMIST (Musio *et.al.*, '95; Amrani *et.al.*, '97) has led to successful attempts to improve the traditionally low specificity of *individual* polypyrrole gas-sensing elements. The application of an "a.c. interrogation" technique, which involves the measurement of the (a.c.) electrical characteristics of a single sensing element at frequencies between 1 MHz and 1 GHz, has resulted in a marked increase in the level of information available from a single polypyrrole element during exposure to an analyte. Indeed, it is claimed that the level of information available (via measurement of conductance, capacitance and inductance at a wide range of frequencies) approaches that of a standard array of 32 polypyrrole sensors (Persaud *et.al.*, '93). However, it may be intuitively expected that information given by the a.c. interrogation technique may be critically dependent on the reproducibility of sensor microstructure; the work presented here suggests that minor fluctuations in deposition parameters may result in significant modifications in device characteristics.

1.4.4 *Parallel Development of Non-Commercial Electronic NOSE Technology.*

Similar research into the development and production of artificial olfactory sensing equipment has been carried out on a smaller scale by many other research bodies throughout the world:

- Researchers at the Tokyo Institute of Technology (Nakamoto *et.al.,* '91) have reported on the development and successful application of a quartz-resonator sensor array, using a number of sensing membrane materials, such as lecithin, cholesterol and ethyl cellulose) to the identification of Japanese whisky odour. An average recognition probability of 94% was quoted. Further work (Nakamoto *et.al.*, '93) reported on the identification of citrus and floral scents with a discriminatory ability approaching that of the human nose. Subsequent collaboration (South Korean) resulted in the development and application of a metal oxide sensor array (Hong *et.al.*, '96) to the identification of twelve gas samples (with 100% recognition probability) and six 'common flavours' (with 93% recognition probability).
- Collaborative research by the University of Rome and the Italian *Instituto Nazionale della Nutrizione* has led to the development (Di Natale *et.al.*, '97) and application (Di Natale *et.al.*, '98) of an electronic nose based on an eight-sensor array of QCM's (quartz crystal microbalances) with tetrapyrrolic cyclic active layers (also known as 'metallo-porphyrins', large rings consisting of four pyrrole groups, often 'complexed' with a central metal atom). This system has been successfully applied to the study of UHT milk and tomato paste odours; the electronic nose was shown to out-perform a human 'smell-panel' during the analysis of tomato paste odour. Further work (Di Natale *et.al.*, '00) has involved the use of the 'University of Rome' nose to analyse the odour of human skin, although sensitivity was not sufficient to allow use of the nose as a diagnostic tool.
- Research at the University of Tübingen, Germany (Schweizer-Berberich *et.al.*, '94) has resulted in the development of an electronic nose based on an array of eight commercially available amperometric sensors. The system utilised complex chemometric techniques to successfully monitor odour changes during the long-term storage of fish, a task traditionally carried out by GC. Further work by the Tübingen group (formerly led by Wolfgang Göpel) has led to the development of a modular sensing system (a 'MOSE' – Modular nOSE) comprising of both MOS and

QCM sensors. The MOSE was found to discriminate well between the odours of [a] sets of rancid vegetable oils, a range of automotive textiles and different brands of tea (Ulmer *et.al.*, '00) .

- Bourrounet *et.al.* ('95) (Toulouse) have developed a lab-based multi-sensor electronic nose based on five commercial (Figaro) MOS sensors. The nose was successfully used to identify the presence of 'boar-taint' during the cooking of pork-fat (an unpleasant odour produced by young 'entire' male pigs when cooked due to the presence of androsterone).
- The University of Linköping, Sweden (in collaboration with the University of Warwick) have reported the use of a hybrid electronic nose (based on CHEMFET devices, but also including Taguchi sensors and an infrared CO_2 sensor) to discriminate between four types of cardboard paper (Holmberg *et.al.*, '95). It was found that only four devices (two CHEMFET, two Taguchi) were required to allow total discrimination.
- The analysis of vapours emanating from citrus peels with 6 semiconductor gas sensors has been presented by Tamura *et.al.* ('94) (Kagawa University). It was found that the analysis of mixed compounds produced responses to the vapour pressures of individual compounds. A 70% probability was quoted for the arrays ability to distinguish between different types of peel.
- Stella *et.al.* ('00) (University of Piza) have utilized an electronic nose to study the aroma of extra-virgin olive oil; results were used to identify a dedicated sensing system for use in the olive oil industry. It was shown by the authors that an array of four polypyrrole sensors (both electrochemically and chemically deposited) was sufficient to result in satisfactory discrimination. The array used was so sensitive as to allow discrimination between the odours of 'handled' and 'non-handled' samples.
- An electronic nose based on an integrated array of 40 metal oxide gas sensors has been developed by Ehrmann *et.al.*, ('00) (Institut für Instrumentelle Analytik, Germany, in collaboration with Kimberly-Clarke) to allow 'self checking' of breath odour quality. Results showed high sensitivity to breath 'malodour'.
- A fully portable electronic nose has been developed by workers in South Korea (Hong *et.al.*, '00). The device utilised six metal oxide sensors, and was successfully used to monitor CO & HC emissions in exhaust gasses.
- Workers at the Chinese Academy of Sciences (Sun *et.al.*, '00) have reported the development of an artificial olfactory sensing array consisting of QCM sensors and

IME devices (see §A1.3) coated with lipids. The use of array members sensitive to mass changes (QCM) and conductivity changes (IME) was an attempt to allow molecular recognition via the deduction of the charge to mass ratio (e^+/m) of analytes. Successful attempts to identify a range of alcohols were reported.

1.5 *Polypyrrole*

The use of polypyrrole and its derivatives is currently very popular in a range of practical applications, not least of all as sensitive elements in artificial olfactory techniques. This popularity has resulted in the formation of a large volume of work in the literature regarding the properties, synthesis and applications of polypyrrole. As a result of this large volume of literature, the first phase of the research presented involved the production of an informal, but thorough literature review, spanning published scientific work between 1993-1996. Review topics included the use of polypyrrole as gas and odour sensors, alternative applications, formation techniques, structural properties, electrical properties and methods of structural determination.

The title of the research project presented, ***"The Structure of Sensor Organic/Polymeric Solids Deposited on Surfaces of Interest for Sensing Devices"*** was non-specific in terms of the polymer used as the gas-sensitive material. The literature search, therefore, was also non-specific with regard to the details of the 'target' polymers; the scientific press was searched for material concerning the structures and gas-sensitivities of many *known* gas sensitive polymers, such as polypyrrole, polyaniline, polythiophene, polyimide and so on. The literature was also searched for details of the performances of rival gas-sensing devices, details of which are included in the review. The body of work collected during the review procedure quickly illustrated that polypyrrole was by far the most popular material for gas and olfactory sensing. It was also of note that Neotronics Scientific Ltd., our industrial collaborators, customarily use pyrrole-based polymers as gas-sensitive elements in the Neotronics Olfactory Sensing Equipment. The research presented therefore concentrates on the study of polypyrrole structure and morphology.

The original intention of the author was to offer the literature review for publication in the peer-reviewed press, but the sheer volume of literature concerned resulted in the production of a lengthy, *informal* document for our own use during the research carried out. The presentation and layout of the review document was therefore tailored to allow its use as a convenient reference text by the authors; its formation and utilisation has subsequently influenced the direction and bias of the work carried out. The review, entitled ***"A Critical Bibliography of the Fundamental Considerations of Conducting***

Polypyrrole Thin-Film Gas-Sensing Ability" is available on request (Lemon and Haigh, '96).

Of the many salient points observed during the collection of the information required, it was especially evident that the structure of electrochemically deposited polypyrrole sensing material had received relatively little attention. Much information was available regarding the traditionally accepted micro/macrostructures of other popular polymers (see §1.5.2), but very little was known about the structure of electrochemically deposited polypyrrole. Miasik *et.al.* ('86) have commented on the poor level of characterisation of *conducting* polymer thin films (including polypyrrole). It was claimed that the difficulty in successful structural characterisation arose from the high degree of amorphous material commonly found in conducting polymer structures. The lack of available information strengthened our belief that the results of investigations into the structure of polypyrrole would be original and novel.

1.5.1 Polymer Structure

The type and level of molecular order present in polymers is a fundamental consideration if their performance is to be understood. The "Fringed-micelle" model (see for example Bunn, '53) was, for many years, the accepted theory as to how polymer chains align to form a multi-molecular sample; this has now been largely discarded. A representation of a fringed micelle structure is shown in Fig. 1.20. It is notable that this model assumes the presence of a finite percentage of fully crystalline material, and a concomitant percentage of less ordered molecular arrangements (it is accepted that the degree of crystallinity present in polymers varies greatly). The model postulated that a single polymer molecule would generally be a part of a number of discrete crystalline regions. The intimate presence of crystalline regions and amorphous areas led to the accepted terminology that most polymers are semi-crystalline.

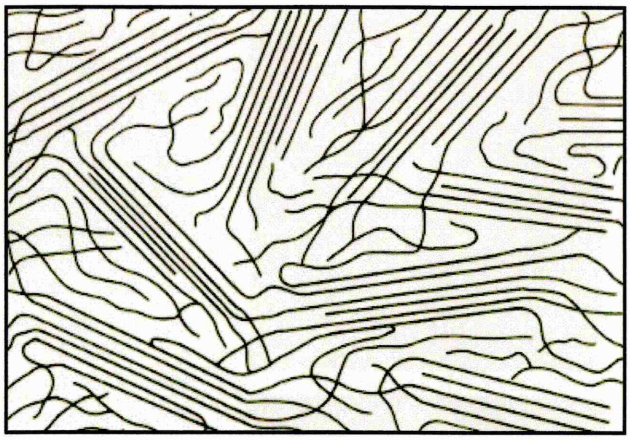

Figure 1.20: *The fringed-micelle model of polymeric texture (from Bassett, '81, after Bunn, '53)*

A more advanced model of polymer structure was introduced soon after (see for example Rees and Bassett, '71), involving the formation of crystalline lamellae consisting of polymer chains oriented perpendicular to the "large" face of a lamellar crystal. The phenomenon known as chainfolding is accepted to be widespread (Bassett, '81); further, the model has been supported by the use of structural determinative techniques which were not available at the time of the introduction of the fringed-micelle model.

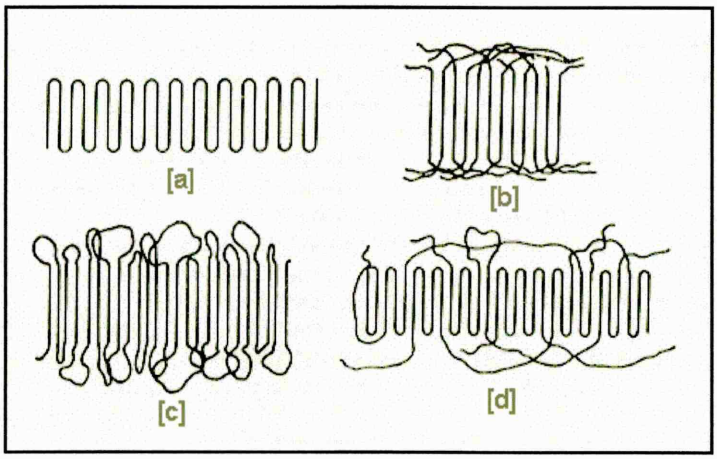

Figure 1.21: *Two dimensional representation of chain-fold models in polymer lamellae, (a) regular, sharp folds, (b) the 'switchboard' model, (c) loose loops with adjacent reentry, (d) combination of several features (from Billmeyer, '84).*

It is known (Billmeyer, '84) that the average length of a polymer molecule is generally much larger than the lamellar thickness. Polymer chains oriented perpendicular to the

lamellar large face must therefore "fold" back on themselves on contact with a crystal face (as represented in Fig. 1.21 [a]). The folding of the polymer chain is not restricted to positions in proximity to the crystal surface, but also occurs at regular intervals throughout the structure. However, it was demonstrated at an early stage that polymers are routinely host to amorphous regions (see Keller, '69) and such regions are not accounted for in a strict chainfolding model. It has therefore been assumed that disordered material is present in the areas of material sandwiched between crystal lamellae. The inter-lamellar amorphous regions may be represented as shown in Fig. 1.21 [b], [c] and [d]. It has also been assumed (see Bassett, '81) that these inter-lamellar regions allow the diffusion of reagents into the polymer.

Spherulites

Early studies regarding the existence of spherulites in polymeric materials were carried out by Keith and Padden (1963, 1964 a&b). Spherulites are, as their name suggests, near-spherical structures, which are often observed in polymers grown in low stress conditions. A classic example of a spherulitic structure (from isotactic polystyrene) is given in Fig. 1.22.

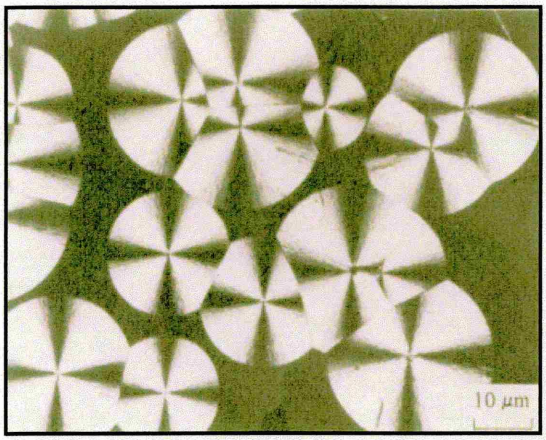

Figure 1.22: *Polarized optical micrograph showing classic spherulites in isotactic polystyrene (from Bassett, '81, after Keith, '63).*

Spherulites are generally peculiar to polymeric materials, but have also been observed in certain minerals, and usually range from 0.5-100µm in diameter. It is well understood that the presence of spherulites is to be expected in almost all melt crystallized semicrystalline polymers (spherulitic morphology is the most common form of unoriented polymeric crystalline structure), with the notable exception of cellulose (Bodor, '91). An optical microscope may be used to view most spherulites, but there are

many spherulitic types which are too small to be observed by use of simple optical instruments. The examination of these structures in electron microscopes is generally not possible, due to the high levels of radiation damage which may result from interaction with the electron beam which can drastically reduce crystallinity. The use of crossed-polars during optical microscopy allows the perception of the levels of order present in spherulitic structures by observation of the classic "Maltese cross" pattern as shown in Fig. 1.22. The high contrast level visible in the cross is the result of the high birefringence levels inherent to mature spherulites.

The growth mechanisms of spherulites have been the subject of much research (see Bodor '91 and Bassett '81 for details). It is accepted that the size of spherulites formed ultimately depends upon two parameters; (a) the density of nucleation sites on the substrate per unit area, and (b) the growth rate employed. Nucleation site density affects spherulite size as would be expected; fewer nucleation sites (fewer nuclei) result in larger spherulites, due to a reduction in the level of interference between neigbouring growth sites. The respective rates of nucleation and growth also affect the spherulitic size; it has been shown (see Bassett '81) that a low number of large spherulites are formed when growth is fast with respect to nucleation rate, and many smaller (immature) spherulites may be formed when nucleation rate is rapid.

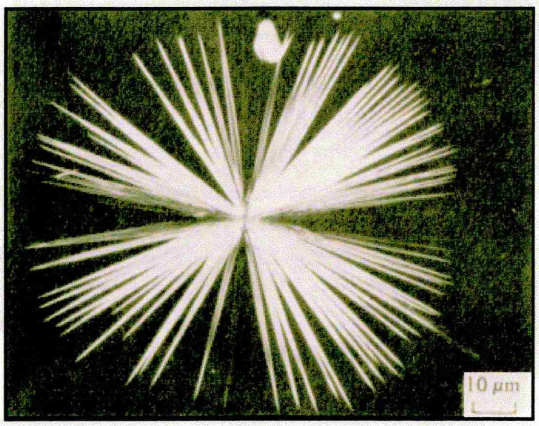

Figure 1.23: *The radiating growth of malonamide from a melt (from Bassett '81 after Keith and Padden '63).*

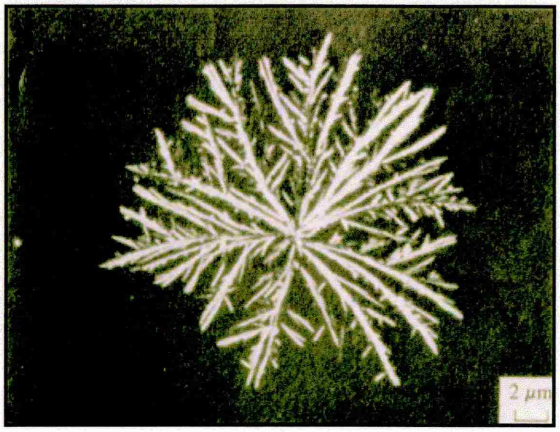

Figure 1.24: *Branching in an isotactic polypropylene spherulite (from Bassett '81 after Keith and Padden '64).*

It is known that spherulites are not single crystals, but are aggregates of many smaller crystalline units (akin to polycrystallinity). These sub-units are known to grow radially from a small central crystallite (this is exemplified by Fig. 1.23, which shows the growth of malonamide in this fashion). Fibrils have been shown to have a thickness which is dependent upon growth speed, and are known to be responsible for the ability of the spherulitic crystal to fill space by their ability to undergo small-angle branching (about which very little is known). Such branching (of polypropylene) is shown in Fig. 1.24. A common process by which a small, central, immature crystallite forms a mature spherulite is shown in Fig. 1.25 (from Bassett '81, after Keith and Padden '73).

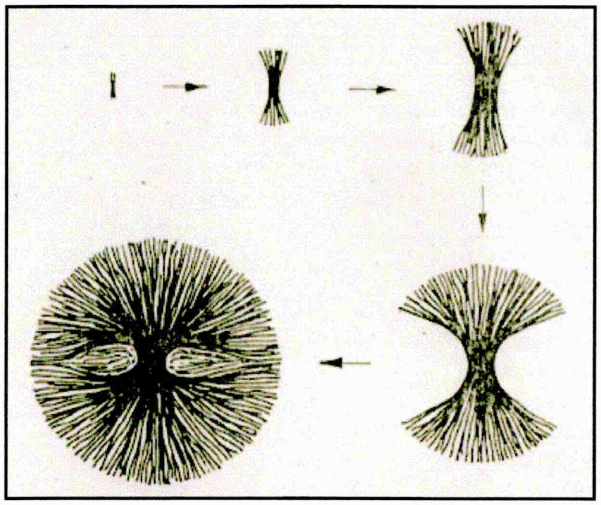

Figure 1.25: *A common form of progressive spherulite formation (from Bassett '81).*

The process shown in Fig. 1.25 is a common example of how spherulites are formed, but is by no means the only growth mechanism observed. This process results in the formation of "negative" spherulites, in which the axes of the polymer chains are perpendicular to the spherulite radius (i.e. fibrils align with radius). An alternative growth method (as observed in polypropylene), is for fibrils to grow radially, but for branching angles to be close to 90°, resulting in the alignment of the polymer chains with the radius (i.e. fibrils lie perpendicular to radius). This type of growth results in the formation of "positive" spherulites. An example of this type of structure is given in Fig. 1.24.

1.5.2 Elucidation of Polypyrrole Structure

Attempts to elucidate the structure of polypyrrole by a range of techniques have been reported in the literature. Morphological studies of polypyrrole are occasionally found, but few workers have successfully applied investigative techniques to the study of the structure of polypyrrole. Attempts have been made to extract chemical and macrostructural information from polypyrrole with many techniques. Reports of work carried out with popular techniques (such as scanning electron microscopy, X-ray diffraction, profilometry and Fourier transform infrared spectroscopy) are documented below. Reports of early work carried out with less popular (and less applicable) techniques are summarised in (Lemon and Haigh, '96). Although a modest amount of work is reported, it is of note that relatively little is still known about the physical structure of polypyrrole (Hodgins, '95).

Scanning Electron Microscopy

Morphological investigations are occasionally carried out by Scanning Electron Microscopy (see, for example, Ren & Pickup, '95; Michalska *et.al.*, '93), although the use of this technique is often intended to provide supporting evidence for results gained from other techniques. Analysis by scanning electron microscopy is far more popular than by transmission electron microscopy due to the ease of sample preparation for SEM observation; the conducting nature of electrochemically polymerised polypyrrole films dispenses with the requirement for gold sputter-coating. More recently, the use of

SEM to study the properties of PPy (polypyrrole) anti-corrosion coatings has been reported by Herrasti and Ocón ('01).

X-Ray Diffraction

Several attempts to apply the X-Ray Diffraction (XRD) technique to the study of polypyrrole structure have been reported in the literature. Brief outlines are given below; details of early work carried out may be found in the literature review.

- Kiani *et.al.* ('92) have used "X-ray scattering" to study the microstructure of polypyrrole. X-Ray scattering was used to assess the effects of the use of 'pulsed' electrochemical deposition (as opposed to traditional potentiostatic deposition) on the molecular anisotropy of polypyrrole films. Samples were prepared by cutting PPy films into 2x4mm rectangles and stacking them whilst preserving their relative orientations. Results suggested that longitudinal and lateral order were subtly different for polypyrrole grown with [a] toluene sulfonate, and [b] naphthalene sulfonate dopants.

- Saunders *et.al.* ('93) have reported XRD studies of PPy formed with each of several (metallophthalocyanine based) dopants. Although the traces produced indicated the presence of substantially amorphous material, several features were identified. These were attributed to the unusually large (tetrasulfonated metallophthalocyanine) counterion used during deposition (see also Wynne & Street '85; Warren, *et.al.* '89) and scattering due to face-to-face pyrrole rings (see also Wynne and Street '85; Buckley *et.al.* '87). It is thought that the significant differences between the work presented by Saunders *et.al.* and the work presented in this thesis in terms of both [a] the deposition conditions used (all films were deposited from propylene carbonate as opposed to aqueous solution), and [b] the dopant material used (phthalocyanine-based, as opposed to sodium benzene sulfonate) render the results presented of little relevance to the materials considered in this thesis.

- Nogami *et.al.* ('94) have used monochromatic Laue-type X-ray diffraction to study the structure of conducting PF_6^- doped polypyrrole. Samples were prepared using a novel synthesis method involving anodic oxidation of pyrrole at –30°C, followed by thermal annealing at 150°C for 5 mins. Laue X-ray patterns for 'twice stretched'

films showed several features, which suggested that "the 'crystalline' domain size along the polymer chain" was "less than 20Å". It should be noted that, as a result of significant differences between the 'histories' of the materials produced by Nogami *et.al.* and the materials considered in this thesis (such as [a] the formation techniques, [b] the growth temperature, [c] the use of annealing, and [d] the use of 'stretching'), the results presented by Nogami *et.al.* bear little relation to the materials studied here.

- Petrillo *et.al.* ('94) have studied polypyrrole and poly(3-n.decylpyrrole) by low angle X-ray diffraction. It was shown that the aromatic rings of the polypyrroles tested were substantially planar. Furthermore, the authors suggested that the presence of the large alkylic group in poly(3-n.decylpyrrole) did not reduce the planarity observed. Again, the non-electrochemical polymerisation technique used by Petrillo *et.al.* (all polypyrroles tested were formed chemically by oxidation with $FeCl_3$ in water at 0°C) result in this work being of limited relevance to the work presented in this thesis.

- Troung *et.al.* ('95) have reported on the use of wide angle X-ray diffraction to study the structural modifications to polypyrrole films doped with *p*-toluene sulfonate or perchlorate ions on heat treatment and/or treatment with aqueous sulfuric acid, sodium sulfate or sodium bisulfate. Modifications to the features observed were noted, but suggestions were not made as to the origins of these modifications.

Film Thickness Measurement

The thickness of polypyrrole thin films have been measured by surface roughness analysis by several workers.

- Rikukawa and Rubner ('94) have used profilometric techniques to study the thickness of polypyrrole films deposited by the Langmuir-Blodgett technique. The average layer thickness of films deposited by the L-B method was found to be around 30Å.

- The surface profile of PPy was measured by Kiani *et.al.* ('92) using a Taylor Hobson Talystep stylus instrument. This gave a reported sensitivity of 0.001 to 0.4μm. The

use of this equipment was problematic as the electrochemically deposited polypyrrole layers had an inherent surface roughness in excess of 4μm.

Fourier Transform Infrared Spectroscopy

Use of the FTIR technique to study the characteristics of polypyrrole has received much attention in the literature. Although the level of information obtainable from this technique (and others derived from it) is impressive, their use was not thought to be suitable for inclusion in the research programme presented here. The information available concerns chemical structure, and therefore does not assist the elucidation of physical structure, as required by our remit. Recent work is now summarised.

- Transmission FTIR has recently been used by Rikukawa and Rubner ('94) to determine the microstructure of "5-layer thick" films of Langmuir-Blodgett deposited polypyrrole. Several features of the FTIR spectrum were observed and attributed to the presence of conducting polypyrrole chains, and to the polypyrrole bipolaron band tail (see §1.5.5).

- Hanawa *et.al.* ('88) have investigated the chemical structure of polypyrrole before and after exposure to NO_2 by FTIR. The authors reported that the spectra obtained for reduced polypyrrole films (after exposure to air) were similar to those presented by Street *et.al.* ('82) for oxidised polypyrrole with anionic dopants. Absorption bands thought to be due to pyrrole were reported at 1530, 1470 and 1410cm^{-1}.

- Hanawa and Yoneyama ('89) have described the use of multi-reflectance FTIR to analyse polypyrrole films. Films were deposited on platinum sputtered ITO glass electrodes chosen for their reflectivity and 2D planarity. FTIR analyses were carried out before and after exposure to SO_2 in order to observe changes in the spectra obtained. It was reported that new peaks appeared which were assumed to be due to SO_2^- and SO_3^{2-}.

- The infrared spectra of polypyrrole on interaction with T_2O has been reported by Kanesaka and Oda ('95). It was shown that the analyte interacted at the pyrrole N position.

- Lei and Martin ('95) have reported on the development of a novel modification to standard FTIR equipment, which allows the characterisation of pristine polypyrrole. This has traditionally been difficult due to the high reactivity of polypyrrole with oxygen. The authors have reported on the use of a 'rigorously airtight infrared spectroelectrochemical cell'. The use of this equipment allowed the authors to investigate, perhaps for the first time, the interaction of molecular oxygen with pristine unoxidised polypyrrole. Mechanisms of oxygen-polypyrrole interaction were documented by the authors.

- Kriván *et.al.* ('00) have used FTIR techniques to study the effects of the exposure of polypyrrole to analyte gases. Spectra taken 'before and after' exposure to H_2S suggested proton transfer between H_2S and the polypyrrole chain.

1.5.3 Polypyrrole Structural Modeling

The low level of understanding of polypyrrole structure formed by empirical observation has been complemented by structural modeling. Ideal structures have been predicted by several workers, often in attempts to describe other material properties, such as electrical transport.

One such study has been presented by Cai and Martin ('91), who have used a simplistic structural model to explain the electrical resistance and capacitive nature of polypyrrole thin films. The model formed described a 'toothbrush' structure, consisting of polymer 'wires' emerging at right angles from the substrate and surrounded by electrolyte. Results suggested that the ionic conductivity of the films was strongly affected by the presence and concentration of the excess free electrolyte present inside the film.

This model is related to a more complex (and more realistic) structural model presented by Ren and Pickup ('95). Impedance measurements from conducting polypyrrole were used by the authors to develop several basic morphological models. The results gained were interpreted as suggesting a structure consisting of polymer aggregates enclosing pores containing electrolyte in the material bulk.

Paasch and co-workers ('94) have considered the electrical properties of polypyrrole and related them to possible chemical structures within the material. The authors suggested that polypyrrole with a two-dimensional macrocyclic structure showed higher electrical conductivity and weaker temperature dependence than conventional 'one-dimensional' polypyrrole. A model was created which aided the explanation of the observed conductivity temperature dependence. This was based on the presence of islands of macrocyclic polypyrrole joined with one dimensional polypyrrole chains.

Veluri *et.al.* ('95) have presented a model of the crystalline microstructure of polypyrrole. The authors used atomistic lattice simulation to describe the optimum packing of polypyrrole chains in 'crystalline' material. The simulation predicted the formation of a unit cell 14.48Å in length, which consisted of five pyrrole repeats.

More recently, Lacroix *et.al.* ('01) have used molecular modeling methods to investigate oligomer-oligomer vs oligomer-monomer coupling during the electrochemical growth of polypyrrole. Molecular modeling suggested that the coupling of long oligopyrroles may be possible *without* oxidation provided that a high doping level is maintained. However, the Authors accepted the severe limitations presented by the use of theoretical molecular simulations.

1.5.4 Polymerisation Mechanisms

Research regarding the polymerisation of pyrrole monomer by electrochemical and chemical means is discussed in Lemon and Haigh, '96. The pyrrole polymerisation reaction is known to be complex (Diaz and Bargon, '86), and involves substitution reactions which proceed via the formation of radical monomer cations, as described below.

The reactions involved in the polymerisation of pyrrole are represented in Fig. 1.26, which illustrates the production of pyrrole radical cations via the oxidation of pyrrole monomer units. The pyrrole monomer radical cations formed may combine via radical cation - radical cation α,α-coupling reactions. Subsequent deprotonation results in the formation of pyrrole dimers.

Note: *Some disagreement exists between workers in this field regarding the possibility of pyrrole dimer production (as described above) by a dissimilar route. Formation by an electrophillic reaction between a monomeric radical cation and a neutral monomer, producing a dimer after further oxidation and deprotonation has been described by Gardner and Bartlett, '99. This process is thought by the author to be highly unlikely (this is supported by Diaz and Bargon, '86), due to the fact that forced electrochemical polymerisation does not occur in the absence of a sufficiently high applied potential. When a suitable potential is applied, the concentration of neutral monomer is zero at the working electrode surface and extremely low in the vicinity of the electrode. It is therefore thought that the reaction must proceed via the direct (α,α-) coupling of radical cation pairs.*

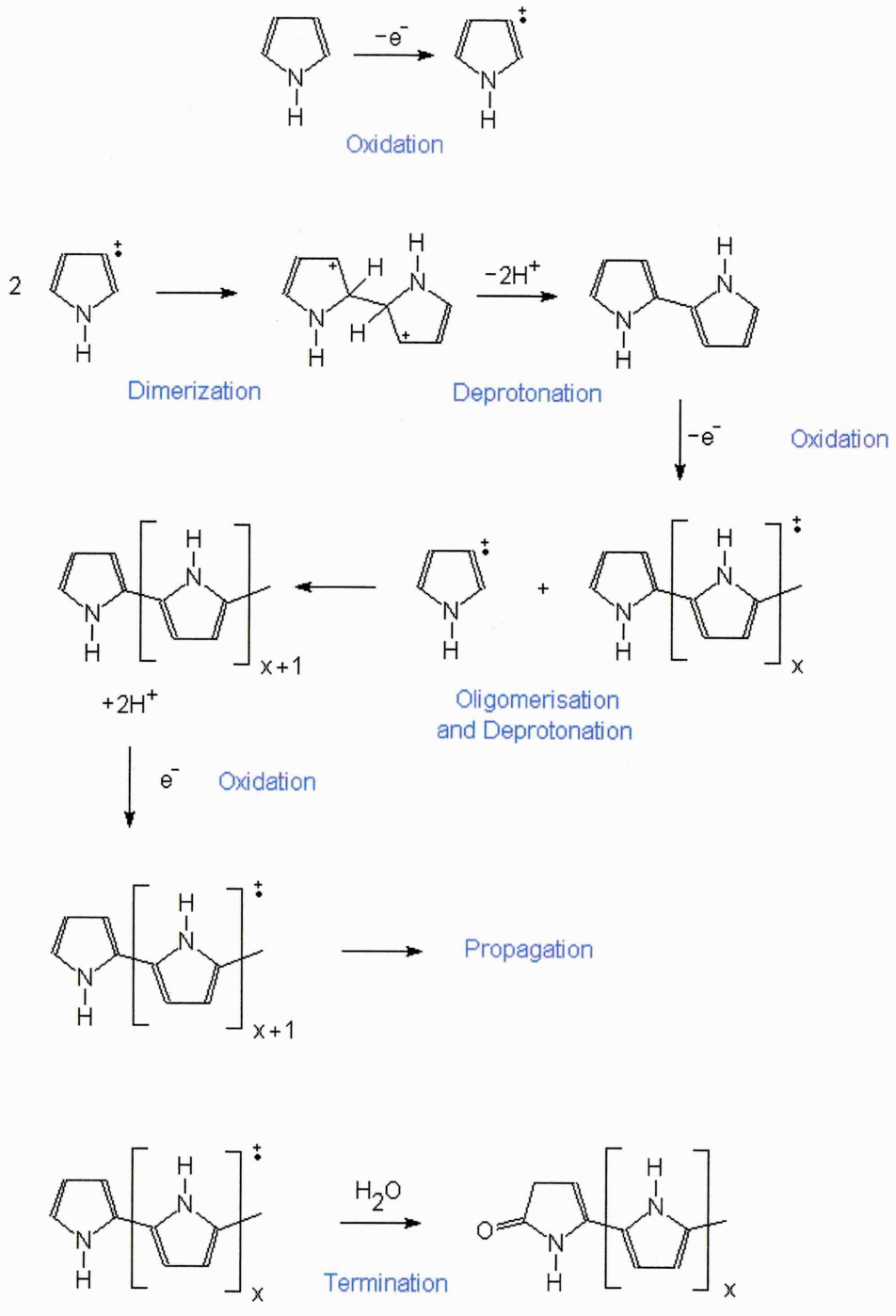

Figure 1.26: *General mechanism for the electrochemical polymerisation of polypyrrole (adapted from Gardner and Bartlett, '99; Diaz and Bargon, '86; Hinton, '96).*

On the formation of neutral dimers (by either route discussed), oxidation results in the formation of pyrrole dimer radical cations. Chain extension (propagation) may be achieved by further coupling reactions between radical dimers and radical monomers, followed by deprotonation and oxidation. Chain extension is unimpeded as dimers, trimers and oligomers are more easily oxidised than monomer (Diaz and Bargon, '86).

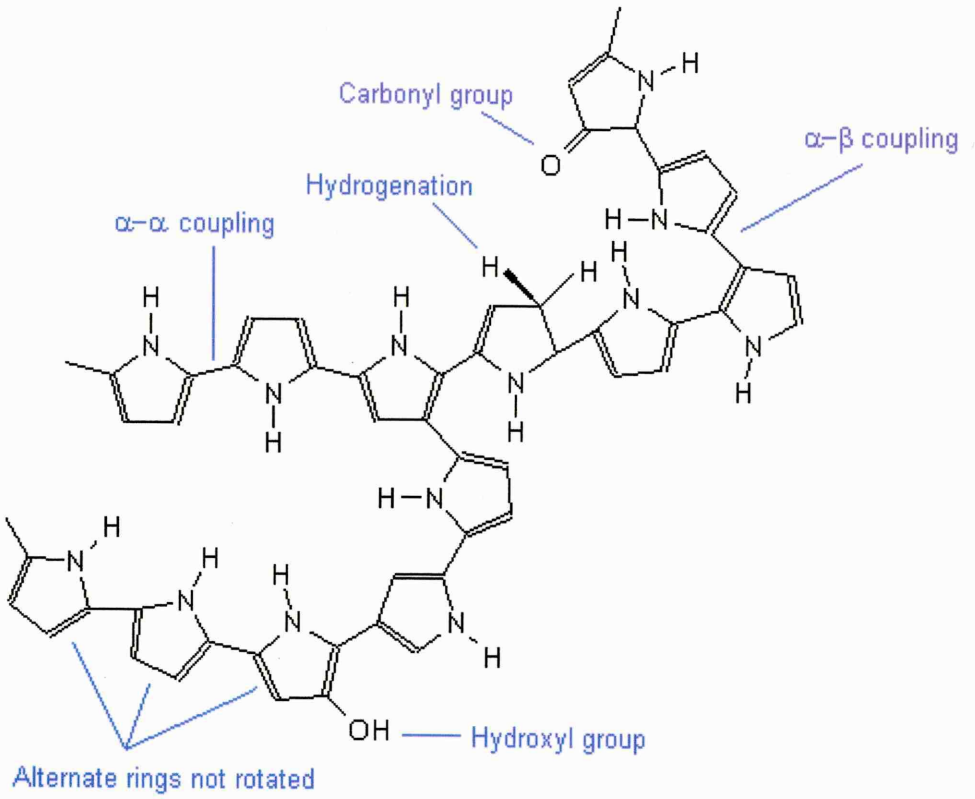

Figure 1.27: *Structural defects known to occur in electrochemically deposited polypyrrole (adapted from Hinton, '96, after Saunders et.al., '95).*

The polymer 'chain' produced by the reaction outlined primarily consists of 2,5- (α,α-) couplings (Street, '86). However, as the likelihood of α,β-couplings increases with increasing chain length (Hinton, '96), the microstructures formed become less ordered as chain length increases. This and other common sources of structural disorder within the electrochemically deposited polymer is shown in Fig. 1.27. Possible termination mechanisms are also shown, such as the formation of carbonyl groups, [which may occur by nucleophillic attack by water (Hinton, '96)] and 'natural' termination [which may occur via the combination of monomer radical cations and oligomeric chain ends, but without subsequent oxidation (Diaz and Bargon, '86)]. *(**Note**: the relative prevalence of each mechanism is as yet unknown, although termination by carbonyl formation is obviously significant during deposition from aqueous electrolyte).*

As chain length increases, the solubility of the oligomers / polymers in solution decreases. Increasing chain length therefore leads to the nucleation and growth of polymer at sites on the working electrode surface.

1.5.5 Electrical Conductivity

The conduction mechanisms of polypyrrole have been the subject of a reasonable amount of research; work in this area is detailed in Lemon and Haigh, '96. The ability of polypyrrole and other 'organic metals' to conduct electricity depends not only on the availability of conducting pathways, but also on the relative abundance of charge carriers and their respective mobilities.

The availability of conducting pathways in polypyrrole is partly due to the presence of a highly conjugated microstructure (see Bredas, '84; Hinton, '96). Conjugation results from extensive overlap between the π-bonds of neighboring pyrrole groups in the polymer chain, and leads to a highly delocalised electron system. Charge transport within polypyrrole may be attributed to a combination of intra-chain (within the same chain) movement *and* inter-chain (between neighbouring chains) movement. Of these, inter-chain transport requires the highest energy; film conductivity is therefore thought by some to be wholly dependent upon inter-chain carrier mobility (Watanabe *et.al.*, '81). However, other workers (Pfluger *et.al.*, '86) argue that the high level of structural disorder within polypyrrole (e.g. crosslinks and branching) lessens the distinction between intra- and inter-chain mobility.

Polaron/Bipolaron Formation

The electrochemical polymerisation of pyrrole monomer (as described previously) is fundamentally dependent on the oxidation of both neutral pyrrole monomer *and* neutral oligomeric chain ends. The anodic oxidation potential of pyrrole oligomers is less than that of pyrrole monomer, and the polymer is therefore automatically oxidised during polymerisation (Diaz *et.al.* '81). This is illustrated in Fig. 1.28, which shows the modifications to nascent polypyrrole (a) on oxidation resulting in the formation of [b] a polaronic defect, and [c] further oxidation resulting in the formation of a bipolaronic defect.

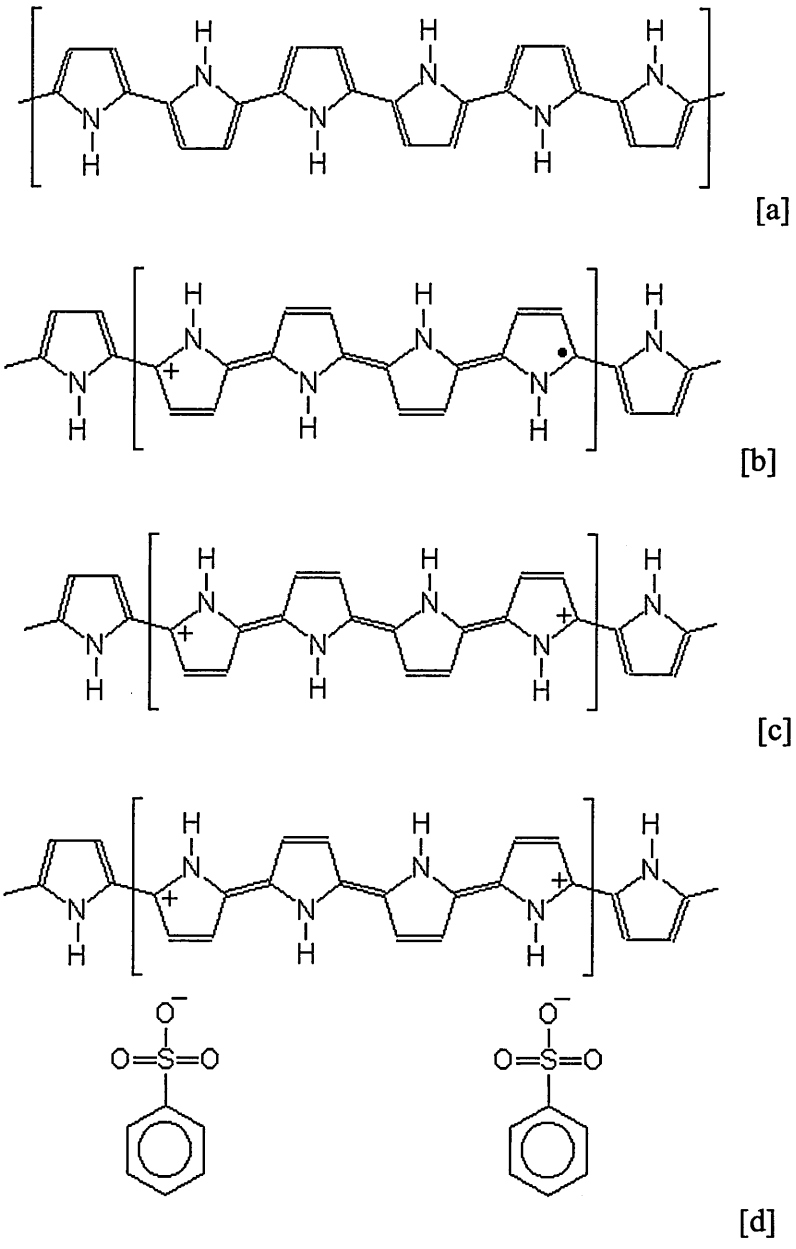

Figure 1.28: *Modifications to a nascent polypyrrole chain [a], by the formation of a polaronic defect [b], and a bipolaronic defect [c]. Charged dopant ions are incorporated to maintain charge neutrality [d].*

The formation of a polaron (as shown in Fig. 1.28 [b]) involves the transition of the polypyrrole backbone from its aromatic to its quinoid form, along with the formation of a radical-cation due to the removal of an electron from the polypyrrole valence band (the transition from stable aromatic to quinoid structure results in a reduction in ionisation energy) (Brédas *et.al.*, '84). The radical-cation formed has been shown to be localised over several monomer groups in the polypyrrole chain (Street, '86).

To counter the presence of positively charged defects (i.e. to maintain electroneutrality) in deposited polypyrrole films, counter-anions from the electrolyte solution are incorporated into the film matrix during deposition (see Fig. 1.28, [d]). The extent of the oxidation of the deposited polymer may be elucidated by analysis of the amount of dopant incorporated into the film during deposition (although the use of this technique is reliant on the presence of sufficient dopant in the electrolyte solution during deposition to allow anion incorporation at each polaronic defect). The use of such techniques has resulted in suggestions that the chain distortion resulting from bipolaron formation is "about four pyrrole rings" (Street, '86; see also Chandler & Pletcher, '85).

Band Theory

To allow an understanding of the electrical conductivity observed with polypyrrole, we should first consider band theory. This theory describes how the well-defined electron occupation energy levels exhibited by isolated atoms are broadened into discrete, narrow bands when atoms are brought together in the solid state. The broadening effect is exaggerated as atoms are brought closer together, and in many circumstances it is possible for atoms to be packed sufficiently closely to result in higher energy bands 'overlapping' those of lower energy, leading to the production of wide energy bands which contain many former energy 'levels' (Kornic, '99).

Molecular orbital theory tells us that lower-energy orbitals (broadened into core and valence bands when brought together in the solid state) are occupied first, whilst higher-energy orbitals (similarly broadened into a conduction band) may be left in the unoccupied state. A substantial energy gap (the band gap, *Eg*) may exist between valence and conduction bands. The extent of this gap is influenced by atomic size (small atoms having a large band gap which decreases with atomic size (Hinton, '96)); this is attributed to the preferential filling of lower energy orbitals. The extent of the band gap of a material has a direct effect on its conductivity (although conductivity may be affected by many other factors such as carrier density and mobility). At zero Kelvin, the valence band is generally completely full in semiconducting materials – promotion of electrons from the valence to the conduction band occurs when the material is heated, so making the material electrically active. Insulating materials have been shown to be host to large band gaps of the order of 10eV or more, semiconducting materials of

around 1eV, whilst metallic materials have no band gap (i.e. valence band conduction bands are not separated *per se*).

The presence of a polaron within the polypyrrole backbone results in the formation of two discrete states (bonding and anti-bonding) within the band gap (Saunders *et.al.*, '95). Subsequent oxidation of the polymer chain results in the formation of a bipolaronic defect (which is energetically favourable to the formation of two separate polarons by 0.45eV (Street, '86)). As the polypyrrole chain is increasingly oxidised up to the oxidation level found in electrochemically deposited material (up to 33%), the states in the band gap are broadened significantly, producing bipolaron bands (Brédas, '86). Brédas ('86) has suggested that further doping would, if possible, result in merging of the bipolaron bands with the valence and conduction bands, resulting in a much reduced band gap. Fig. 1.29 illustrates the modifications to the band structure of polypyrrole as described. (*Note: several workers in this field have published contradictory accounts of the band structure of polypyrrole, see for example Hinton, '96; Brédas, '86; Pfluger et.al., '86. This is thought to be due to [a] variations due to doping and formation regimes, and [b] considerable band tailing caused by the high level of disorder within the polymer (Pfluger et.al., '86)).*

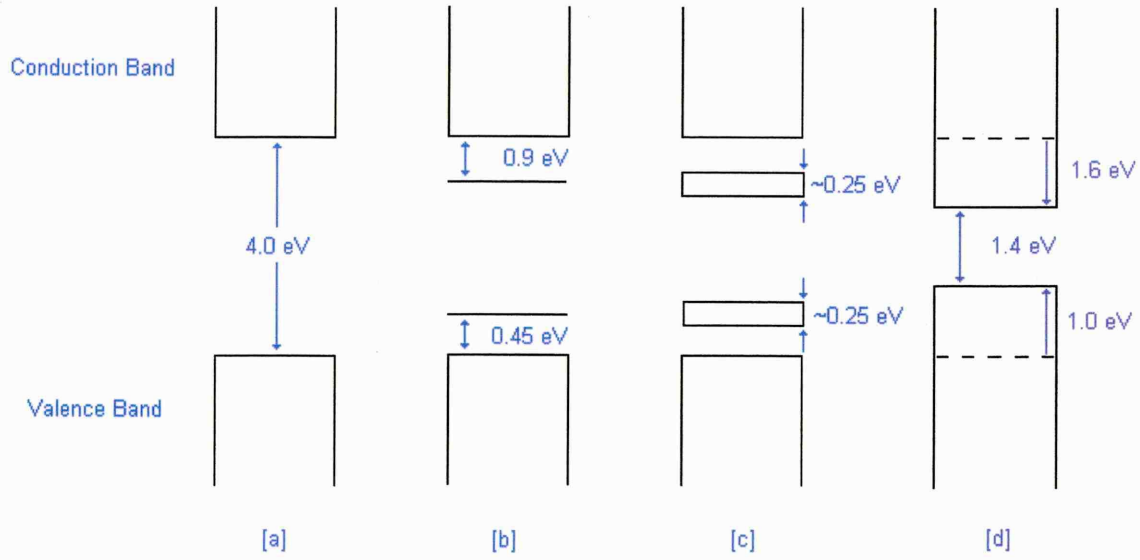

Figure 1.29: *Energy Level Diagrams representing [a] undoped polypyrrole, [b] polypyrrole doped to allow the formation of non-interacting bipolaronic defects, [c] further doped to produce bipolaron bands (~33% doping, as found in typical electrochemically deposited material), and [d] theoretically 100% doped material (adapted from Brédas, '86).*

Summary, Chapter 1

- Methods of artificial olfaction are required due to the low repeatability, low reproducibility and expense of human-based 'organoleptic panels'.
- 'Neotronics Olfactory Sensing Equipment' (N.O.S.E.) was designed to mimic the mammalian olfactory process.
- The NOSE technique uses an array of gas-sensitive, electrically conducting polymeric sensors with subtly different response characteristics.
- Sensors are non-selective, but react subtly differently to common odourants. Results from each sensor are fed to an intelligent neural network to allow recognition of, and discrimination between, odours.
- Polypyrrole is used as the basis for the majority of the sensors used in the NOSE, but the structure of this material is not well understood; assumptions have traditionally been made linking polypyrrole structure to accepted structural models.
- The electrical conductivity, and therefore the response of polypyrrole, is thought to be closely related to the structure of the sensing material, about which little is known.

2. Experimental

In this chapter, the fabrication techniques employed during the electrochemical deposition of polypyrrole are illustrated and discussed, along with the equipment and investigative techniques used during the characterisation and analysis of the polypyrrole sensing elements studied.

2.1 Device Fabrication

The study presented was broadly inspired by a desire to increase the level of understanding of the morphology, structure and growth mechanisms of the gas sensing elements under development by Sheffield Hallam University and our industrial collaborators, Neotronics Scientific Ltd.

A large range of standard 'sensor types' (each using a unique combination of monomer, dopant and deposition parameters) were used by Neotronics Scientific in the e-NOSE 4000 olfactory sensing equipment; the use of an array consisting of broadly similar (yet unique) materials is the basis of the artificial olfactory technique used. As it was not at all practicable to carry out in-depth morphological and structural studies of the range of materials used (or even a representative sample of the range), the work presented therefore concentrates on the analysis of the properties of the polymeric material used in a popular 'all-round' standard sensor type – the type 283. The material used in the 283 sensor is based on electrochemically deposited polypyrrole, with benzene sulfonic acid (sodium salt) [sodium benzene sulfonate] used as dopant during deposition from an aqueous electrolyte as described in §2.1.1. This configuration is routinely abbreviated as [PPy\BSA(Na)\H_2O] – i.e. [monomer\dopant salt\electrolyte]. Other combinations of monomer, dopant and electrolyte were used during the work presented; the configurations used are summarised in Table 2.1.

CODE	MONOMER	DOPANT	ELECTROLYTE
PPy/BSA(Na)/H_2O	Pyrrole	Sodium benzene sulfonate	Water
PPy/$LiNO_3$/H_2O	Pyrrole	Lithium nitrate	Water
PPy/$NaPF_6$/H_2O	Pyrrole	Sodium hexafluoro-phosphate	Water
PPy/$NaClO_4$/H_2O	Pyrrole	Sodium perchlorate	Water
PPy/BSA(Na)/CH_3CN	Pyrrole	Sodium benzene sulfonate	Acetonitrile

Table 2.1: *'Abbreviated Polymer Code' describing the monomer/dopant/electrolyte combinations used during the work presented.*

Deviations were made from the standard configurations (i.e. type-283) and electrochemical deposition techniques used in order to [a] study the effects of deposition parameter modification, and [b] allow the formation of samples on non-standard substrates in order to allow analysis with the structural investigative techniques used. Standard deposition techniques were, however, adhered to at all other times throughout the work presented unless stated otherwise. The standard formation techniques used are discussed in §2.1.1; the investigative techniques used to characterise the materials produced are discussed in §2.2.

2.1.1 Electrochemical Deposition

Electrolyte Materials

Pyrrole monomer (Aldrich) was stored under nitrogen at low temperature (5°C) in low light conditions. Monomer was typically purified immediately before use by solid liquid chromatography; this was achieved by slowly passing through two separate alumina filled columns, each of around 3ml volume. This process was used prior to the formation of type-283 polypyrrole films, and served to purify the monomer by the removal of the majority of the oligomers and polar oxidation products present in 'as-supplied' material (Hinton, '96). The bulk of the work presented involved the use of monomer purified by this technique. The effects of monomer purification have been investigated in some detail; the use of [a] as supplied monomer, [b] monomer purified by the standard technique outlined above, and [c] distilled monomer are reported in §4.2, along with the associated affects on the growth mechanisms and resultant morphology of the polymer films produced.

Benzenesulfonic acid (sodium salt) (Aldrich) was used as dopant in the as supplied state for type-283 material. Investigations were carried out into the morphological and structural effects of the use of other dopant salts, such as lithium nitrate, sodium perchlorate and sodium hexafluorophosphate, all of which were supplied by Aldrich and used in the 'as supplied' state without further purification. All aqueous electrolyte solutions were prepared using water which had previously been distilled and passed through a Millipore (Milli-Q) cartridge purification system. Millipore water was stored in sealed Winchesters after purification.

Substrate Materials

Type-283 and other sensor materials were routinely deposited on 'Mk-III' Neotronics gas-sensor substrates (see A1), which allow polymer deposition over two adjacent gold contacts, each of around 0.5mm^2, separated by a 10μm insulating gap. The presence of this gap allows simple measurement of the electrical conductivity of materials spanning the gap, provided that suitable electrically conductive contact is made with both contacts.

In situations where a larger area of polymer was required, such as for analysis by X-Ray diffraction, gold gas-sensor substrates were replaced with indium tin oxide (ITO) coated glass slides (Balzers), cut to allow deposition over an active area of around 200mm^2. The absence of an insulating gap complicated the measurement of the electrical conductivity of the polymer films deposited on ITO glass slides; a standard four-point-probe technique was used to achieve this when necessary.

Whilst reviewing the literature, it became apparent that the use of interdigital substrate designs was often of benefit to the ultimate performance of gas sensing devices. Several effects of the use of interdigital substrates on the growth mechanisms and structure of the sensing material were therefore investigated. Attempts were made to fabricate interdigital electrodes 'in-house' as a result of the prohibitively high cost of commercially available designs. However, a source of proprietary research grade interdigital substrates was identified via Ehime University, Japan before the completion of this work (as described in A1). The devices (known as "Yoshi" electrodes) consist of two discrete, interlocking comb electrodes formed photolithographically from sputter

coated platinum. Polymer deposition over the comb electrodes (an area of around 50mm^2) allows measurement of the electrical conductivity of the polymer which bridges the insulating gap between the comb electrodes. Electrically non-conductive low alkali metal content glass is used as a substrate.

Equipment / Instrumentation

Forced electrochemical deposition of polypyrrole was carried out using a custom-made Oxford combination potentiostat / galvanostat. This was used to control deposition in a standard three-electrode electrochemical cell (see, for example, Kissinger and Heineman '96) (Fig. 2.1).

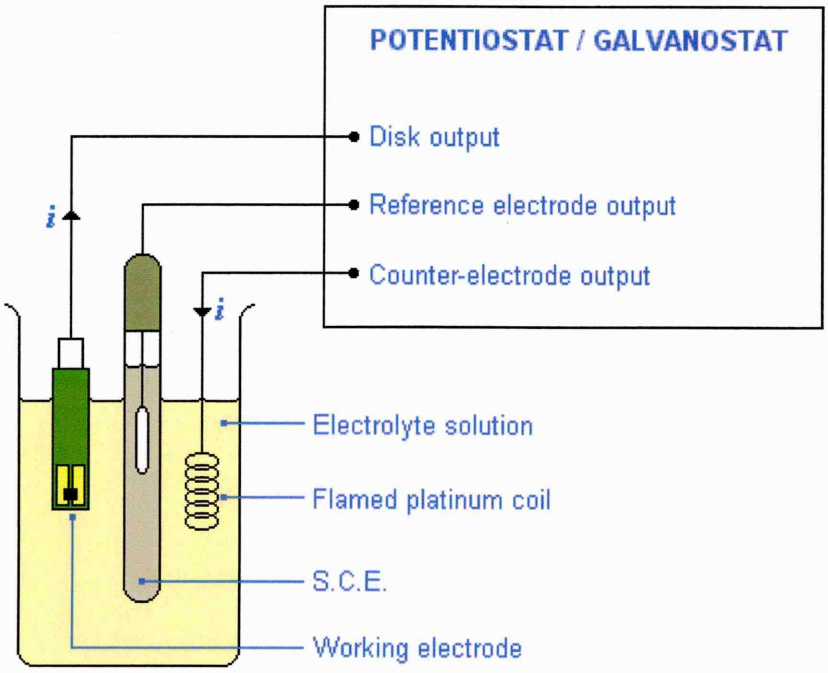

Figure 2.1: *A Standard three-electrode electrochemical cell used for polypyrrole deposition. Polymer is deposited on the non-insulated areas of the working electrode.*

A saturated calomel electrode (SCE) was used as a reference, and all potentials are quoted with respect to this. The SCE was stored between uses in an aqueous solution of KCl (3 Molar), and was rinsed well with Millipore water before use. A high purity platinum coil was used as counter electrode (auxiliary electrode). This was cleaned before use by a thorough rinse in Millipore water, heating to incandescence, rinsing well in fresh Millipore water and washing in propan-2-ol (isopropanol, IPA). The working electrodes used for deposition (the substrate materials) were rinsed well in Millipore water before use, followed by an IPA rinse and drying under a high velocity jet of

oxygen-free nitrogen (care was taken not to allow large droplets of IPA to evaporate on the surface of the substrate materials; the gas-jet was used to quickly remove as much solvent as reasonably practicable before evaporation).

A digital multi-meter (DMM) was used to measure the electrical resistance of the devices produced on Neotronics gold electrodes. This was aided by the use of connectors modified to allow direct insertion of electrodes, so overcoming inconsistencies brought about by the electrical contact between electrode contacts and crocodile clips / probes.

Method / Procedure

Electrolyte solutions were prepared using the reagents outlined previously. The mass of dopant salt (typically benzenesulfonic acid, sodium salt [sodium benzene sulfonate]) required to produce the desired monomer concentration was measured (by weight) in a 50ml beaker. A predetermined volume of solvent (usually 25ml of Millipore water) was added to the beaker, and stirred until a homogeneous solution was obtained. Monomer (pyrrole) was then added to the solution by pipette (whilst monitoring mass increase) until the desired monomer concentration was reached. The solution was stirred until a homogeneous solution was obtained. If prolonged stirring did not produce a homogeneous solution (i.e. under conditions of excess monomer or dopant concentration), then the solution was discarded.

The counter electrode, SCE and a single working electrode were then lowered into the electrolyte solution until the counter electrode coil was completely submerged and the active area of the working electrode was well below the meniscus of the solution (as shown in Fig. 2.1). Potentiostatic electrochemical deposition of the polymer film was then carried out by the application of a fixed step potential from 0.00V to (typically) +0.85V between the working electrode and counter electrode for a specific time. The potential was then stepped back to 0.00V and the deposited polymer left in the solution for a further 30s. This 'decay period' controlled the oxidation state of the polymer and allowed the current to decay until the system reached a stable state (Hinton, '96).

The counter electrode, SCE and working electrode (with freshly deposited polymer film) were then removed from the electrolyte solution, rinsed well under a stream of

clean solvent used in the electrolyte solution (typically Millipore water) and dried under a jet of oxygen-free nitrogen. The working electrode was then detached from the system, was dried, and branded with a unique label. Measurements of electrical conductivity were then carried out.

Fresh electrolyte solutions were used for each set of polymer films deposited on Neotronics gold electrodes, where a set would usually consist of no more than 10 sensors. The use of ITO substrates generally resulted in the deposition of large amounts of polymer; fresh solutions were therefore used for each film.

2.2 Materials Characterisation

2.2.1 Scanning Electron Microscopy

The Scanning Electron Microscopy (SEM) technique was used throughout the work presented to study the topographical and morphological characteristics of polypyrrole. The SEM technique is based on the controlled interaction of a finely focussed beam of electrons with the surface of a suitably prepared sample (Bowen and Hall, '75; Gabriel, '85). Individual electrons within the beam may pass into the bulk of the material under study, or may interact with the surface of the material via scattering, absorption or reflection.

The electron beam is formed by the generation of a stable electron supply from an electron gun positioned at the head of the microscope column, which is maintained at a vacuum of 10^{-7} mbar (see Fig. 2.2). The gun consists of a tungsten filament (although LaB_6 may also be used), which is heated to incandescence (around 2850K) where thermionic electron emission occurs; saturation results in the most effective operation (Gabriel, '85). The beam of electrons produced is subjected to a coarse 'pre-focus' by a small negatively biased electrostatic field generated by a Wehnelt Grid (Fig. 2.2). This reduces the diameter of the electron beam to around 50μm before it is systematically focussed and demagnified by a series of electromagnetic condenser lenses in the microscope column. Demagnification and focussing results in the formation of an image of the electron source which is suitably small to allow high resolution imaging.

The beam is then manipulated further by a final 'probe forming' lens which scans the beam across the surface of the sample under study in a 'television-like' raster.

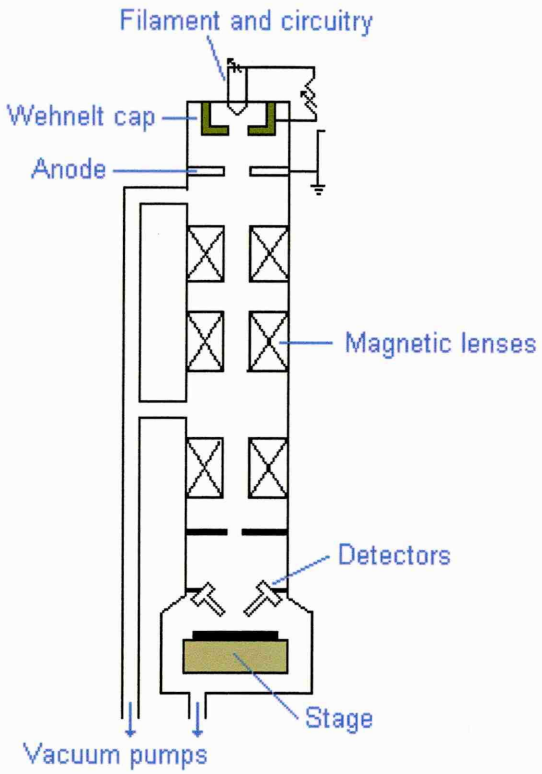

Figure 2.2: *Schematic representation of the Scanning Electron Microscope (adapted from Donohue, '95).*

As the electron probe is scanned across the sample surface, various signals are generated from the surface material. These include emitted secondary electrons, which are produced via inelastic collisions between incident electrons and outer electrons bound loosely to sample ('target') atoms. The majority of the work presented here was carried out in 'secondary electron emission' mode due to the high level of topographical information available. A significant proportion of the secondary electrons produced in this way are emitted from the sample surface, where detection is carried out by a scintillation photomultiplier. The detector is positioned at an angle to the incident electron beam; secondary electrons are attracted to it by a positively biased grid.

Imaging is achieved by the collection of the signals produced throughout the sample scan; a magnified image is traditionally produced by the synchronisation of the electron beam raster with the raster of a CRT. Signal strength at each point throughout the raster

is used to control image brightness. Contrast is achieved due to 'shadowing' which results from the angular difference between the incident electron beam and the detector used (regions of the specimen surface which are in the 'shadow' of the field produced by the positively biased grid are not attracted to the detector and therefore appear as dark areas). The information derived in secondary electron emission mode is therefore highly topographically sensitive.

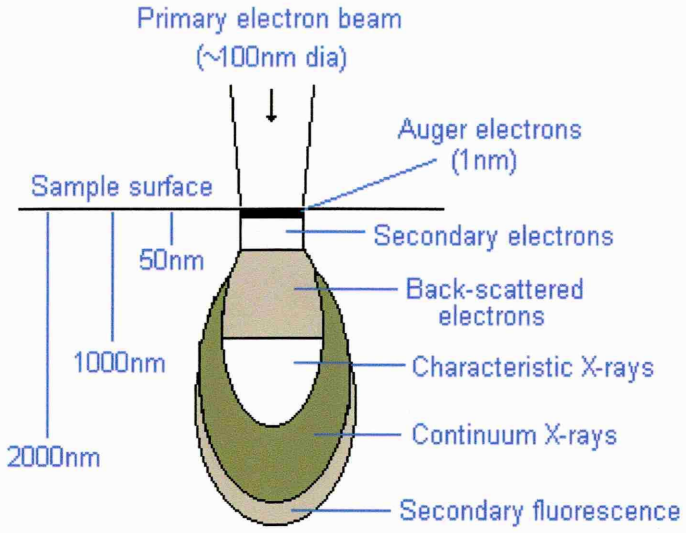

Figure 2.3: *Electron beam interaction volume and analysis resolution.*

Interaction of the incident electron beam with the sample surface also produces other signals, as shown in Fig. 2.3. The use of the SEM in 'back-scattered-electron mode' gives complementary information to that obtainable in secondary-electron-mode. Energetic primary electrons (electrons from the incident beam) may be back-scattered by atoms in the sample surface. The efficiency of back-scattered primary electron production differs between elements; the detection of back-scattered electrons therefore gives information regarding variations in elemental composition. The information derived in back-scattered electron mode is far less topographically sensitive than in secondary electron mode.

Inelastic collisions between primary electrons and electrons in the inner shells of sample atoms may result in the ejection of the inner-shell electron, so producing an ion in an excited state. Such ions may 'relax' via the transition of an electron from an outer shell into the vacancy produced in the inner shell. Such transitions generally result in the emission of an X-ray photon, the energy of which is characteristic of the energy gap

between the energy levels in the element from which it came. The detection of the X-rays produced can therefore provide detailed information regarding the elemental composition of the material under study. Energy dispersive X-ray detectors (and often wavelength dispersive X-ray detectors) are generally mounted within the SEM sample chamber in order to allow elemental analysis to be carried out during electron imaging (Lawes, '87).

A JEOL 840A Electron Probe Microanalyser was used for both Scanning Electron Microscopy and Energy Dispersive X-Ray Analysis (via a Link AN10000EDX facility) during the work presented.

2.2.2 θ-2θ X-Ray Diffraction

X-Ray diffraction (XRD) is a powerful and popular analytical technique which relies on the diffraction of a parallel beam of X-rays by atomic planes in the near-surface region of a sample under study. This technique has been shown to provide structural information regarding the degree of crystallinity, crystal lattice parameters and grain orientation of solid samples (Whiston, '87; Cullity, '78).

The diffraction phenomenon utilised in the XRD technique essentially depends on a phase relationship between a number of waves from an incident X-ray beam which have been scattered by a periodically repeating array of atoms in a crystalline solid (or indeed scattered by a non-regular array in a disordered or amorphous solid).

Diffraction will only occur if the wavelength of the incident electromagnetic waves is of the same order of magnitude as the repeat distance of the scattering centres. As many crystalline materials have repeat distances in the nanometre scale, the use of X-rays is ideal (the wavelength of the radiation typically used is ~ 1.5 Å). If the repeat distance of the crystal under investigation and the wavelength of the incident x-rays *are* of the same order of magnitude, then waves will interact with the solid material and scatter in a predictable manner. If the angle of incidence of the 'input' X-ray beam is such that the paths traveled by diffracted x-rays are of equal distance, or the path difference between diffracted X-rays differs by a whole number of wavelengths, then constructive

interference will occur. However, if this is not the case, then phase cancellation will result in destructive interference. This is represented in Fig. 2.4.

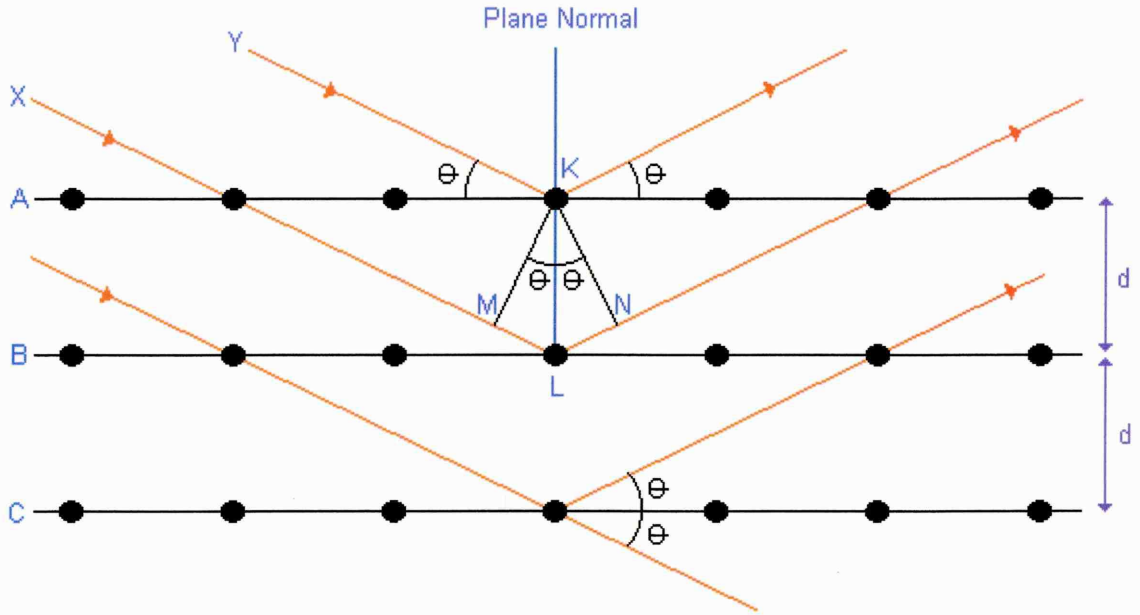

Figure 2.4: *Schematic representation of the diffraction of X-rays by a crystal.*

If an X-ray beam is incident on an atomic lattice with an interplanar spacing *d*, and is diffracted at an angle θ (the Bragg angle) by atoms (or other scattering centres) K and L lying in parallel atomic planes A and B, then the path difference between X-rays X and Y may be shown to be:

$$ML + LN = d.\sin\theta + d.\sin\theta$$

After scattering, the two rays X and Y will be in phase (and so will interfere constructively) when the path difference between them is equal to an integer number of wavelengths (nλ). It may therefore be shown that constructive interference will occur when the following expression (the Bragg equation) is satisfied:

$$n\lambda = 2d.\sin\theta$$

The theory described above is utilised in several practical techniques; the most suited to the analysis of the materials studied here is the θ-2θ X-ray diffractometer, as shown in Fig. 2.5. The θ-2θ diffractometer used during the work presented consists of a fixed X-

ray source emitting radiation of a known wavelength, with a sample stage and x-ray detector able to rotate around a fixed central axis *C*, perpendicular to the incident beam.

The sample under study is placed with its analysis plane on the *C*-axis, and is set to rotate at an angular velocity ω about the *C*-axis, so subtending an angle θ to the beam direction. The X-ray detector assembly is also set to rotate around the *C*-axis, but does so at an angular velocity of 2ω, so subtending an angle of 2θ to the beam direction. This constant angular relationship is maintained between source, sample and detector by a direct mechanical linkage, and ensures that the Bragg condition is maintained.

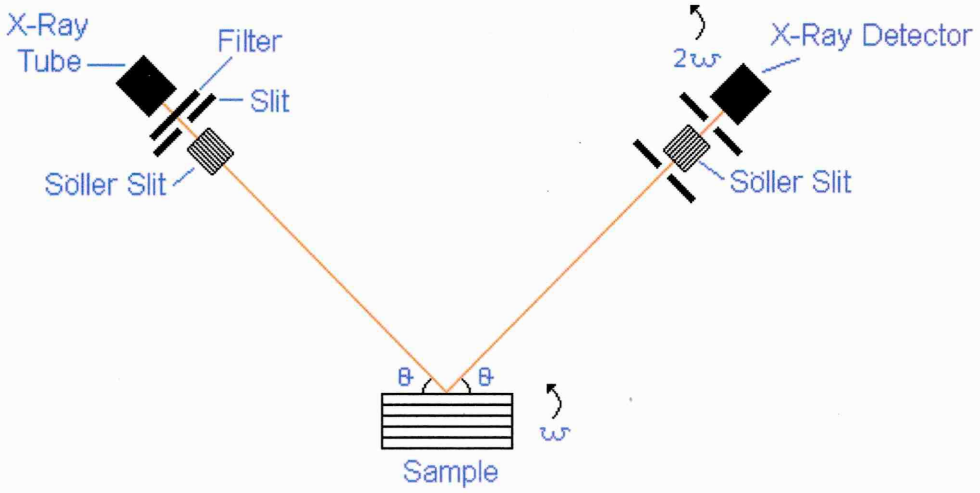

Figure 2.5: *Schematic representation of the X-Ray Diffractometer used.*

The number of X-rays picked up by the detector (the count) is continually monitored and stored as the detector passes through its 2θ scan range (from 5° to 130° under normal operating conditions). The scan range is split into many user definable channels; a 'tally' of the X-rays detected in each channel is displayed and automatically stored during analysis. The resultant plot (or *diffractogram*) shows the X-ray count (representing X-ray intensity) as a function of the diffraction angle, 2θ. Analysis of crystalline (or partly crystalline) material generally results in the production of a series of peaks, characteristic of the unit cell of each crystal structure encountered. Analysis of peak position yields information regarding the size and shape of the unit cell. Peak heights may also be used, in combination with peak positions, to determine crystal structures (Windle, '77).

The X-ray diffraction (XRD) studies presented here were carried out using Philips PW1130/60 and PW1810 θ-2θ horizontal axis powder diffractometers with CuKα radiation (λ = 1.542 Å); results were analysed by a Philips PW3710 control unit via Philips APD 3.6 analysis software.

2.2.3 Glow Discharge Optical Emission Spectroscopy

The Glow Discharge Optical Emission Spectroscopy (GDOES, or GDOS) technique is a novel method of elemental analysis which produces qualitative, and often quantitative analysis of the components of a sample. Information is presented as a function of depth; this is achieved by the systematic removal of atoms from the sample surface during analysis via an argon glow discharge.

As material is removed from the sample by the argon discharge, information regarding elemental composition is collected via the stable excitation of the sample material. If the energy transferred to the sample material during argon abalation is sufficient, then orbital transitions to higher energy levels occur in the sample material atoms. These transitions result in vacancies in lower energy levels from which electrons were excited. On 'relaxation' of the excited atoms (electron transitions back to the lower energy level), energy is emitted as a photon, the energy of which will be characteristic of the material from which it was emitted. The energy of the emitted photon is characterised by:

$$(E_1 - E_2) = h \,.\, c / \lambda$$

where:

	E_1	=	Excited state energy
	E_2	=	Ground state energy
	h	=	Plank's constant
	c	=	Speed of light
	λ	=	Wavelength

As each element has its own characteristic electron orbital energy levels, excitation will give rise to the emission of characteristic spectral lines. The analysis of the wavelength of the photons produced therefore allows elemental analysis of the material under study.

Further, the intensity of the emission lines produced is proportional to the number of emitted quanta (Ives, '94), and is therefore proportional to the elemental concentration (Strobel, '77).

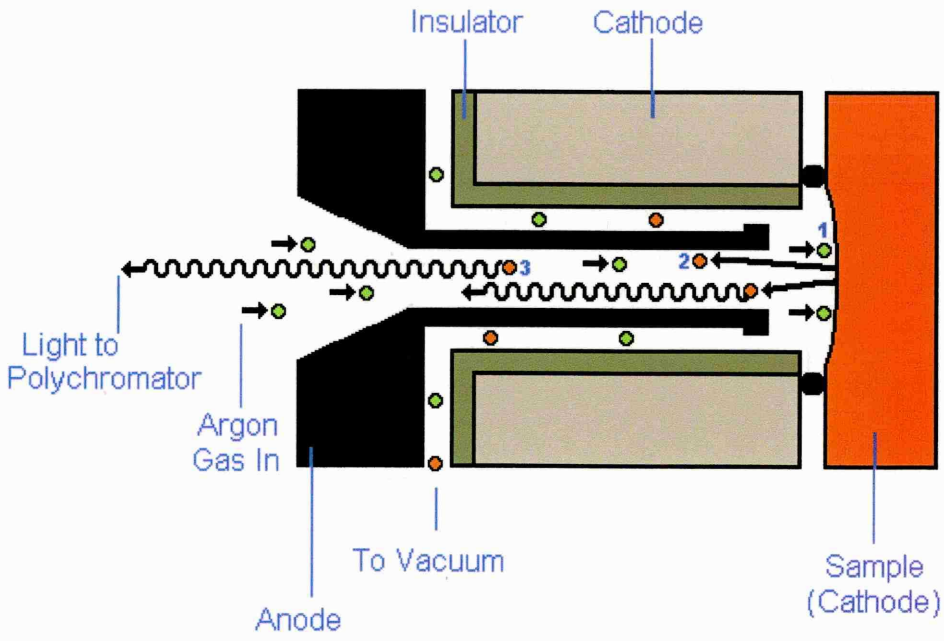

Figure 2.6: *Schematic representation of the Glow Discharge Lamp used in the LECO 750-GDS (adapted from Ives, '94).*

A LECO 750-GDS Glow Discharge Optical Spectroscope was used for the GDOES work presented. The equipment consists of a glow discharge lamp housing a small vacuum chamber with a hollow, cylindrical anode and a 4mm diameter aperture over which the sample is placed. Argon is bled into the vacuum chamber and is broken down (ionised) by a potential applied across the anode and cathode (from 500 to 1500 V). Argon ions are then accelerated towards the cathode material; impact (see step **1** , Fig. 2.6) results in the ejection of neutral cathode atoms (sputtering, see step **2**, Fig. 2.6) along with secondary electrons. Secondary electrons are repelled by the cathode, and sustain the discharge by ionising argon atoms. Sputtered atoms from the cathode collide with either secondary electrons or argon ions resulting in their transition to an excited state or their ionisation. The relaxation of excited cathode ions (see step **3**, Fig. 2.6) results in the emission of a photon of characteristic energy. The light photons emitted then pass to a polychromator for detection. Input light is focussed and diffracted by a

concave reflective diffraction grating (Ives, '94). Diffraction allows the separation of characteristic wavelengths, which are fed to a series of 44 etched slits, each of which leads to an individual photomultiplier tube.

2.2.4 Gas Chromatography (Mass Selective Detection and Flame Ionisation Detection).

Gas chromatography (GC) was utilised on the author's behalf by Dr. N. Szczur and Dr. D. Douce to determine chemical information from pyrrole monomer of a range of purities (see §4.2).

The GC technique involves the vaporization of a sample and subsequent injection/transportation through a chromatographic column via the movement of an inert gas. Volatile organic compounds are separated due to differences in their partitioning behavior between (mobile) gaseous phase and the stationary phase.

Gas chromatographic studies were carried out using Hewlett Packard model 5890 gas chromatograph, as described in §4.2.1.

2.2.5 Surface Profilometry.

Surface profilometry was used to study the dimensions and morphological characteristics of the sensing elements used as substrates for polymer deposition (i.e. Mark-4 Neotronics gas-sensor substrates and 'Yoshi' platinum interdigital electrodes; ITO substrates were not studied).

Throughout the work presented, surface microroughness was studied with a Taylor Hobson Precision (formerly Rank Taylor Hobson) Surtronic 3+ Portable Surface Microroughness Transducer, calibrated to a NAMAS 'Ra' roughness standard. Surtronic hardware was operated in "Data Dump" mode, and was linked to a portable P.C. running Taylor Hobson 'Talyprofile' Expert Mode Version 1.2.12 Beta software. This allowed visualisation and appropriate manipulation of the traces taken.

Summary, Chapter 2

- The work presented concentrates on a popular conducting polymer sensor used in the Neotronics NOSE, the 'type-283'. This material is based on pyrrole electrochemically deposited from aqueous solution with benzene sulfonic acid, sodium salt used as dopant (also known as sodium benzene sulfonate).
- Three substrates have been used for polypyrrole deposition, [i] gold microelectrodes, as used by Neotronics, known as 'MkIII Bass-Warwick electrodes', [ii] ITO coated glass slides, and [iii] platinum interdigitated electrodes (identified at a late stage).
- Polypyrrole deposition was carried out electrochemically from aqueous electrolyte throughout the work presented.
- Polymer films were studied by SEM, θ-2θ XRD, GDOES, GC and surface profilometry.

3. *The Electrochemical Formation of 'Type-283' Polypyrrole.*

The research presented concentrates on the characteristics of sensing material type-283; electrochemically deposited polypyrrole with benzene sulfonic acid (sodium salt) dopant and with water as the supporting electrolyte. Although many other material types are used in artificial olfactory technology, type-283 polymer is extraordinarily popular, and currently (at the time of writing) represents a common material choice for inclusion in Neotronics artificial olfactory arrays.

In this chapter, investigations into the effects of variations in the electrochemical parameters and practices used during electrochemical polymer deposition are reported and discussed.

3.1 *The Effects of Dopant Concentration Variation.*

The effects of dopant concentration variation on sensor properties were studied by deposition of a range of type-283 polymer films on MkIII Bass-Warwick electrodes (Note: Polymer depositions in §3.1 were carried out on the author's behalf by Dr. Andrew Hinton, Dept. of Chemistry, SHU. This formed the basis of the author's training in the operation of the equipment and reagents used during deposition).

Devices were produced from discrete electrolyte solutions, prepared with standard (0.25M) concentrations of pyrrole monomer in 50 ml of Millipore water. Dopant concentrations from 0.010M to 0.250M were used, and five devices were deposited in turn from each solution, each at +0.85V vs SCE for 120s (+30s @ 0V vs SCE) (as reported in Lemon, '96 (Registration Transfer from M.Phil. to Ph.D. Report)).

Device D.C. electrical resistance measurements were taken from each device after a set 'post-deposition' period of 24 hours using a calibrated DMM. A selection of devices were set aside for SEM and EDAX measurements; the resistances of these devices were not measured as it was considered that electron interaction could result in localized heating, possibly leading to resistance modification. It was also unclear as to how the

moderate vacuum conditions used during SEM analysis would affect sensor resistance. Mean resistances of the remaining devices are presented in Fig. 3.1.

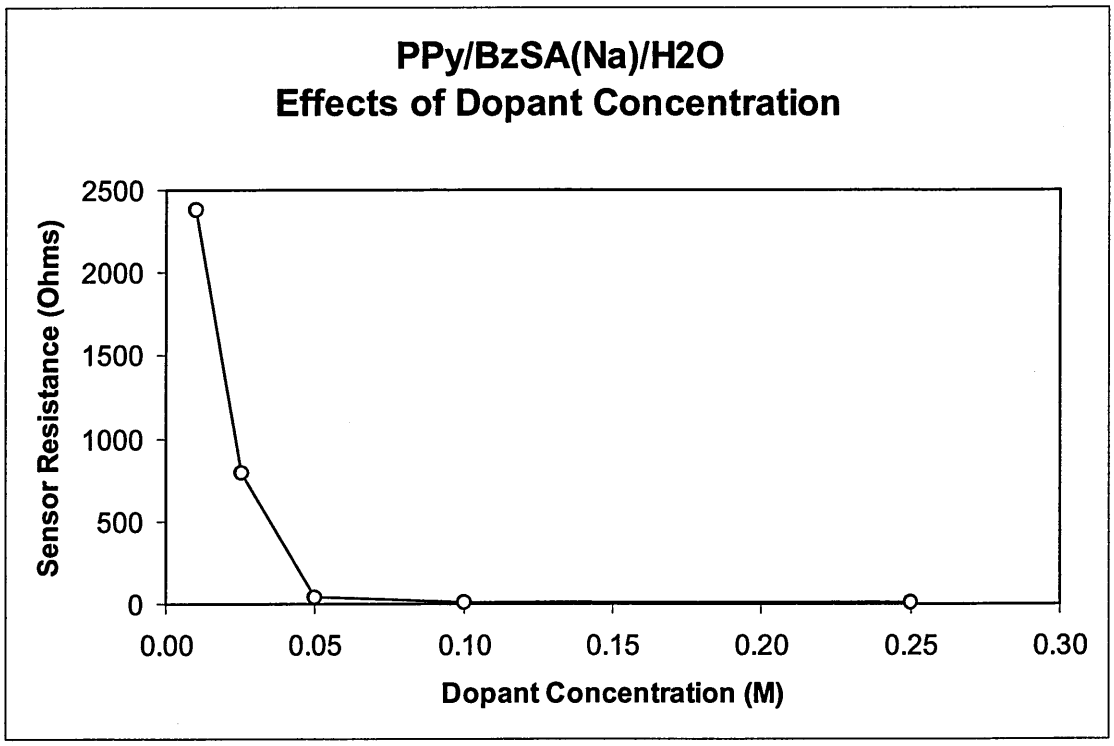

Figure 3.1: *The effects of dopant concentration variation on sensor resistance.*

The rapid decrease in sensor resistance observed from 0.010M, through 0.025M to 0.050M dopant concentrations, and the gradual decrease in sensor resistance from 0.050M through 0.100M to 0.250M suggests that increasing dopant concentration results in either; [a] increased film thickness per unit deposition time, or [b] a simple increase in dopant incorporation.

It is known that the presence of dopant in solution during electrochemical deposition is a prerequisite for the growth of electrically conducting polypyrrole (Stubb *et.al.*, '93; Biswas & Roy, '94); the relationship shown in Fig. 3.1 supports this. Further work is now presented which aims to identify the origins of the observed relationship.

Electron Probe Microanalysis (EDAX and SEM) studies of the films produced were carried out in order to test the hypothesis of film thickness increases being responsible for resistance decrease with increasing dopant concentration. A selection of the devices prepared above were examined by EDAX; results are presented in Fig. 3.2.

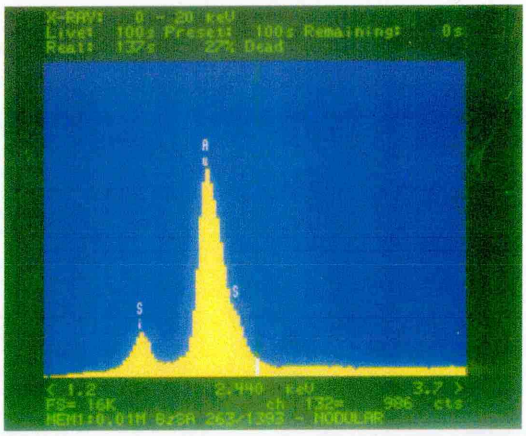

▲ [a] 0.010M

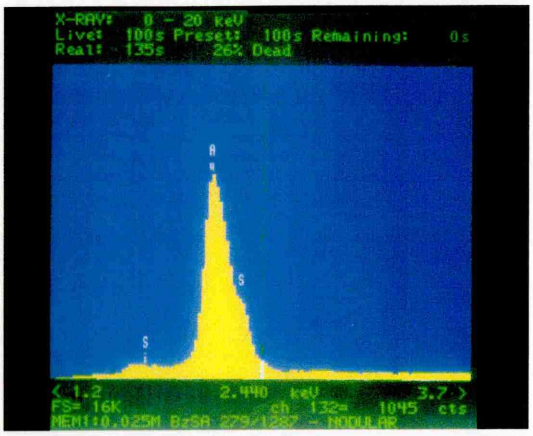

▲ [b] 0.025M

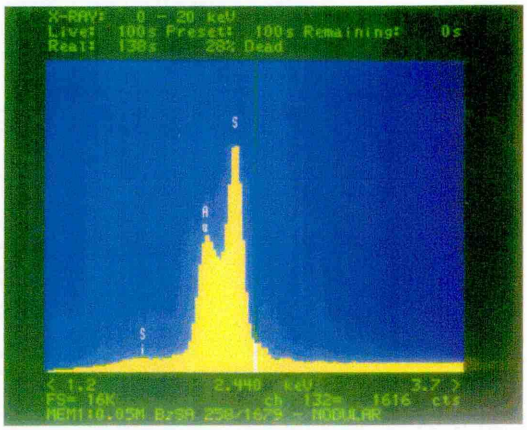

▲ [c] 0.050M

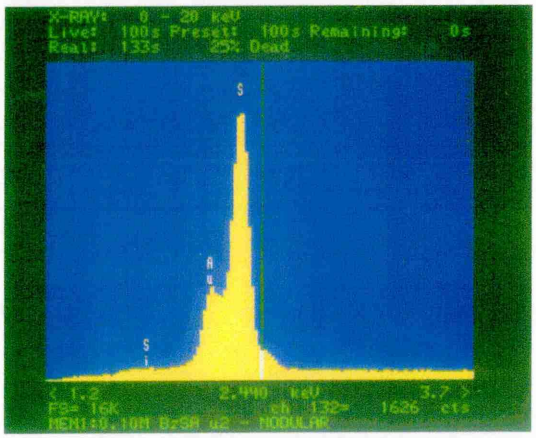

▲ [d] 0.100M

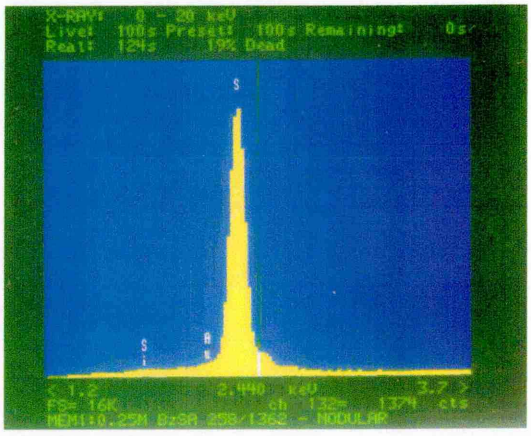

▲ [e] 0.250M

Figure 3.2: *EDAX analyses ($1x10^{-9}A$, 100s) of polypyrrole films electrochemically deposited from solutions with dopant concentrations of [a] 0.010M, [b] 0.025M, [c] 0.050M, [d] 0.100M, and [e] 0.250M.*

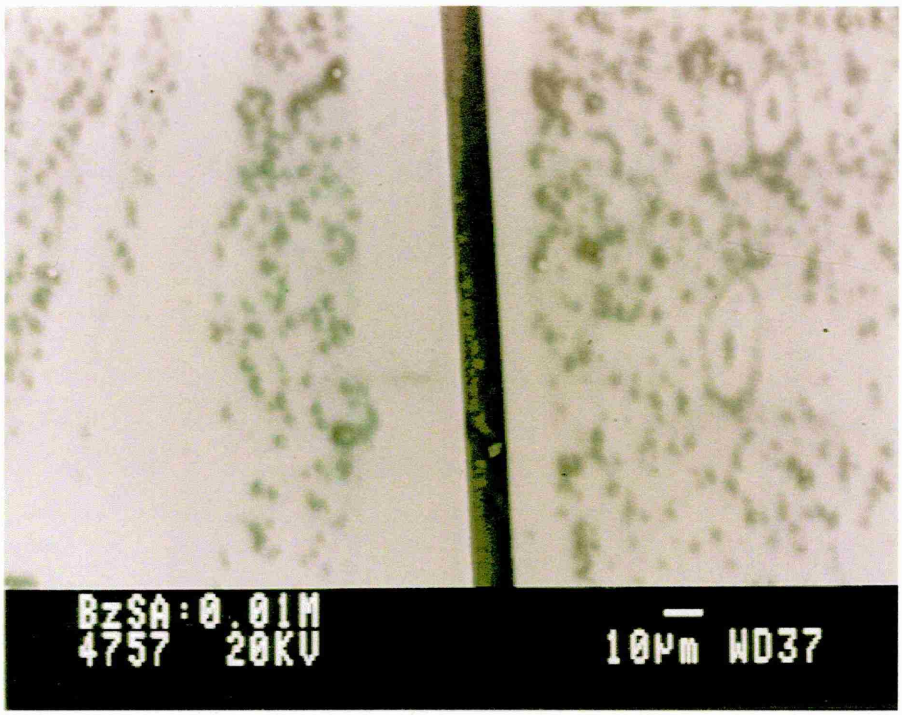

▲ [a] 0.010M

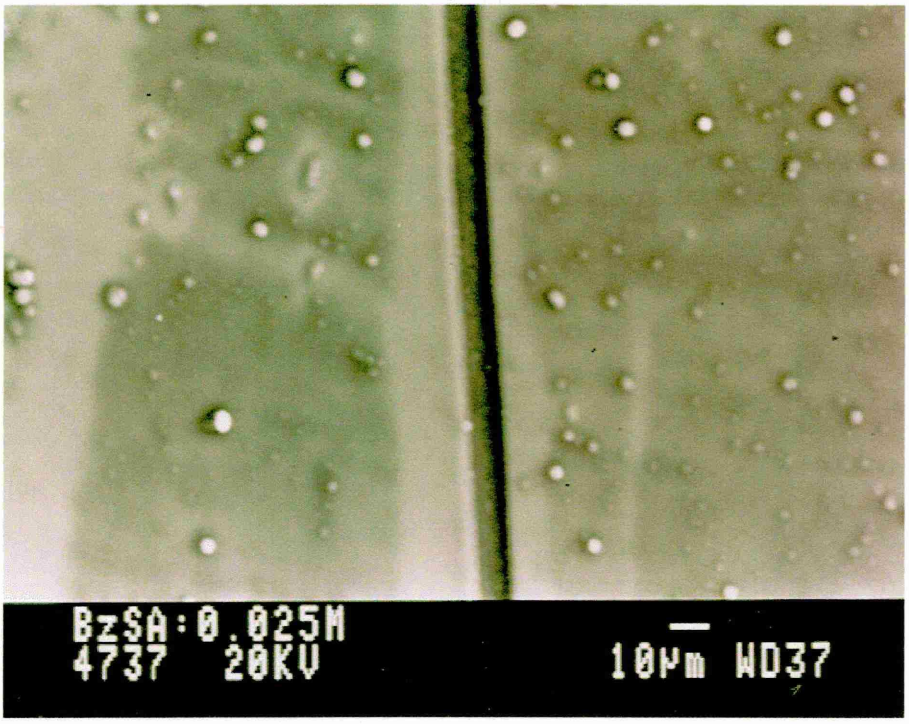

▲ [b] 0.025M

Figure 3.3: *SEM micrographs of polypyrrole films electrochemically deposited from solutions with dopant concentrations of [a] 0.010M, [b] 0.025M, [c] 0.050M, [d] 0.100M, and [e] 0.250M.*

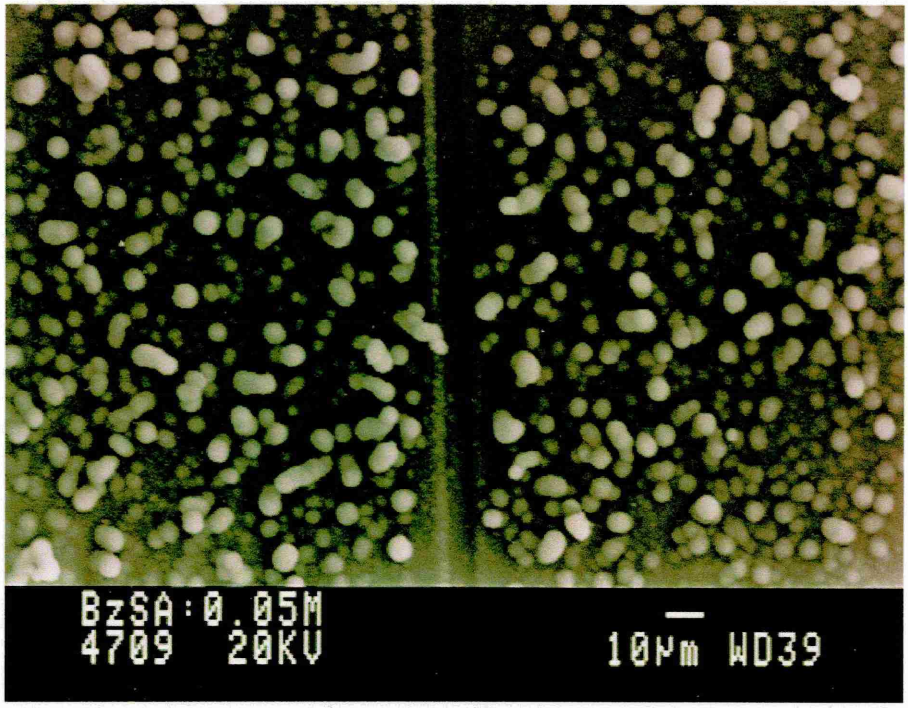

▲ [c] 0.050M

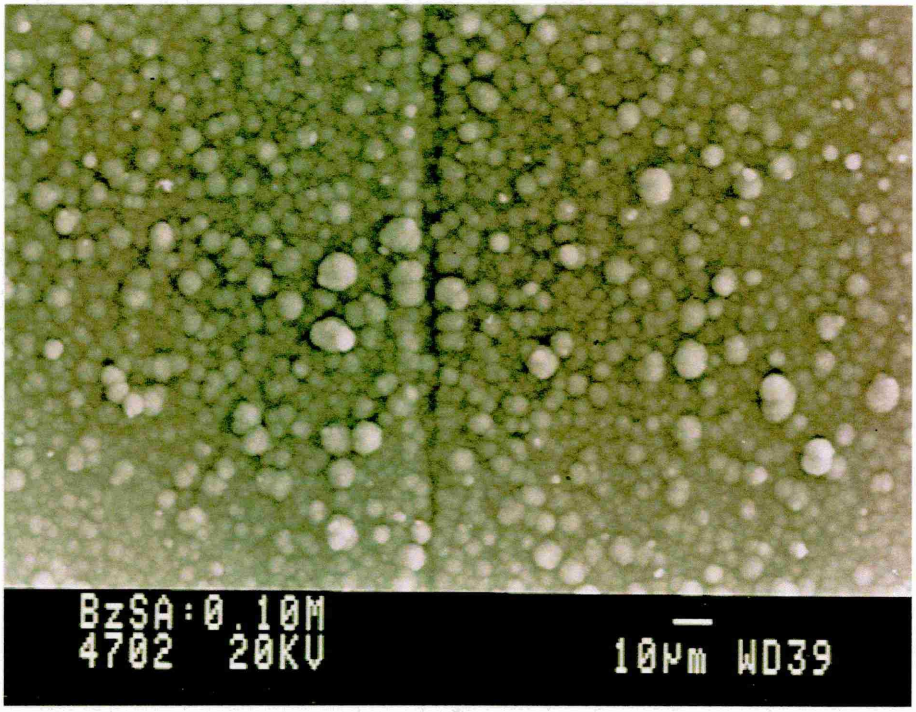

▲ [d] 0.100M

Figure 3.3.

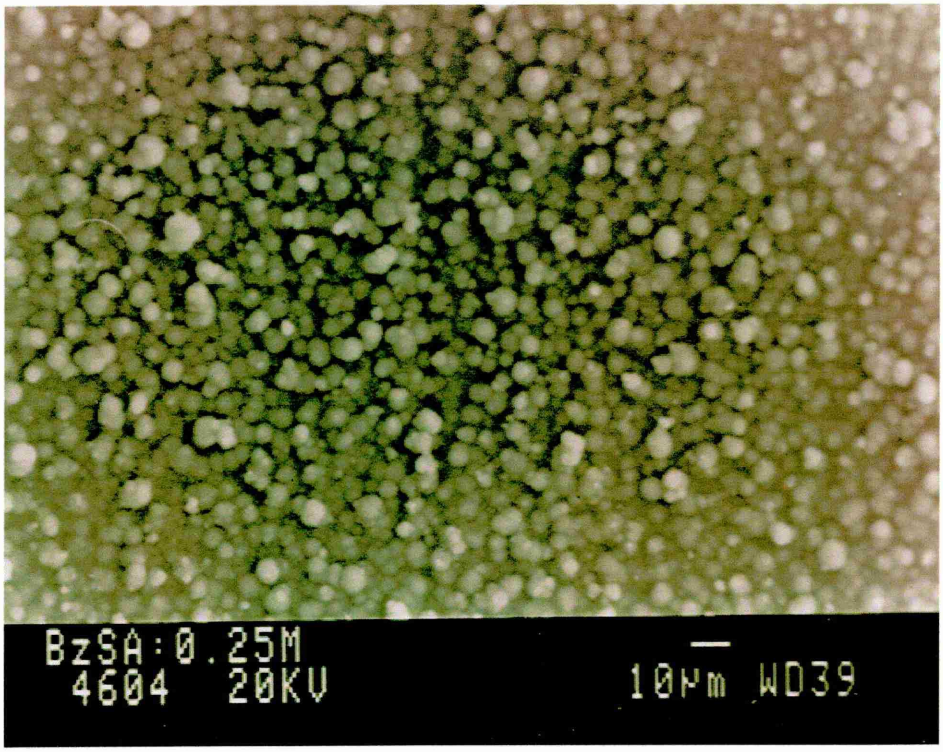

▲ [e] 0.250M

Figure 3.3.

The EDAX spectra presented in Fig. 3.2 consistently exhibit three discrete peaks; characteristic of silicon (the active element bulk substrate), gold (the active element surface), and sulfur (postulated to originate from the dopant group used in type-283 material (benzenesulfonic acid, sodium salt)). The observed effects of dopant concentration increase on the EDAX spectra produced (i.e. reduction in silicon (Si) peak intensity; reduction in gold (Au) peak intensity; increase in sulfur (S) peak intensity) strongly suggests that dopant concentration increase results in the deposition of a more substantial polymer film per unit time, so supporting the hypothesis of increasing dopant concentration resulting in increased film thickness. It was considered that an increase in sulfur peak intensity with increased dopant concentration *could* represent an increase in the level of dopant incorporated into films during deposition. However, reduction of gold peak intensity cannot easily be explained by an increase in dopant incorporation.

Scanning Electron Microscopy was used to ascertain the origins of the x-ray peak intensity changes observed on dopant concentration change. Fig. 3.3 shows micrographs of the morphology of devices grown at each dopant concentration as

described. It is immediately apparent that more substantial films are formed at higher dopant concentrations, as supported by increase in film nodularity.

EDAX and SEM evidence therefore suggests that dopant concentration increase results in an increase in polymer film thickness during (fixed deposition time) deposition as described. It is thought that increased film thickness is due to an increased deposition *rate* which in turn results from increased electrolyte solution conductivity on dopant concentration increase (the ionic dopant species are the dominant conductors in the electrolyte solution).

3.2 The Effects of Deposition Potential Variation.

The effects of deposition potential variation on sensor properties were studied by deposition of a range of type-283 polymer films on MkIII Bass-Warwick electrodes. Devices were produced from discrete electrolyte solutions, prepared with standard concentrations of pyrrole monomer (0.25M) and benzenesulfonic acid (sodium salt) dopant (0.25M) in 50 ml of Millipore water. Deposition potentials from +0.75V to +1.05V (all vs SCE) were used; five devices were deposited in turn from each solution.

As per §3.1, device resistances were measured after a set 'post-deposition' period by DMM. Devices were selected at random for SEM and EDAX investigation; resistance measurements were not taken from these devices. Mean resistances of the remaining devices are presented in Fig. 3.4.

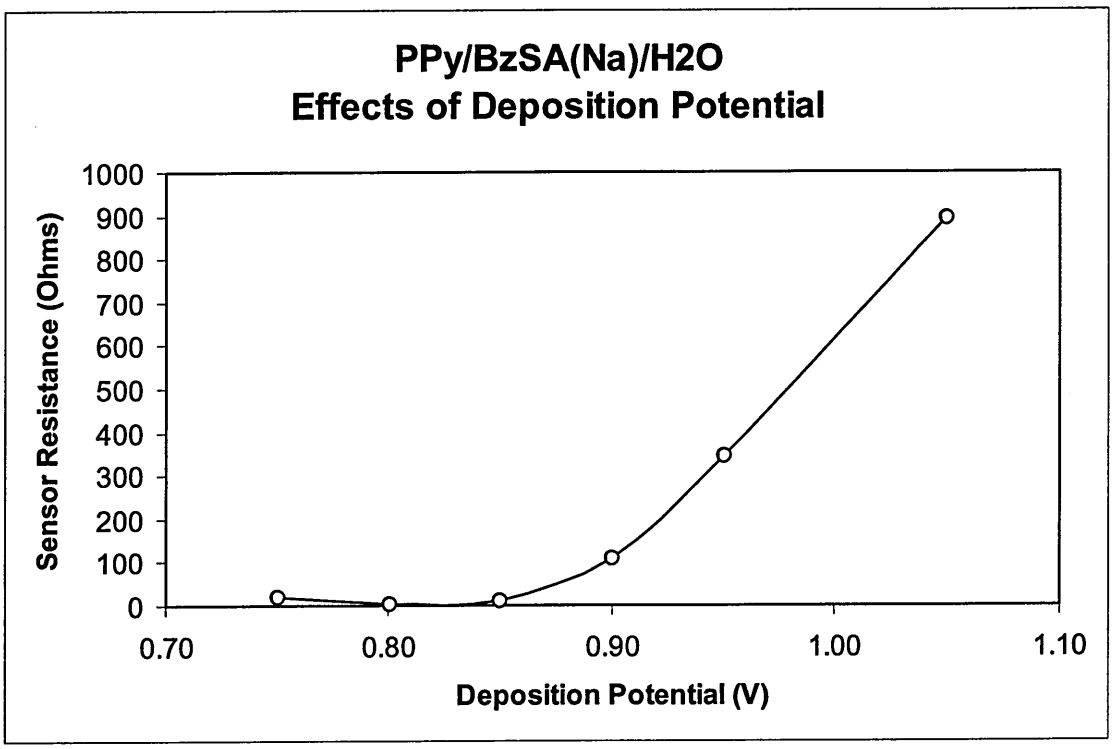

Figure 3.4: *The effects of deposition potential variation on sensor resistance.*

The slight variation in sensor resistance observed from +0.75V to +0.85V is not thought to be significant, given the moderate standard deviations observed between sets of devices. The rapid increase in sensor resistance with increasing deposition potential from +0.85 to +1.05V may be suggestive of film thickness changes (although one would intuitively expect that an increase in deposition potential would result in a more substantial film, and therefore *lower* film resistance). It is thought that variations in film microstructure may be responsible for the resistance changes observed; increased deposition potential may lead to less ordered growth as is often the case in melt-grown polymers and crystalline matter (Bassett, '81; Billmeyer, '84) (see also discussions in §5.2).

SEM and EDAX were used to study the morphological effects of deposition potential variation, such as film thickness changes, in order to test the hypotheses presented above. A selection of the devices prepared above were examined by EDAX; analysis of the relative intensities of emission peaks characteristic of silicon, gold and sulfur (as in §3.1) suggest that insubstantial films were produced at a deposition potential of +0.75V vs SCE, whilst deposition at all higher potentials used resulted in the formation of

substantial films, with film thickness appearing to increase slightly with increasing deposition potential.

SEM analysis supported the film thickness model based on EDAX results presented above, showing that substantial films were produced during deposition at all potentials greater than +0.75V vs SCE, as shown in Fig. 3.5.

EDAX and SEM evidence therefore suggests that deposition potential increase results in an increase in polymer film thickness over a standard deposition period. It is thought that increased film thickness is due to an increased deposition *rate* due to increased deposition potential. It is thought that this supports the idea presented previously that increasing deposition potential results in less ordered polymer growth, so resulting in increased device resistance.

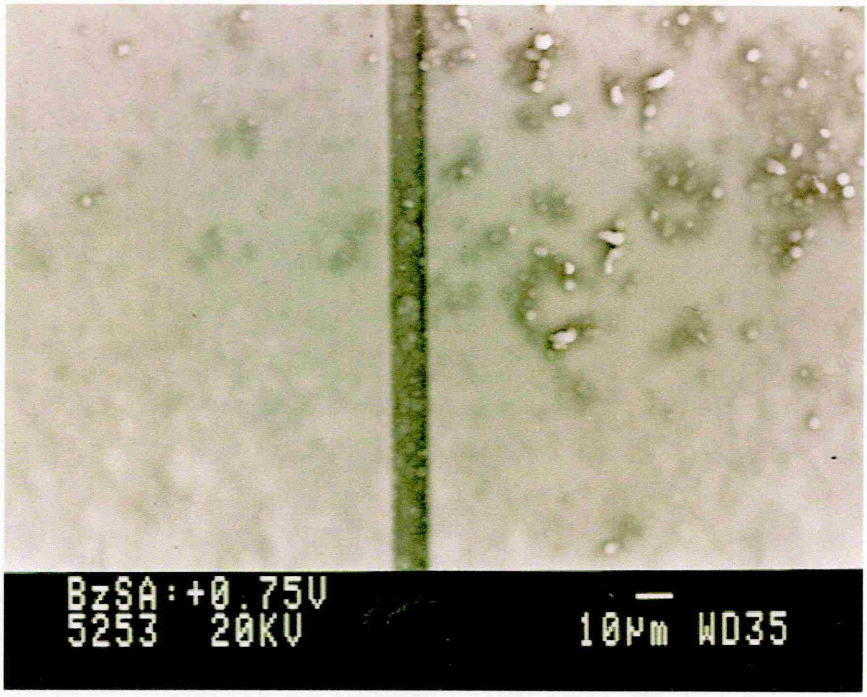

▲ [a] +0.75V

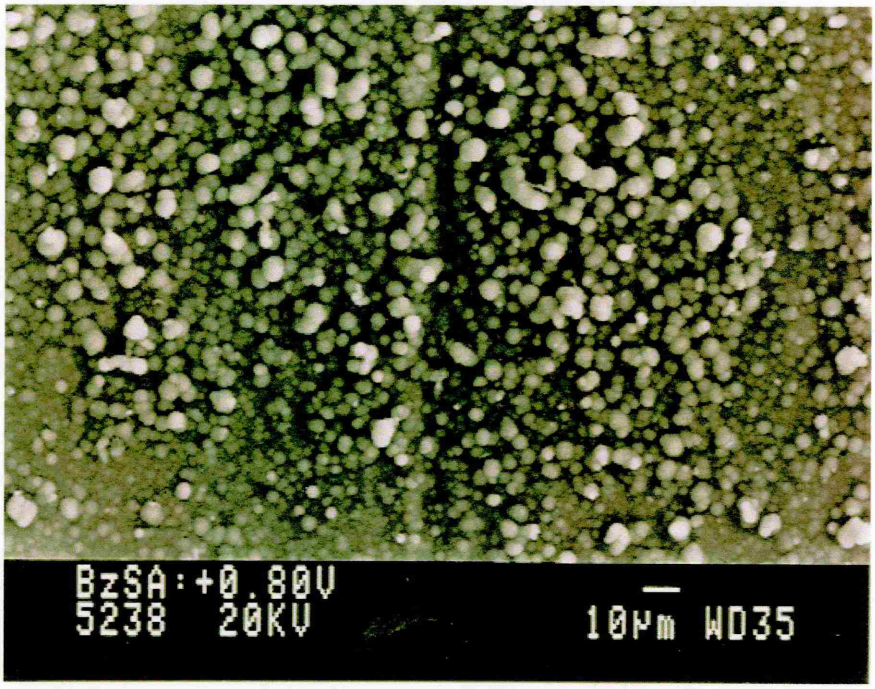

▲ [b] +0.80V

Figure 3.5: *SEM micrographs of polypyrrole films electrochemically deposited from standard solutions at deposition potentials of [a] +0.75V, [b] +0.80V, [c] +0.85V, [d] +0.90V, [e] +0.95V, and [f] +1.05V (all vs SCE).*

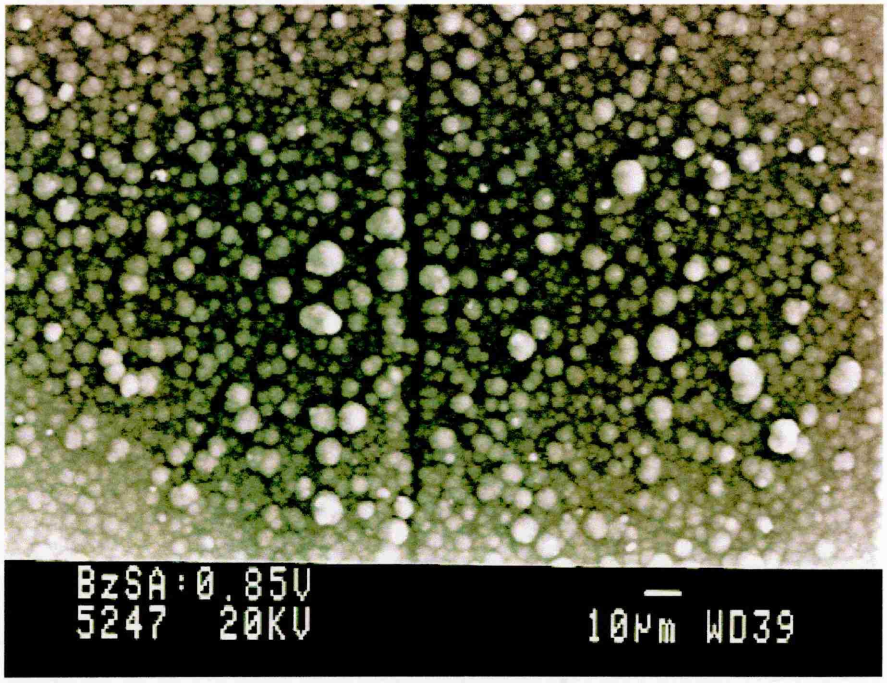

▲ [c] +0.85V

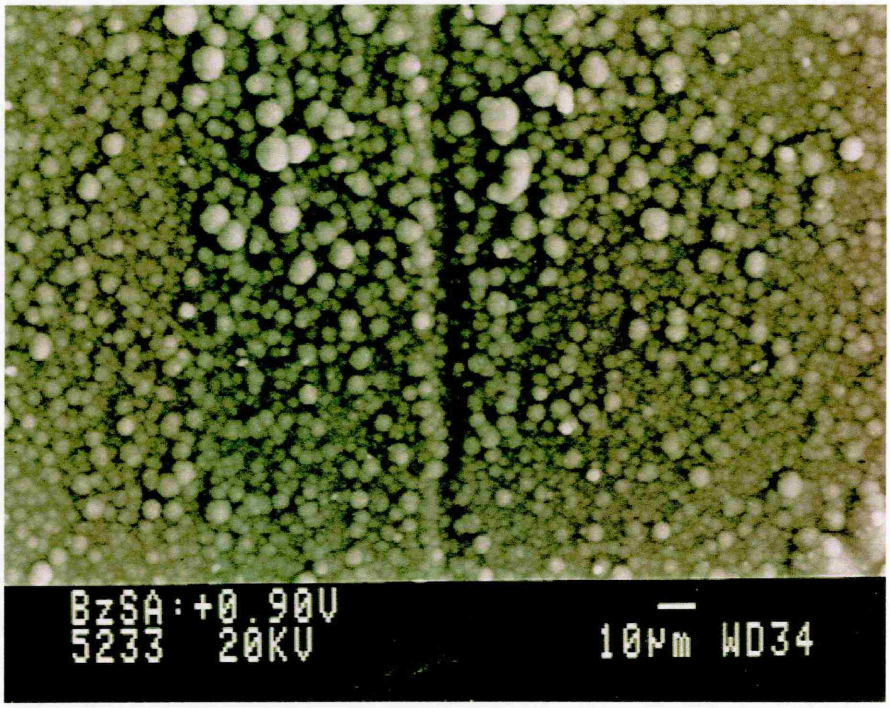

▲ [d] +0.90V

Figure 3.5.

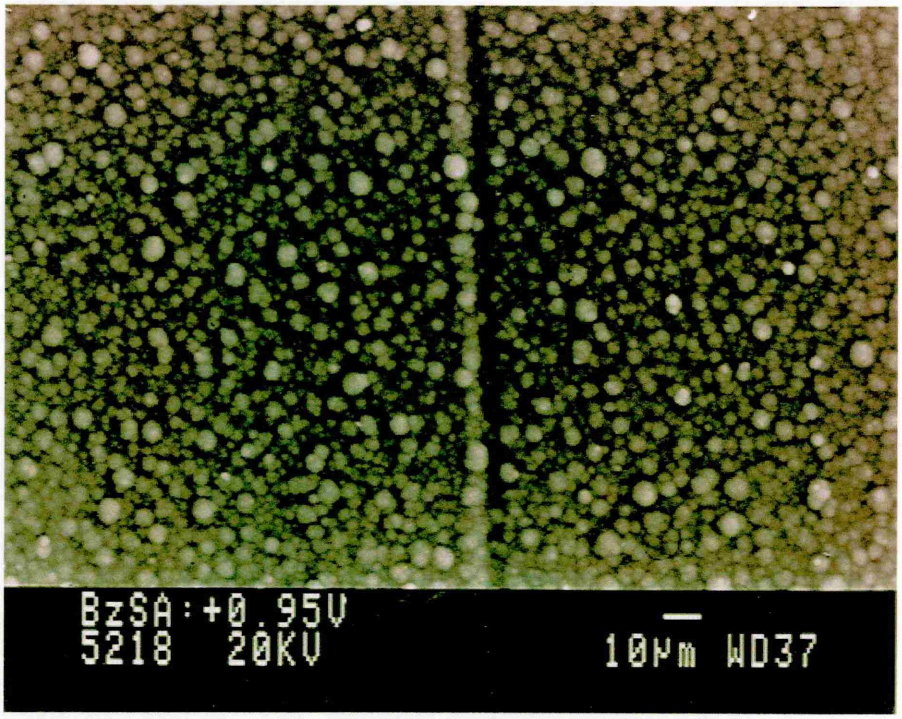

▲ [e] +0.95V

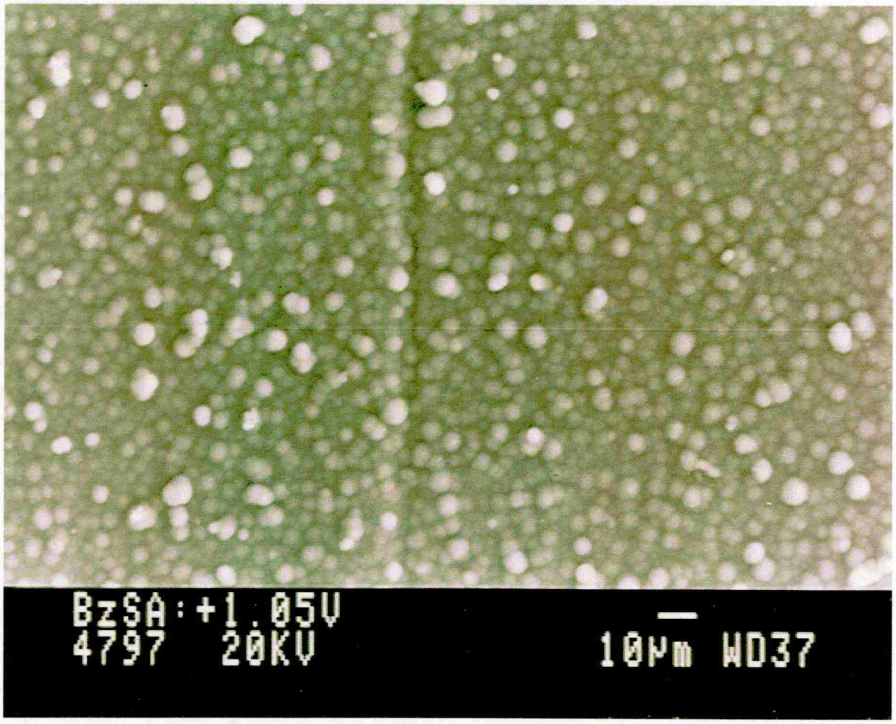

▲ [f] +1.05V

Figure 3.5.

3.3 *The Effects of Growth Time Variation*

The effects of growth time variation on sensor properties were studied by deposition of type-283 polymer films on MkIII Bass-Warwick electrodes for a range of deposition times.

Devices were produced from discrete, standard electrolyte solutions containing pyrrole monomer (0.25M) and benzenesulfonic acid (sodium salt) dopant (0.25M) in 50 ml of Millipore water. A deposition potential of +1.00V (vs SCE) was used throughout; five devices were deposited in turn from each solution.

As per §3.1, device resistances were measured after a set 'post-deposition' period by DMM; devices used for SEM and EDAX investigation were not used during resistance studies. Mean resistance values of the remaining devices are presented in Table 3.1 and Fig. 3.6.

GROWTH TIME (s)	MEAN D.C. RESISTANCE (Ω)
1	∞
2	∞
5	25.65k
10	6.17k
15	4.46k
20	4.29k
30	1.95k
40	589
60	334
120	179

Table 3.1: *The effects of growth time variation on sensor resistance.*

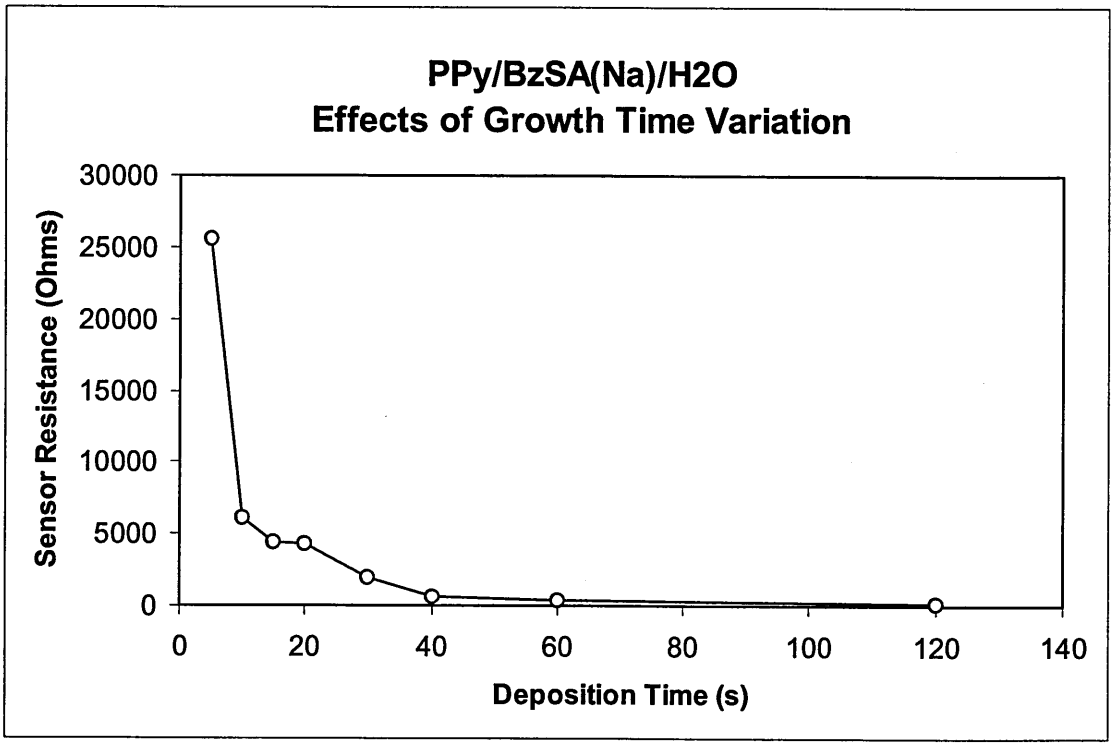

Figure 3.6: *The effects of growth time variation on sensor resistance.*

The relationship found between deposition time (growth time) and sensor resistance, as shown in Fig. 3.6, is as expected. Increasing deposition time reduced sensor resistance over the range tested. It is of particular interest to note that sensors grown for 1s and 2s had 'infinite' resistance. This suggests that the amount of polymer deposited after 2s was not sufficient to result in 'bridging' of the 10μm insulating gap, as described in A2. Table 3.1 shows that electrical contact between the two sides of the electrode active area was made at some point between 2s and 5s.

SEM and EDAX were used to study the morphological effects of deposition time variation. A number of the devices prepared above were examined by EDAX; analysis of the relative intensities of emission peaks characteristic of silicon, gold and sulfur (see §3.1) supports the resistance data presented. Peak intensities suggest that increased deposition time resulted in the formation of increasingly substantial films (resulting in reduced silicon and gold peak intensity, and increasing sulfur peak intensity).

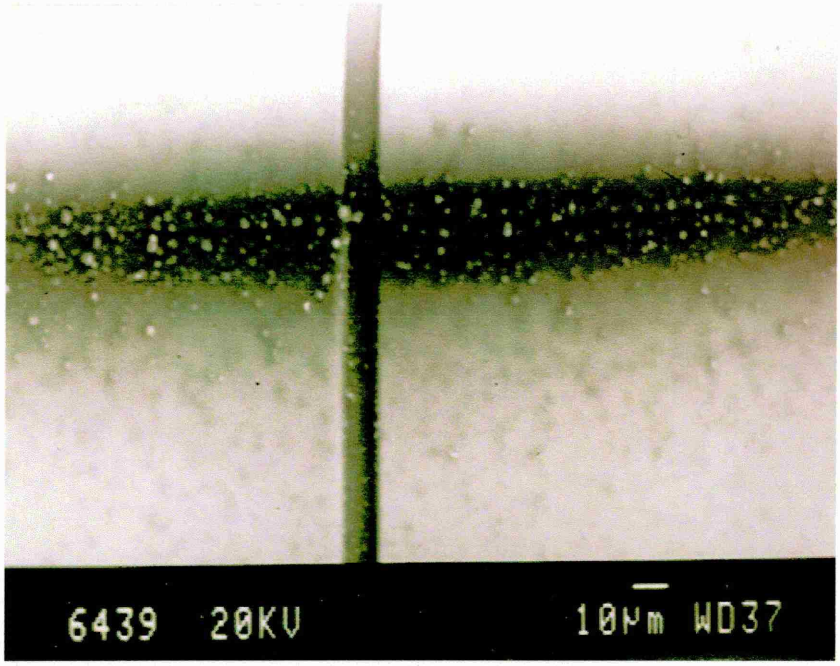

▲ [a] 40s

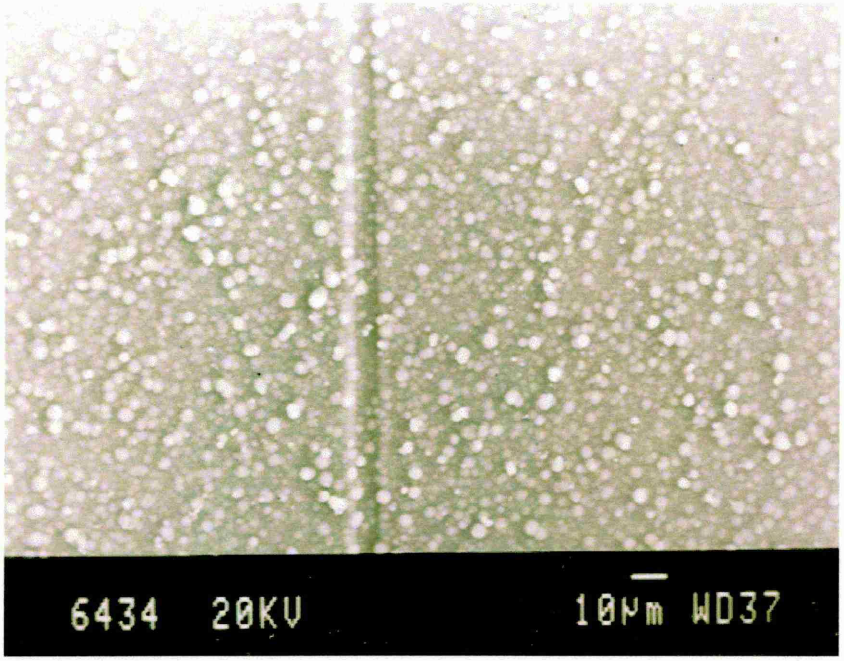

▲ [b] 120s

Figure 3.7: *SEM micrographs of polypyrrole films electrochemically deposited from standard solutions for [a] 40s and [b] 120s.*

SEM morphological analysis shows that film maturity and nodularity increase with deposition time (as shown in Fig. 3.7), so giving further support to the resistance data presented. However, despite the superior resolution of the electron microscope used to standard optical techniques, the polymer 'bridging' predicted by resistometry data was not observed by SEM.

Optical microscopy (Olympus VANOX) was therefore used in an attempt to observe the coalescence of polymer grown on either side of the electrode active area. Fig. 3.8 shows that contact does indeed occur at some point between 2s [a] and 5s [b].

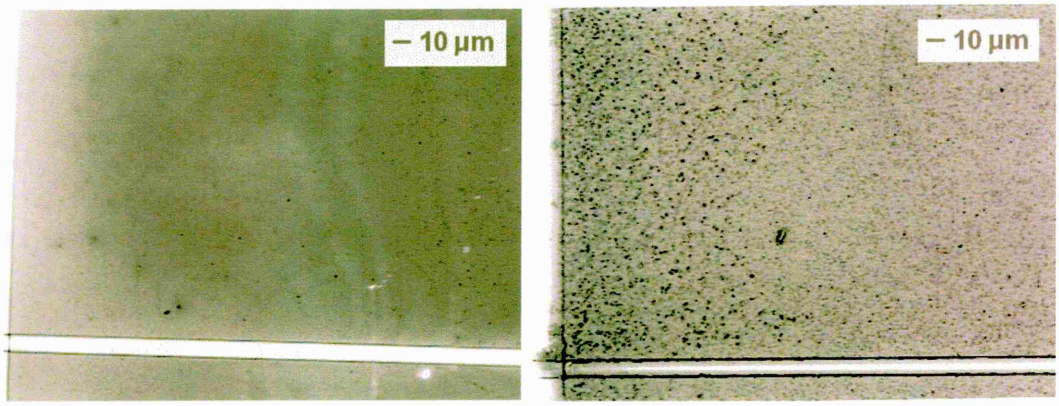

▲ [a] 2s ▲ [b] 5s

Figure 3.8: *Optical micrographs of polypyrrole films electrochemically deposited from standard solutions for [a] 2s and [b] 5s.*

3.3.1 Dependence of Device Resistance on Insulating Gap Coverage

The 'type-283' devices produced during the study presented in §3.3 were also used to form a relationship between gap coverage and device resistance.

It was noted during optical microscopy studies that the extent of coverage of the 10 µm insulating gap increased with deposition time, as would be intuitively expected. Resistance data was also noted to be dependent on the extent of gap coverage. Therefore, gap coverage was carefully measured in order to investigate the relationship between it and device resistance. This was thought to be valuable, given the fundamental manner in which interfacial matter may affect device properties (see discussions in A2).

A selection of devices were studied by optical microscopy (Olympus Vanox); it had been previously shown that SEM was not ideally suited to the work presented, as contrast between polymer grown over the insulating gap and the gap material (SiO_2) was poor. The gap length of each device was measured individually; the total length of the insulating gap over which polymer from either side of the electrode active area had coalesced was also measured. 'Gap coverage' was calculated and expressed as a percentage.

GROWTH TIME (s)	MEAN D.C. RESISTANCE (Ω)	GAP COVERAGE (%)
1	∞	0.2
2	∞	0.2
5	25.65k	12
10	6.17k	82
15	4.46k	96
20	4.29k	96
30	1.95k	98
40	589	100
60	334	100
120	179	100

Table 3.2: *The relationship between device resistance and gap coverage.*

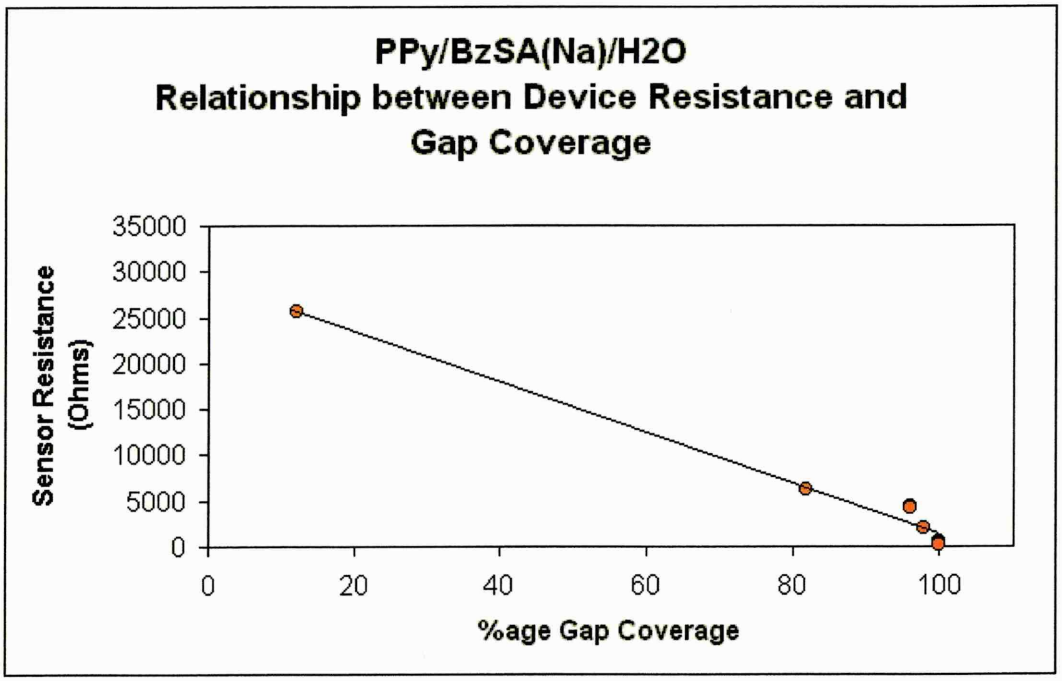

Figure 3.9: *The relationship between device resistance and gap coverage.*

The relationship shown in Fig. 3.9 suggests that there is a linear relationship between device resistance and gap coverage. Although the correlation appears to be strong (R^2=0.979), it is of note that the linear relationship presented must break down when gap coverage approaches 0% (as 0% gap coverage will yield infinite device resistance) or reaches 100% (as further deposition will reduce device resistance, but not increase percentage gap coverage).

The data presented in Table 3.2 is heavily biased towards complete gap coverage; this is due to the rapid deposition of polymer onto the gold electrode active area at the deposition potential and monomer / dopant concentrations used. As a result, a second study was carried out to allow validation (or otherwise) of the relationship presented in Fig. 3.9, using a range of devices deposited at lower monomer / dopant concentrations.

A range of devices were prepared, as described in §3.3. Type-283 polymer was deposited onto MkIII electrodes, and deposition time was varied as described previously. However, electrolyte solutions were used with pyrrole monomer concentrations of 0.05M, and benzenesulfonic acid (sodium salt) dopant concentrations of 0.07M. Deposition potential was also lowered to +0.85V vs SCE. Resistance data were collected by DMM after a set 'post-deposition' period. Mean resistance values of the remaining devices are presented in Table 3.3 and Fig. 3.10.

GROWTH TIME (s)	MEAN D.C. RESISTANCE (Ω)	GAP COVERAGE (%)
1	∞	0
2	∞	0
5	∞	0
10	∞	0
15	∞	0
20	∞	0.2
35	59.36k	26
50	37.56k	50
80	8.46k	100
120	4.92k	100

Table 3.3: *The relationship between device resistance and gap coverage – low concentration and reduced deposition potential.*

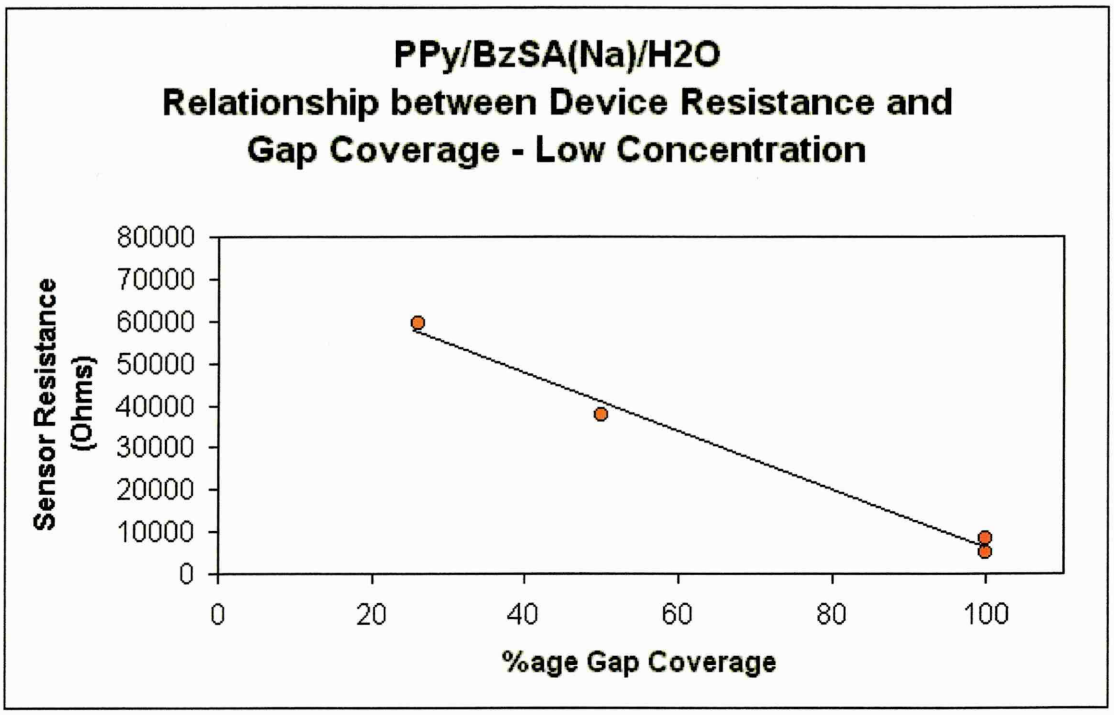

Figure 3.10: *The relationship between device resistance and gap coverage – low concentration and reduced deposition potential.*

The relationship shown in Fig. 3.10 supports that shown in Fig. 3.9; sensor resistance and percentage insulating gap coverage correlate highly (R^2=0.989) and appear to be linearly related between >0% and <100% boundary conditions (given the limited amount of available data).

3.4 *The Effects of Electrolyte Recycling*

The regular deposition of full sets of twelve devices from a single 50ml electrolyte solution resulted in an investigation being carried out into the effects of electrolyte depletion during multiple depositions. The low volume of polymer required for device formation (~1mm^2 x 1 to 100μm) was expected to result in extremely low depletion of monomer and dopant; the effects of depletion on sensor properties (electrical resistance, morphology and chemical content (EDAX)) were investigated to verify this.

A set of 14 devices were produced from a single electrolyte solution in order to assess the effects of electrolyte 'recycling' (i.e. the re-use of an electrolyte solution to deposit a number of polymer layers). Type-283 polymer was deposited onto MkIII electrodes; reduced concentrations of monomer (0.08M) and dopant (0.17M) were used in order to intensify the effects observed. Depositions were carried out at +1.00V vs SCE for 120s. Resistance data were collected by DMM after a set 'post-deposition' period of 24 hours. Devices were examined by SEM and EDAX subsequent to resistance measurement. Individual resistances are presented in Table 3.4 and Fig. 3.11.

DEPOSITION NUMBER	D.C. RESISTANCE (Ω)
1	186
2	204
3	244
4	207
5	179
6	267
7	257
8	243
9	256
10	298
12	326
14	398

Table 3.4: *The relationship between device resistance and deposition number.*

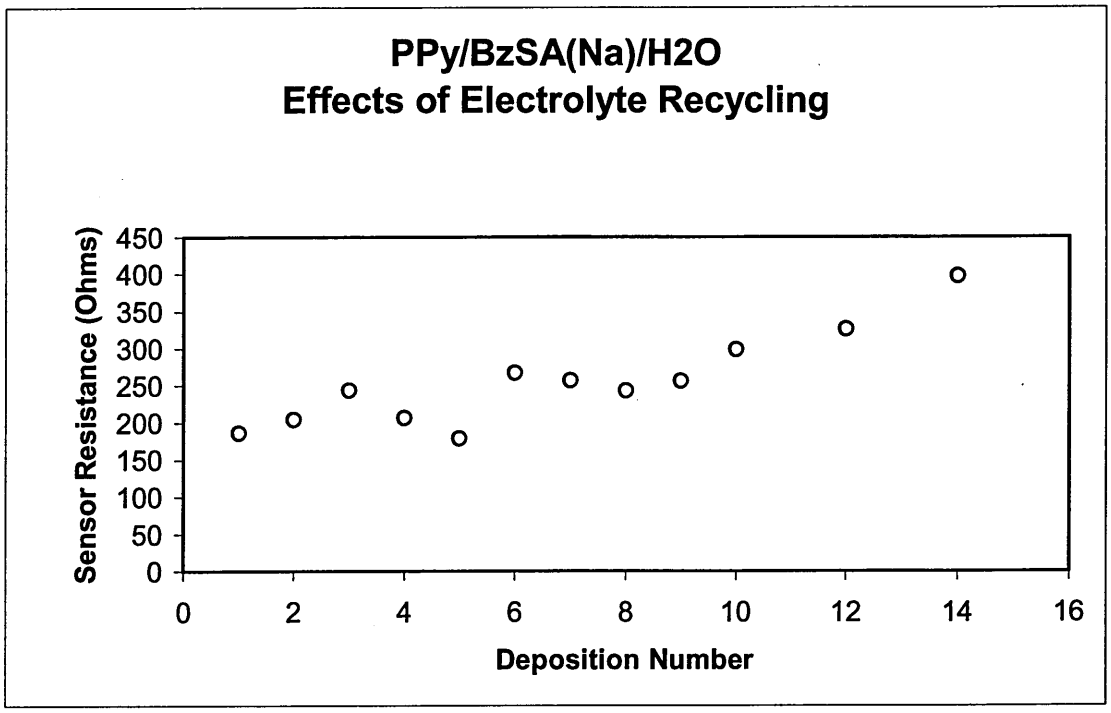

Figure 3.11: *The relationship between device resistance and deposition number.*

Fig. 3.11 suggests that the repeated deposition of a number of devices from a single electrolyte solution gradually increases device resistance. This is considered to be due to gradual reductions of the concentrations of dopant and/or monomer in the electrolyte solution. Dopant/monomer depletion may directly increase device resistance (through a reduction in the level of dopant available for incorporation into the polymer matrix, and therefore a decrease in the width of the 'bipolaron bands' within the bandgap (see §1.5.5)). Changes in the deposition rate were also considered to have a possible effect on device resistance, however logic suggests that depletion would *reduce* the rate of deposition, and so arguably result in a more ordered matrix, so reducing device resistance.

SEM examination subsequent to resistance measurement did not reinforce the relationship shown in Fig. 3.11 *per se*, as all device polymer layers were observed to be fully mature and nodular. However, variations in film maturity would be expected to result in much greater resistance variation than that shown in Fig. 3.11. EDAX examination supported SEM evidence; it was suggested that layer maturity (thickness) was not markedly affected by electrolyte recycling. Optical microscopy, as would be reasonably expected, supported SEM evidence.

The above data suggests that, with the exception of an acceptable degree of device resistance increase with deposition number, the use of a single sample of electrolyte for the deposition of a set of devices (12) does not adversely affect the properties of the devices produced. However, it was considered that the use of relatively low monomer and dopant concentrations may have exaggerated the effects of electrolyte recycling on device resistance. In order to verify this, the above study was repeated using still lower concentrations of monomer and dopant.

A further set of 14 devices was produced from a single electrolyte solution as described above. Further reduced concentrations of monomer and dopant were used (0.05M and 0.07M respectively) in order to intensify the effects observed. Depositions were carried out at +1.00V vs SCE for 120s, and resistance data were collected by DMM as described. Devices were, again, examined by SEM and EDAX subsequent to resistance measurement. Individual resistances are presented in Table 3.5 and Fig. 3.12.

DEPOSITION NUMBER	D.C. RESISTANCE (Ω)
1	839
2	942
3	1730
4	1475
5	1671
6	1675
7	1068
8	995
9	1589
10	2059
12	4060
14	4560

Table 3.5: *The relationship between device resistance and deposition number – low Concentration.*

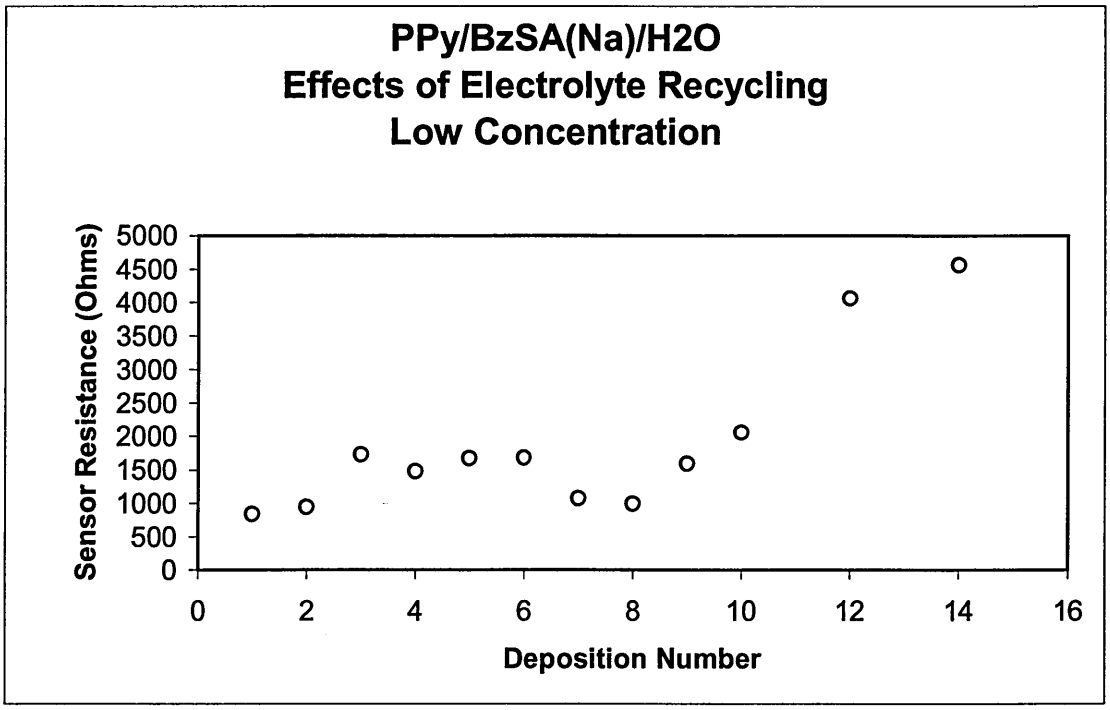

Figure 3.12: *The relationship between device resistance and deposition number – low concentration.*

As was the case for Fig. 3.11, Fig. 3.12 (above) suggests that device resistance increases on electrolyte recycling. However, resistance increases are relatively low, considering the low electrolyte concentration used; it is therefore expected that relative resistance increases will be negligible during electrolyte recycling using standard concentrations.

Examination by optical microscopy subsequent to resistance measurement again suggested that polymer morphology and layer thickness were not greatly affected by electrolyte recycling.

It has been shown that the effects of electrolyte recycling on device resistance on deposition from low concentration electrolyte are greater than those on deposition from electrolyte solutions of greater concentration. This supports the hypothesis that the effects of electrolyte recycling on devices deposited from electrolyte solutions of standard concentrations will be extremely low.

3.5 *The Effects of Solution Agitation*

Although standard Neotronics sensing devices were deposited from a 'still' solution, as were standard SHU research devices, the effects of electrolyte solution stirring during deposition have been studied. It was assumed that solution stirring during deposition may be advantageous in that the build up of [a] depletion regions, and [b] impurities at the polymer growth face may be reduced (see Ch.4). However, it was also considered that the rapid movement of the electrolyte solution in the vicinity of the polymer growth face during deposition may reduce growth by the removal of intermediate polymerisation products. The polymerisation mechanisms discussed in Ch.1 describe how polymer growth is dependent upon oxidation, dimerization and subsequent deprotonation. Rapid movement of solution during this process may result in the removal of radical cations and/or dimers from the growth face, so inhibiting the growth process.

A set of four devices was produced from a single electrolyte solution in order to assess the effects of electrolyte solution agitation on device resistance. Type-283 polymer was deposited onto MkIII electrodes from 50ml electrolyte with monomer and dopant at concentrations of 0.08M and 0.17M respectively. Depositions were carried out @ +1.00V vs SCE for 120s. Resistance data were collected by DMM after a set 'post-deposition' period prior to VANOX, SEM and EDAX examination. Resistance data are presented in Fig. 3.13.

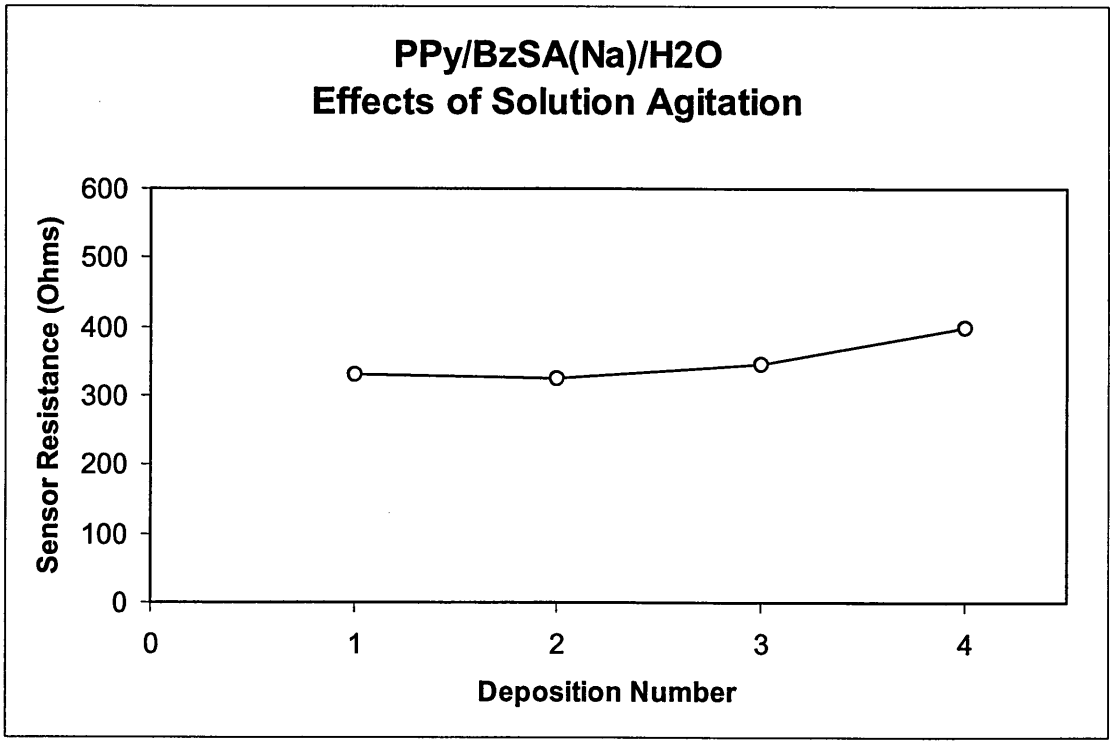

Figure 3.13: *The effects of electrolyte solution agitation during device deposition. Devices No.1 & No.3 stirred during deposition, devices 2 & 4 deposited without artificial agitation.*

The relationship illustrated in Fig. 3.13 suggests that solution agitation does not greatly affect device resistance. However, observation by VANOX suggested that the thickness of polymer films deposited from agitated solution was far greater than those deposited from 'still' films (this was assessed by variation of the limited depth-of-field focus and by observation of the 'apparent gap width' of devices).

Further, SEM examination supported VANOX observations; it was shown that film maturity (i.e. nodularity level and apparent thickness) was greater for film deposited from agitated electrolyte. The 'frame effect' (the growth of polymer onto the insulator around the device active area), generally observed on mature device polymer layers, was observed to be more pronounced on solution agitation (again, indicative of greater film maturity, see Fig. 3.14). It is also of note that the geometry of the frame is skewed to the right hand side of the active area of the device shown, illustrating the direction of electrolyte stirring.

EDAX examination also supported the evidence presented above; devices deposited from agitated electrolyte showed a far stronger sulfur signal than those deposited from still electrolyte. The opposite was observed for gold peaks, so suggesting that film thickness increased with solution agitation.

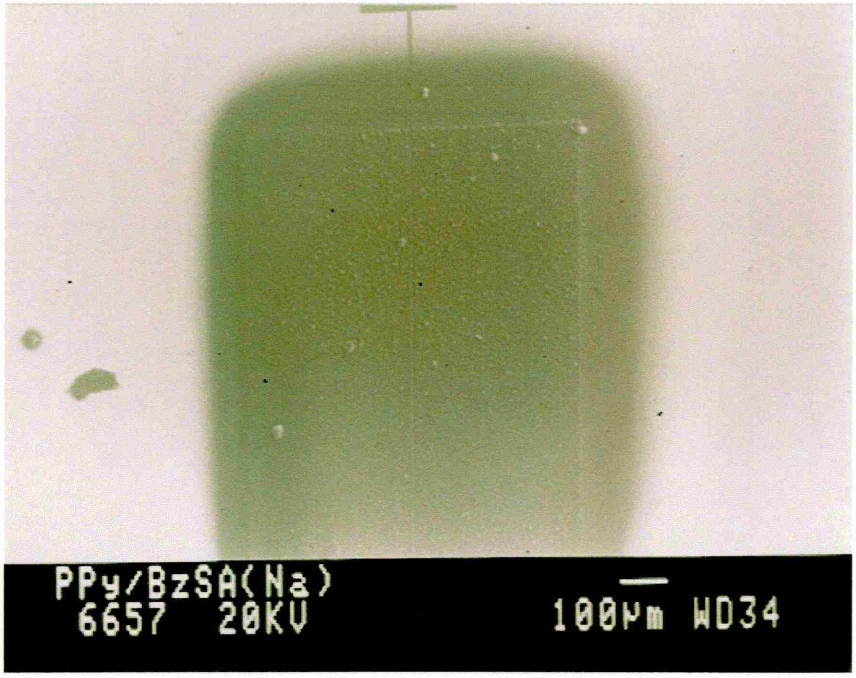

Figure 3.14: *Device active area after polypyrrole deposition from agitated electrolyte solution. Note the high level of film maturity, also the skewed dimensions of the polymer 'frame' showing the direction of stirring.*

The results presented suggest that solution agitation during polymer deposition *does* affect the properties of the films produced. As a result, all films deposited during the work presented are from still electrolyte wherever reasonably practicable. Although it has been identified that thicker polymer films may be produced during solution agitation, such techniques will not be used here in fear of introducing inconsistency / irreproducibility into the film deposition process. However, if carefully controlled, solution agitation could be utilized during commercial device production.

A second set of polypyrrole devices were prepared as described above, but electrolyte concentration was reduced (pyrrole monomer at 0.05M and dopant at 0.07M) in order to study the effects of solution agitation on 'immature' polypyrrole films.

Resistance measurements showed that films deposited from agitated solution had infinite resistance (i.e. significant polymer bridging had not occurred), but that films deposited from still solution had resistances of around 3kΩ, as expected given the deposition parameters used.

Optical microscopy (VANOX) showed that films deposited from agitated electrolyte solution were far less mature than those deposited from still solution. Film thickness, nodularity levels and insulating gap coverage were extremely poor (polymer bridging had not occurred). However, interesting growth mechanisms were observed on films grown from agitated electrolyte solution. Fig. 3.15 [a] and [b] show that the ordinarily 'random' distribution of nodules observed from films grown under still conditions has been replaced by a far more ordered pattern of nodule growth. It is assumed that this patterning is the result of the presence of a transverse 'current' of electrolyte during deposition. It is postulated that the movement of radicals in this 'current' is responsible for the formation of the observed pattern.

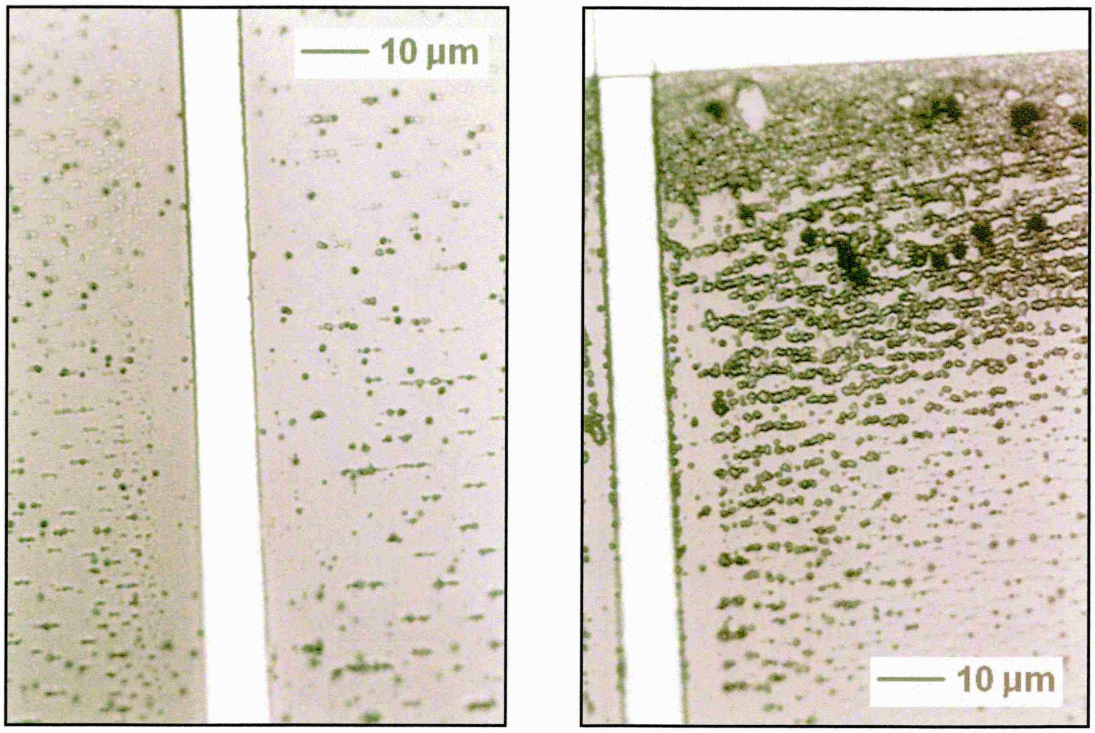

▲[a] ▲[b]

Figure 3.15: *Optical micrographs of immature polypyrrole films deposited from 'agitated' solution showing linear nodule distribution.*

The studies presented above suggest that, at moderate electrolyte concentrations, solution agitation results in an increase in deposition rate and therefore an increase in film thickness per unit deposition time, although device resistance is not greatly affected. At lower electrolyte concentrations however, solution agitation results in a marked reduction in film thickness, presumably resulting from a reduction in deposition rate.

At the electrolyte solution concentrations normally used for the production of commercial devices, the evidence presented leads to the following hypotheses:

When a still electrolyte is used, deposition occurs via oxidation, dimerization and deprotonation (as described in §1.5.4) at the polymer growth face. The availability of requisite monomer and dopant depends on monomer and dopant concentrations, the rate at which the concentrations of monomer and dopant are used (depleted) by the growth face, and the rate at which 'depleted' monomer and dopant can diffuse towards the growth face. However, when the electrolyte solution is stirred during deposition, a greater number of monomer and dopant groups pass over the growth face per unit time, so resulting in an increase in deposition rate, and hence the growth of a thicker film per unit time.

Further, this increased deposition rate is thought to result in less ordered, therefore more electrically resistive, films. Resistance increases as described are, however, offset by the deposition of thicker films, resulting in similar resistance values being observed for films deposited in 'still' and 'stirred' conditions.

At reduced monomer and dopant concentrations, the principles described above apply. However, the production of far less mature (thinner) polymer films during solution stirring at reduced concentration is thought to be due to the dimerization stage in the polymerization reaction described in §1.5.4. It is postulated that the oxidation of pyrrole may occur at the growth face at a greater rate during solution stirring, due to increased availability of monomer. However, at the very low concentration of monomer used (0.05M), it is thought that dimerization may be the limiting step in the polymerization process. Over the short timescale involved, any delay between oxidation and

dimerization of pyrrole monomer (due to reduced monomer concentration) may result in removal of radical monomers/dimers from the growth face due to the solution current. Therefore, under these conditions, the presence of a solution 'current' is thought to be responsible for the production of a less mature film. Lack of film maturity is observed in Fig. 3.15 to result in a complete lack of polymer bridging of the insulating gap.

3.6 *The Effects of Substrate Cleaning Regimes*

During the research presented, MkIII Bass-Warwick electrodes, Yoshi interdigital electrodes and Indium Tin Oxide (I.T.O.) glass slides (as used for investigations by XRD, as described in Ch. 5 and A3), were generally cleaned before polymer deposition by gentle agitation in propan-2-ol (isopropyl alcohol, IPA). After cleaning, IPA was removed as soon as possible by blowing with a high velocity jet of oxygen-free nitrogen. Use of IPA allowed the simple removal of grease and dust; however, evaporation of the IPA during use could result in the deposition of contaminants onto the electrode surface.

The effects of the use of differing substrate cleaning regimes have been studied and are reported here.

The following points are of note:

- As described in §A1.2.3, the use of an aggressive H_2SO_4 electrode pre-clean was not found to be effective at removal of common electrode contaminants.
- The use of a standard IPA cleaning regime may result in lost time due to the slow rate of evaporation of IPA at room temperature. As a result, an acetone rinse was often used subsequent to IPA wash in order to allow quicker substrate drying. The use of an acetone rinse was observed not to affect sensor resistance or morphology. As a result of the information presented in §3.6.1 & §3.7, substrates 'wetted' with IPA or acetone were blown with a high velocity jet of oxygen-free nitrogen to allow thorough drying.
- Due to the limited supply of Yoshi interdigital electrodes, some plates of devices were used which were subject to an unidentified, but tenacious contaminant. For these devices, a more aggressive cleaning regime was used, involving successive agitation in string of solvents. Dichloromethane, water, acetone, IPA, water and acetone were used consecutively, before rapid drying with a high velocity jet of oxygen-free nitrogen. Although a marked improvement in the conductivities of the devices formed on formerly contaminated Yoshi devices was observed, it was noted that the use of the above regime on electrodes subject to expected contaminants (dust, grease etc.)

did not result in modifications to device performance when compared to electrodes cleaned with the standard IPA cleaning regime.

- The use of a hot dichloromethane reflux cleaning regime was also considered, however, sufficiently tenacious contamination was not encountered to necessitate the use of this technique.

3.6.1 Solvent Droplet Evaporation

The use of solvent based cleaning regimes to remove / reduce the level of electrode contamination prior to polypyrrole deposition as described above was found to be effective in the vast majority of cases. However, several instances were identified where failure to remove solvent by nitrogen jet before evaporation resulted in the formation of 'rings' of non-volatile contaminants at the solvent evaporation site (i.e. non-volatiles previously present in the impure solvent used). An example of this is shown in Fig. 3.16, taken from an ITO glass slide by VANOX optical microscopy after cleaning with IPA.

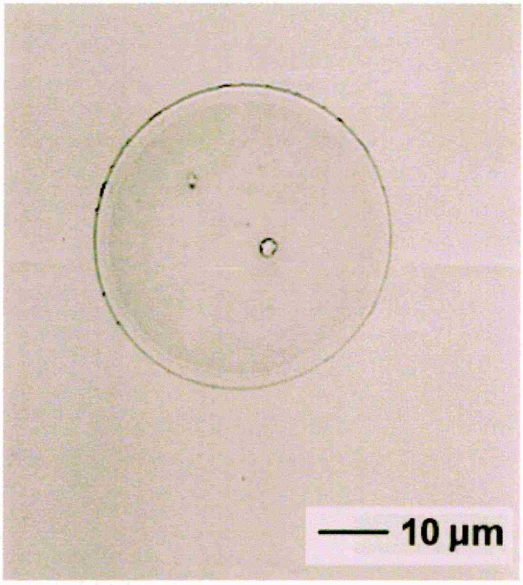

Figure 3.16: *Optical micrograph of a circular contaminant on ITO glass, postulated to result from the evaporation of impure solvent.*

The presence of such contaminant rings on electrodes prior to electrochemical deposition may be a potential source of irreproducibility during the production of research (and commercial) devices.

Further, it is thought possible that contaminant rings may act as preferential nucleation sites for polymer growth during electrochemical deposition. Bassett ('81) reported that during the nucleation of polymers onto non-polymeric materials, preferential deposition often takes place around impurities and scratches. Assuming that the contaminant is not electrically conductive, it is reasonable to assume that preferential nucleation may occur at the circumference of the ring, as nucleation *within* the non-conducting ring would be extremely unlikely due to the resistance of the contaminant material. Subsequent growth of substantial polypyrrole films may result in the formation of the common nodular structure (depending upon deposition conditions), which, it is postulated, may result in the formation of 'rings' of nodules on the polymer growth face, corresponding to the nucleation positions around the circumference of the circular contaminant, as shown in Fig. 3.17.

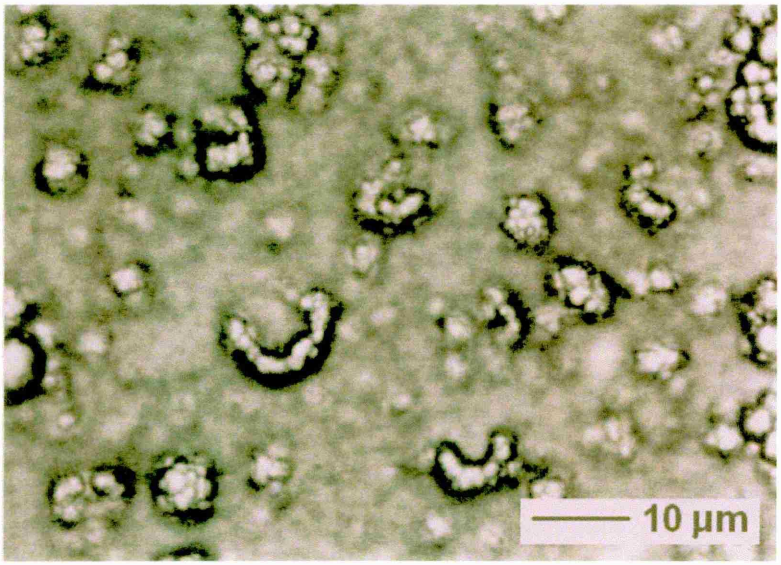

Figure 3.17: *Optical micrograph showing a pair of semicircular arrangements of nodular growths.*

Results presented in Lemon, '96 (Registration Transfer from M.Phil. to Ph.D. Report) suggested that such arrangements may be the result of larger, nodular structures formed around gas bubbles (gaseous spheroids) which had subsequently collapsed inwardly. Although subsequent work has strongly supported the formation of such structures (see [a] Ch. 4 and [b] Lemon and Haigh, *Materials Research Bulletin*, 1999), their appearance is far removed from that of the semicircular morphology shown in Fig. 3.17.

Although the effects of circular contaminants on the performance of polypyrrole devices may not be as fundamental as that of gas-void formation (as discussed in Ch. 4), it is reasonable to assume that the presence of sections of non-conducting matter at the interface between substrate and polymer will affect device performance to a degree. The careful removal of solvent from electrodes before evaporation is therefore advised.

The hypothesis presented above that nucleation of polypyrrole on surface features of the substrate may result in nodular 'patterns' is strongly supported by the occasional formation of parallel lines of nodules as shown in Fig. 3.18. Observation of polypyrrole growth on both ITO glass slides and on gold microelectrodes suggests that significant polypyrrole deposition results in the formation of primary nodular growths. Consideration of the surface morphology of the substrates used suggests a reasonably flat topography with a high probability of the presence of surface defects, such as scratches etc.. The presence of substrate scratches would present preferred nucleation sites for polymer growth (Bassett, '81), so resulting in the formation of nodular material over these sites. As reported in Lemon, '96 (Registration Transfer from M.Phil. to Ph.D. Report), a well-known example of a similar phenomenon is that of the adsorption of previously dissolved gas from a liquid onto a glass surface. Gas atoms adsorb onto the (microscopically rough) glass surface, but adsorb preferentially onto areas of higher surface roughness, such as scratched or worn areas, therefore congregating on imperfections.

Although it is not considered that the presence of sundry light scratches on an electrode would adversely affect polypyrrole structure or sensor properties, it is interesting to note that nodule 'patterns', and therefore the distribution of nodular material throughout polypyrrole sensing layers, may be actively controlled by subtle patterning on the electrode surfaces used. The application of crosshatched patterns (or a multitude of alternative patterns) onto device substrates *could* allow the production of polypyrrole material with carefully controlled nodular distribution. Such control of nodular distribution, and indeed control of original nucleation sites, could allow the electrochemical production of polypyrrole films with greater *structural* reproducibility and/or improved device performance reproducibility.

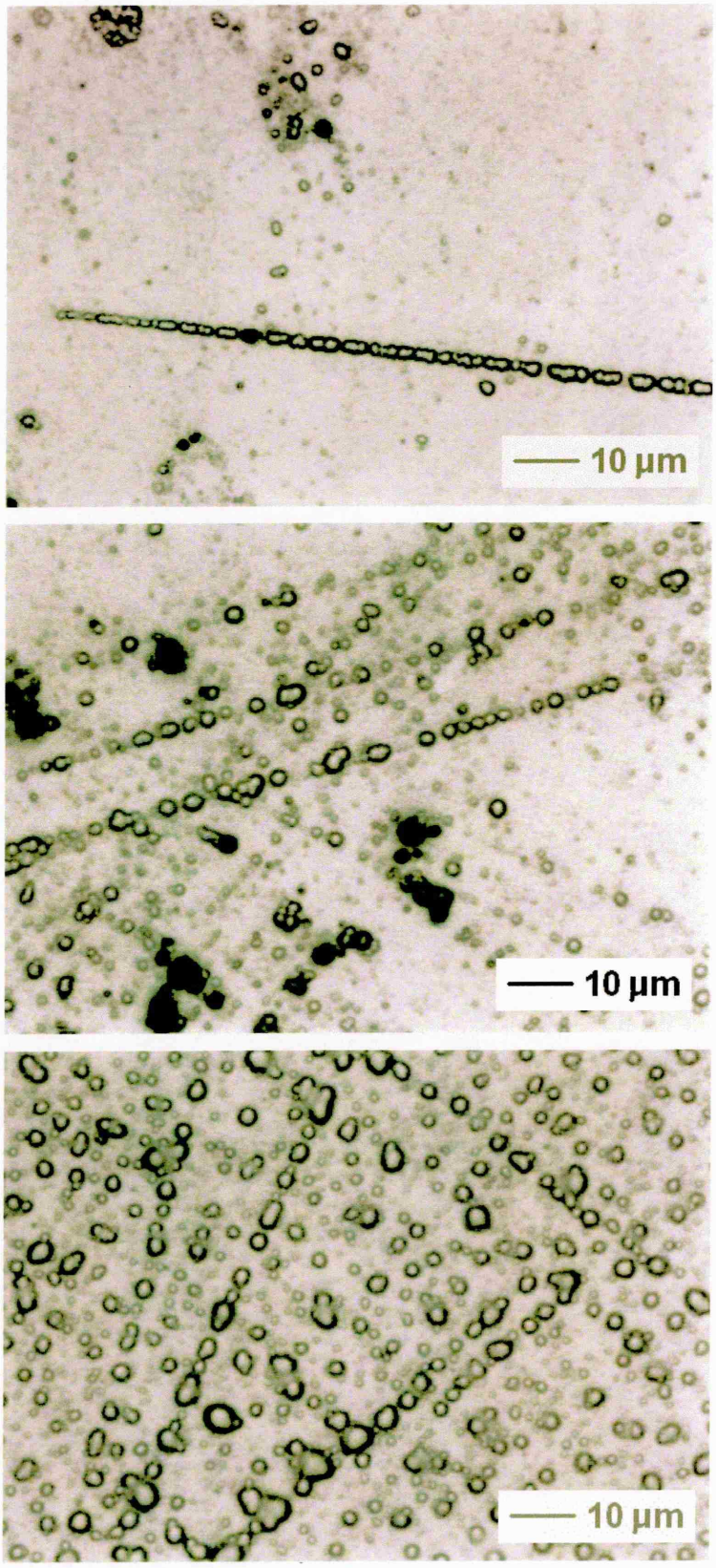

Figure 3.18: *Optical micrographs illustrating the nucleation of nodular polypyrrole growth on substrate scratches.*

3.7 *The Effects of Polypyrrole Layer 'Post-Deposition Treatment'*

In an attempt to further standardize the methods used to deposit research-grade polypyrrole films (and therefore to improve control of the structure of the polypyrrole produced), the effects of 'post-deposition treatment' of polymer films were assessed (i.e. the methods used to rinse and dry polymer films subsequent to deposition).

Two sets of five devices were deposited from standard type-283 solutions. Depositions were carried out at +0.85Vvs SCE for 120s in all cases. Each set of five devices was deposited from a fresh electrolyte solution. After deposition, devices were removed from the electrolyte solution and treat in the following ways:

Type I films were neither rinsed nor dried (i.e. were allowed to dry naturally).
Type II films were rinsed well in electrolyte (Millipore water) and allowed to dry naturally.
Type III films were similarly rinsed, but dried with a high velocity jet of oxygen-free nitrogen as described previously (random jet direction).
Type IV films were treated as Type III films, but were dried with a nitrogen jet oriented perpendicular to the meniscus.
Type V films were also treated as Type III films, but were dried with a nitrogen jet oriented parallel to the meniscus.

It was noted during subjective, visual examination of the films produced by optical microscopy (VANOX) that Type III, IV and V films (i.e. those dried with a nitrogen jet) were appreciably less contaminated than Type I and II films (i.e. those allowed to dry naturally). As would be reasonably expected, Type I and Type II films were observed to be heavily contaminated, Type I more so than Type II. Type III films were noted to be host to far lower contamination levels than Type I or II films, presumably as a result of the removal of (relatively pure) Millipore water electrolyte by nitrogen jet. The level of contamination remaining after natural drying of electrolyte was far higher than expected; all research devices were therefore thoroughly dried with a nitrogen jet after rinsing in 'clean' electrolyte.

The nucleation and growth of polypyrrole observed during this study, was noted to result in the formation of lines, or bands, of polymer, as was often observed during routine deposition. Several mechanisms were considered to be potentially responsible for this, [a] the action of the high velocity nitrogen jet used to remove the 'fresh electrolyte rinse' from films after deposition, [b] the flattening of tendrillar growth, or [c] patterning of the substrate by some means prior to deposition. Each of these will now be discussed.

[a] Jet Action

Type IV and V films were incorporated into this study in a direct attempt to ascertain whether nitrogen jet action could be responsible for the orientational banding effect. VANOX optical microscopy was therefore used to examine Types IV and V films in order to investigate this. From the limited number of films incorporated into this study, it was clear that the direction of the banding observed did not correspond with the direction of the nitrogen jet used to dry films after post-deposition rinsing.

[b] Tendril Formation

It was thought possible that the formation of tendrils (finger-like growths protruding out from the polymer growth face, resulting from particular deposition conditions, as described in Ch.4, in Lemon, Szczur and Haigh, '97 and in Lemon, Szczur and Haigh, '98), and the subsequent use of a high velocity nitrogen jet drying procedure may result in the flattening of tendrillar growths in a direction parallel to the jet direction, so resulting in a 'banding' effect as described. However, the conditions required to result in tendril formation were not used during this study, so strongly suggesting against this.

[c] Substrate Patterning

It was also considered that the patterning of substrates before deposition *may* result in the formation of 'banded' polymer as described. It was thought that a possible means of such substrate patterning may be the drying procedure used during substrate cleaning, as described in §3.6. In order to investigate this, two further sets of films were produced;

Type VI films were deposited onto substrates cleaned with IPA and dried by nitrogen jet oriented perpendicular to the electrolyte meniscus.

Type VII films were deposited onto substrates cleaned with IPA and dried by nitrogen jet oriented parallel to the electrolyte meniscus.

The substrate drying procedure used is illustrated in Fig. 3.19, which shows the possible formation of parallel lines of contaminant on the substrate resulting from the directional use of the nitrogen jet to remove solvent after substrate cleaning.

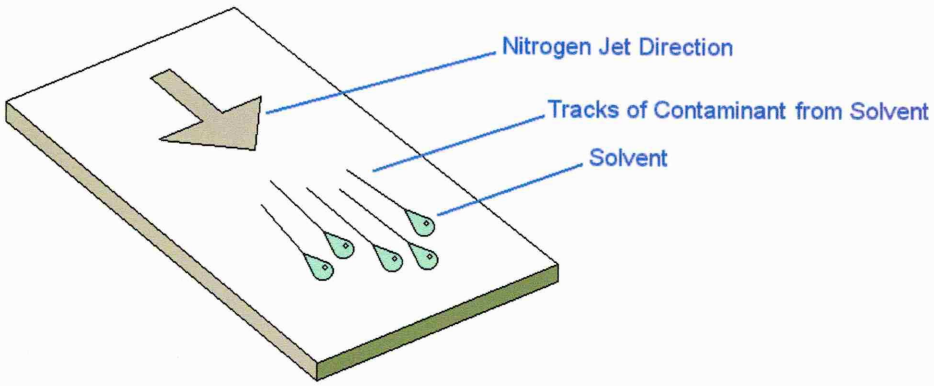

Figure 3.19: *Nitrogen-jet substrate drying regime resulting in the formation of 'tracks' of contamination leading to subsequent patterning of polypyrrole growth.*

Optical microscopy was used to investigate the morphology of Type VI and VII films; VANOX micrographs are shown in Fig. 3.20. It is evident that polymer banding is strongly affected by the orientation of the nitrogen-jet used during substrate cleansing. The confirmation of the hypothesis that nitrogen jet orientation during substrate cleaning could affect the morphology of deposited polypyrrole resulted in the adoption of a standard jet orientation, perpendicular to the position of the electrolyte meniscus during deposition. Further, possible sources of contamination of the IPA used during substrate cleaning were minimized where possible. The morphological (and hence structural) modifications identified above illustrate the dependency of polypyrrole structure on not only deposition methods and parameters, but also on the preparation and treatment of substrate materials.

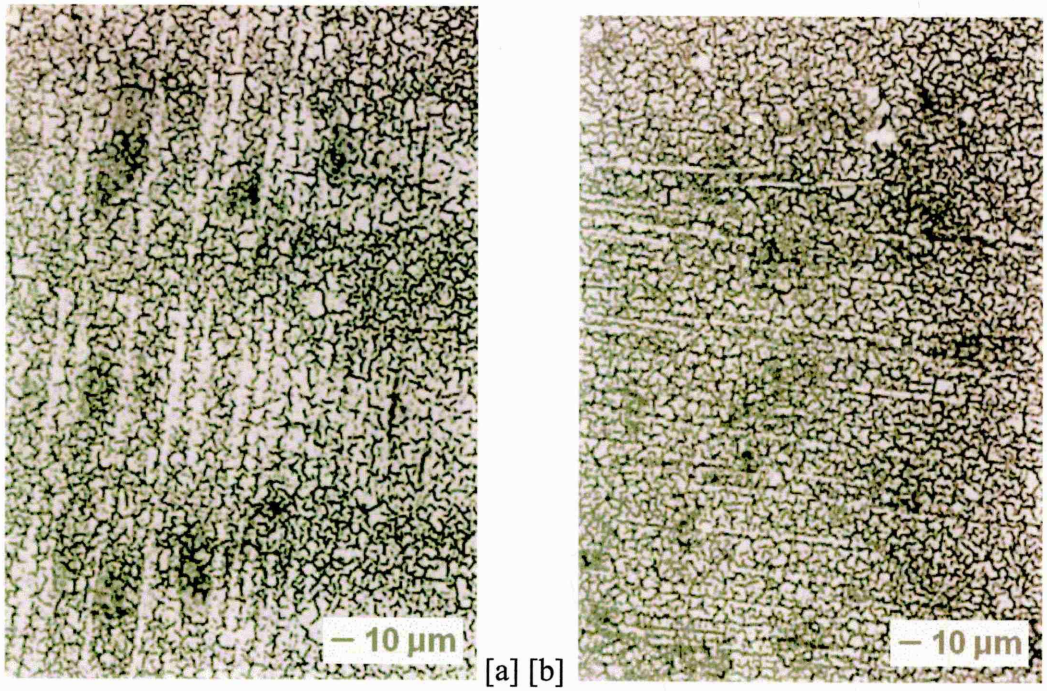

[a] [b]

Figure 3.20: *Banding observed during polymer deposition resulting from the re-contamination of substrate materials during cleaning prior to deposition. Nitrogen jet orientations [a] parallel, and [b] perpendicular to the electrolyte meniscus were used.*

Summary, Chapter 3

- The variation of electrolytic dopant concentration has a significant effect on the electrical conductivity of polypyrrole devices. These effects have been shown to be due to an increase in film structural maturity (film thickness, nodularity level etc.) with increasing dopant concentration.
- The variation of deposition potential also has a significant effect on the electrical conductivity of polypyrrole. Conductivity effects have been shown to be due to increased deposition rate with increasing potential leading to increased film structural maturity per unit deposition time.
- The relationship between deposition time and sensor resistance has been studied; after 'bridging' of the insulating gap, the relationship observed was as intuitively expected. Microscopic evidence of gap bridging has been presented, and shown to occur between 2s and 5s of deposition under normal conditions. The level of gap bridging was shown to correlate well with sensor resistance.
- The effects of electrolyte re-use have been studied; it has been shown that the (well accepted) deposition of 12 Mk-III devices from a single electrolyte solution did not affect polypyrrole morphology. Low-level increases in sensor resistance were observed over the deposition of 12 devices; resistance increases were observed to be more significant on deposition from lower concentration electrolyte solutions.
- Solution agitation during deposition has been demonstrated not to greatly affect sensor resistance, although gentle agitation was shown to result in increased film maturity over standard deposition times. Immature polymer growth was found to orientate with 'current' during solution agitation.
- Studies of the effects of substrate cleaning regimes suggested that evaporation of solvent from working electrodes before polymer deposition could result in the adoption of morphological traits by mature films, as could the presence of scratches (etc.) on the working electrode.
- The effects of post-deposition film treatment have also been studied; it was shown that rinsing of films in Millipore water after deposition greatly reduced the level of observed contamination (as would be intuitively expected). Film 'drying' by high velocity nitrogen jet also greatly reduced contamination levels. The 'blow-drying' of substrates before deposition was also found to affect morphological characteristics of immature films.

4. *The Macrostructure of Polypyrrole*

The work presented in this chapter concentrates on the elucidation of the macrostructure of type 283 polypyrrole, although the morphologies and macrostructures of other polypyrrole-based sensor polymers (PPy/$LiNO_3$, PPy/$NaClO_4$, PPy/$NaPF_6$) are studied and discussed.

The structural studies presented are exclusively based on polypyrrole formed by electrochemical means. It is known that polypyrrole formed by alternative techniques such as the Langmuir-Blodgett method (see Rikukawa and Rubner, '94) and chemical polymerisation (see Sak-Bosnar *et.al.*, '92; Myers, '86) may have morphological characteristics dissimilar to those of electrochemically deposited material. A thorough investigation of the morphological and structural characteristics of polypyrrole formed by non-electrochemical techniques is therefore beyond the scope of this thesis.

As stated in the 'Abstract', the level of understanding concerning the growth dynamics and structural characteristics of electrochemically deposited polypyrrole was poor prior to the work presented. Indeed, early discussions with industrial collaborators (Hodgins, '95) suggested that polypyrrole sensing elements were thought to possess micro- and macrostructures which were isotropic (i.e. equivalent in x-, y- and z- orientations). The work presented is therefore novel, and has resulted in a marked improvement in the industrial understanding of polypyrrole macrostructure and its relationship to the characteristics of olfactory sensing elements. Much of the work presented in this chapter has resulted in peer-reviewed publication; sections of published work are referenced as required.

4.1 *The Nodular Morphology of Electrochemically Deposited Polypyrrole*

The majority of the work presented in this chapter concerns the formation of novel polypyrrole morphological characteristics (either unreported in the literature or reported in passing) during electrochemical deposition under specific (although not necessarily non-standard) circumstances. Further, although the presence and the effects of nodular morphology on electrochemically deposited polypyrrole have been reported

(Charlesworth *et.al.*, '93; Maddison, '93), very little work has been reported concerning the formation/structure of polypyrrole nodules. In this section, salient observations regarding the formation of nodular macrostructure are discussed.

Studies presented previously in §3.1 to §3.3 amply illustrate the generation of characteristic nodular morphology with increasing dopant concentration, increasing deposition potential, and increasing deposition time. It is apparent that increasing film maturity (thickness) correlates strongly with increases in film nodularity levels. A series of studies concerning the formation of type-283 polypyrrole morphology is now presented.

4.1.1 'Pre-Nodular' Morphology of Type-283 Polypyrrole

It has been shown, by VANOX optical microscopy and SEM, that the 'pre-nodular' growth of type-283 polymer (i.e. the immature films formed before nodular morphology develops) is in the form of a sub-micron thick film (as per Surtronic 3+ surface microroughness data). Such pre-nodular growth is responsible for the *initial* contact between the two discrete areas of the MkIII Bass-Warwick electrode active area (i.e. the initial contact over the '10µm insulating gap', see Appendix 1), and has been noted to be responsible for *all* of the polymer contact (and therefore charge transport) over the insulating gap in the early stages of polymer growth. It was therefore assumed that the structure and properties of the immature material deposited during the early stages of growth would strongly influence the electrical resistance and sensing properties of complete devices.

It has been shown that further deposition involves the thickening of the immature polymer film (Ch. 3), along with significant increases in the deposition *area* where possible. Deposition onto MkIII Bass-Warwick electrodes typically resulted in the formation of a polymer 'frame' around the electrode active area, as shown in Fig. 3.14 (Ch. 3); frames of up to ½mm wide have been observed during the work presented. It is widely reported (Bassett, '81) that the nucleation of polymers is invariably heterogeneous (i.e. is initiated on non-polymeric sites); the observation of polypyrrole deposition onto the area surrounding the electrode active area was therefore no surprise.

However, growth of polypyrrole frames was unexpected due to the insulating nature of the substrate material around the electrode active area. The successful electrochemical polymerisation of polypyrrole fundamentally depends on the oxidation of pyrrole monomer, as reported in Ch.1. This is achieved by the deposition of polypyrrole onto a working electrode at or above the deposition potential required for pyrrole oxidation, so strongly opposing the *deposition* (i.e. the nucleation and growth) of polypyrrole onto non-conducting substrates by electrochemical means.

It is therefore suggested that immature polypyrrole layers around MkIII Bass-Warwick electrode active areas ('frames') grow as a result of the electrical conductivity of polypyrrole; oxidized and polymerized polypyrrole is used to carry the potential required to oxidize surrounding monomer groups. Further, it is suggested that the finite resistance of electrochemically deposited polypyrrole results in a reduction of the local deposition potential as a function of distance from the electrode active area; this reduction of potential limits the 'frame' area over which polymer may grow.

The observation of the frame-effect, as described above, suggests that the initial, immature growth of electrochemically deposited polypyrrole occurs preferentially in the *plane* of the polymer growth face as opposed to in the *direction* of the growth face. It is known that typical film thicknesses of commercial devices range from 1 to 10μm; observation of polymer frames of ½mm width suggests a disparity in the ability of polypyrrole to grow in the 'x-z plane' and in the 'y-direction' during early 'pre-nodular' growth stages, as illustrated in Fig. 4.1.

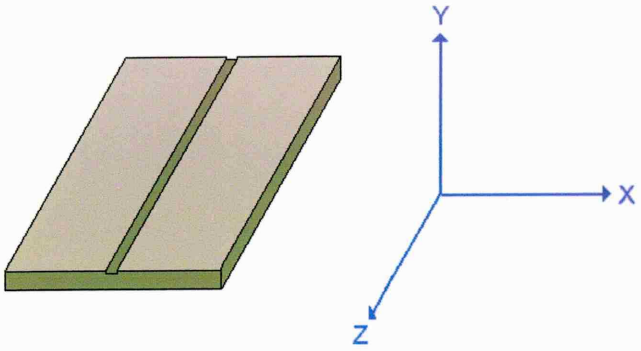

Figure 4.1: *Orientational dependence of polypyrrole growth; observations suggest a preference towards growth in the x-z plane over growth in the y-axis during early stages of film formation.*

The apparent orientational dependence of initial polypyrrole growth reported above is supported by equivalent observations of polypyrrole deposition onto platinum 'Yoshi' electrodes, as described in Appendices 1 & 2. Deposition onto Yoshi electrodes has been observed to involve polymer bridging of the 75µm insulating gap (i.e. electrical contact via polymer contact) at very immature stages of polypyrrole development. Film thickness at the time of bridging has been estimated as *around* 1µm by profilometry (although the polypyrrole films used to assess thickness were repeatedly damaged during contact with the diamond stylus used). Despite the potential inaccuracy involved in the film thickness measurement technique used, it may be safely stated that the immature electrochemical growth of polypyrrole if *far* more vigorous in the x-z plane than in the y-axis. This strongly suggests against the industrially accepted view of three-dimensionally equivalent polypyrrole structure; industrial accounts of the microstructure of electrochemically deposited polypyrrole suggested a three-dimensionally equivalent structure (as stated previously in this Chapter).

4.1.2 Nodular Morphology – Growth Models.

Although the nodular morphology of mature polypyrrole films is well reported (references cited previously), very little work has been reported in the literature regarding the *formation* of nodules. The growth models reported in this chapter relate to the author's published work where appropriate, but are all novel.

The 'immature-growth' model presented in §4.1.1 does not support the original growth model assumed (without empirical evidence) by the author, as reported in Lemon, '96 (Registration Transfer from M.Phil. to Ph.D. Report). The model (reproduced in Fig. 4.2) described polypyrrole growth via primary nucleation on numerous substrate sites, coalescence, the formation of a columnar structure, and the maturation of dominant columns into nodules. It was also thought likely that nodular structure would be strongly spherulitic.

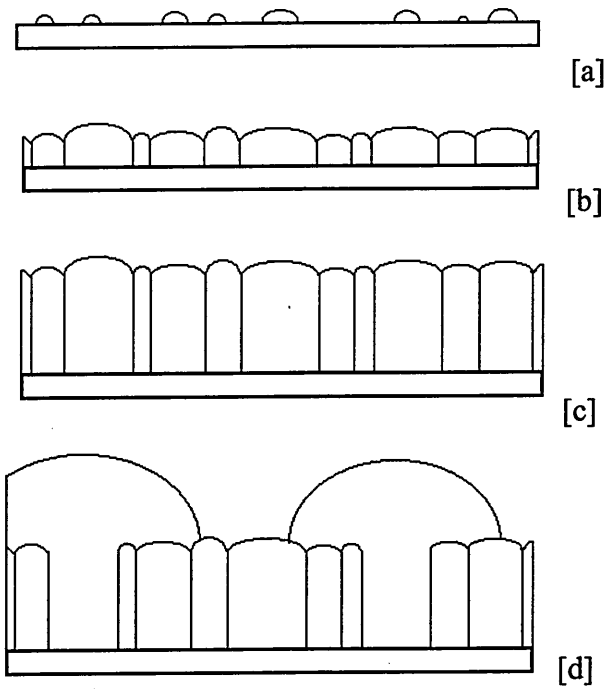

Figure 4.2: *"Dominant Column Nodule Formation" growth model previously suggested involving [a] primary nucleation on numerous substrate sites, [b] coalescence, [c] the formation of a columnar structure, and [d] the maturation of dominant columns into nodules (reproduced from Lemon, '96).*

Work carried out since the formation of the model illustrated in Fig. 4.2 does not suggest against steps [a] and [b] *per se*; it is difficult to visualize the initial stages of electrochemical polypyrrole growth by means other than nucleation and coalescence. However, the observations reported in §4.1.1 show that the growth of polypyrrole over relatively large areas of non-conducting substrate materials is possible. This suggests that either an unknown growth mechanism is responsible for immature film formation, or 'unbounded coalescence' is responsible for polymer growth over insulating areas. To explain the spread of polypyrrole over insulating material, consider Fig. 4.3. It is

postulated that the nucleation suggested in Fig. 4.2 is dependent on nucleation density (i.e. the number of nucleation sites per unit area) and the growth rate of the polymer (high growth rate may reduce nucleation density). Coalescence of growth from neighbouring nucleation sites is thought to result in the formation of a small-scale columnar structure (as illustrated in Fig. 4.2 [b]), as a result of the boundaries encountered by each nucleation site. However, nucleation sites at the edges of conducting areas are essentially unbounded, as illustrated in Fig. 4.3. This model sits comfortably with the observation (as reported in Ch. 3) of the formation of substantial 'frames' of polymer onto insulating areas around the electrode active area of MkIII Bass-Warwick devices.

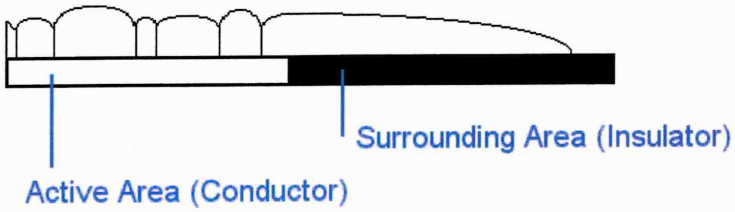

Figure 4.3: *Unbounded polypyrrole growth over insulating material.*

Steps [a] and [b] of the "Dominant Column Nodule Formation" growth model (as shown in Fig. 4.2, reproduced from Lemon, '96) are therefore supported by the author's subsequent work. However, steps [c] and [d] are not supported. An alternative growth model (supported by empirical evidence) is now presented.

4.1.3 The Development of Nodular Morphology – Stage 1 & 2 Growth

A study of the morphological effects of growth time variation is discussed in §3.3. However, the work presented concentrated on the resistance characteristics of MkIII Bass-Warwick devices; morphological changes were considered only as evidence of film thickening (in corroboration with EDAX evidence).

A more focused study was carried out in order to investigate the morphological development of type-283 polypyrrole during electrochemical growth, with particular attention paid to the first ten seconds of deposition, during which significant 'blackening' of the substrate is routinely observed, indicating the growth of a substantial

film. In order to directly observe the early stages of polypyrrole film formation, a set of films were deposited under standard conditions onto Indium Tin Oxide (ITO) coated glass slides (area $100mm^2 \pm \sim 5mm^2$) for a range of deposition times between 0 and 300s. ITO substrates were used in preference to gold microelectrodes in order to allow XRD analysis at a later stage (as reported in Ch.5). It was noted by the author during previous work that deposition of mature layers of type-283 polypyrrole onto ITO electrodes resulted in the formation of an identical morphology to that formed from deposition onto gold microelectrodes. It was therefore thought reasonable to assume that immature morphologies and growth mechanisms involved during deposition onto gold and onto ITO would *not* be dissimilar. Further, previous experience of the SEM technique suggested that, although resolution was excellent, the study of immature polypyrrole layers was made difficult by poor contrast/definition during the analysis of the early stages of film growth (see Fig. 3.7 [a], §3.3 for example). VANOX optical microscopy was therefore used during this study in preference to SEM.

ITO glass electrodes were cleaned with IPA prior to deposition, and were dried as described previously. VANOX microscopy showed that, for deposition times of 2s and 5s, extremely immature films (termed 'Stage 1' films) of polypyrrole were formed on the ITO substrates. The position of the observed growth relative to the orientation of the electrode during deposition supported the assumption that the observed material was polypyrrole as opposed to cleaning residues etc. The production of several '0 s' (zero seconds) samples (ITO electrodes handled, washed, dried, dipped in electrolyte, rinsed and dried using identical techniques to those used for deposition of 2s and 5s samples) confirmed that the growth patterns observed were not due to cleaning or electrolyte contamination (etc.) but were the result of immature polypyrrole growth.

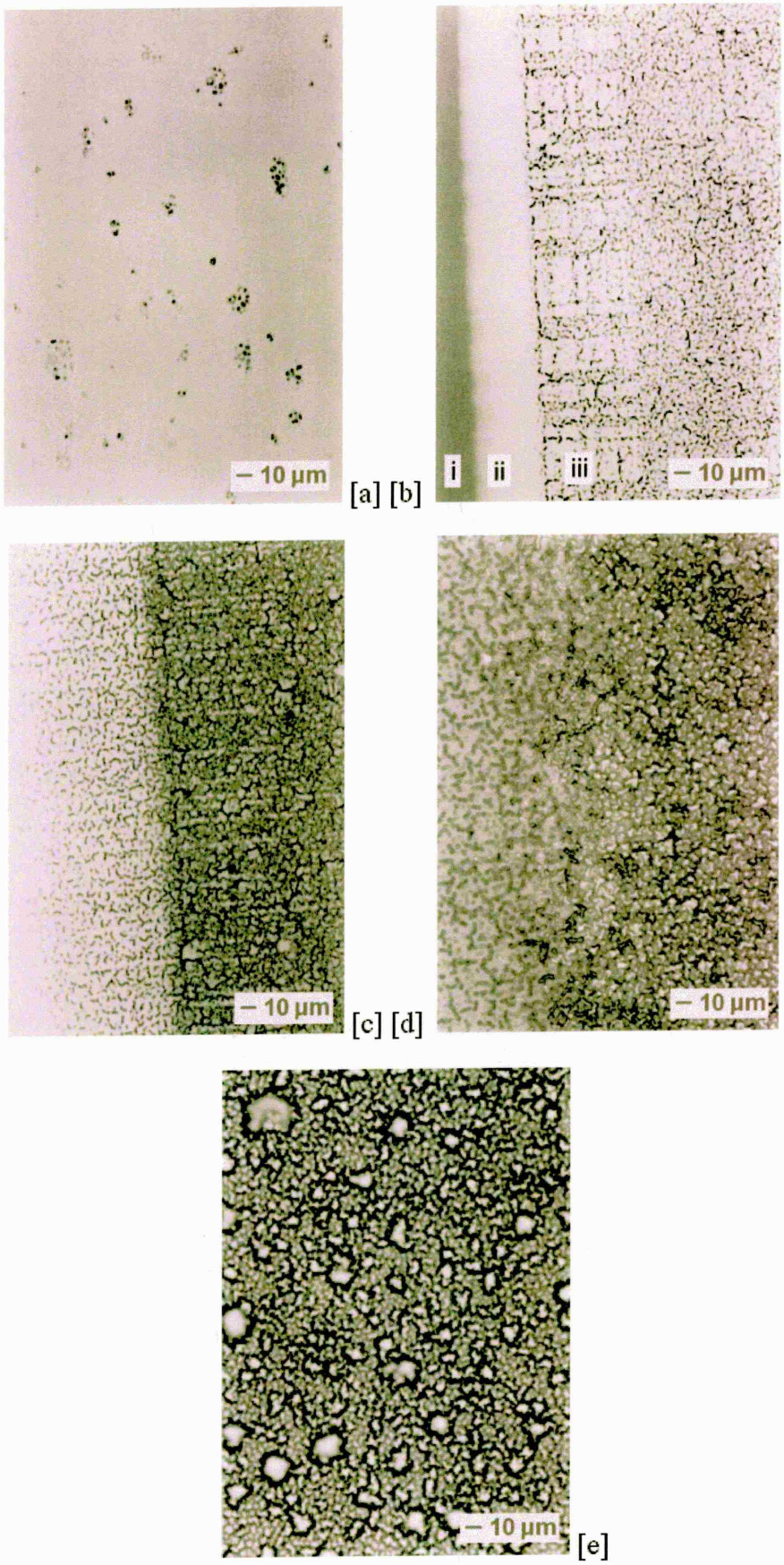

Figure 4.4: *Polypyrrole growth on ITO glass electrodes (VANOX optical microscope). See text for details.*

The growth patterns observed (as per Fig. 4.4 [a] (2s deposition)) supported the nucleation of polypyrrole at discrete sites between 2 and 5 seconds of growth. Direct evidence of coalescence was not observed; the morphology observed after 10s of deposition was significantly more mature, displaying evidence of the formation of a second layer (termed 'Stage 2' growth) of polypyrrole over the Stage 1 layer. Fig. 4.4 [b] (10s deposition)) shows both Stage 1 and immature Stage 2 polypyrrole growth (immersion in the electrolyte solution increases from left to right as shown). Area [i] represents pristine substrate material, area [ii] Stage 1 growth, and area [iii] the early stages of Stage 2 growth (Note that SEM was used to confirm this). Further deposition (Fig. 4.4 [c] (30s deposition)) was observed to result in maturation of the Stage 2 layer; it was of note that the original discrete Stage 2 nucleation sites shown in [b] had matured via the growth of several stalks radiating from the original nucleation sites (note also that Stage 2 growth occurs over the area occupied by Stage 1 growth in [b]). Further growth (Fig. 4.4 [d] (60s deposition) was observed to result in coalescence of the Stage 2 film and immature nodular formation. Further deposition (Fig. 4.4 [e] (120s deposition) resulted in the formation of a mature nodular morphology.

The observations discussed above have allowed the production of a growth model relating to the development of polypyrrole films during electrochemical deposition. The model, illustrated in Fig. 4.5, involves:

[1] the nucleation of polypyrrole at discrete sites onto the electrode surface, with a heavy bias towards growth *in the plane* of the electrode (the 'XZ-plane', see Fig. 4.1),

[2] coalescence of the nucleation sites described in [1],

[3] complete coalescence forming the 'Stage 1' layer,

[4] secondary (homogeneous) nucleation (although it is reported that polymer nucleation is invariably heterogeneous, it is thought that the electrical conductivity of polypyrrole allows homogeneous nucleation, i.e. the nucleation of polypyrrole *on* the 'Stage 1' polypyrrole layer; this is supported by empirical evidence as shown in Fig. 4.4). *Note that it is not assumed that secondary nucleation (i.e. nucleation of the Stage 2 film) takes place on Stage 1 nucleation sites, as would normally be expected. Secondary nucleation is thought to occur on the stage 1 film, which would mask features of the original substrate. However, macro-scale defects of the original*

substrate may lead to nucleation of stage 2 material on substrate defects; it is thought that evidence of this effect is shown in Fig. 3.18, §3.6.1.

[5] further polypyrrole growth on the nucleation sites described in [4], with growth far less biased towards the electrode plane, but with growth extending on the axis perpendicular to the electrode plane (the 'Y-axis', see Fig. 4.1),

[6] the formation of radial polymer stalks from the secondary nucleation sites described in [4], often resulting in either a 'tripartite radial stalk' morphology, or a 'sheaf' morphology [as shown in Lemon and Haigh, '99 (a) (Fig. 1)].

[7] maturation via massive growth in the 'XZ-plane' *and* along the 'Y-axis'

[8] the formation of a nodular morphology.

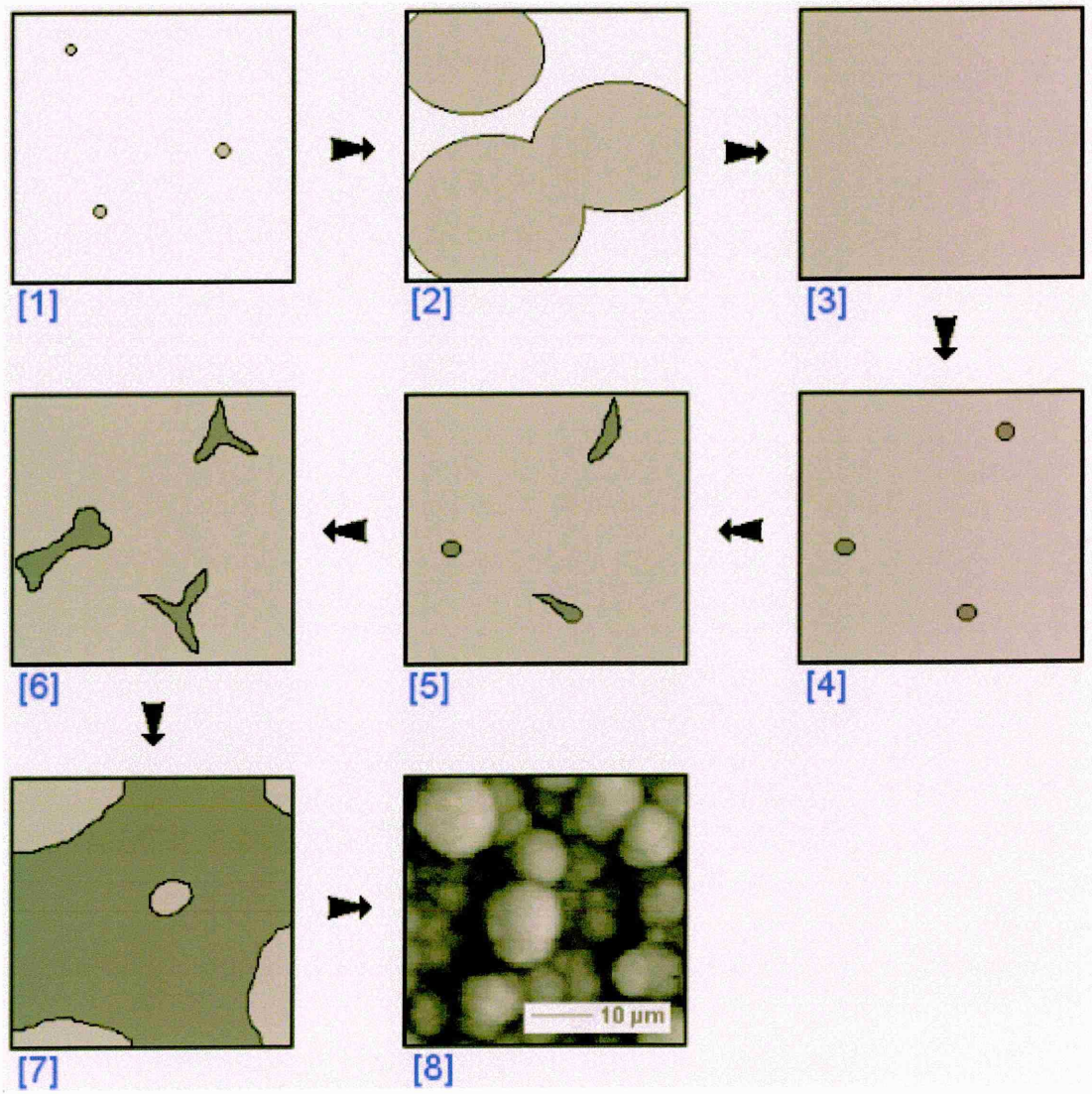

Figure 4.5: *Type-283 polypyrrole growth model.*

It is of note that step [8] above (the formation of nodular morphology) is thought to be the result of the production of gas at the working electrode interface during electrochemical deposition. The effects of such gas production are discussed in depth in §4.3 (and are reported in Lemon and Haigh, '99 (a)). However, it is not thought that nodules nucleate *per se*. Rather, gas generation at the polymer/substrate interface is thought to result in the partial, localised detachment of the polymer film from the substrate surface. It is postulated that gas production, and subsequent localized film detachment results in the formation of gas 'pockets' at the film/substrate interface. The 'maturation' of these gas pockets is thought to result in the development of the commonly reported polypyrrole nodular morphology (see §4.3 and Lemon and Haigh, '99(a)).

Empirical evidence is presented in §4.3, which supports the hypothesis of nodule formation resulting from gas production during film deposition. The development of nodular morphology on non-conducting substrate areas is also discussed, with relation to the production of gas at the working electrode; it is suggested that gas production may also occur at an interface between the previously described 'Stage 1' and 'Stage 2' polypyrrole layers, so supporting the growth model presented.

4.1.4 The Development of Nodular Morphology on Non-Conducting Substrates

The electrochemical deposition of polypyrrole onto non-conducting areas of otherwise conducting substrates has been discussed (§4.1.1), as has the development of nodular morphology (§4.1.3).

Close scrutiny of mature layers of type-283 electrochemically deposited polypyrrole has revealed a novel morphological trait that is occasionally observed during growth under 'normal' conditions. As shown in Fig. 4.6, it appears to be possible for nodular growth to occur not only on conducting substrates, but also on non-conducting substrate areas, such as within the MkIII Bass-Warwick electrode 10μm insulating gap. Although the mechanisms involved are discussed in length in §4.3, it is necessary at this stage only to state that the application of a sufficient deposition potential to conducting areas of the typical substrate materials used is thought to be responsible not only for the

polymerisation chain reaction discussed in §1.5.4, but also for the generation of gaseous oxygen. This oxygen production is thought to result in the well-reported nodular morphology of polypyrrole.

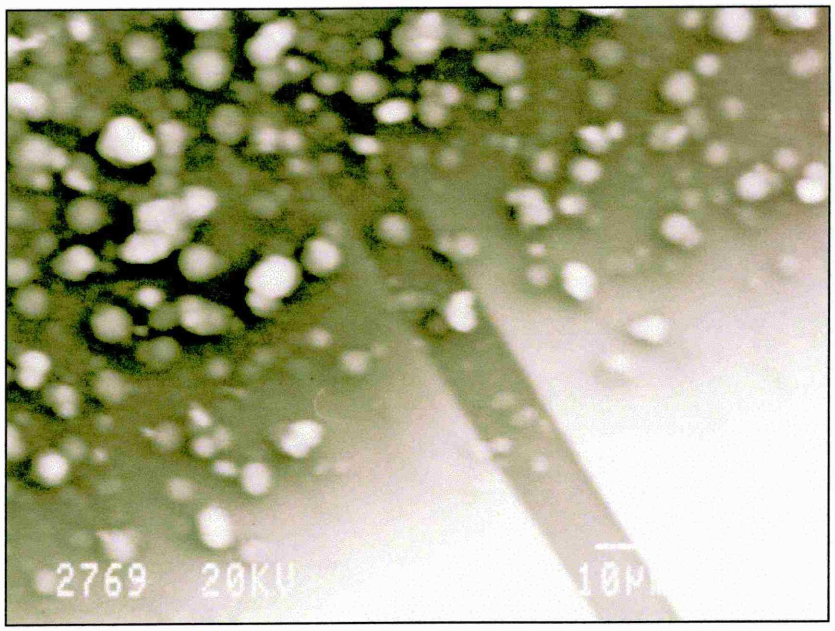

Figure 4.6: *The formation of nodular polypyrrole morphology over non-conducting substrate areas (black strip from top left to bottom right of frame is insulating).*

It is postulated that the architecture of the 'Stage 1 & 2' film structure as discussed in §4.1.3 may be responsible for the production of nodular morphology over non-conducting substrate regions. As stated, oxygen generation is thought to be responsible for nodule formation; the presence of a suitable deposition potential at the working electrode is responsible for oxygen generation. It is postulated that the formation of a 'Stage 1' conducting polypyrrole layer over the insulating areas of the substrates used directly results in the presence of a significant potential over non-conducting substrate areas. The presence of this potential, given the significantly conducting nature of type-283 polypyrrole, is thought to be sufficient to result in the generation of oxygen, and so nodule formation.

4.1.5 Profilometric Morphological Investigation

Attempts were made to investigate the development of nodular morphology (as described above) via contact profilometry.

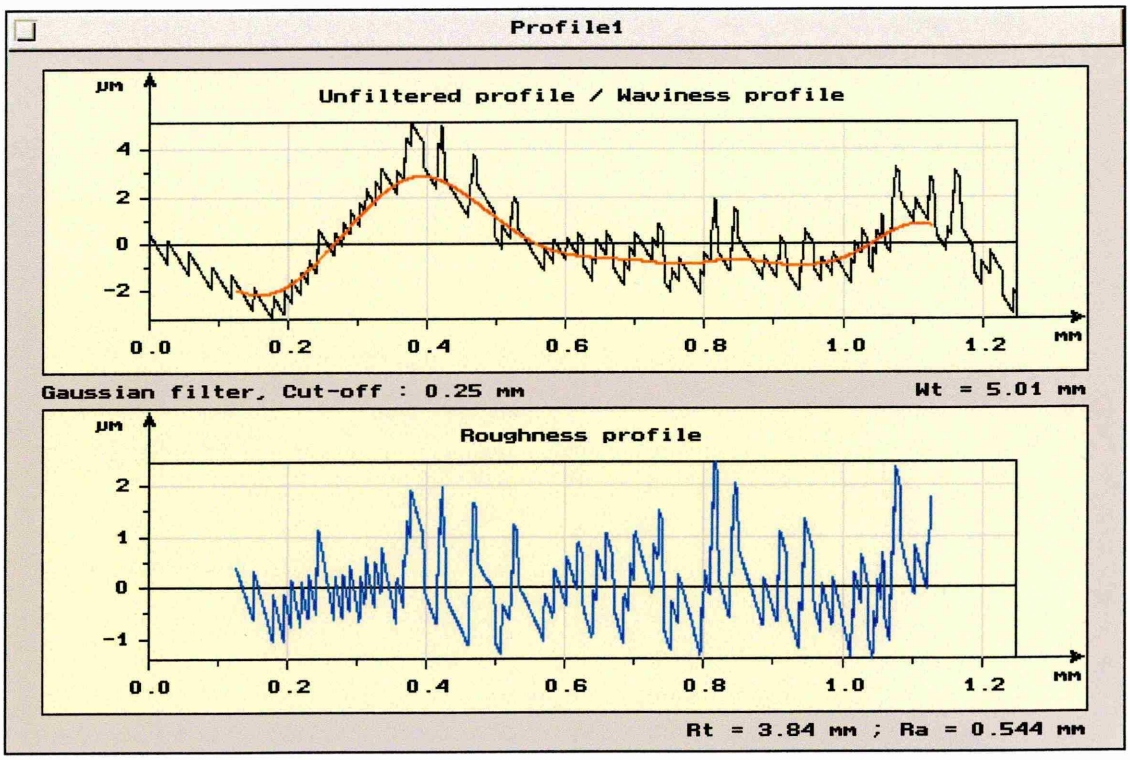

Figure 4.7: *Surtronic 3+ analysis of the microtopography of a mature electrochemically deposited polypyrrole film.*

A Taylor Hobson Surtronic 3+ (see §2.2.5) was used with Talyprofile visualization software in order to investigate the morphological development of polypyrrole films at various stages of maturity (films prepared during the study presented in §4.1.3 were used).

Traces were taken from a single film representing each stage of deposition as described in §4.1.3; a set of 5 traces were taken from each film. Analysis of the data collected showed that the equipment used was unsuited to the analysis of the very fine morphologies formed by type-283 polypyrrole. Traces taken from early stages of growth suggested that films were damaged by the diamond stylus used by the Surtronic (a contact method); this was confirmed by the observation of 'tracks' left on polypyrrole films by the stylus after measurement. Analysis of fully mature films did not result in visual damage by the Surtronic stylus, but traces were not representative of the polypyrrole morphology observed during SEM analysis (peak width (i.e. nodule size) and peak spacing (i.e. nodule spacing) were not found to agree with SEM examination). A typical trace is shown in Fig. 4.7; the true roughness trace (shown in black on the upper trace) does not confirm the nodular spacing observed during optical and SEM

analysis. This is thought to be the result of the 90°, 5µm radius stylus used by the Surtronic instrument, which is known to result in the production of spurious data when used to analyse the morphology of samples with very fine morphological features (Lemon, '97).

4.1.6 The Morphological Effects of Dopant Group Selection

The effects of dopant group choice on the morphologies of electrochemically deposited polypyrrole films were assessed via direct morphological examination by SEM and VANOX optical microscopy.

Dopant groups reportedly used in the literature during the electrochemical deposition of polypyrrole were used to assess the morphological effects of the use of dopant groups other than Sodium Benzene Sulfonate (as used in type-283 polypyrrole). Lithium Nitrate ($LiNO_3$) (Neotronics, '94(c)), Sodium Perchlorate ($NaClO_4$) (Nagase *et.al.*, '93(a), Liang *et.al.*, '92; Truong *et.al.*, '95) and Sodium Hexafluorophosphate ($NaPF_6$) (Rikukawa and Rubner, '94; Miasik *et.al.*, '86) were used.

Depositions were carried out under standard conditions, using pyrrole monomer at 0.25M concentration and 0.25M dopant concentration in 50ml of Millipore water. A deposition potential of +0.85V vs SCE was used throughout. Two discrete solutions were prepared using each dopant type: the first of each was used to deposit a set of five films onto individual Mk-III Bass Warwick electrodes, the second used to prepare large-scale films on ITO glass slides (as described in §4.1.3).

Lithium Nitrate ($LiNO_3$)

Films deposited onto MkIII Bass-Warwick electrodes were found to have a mean resistance of 150.2Ω, with a standard deviation of 103.0Ω. In comparison to type-283 devices, the mean resistance calculated for $LiNO_3$ doped devices is high, although this need not be a disadvantage if devices are used as members of a multi-sensor array. However, the large standard deviation calculated is considered to be a significant disadvantage of the use of $LiNO_3$ doped polypyrrole as a sensing material; low

device-to-device reproducibility significantly reduces the practicability of like-for-like sensor replacement in the event of sensor failure (the replacement of a sensor with one of dissimilar resistance and response characteristics is known to limit the effectiveness of the knowledge base within the Neotronics NOSE during the identification of, or discrimination between, odours).

The morphology of $LiNO_3$ doped polypyrrole deposited onto MkIII Bass-Warwick (gold) electrodes under standard 'device formation' conditions (i.e. +0.85V vs SCE, 120s) resembled that of type-283 polypyrrole deposited under similar conditions. However, although the characteristic nodular morphology was observed, it is of note that the spacing of the nodules observed was greater than for type-283 material (see Fig. 4.8); film thickness was also noted to be lower than would be expected from type-283 material (estimated using the limited depth of field of the VANOX optical microscope). It is considered that this may be partly responsible for the observed high resistance of the devices produced. As for type-283 material, film adhesion was observed to be good, although adhesion was tested subjectively.

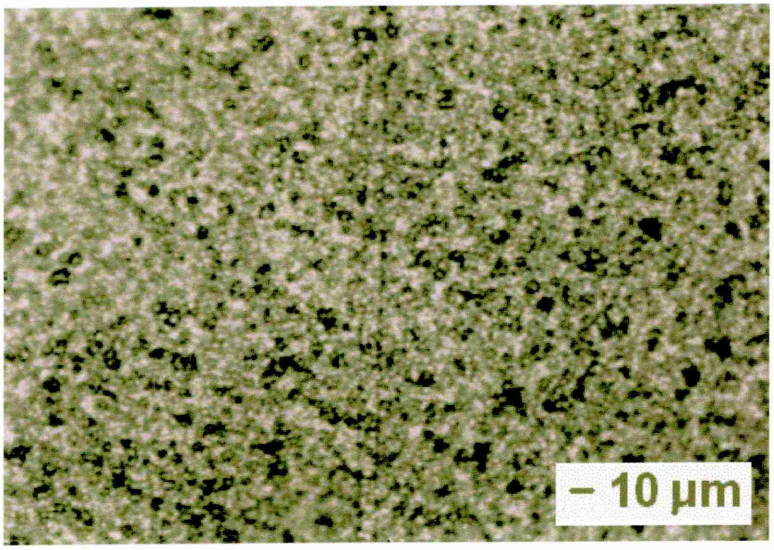

Figure 4.8: *The nodular morphology of electrochemically deposited polypyrrole doped with lithium nitrate (standard conditions on gold).*

Deposition of $LiNO_3$ doped polypyrrole onto ITO glass under standard conditions (120s) resulted in the formation of a thin film (with thickness increasing with increasing

vicinity to the meniscus) with similar nodular morphology to that observed on deposition onto gold microelectrodes. Analysis of growth patterns on ITO suggests that film formation is via nucleation (as illustrated for type-283 growth in Fig. 4.5, §4.1.3, steps [4] & [5]), followed by growth of polypyrrole as radial stalks (as described for type-283 growth). However, stalks routinely appear to be thicker than those formed during type-283 growth, so leading to a more dense polymer film. Further growth is observed to lead to coalescence and formation of nodular morphology. The use of an extended deposition time (30 mins, to allow the production of a thick film used during XRD analysis in Ch. 5) produced a similar morphology. However, this morphology was superimposed onto a large-scale texture, similar to that described previously by Stankovic *et.al.*, '94 as 'brain skin' (indicating a texture similar to that of the surface convolutions and depressions of the brain's 'cortical substance' (Gray, '98) (see Fig. 4.9). It is *not* considered that this large-scale texture is formed via the same mechanism as suggested by Stankovic *et.al.*; this is discussed further in §4.3. It is thought that this large-scale morphology is the result of stresses within the unusually thick films produced on settling after the extended growth period. It is not, therefore, considered that this morphology is of structural significance.

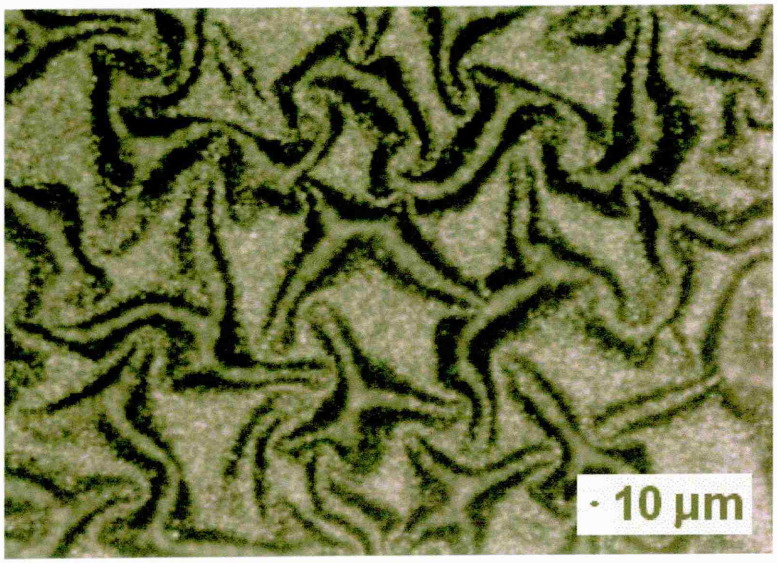

Figure 4.9: *The large-scale 'Brain-Skin' morphology of electrochemically deposited polypyrrole doped with lithium nitrate (extended growth period).*

Sodium Perchlorate ($NaClO_4$)

Polypyrrole films doped with sodium perchlorate deposited onto MkIII Bass-Warwick electrodes were found to have a mean resistance of 1476Ω, with a standard deviation of 1169Ω. Electrical resistance of this magnitude is far higher than that of type-283 polymer, but need not count against its use as a sensing array member. However, as for lithium nitrate doped material, the large resistance standard deviation observed is considered to be a significant disadvantage for reasons discussed previously.

The morphology of $NaClO_4$ doped polypyrrole deposited onto gold electrodes under standard conditions (i.e. +0.85V vs SCE, 120s) again resembled that of type-283 polypyrrole deposited under similar conditions. Two morphological traits distinguished $NaClO_4$ doped material from type-283 material. Firstly, the level of nodularity observed consistently exceeded that of type-283 material by a considerable margin (see Fig. 4.10). Secondly, despite the standard rinsing and blow-drying technique used after deposition (see §2.1.1), $NaClO_4$ doped material was consistently observed to develop crystals shortly after deposition. These crystals were easily resolved by optical microscopy, as shown in Fig. 4.11. The development of post-deposition crystallinity is considered in depth in §4.4.

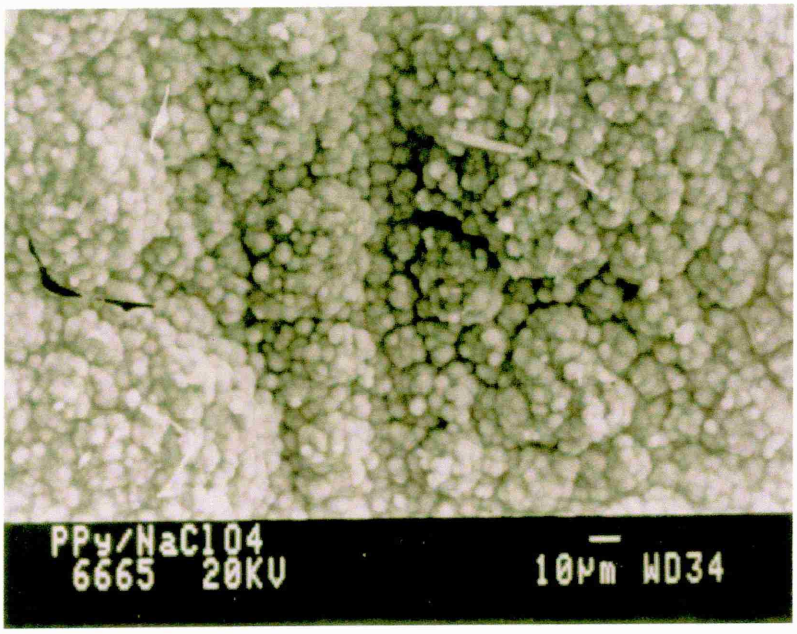

Figure 4.10: *The nodular morphology of electrochemically deposited polypyrrole doped with $NaClO_4$ (standard conditions on gold).*

Film thickness was noted to be greater than would be expected from type-283 material. This conflicts with the electrical resistance data collected, which suggested that either the film thickness of the $NaClO_4$ doped devices formed was lower than typical type-283 devices, or that the resistivity of the $NaClO_4$ doped material was significantly higher than type-283 material. It is suggested by the author that the observed increased device resistance is not the effect of an unusually high material resistivity (and it is known that it is not the result of low film thickness), but is rather the effect of gas production at the working electrode during deposition resulting in widespread detachment of the film from the substrate (i.e. the polymer/gold interface). Further evidence is given to support this hypothesis in §4.3.

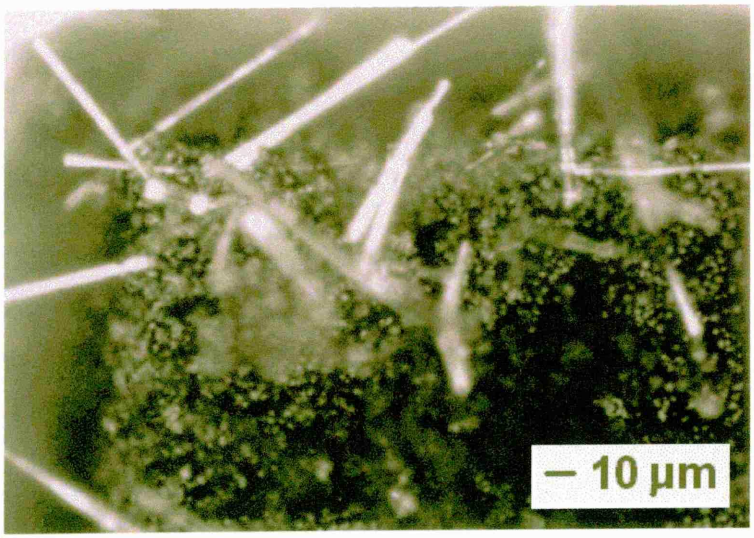

Figure 4.11: *Electrochemically deposited polypyrrole doped with $NaClO_4$, showing the presence of a well developed crystal structure.*

Deposition of $NaClO_4$ doped polypyrrole onto ITO glass under standard conditions (120s) resulted in the formation of a substantial, robust film in the vicinity of the meniscus, becoming thinner and less opaque with solution depth. Nodularity levels were observed to be equivalent to material produced on gold microelectrodes. Analysis of various levels of film maturity suggested that film formation occurs via nucleation, radial stalk growth, coalescence and nodule formation. As for films deposited onto gold microelectrodes, films grown on ITO substrates were observed to contain many fibrous crystallites, the origins of which are discussed in §4.4.

Films grown for an extended 30 minute deposition time were observed to possess a similar morphology to '120s' films grown on ITO. Again, the production of thick, very substantial films led to the superimposition of this morphology onto a large-scale 'brain-skin' texture as described previously, thought to be the result of stresses produced within the films after deposition.

Sodium Hexafluorophosphate ($NaPF_6$)

Polypyrrole films were deposited onto gold electrodes from electrolyte solution containing $NaPF_6$ dopant. Films were observed to grow well, but polymer/gold adhesion was so poor as not to withstand the standard rinse & dry technique used subsequent to deposition. Resistance data and morphological evidence were therefore not collected from polypyrrole doped with $NaPF_6$ on gold microelectrodes.

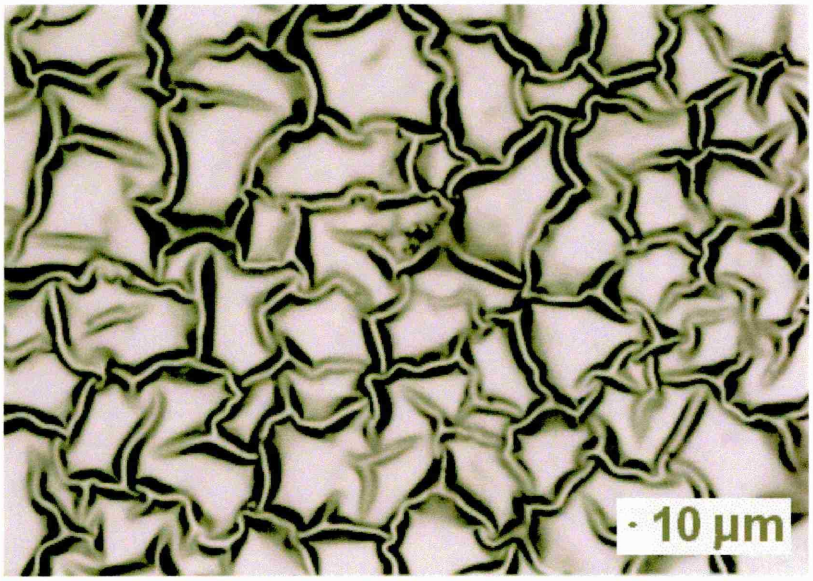

Figure 4.12: *Electrochemically deposited polypyrrole doped with $NaPF_6$.*

Deposition of polypyrrole doped with $NaPF_6$ onto ITO glass for [a] standard deposition time (120s) and [b] extended deposition time (30 mins) resulted in the formation of substantial, robust films with subjectively identical morphologies. The 'brain-skin' texture described previously was evident in all cases (Fig. 4.12), along with a complete lack of nodular morphology. Information regarding film growth mechanisms was not

available due to the vigorous growth observed; no areas of immature polymer were found on any sample.

It is therefore clear that dopant choice affects not only the electrical characteristics of polypyrrole, but also the growth mechanisms and morphologies of material produced by electrochemical means. The discussion points raised in this section are of great relevance to the direction of the work programme presented; many of the morphological characteristics noted are discussed at great length later in this chapter, the majority leading to peer-reviewed publication.

Sodium Benzene Sulfonate (Benzenesulfonic acid, Sodium Salt, $C_6H_5SO_3Na$) – Extended Deposition Time

The characteristic morphology of polypyrrole films doped with sodium benzene sulfonate (type-283 films) grown by electrochemical means from aqueous electrolyte is [a] illustrated at length in Ch. 3, and [b] discussed and modeled in this chapter. As stated previously, the morphologies of type-283 polypyrrole deposited onto gold electrodes and onto ITO glass slides are subjectively identical, both exhibiting a well developed nodular structure. The morphologies of 'extended deposition time' type-283 polypyrrole films were studied by the growth of type-283 polypyrrole films onto ITO glass at +1.00V vs SCE for 30 mins. The resultant films were substantial and robust, but were observed to delaminate during deposition. This delamination was observed to be the result of gas production at the polymer/substrate interface (as discussed at length in §4.3, and in Lemon and Haigh, '99 (a)); delamination was observed to result in the growth of a secondary polypyrrole film at the polymer/substrate interface, which, on further deposition and further gas production, was observed to delaminate. This process was observed to continue during the 30 minute deposition; the final structure is described by the author as resembling 'choux pastry', due to its many layers of thin material. Similar deposition conditions were used to confirm that this morphology was not reproduced during deposition onto gold microelectrodes; it was observed that gas production was significant, but did not lead to delamination. It is thought that this is the result of the superior adhesional characteristics of polypyrrole/gold over polypyrrole/ITO interfaces.

With reference to the performance of commercial polypyrrole devices in artificial olfactory systems, the discrepancy between the properties of films formed on gold substrates is thought to be of fundamental importance. However, it is assumed by the author that the morphological differences observed between 'extended deposition time' films (although of scientific interest) should not be of great concern during the production of commercial devices (which are routinely deposited for 120s).

4.2 *The Effects of Monomer Purity on Polypyrrole Morphology*

It is accepted that pyrrole monomer (and other nitrogen-containing aromatic compounds) are prone to contamination with oxidation products on exposure to air (Gilchrist, '85). The degradation of pyrrole is immediately apparent via a visible colour change; the yellow hue of pristine pyrrole is observed to rapidly degrade to deep brown on exposure to the atmosphere / ageing.

As a result of the rapid degradation of pyrrole monomer, the use of several techniques to purify pyrrole before experimental use have been reported in the literature. These include purification by passing through alumina (Hinton, '96; Cho *et.al.*, '00), vacuum distillation (Hulkanicki *et.al.*, '94; Biswas and Roy, '94), and double distillation (Michalska *et.al.*, '93; Saoudi *et.al.*, '00). Of greater importance are the number of authors who do not report the use of a purification regime prior to the use of as-supplied pyrrole.

In order to reduce the extent of characteristic degradation, the 'as-supplied' pyrrole monomer used during the work presented was stored in a sealed container under low light conditions in a domestic refrigerator. Further, the 'headspace' above the stored monomer was flushed with dry nitrogen before sealing to reduce the extent of oxidation product formation. Before use in the work presented, pyrrole monomer was purified by passing in series through two alumina filled columns (each of around 3ml volume) as referenced above (this technique was routinely used by Neotronics during the production of commercial devices). This technique resulted in the restoration of the characteristic yellow hue of pristine pyrrole; the brown hue of the as-supplied pyrrole was retained by the (pristine white) alumina used, and this discolouration was observed to gradually spread down the alumina columns during the purification of large volumes of pyrrole. Alumina columns were replaced before the progress of brown contamination neared the end of the second column. Purified monomer was used immediately when this was reasonably practicable.

Despite the reported use of a range of purification techniques, a systematic study of the effects of monomer purity on the morphology / structure of electrochemically deposited

polypyrrole has not been reported in the literature; such a study is reported here. The work outlined in this section has been published by the author (Lemon *et.al.*, '97; Lemon *et.al.*, '98). Both pieces of published work concentrate on the elucidation of the effects of monomer purity (studied by Gas Chromatography) on the morphology of electrochemically deposited polypyrrole (studied by SEM). All GC experimental work was carried out on the author's behalf by Dr. D. Douce and Dr. Natalka Szczur; assistance was given by the author.

4.2.1 The Assessment of the Efficacy of Pyrrole Purification Techniques

Pyrrole monomer was used in three purity states, [a] as supplied, [b] twice passed through alumina-filled columns (each of around 3ml volume), and [c] distilled under oxygen-free nitrogen at 23-24°C at a pressure of 2mmHg (Note: all distillation was carried out on the author's behalf by Dr. Natalka Szczur). All samples, regardless of purity state, were stored in low light conditions with an oxygen-free nitrogen headspace in a domestic refrigerator (at around 5°C) after purification.

The purity of the three monomer grades used were assessed by gas chromatography; GC-MSD (Mass Selective Detection) and GC-FID (Flame Ionisation Detection) were used for the analyses. GC-MSD was carried out using the hardware described in §2.2.4, comprising a Hewlett Packard model 5890 series II gas chromatograph with a Hewlett Packard 5971A series mass selective detector and a Restek RTX-5 column (5% diphenyl, 24m, 0.250mm i.d., 0.25μm film thickness) with helium as the carrier gas (1 ml/min flow). A solvent delay of 10 mins was used on the mass spectrometer with a m/z range of 30 to 400. The oven temperature was held at 40°C for 5 mins, then ramped to 280°C at 10°C min^{-1} and held for 10 mins, giving a total run time of 39 mins. All samples were injected splitless in a volume of 1μl. GC-FID was carried out using a Hewlett Packard model 5890 gas chromatograph with nitrogen as the carrier gas (1 ml/min). An RTX-5 Restek column was fitted (5% diphenyl, 30m, 0.250mm i.d., 0.25μ m film thickness). The oven temperature was held at 50°C for 1 min then ramped to 170°C at 10°C min^{-1} and then to 270°C at 30°C min^{-1} and held for 6 mins, giving a total run time of 22.3 mins. All samples were injected split in a ratio of 30:1. C_{20} at 20ppm was used as the internal standard (Peak #3, Fig. 4.13).

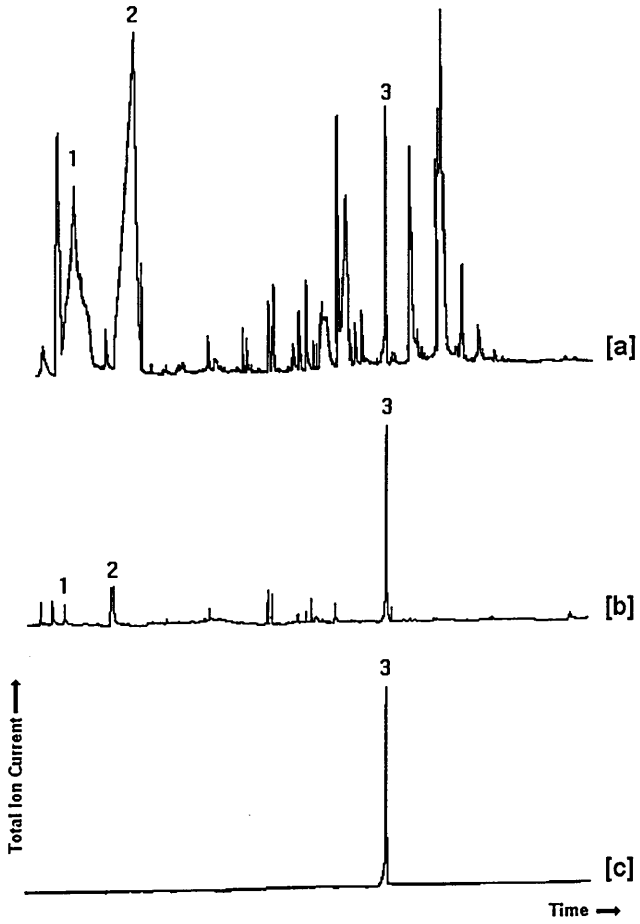

Figure 4.13: *Gas Chromatography traces of pyrrole monomer in three purity states, [a] as supplied, [b] after Al_2O_3 purification, and [c] after distillation. Peaks identified above represent a pair of isomeric oxidation products ([1] & [2]), which appear to dominate the 'as-supplied' monomer, and the internal standard [3]. Note: pyrrole peak not shown (off scale).*

Gas chromatography traces taken from the three monomer purity grades are shown in Fig. 4.13. Trace [a] is taken from as-supplied monomer (deep brown) and shows a range of very strong peaks. It is considered that the presence of the majority of the observed peaks is due to oxidation and / or polymerisation products of pyrrole, as shown in Fig. 4.14.

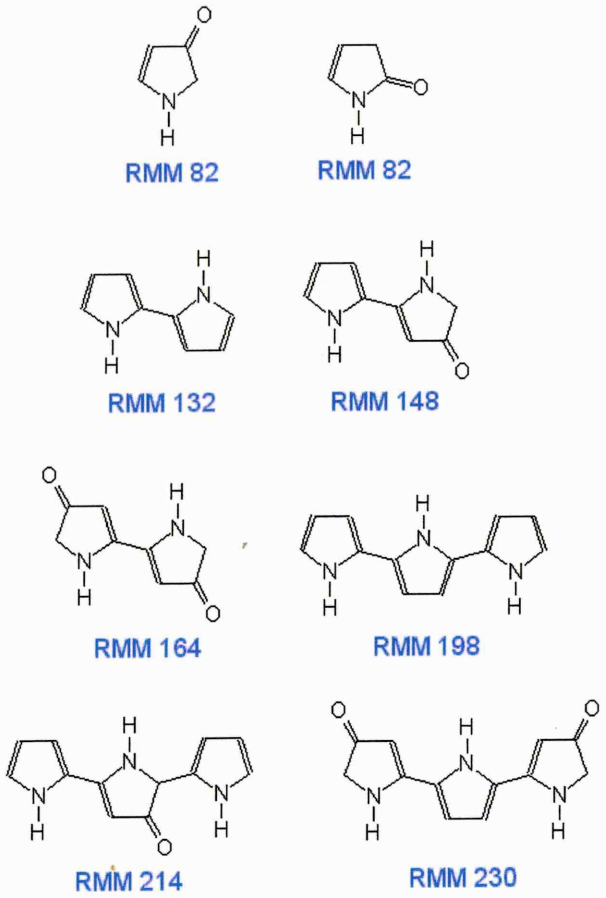

Figure 4.14: *Possible pyrrole impurity structures.*

As shown, it is considered that impurities are based on oxides of pyrrole (as RMM 82 above), short-chain polypyrrole (dimers and trimers, as RMM 132 and RMM 198), and oxides of short-chain polypyrrole. Gas chromatography traces of impure (as supplied) monomer (Fig. 4.13, trace [a]) were found to be consistently dominated by two peaks (labelled as 1 & 2) representing two isomers of oxidized pyrrole (both of RMM 82, as shown in Fig. 4.14). Traces taken after Al_2O_3 purification (Fig. 4.13, trace [b]) consistently showed a drastic reduction of the peak size corresponding to both RMM 82 groups; the magnitude of the reduction was consistent with the reduction of all other peaks, with the obvious exception of the 20ppm C_{20} internal standard used. Traces taken immediately after distillation (Fig. 4.13, trace [c]) show zero concentrations of both RMM 82 groups, to within the resolution of the instrument.

A comparative method was used which allowed assessment of the efficacy of each of the purification techniques employed. This involved comparison of the *areas* of impurity peaks against the (constant) peak area of the 20ppm C_{20} internal standard

used. Rather than producing quantitative concentration information, this technique allowed the relative concentrations of impurities to be expressed as an 'Impurity Peak Area Ratio'. The ratio of the C_{20} standard peak area to those of the RMM82 impurities (the two isomeric oxidation products shown in Fig. 4.14, pyrrol-2-en-4-one and pyrrole-2-en-5-one) was used as a measure of relative concentration, with C_{20} peak area normalized to unity to simplify interpretation. The Impurity Peak Area Ratios for both RMM82 impurities are given in Table 4.1.

PURIFICATION TECHNIQUE		IMPURITY PEAK AREA RATIO (vs MONOMER AGE)			
		0	30 mins	180 mins	3 days
None	Peak 1	1 : 9.12	---	---	---
	Peak 2	1 : 16.90	---	---	---
Alumina	Peak 1	1 : 0.11	1 : 0.12	1 : 0.18	1 : 5.07
	Peak 2	1 : 0.34	1 : 0.42	1 : 0.94	1 : 12.95
Distillation	Peak 1	1 : 0.00	1 : 0.00	1 : 0.03	---
	Peak 2	1 : 0.00	1 : 0.00	1 : 0.02	---

Note: the above ratios are between the GC internal standard peak area and impurity peak areas.

Table 4.1: *Pyrrole impurity level ratio against purification technique and post-purification period. Peaks 1 & 2 represent pyrrol-2-en-4-one and pyrrol-2-en-5-one respectively (the pair of isomeric oxidation products with RMM82 shown in Fig. 4.14).*

Data calculated from GC traces taken immediately after alumina purification (shown in Table 4.1) showed that a significantly high proportion of the impurities (oxidation products, oligomers and oxidized oligomers) found in as-supplied pyrrole were removed. Alumina purification resulted in considerable reductions in pyrrol-2-en-4-one and pyrrol-2-en-5-one (RMM 82, Fig. 4.14) peak area ratios from 1:9.12 to 1:0.11 and from 1:16.90 to 1:0.34 respectively. GC analyses were also carried out on samples of alumina-purified monomer, which had been allowed to age in standard laboratory conditions for 30 mins, 180 mins and 3 days. Table 4.1 shows that ageing results in a steady increase in the peak areas (and therefore the relative concentrations) of pyrrol-2-en-4-one and pyrrol-2-en-5-one. Impurity levels after 3 days were found to near those of as-supplied monomer.

Traces collected immediately after monomer distillation showed the presence of no impurities (to within the resolution of the instrument used). Similarly, monomer aged for 30 mins was found not to contain the impurities previously encountered. However, after ageing for 180 mins, small peaks corresponding to pyrrol-2-en-4-one and pyrrol-2-en-5-one were found.

Therefore, although distillation has been shown to be a far more effective method for the purification of pyrrole monomer than alumina-purification, it is considered that the low residual impurity levels found after alumina-purification are tolerable. Further, the simplicity of the alumina-purification technique allows purification to be carried out immediately prior to pyrrole use. Conversely, distillation is not considered by the author to be a practical method for *ad hoc* use, due to the considerable time required by the distillation procedure. The inconvenience of distillation, in the experience of the author, results in the production of large volumes of distilled pyrrole per distillation, therefore leading to storage of distilled pyrrole between uses. Time-dependent degradation of distilled pyrrole will increase impurity concentration to a level comparable to that found in alumina-purified pyrrole immediately after purification.

4.2.2 Film Preparation

In order to allow the systematic study of the morphological effects of monomer purity, several sets of MkIII Bass-Warwick devices were prepared using monomer of a range of purities and ages.

Substrates were prepared by thorough cleaning in propan-2-ol, followed by rapid drying under a high velocity jet of oxygen-free nitrogen. All electrolyte solutions were prepared immediately before film deposition, and consisted of standard type-283 materials (PPy/BSA(Na)/H_2O) with monomer and dopant at a standard 0.25M concentration.

Sets of five devices were prepared from discrete 50ml solutions with pyrrole monomer in the following states of purity: [a] purified by filtering through a pair of alumina-filled columns in series as described previously (clear with a pale yellow hue), [b] as-supplied without purification (mid brown in colour), [c] aged (>24 months old) without

purification (very deep brown/black in colour), and [d] freshly distilled as described previously (clear with a pale yellow hue). Depositions were carried out at +1.00V vs SCE in all cases.

Devices were rinsed and dried after deposition (as described in Ch. 2) and individual resistance measurements taken one hour after deposition using a calibrated DMM. The temporal stability of the devices formed was not studied, therefore no devices were 'withheld' from SEM analysis. All devices were studied by VANOX optical microscopy; SEM was used to verify the morphology of select devices where appropriate.

Equivalent polypyrrole films were deposited onto ITO coated glass slides, cut to allow deposition over an area of around 200mm^2; the dimensions of these films were tailored for XRD analysis, as reported in Ch. 5.

4.2.3 The Effects of Monomer Purity on Device Resistance

Mean resistance values were calculated for each of the four sets of devices produced in §4.2.2, as shown in Table 4.2; mean resistance values were shown to lie within one standard deviation of each other. It was therefore considered that the electrical resistances of devices formed using [a] alumina purified, [b] as-supplied, [c] aged, and [d] freshly distilled monomer were not significantly different.

FILM I.D.	MONOMER TREATMENT	MEAN RESISTANCE (Ω)	STANDARD DEVIATION (Ω)
AL2X	Al_2O_3 purified	21.3	2.4
ASX	As supplied	20.6	5.2
ANPX	Aged	21.2	15.4
FDX	Freshly distilled	18.2	1.9

Table 4.2: *The effects of monomer purification on device resistance.*

The lack of variation between the resistance characteristics of devices formed from each of the four monomer samples used may suggest that the impurities described in Fig. 4.14 are *not* incorporated into the advancing film during polymerisation. The

incorporation of dimers, trimers and more mature oligomers into the film is, of course, an integral part of the polymerisation process (as the oxidation potentials of di-, tri- and oligomers are lower than that of nascent pyrrole, as described in §1.5.4). Incorporation of such groups would therefore not be expected to be revealed by resistometry. However, the incorporation of oxides (such as RMM 82, 148, 164, 230 shown in Fig. 4.14) would certainly have a marked effect on the electrical characteristics of the films, including their conductivity. It is therefore postulated that pyrrole-based oxides are *not* incorporated into polypyrrole films during electrochemical deposition as described. If this *is* the case, then the growth dynamics of electrochemically deposited polypyrrole may vary with monomer oxide-based impurity level. It is postulated that the presence of oxide-based impurities in the electrolyte in the vicinity of the polymer growth face during electrochemical deposition may impede the advancement of the growth face (as relative concentrations of impurity may increase as 'pure' pyrrole is depleted). Further, it is logically assumed that the rates of diffusion of pyrrole *towards* the growth face, and the rate of diffusion of oxide-based impurities *away from* the growth face may affect the growth rate, and possibly the morphological characteristics, of polypyrrole films formed under these conditions. A study of the effects of monomer purity on film morphology is now presented, with reference made to the relevance of monomer and impurity diffusion.

4.2.4 Assessment of the Effects of Monomer Purity on Polypyrrole Morphology

VANOX optical microscopy was used to assess the morphological characteristics of the devices formed using the four monomer purity 'grades'. Devices formed from alumina-purified monomer were observed to display the nodular morphology characteristic of type-283 polypyrrole deposited in this manner; this is illustrated in Fig. 4.15, which is formed from two frames of VANOX thermal image prints, each taken using a subtly different focus (the focal modification between frames is one arbitrary unit, the difference between the maximum and minimum focal setting is one 'unit'). This method was used to allow visual representation of the 'depth' of texture (which represents the peak-to-valley (Rt) roughness of the surface under study, see references cited in HSE, '99).

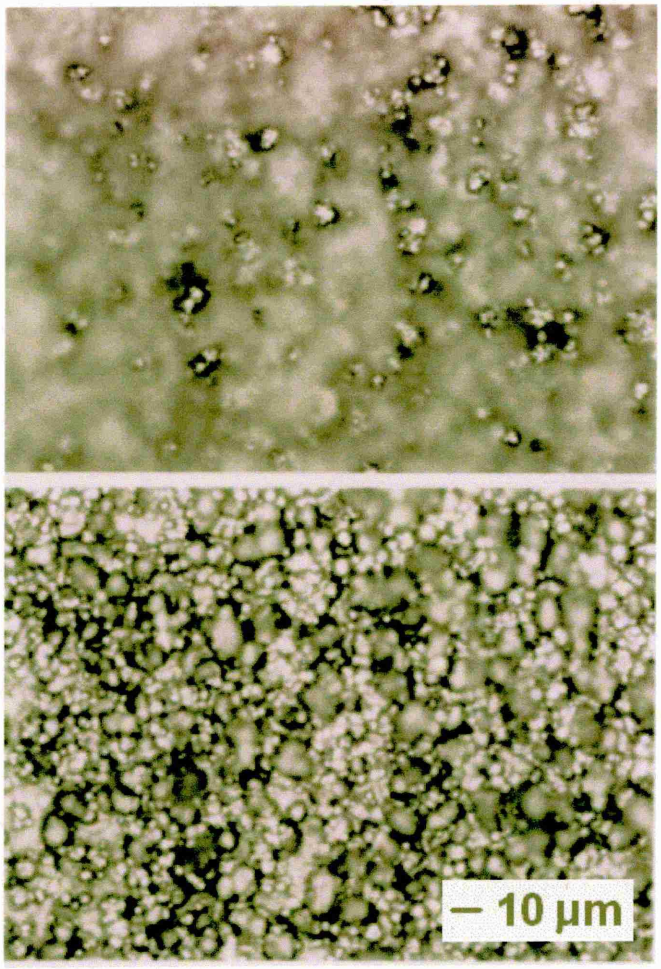

Figure 4.15: *VANOX optical micrographs of type-283 polypyrrole formed from alumina-filtered monomer, showing characteristic nodular morphology (see text for details).*

Devices formed from non-purified, as-supplied monomer were observed *not* to display the nodular morphology characteristic of type-283 polypyrrole. Rather, they were consistently and reproducibly observed to have fibrillar excrescences, grown outward from the substrate plane. This morphology is thought to be novel, and has been reported by the author in the scientific press via the two papers previously referenced in this section (similar polypyrrole morphology has been reported in passing in the literature (Kaynak, '97), but attempts to explain the formation of this morphology have been ambiguous).

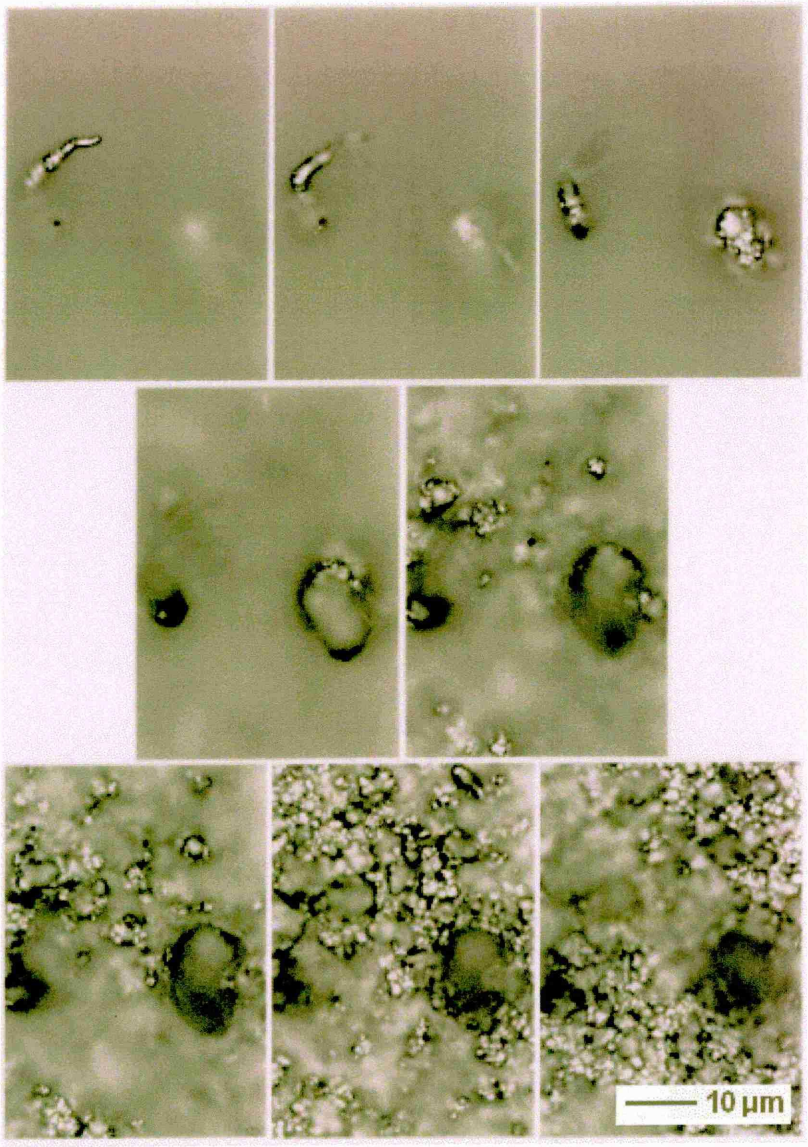

Figure 4.16: *VANOX optical micrographs of type-283 polypyrrole formed from non-purified, as-supplied monomer, showing novel tendrillar morphology (see text for details).*

This novel morphology, termed 'tendrillar' by the author, is illustrated in Fig. 4.16, which is formed from eight frames of VANOX thermal image prints, each taken as described above (the focal modification between frames is two arbitrary units, the difference between the maximum and minimum focal setting is fourteen 'units'; the surface roughness of the two films shown (Figs. 4.15 and 4.16) therefore differ by a factor of 14). Fig. 4.16 shows that several tendrils extend significantly from the polymer growth face; the formation mechanisms and potential effects of tendrillarity are discussed in §4.2.5.

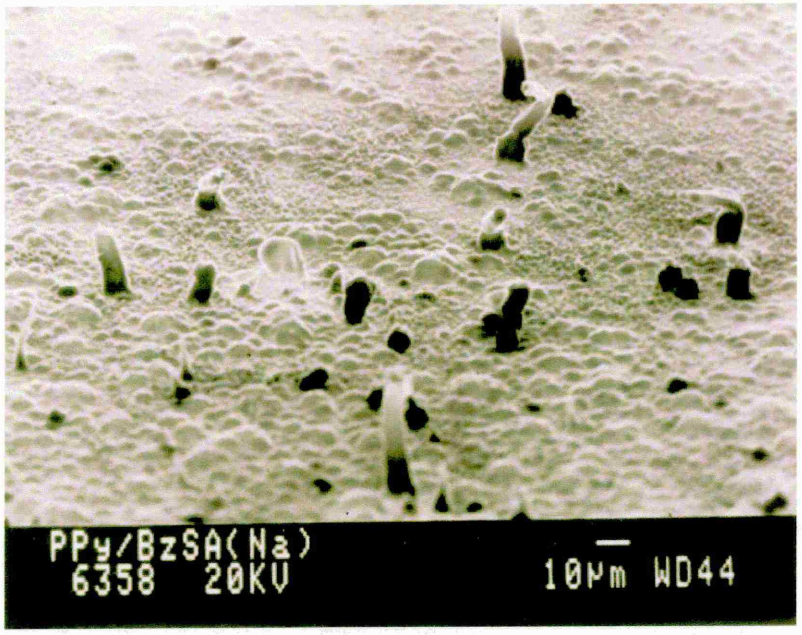

[a] ▲ [b] ▼

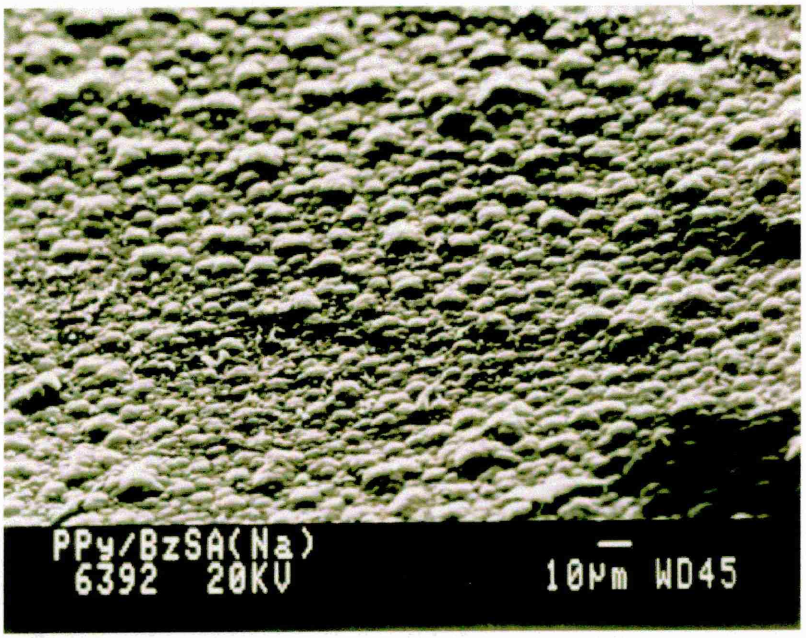

Figure 4.17: *Scanning electron micrographs of [a] tendrillar, and [b] nodular polypyrrole morphologies. Tendrillar polypyrrole, [a], was grown from non-purified, as-supplied monomer; nodular polypyrrole, [b], was grown from alumina-purified monomer.*

The morphologies of devices formed from non-purified, aged monomer were observed to be tendrillar, as per devices formed from as-supplied, non-purified monomer (as would be intuitively expected). Similarly, devices formed from distilled monomer were characteristically nodular.

Scanning electron micrographs of nodular and tendrillar polypyrrole morphologies (taken from purified and non-purified monomer respectively) are presented in Fig. 4.17 [a] and [b] (as presented in Lemon, Szczur and Haigh, '97 and Lemon, Szczur and Haigh, '98).

4.2.5 The Formation of Tendrillar Morphology

If tendril formation is related to monomer purity during electrochemical deposition, no pre-existing theories directly explain why this should be so. The considerations given in §4.2 suggest that the formation of tendrillar morphology may be related to the presence of impurities based on the oxides of both pyrrole and of pyrrole 'low oligomers' (i.e. dimers, trimers etc.) in the vicinity of the growth face during electrochemical deposition. As considered in this section, it is thought that the presence of solution impurities at the growth face may impede growth due to pyrrole depletion and a simultaneous increase in impurity concentration. This is thought to result from the sustained preferential incorporation of pyrrole monomer into the polymer matrix over the incorporation of oxide-based impurities, possibly leading to the exhaustion of available pyrrole. The diffusion rates of [a] pyrrole *towards* the growth face, and [b] oxide-based impurities *away from* the growth face is intuitively expected to affect the state of pyrrole depletion, *ergo* the growth rate, *ergo* the morphological characteristics of polypyrrole films formed under these conditions.

In pyrrole depletion conditions as described, it is known that impurities will diffuse away from the polymer growth face to areas of lower impurity concentration, due to the inherently high local impurity concentration. In conditions where the rate of 'outward diffusion' of impurities exceeds the rate of advancement of the polymer growth face, polymer growth may be sustained. However, if the converse is the case then sustained pyrrole depletion will occur resulting in a 'stalemate', which will drastically reduce the advancement of the growth face. This growth rate reduction may allow impurity diffusion *away* from the growth face along with pyrrole diffusion *towards* the growth face, so leading to the possible recovery of polymer growth.

The above considerations are strongly related to the formation of tendrillar morphology. If one considers the advancement of a *flat* growth face (with respect to the dimensions of the impurity (pyrrole depletion) layer), an increasing concentration of oxide-based impurities at the growth face and depletion of pyrrole monomer will greatly reduce growth rate. However, the advancement of an *uneven* growth face (again with respect to the dimensions of the impurity (pyrrole depletion) layer) will result in any protrusion peaks present on the film surface growing in an area of electrolyte with both lower oxide-based impurity concentration, and higher pyrrole concentration (as the protrusion 'breaks through' the impurity / depletion layer). This situation (illustrated in Fig. 4.18) may result in the concentration of polymer growth on growth face protrusions, leading to the formation of a morphology consisting of tendrillar excrescences, whose length is far greater than their diameter (similar in principle to growth resulting from constitutional supercooling, (Haigh, '01)).

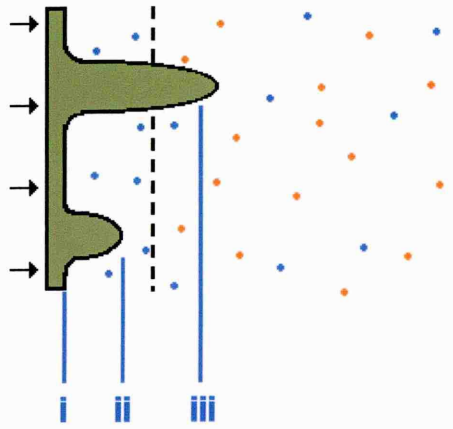

Figure 4.18: *Advancement of an uneven polypyrrole growth face [i] during electrochemical deposition. Continued growth results in the formation of an 'impurity (pyrrole depletion) layer' [ii], in which pyrrole (represented in red) concentration is depleted, and oxide-based impurity (represented in blue) concentration in increased. 'Protrusions' [iii] on the uneven growth face break through the impurity (pyrrole depletion) layer resulting in the unimpeded growth of polymer tendrillar excrescences.*

The situation described above is logically thought to be responsible for the formation of tendrillar polypyrrole morphology; this sits comfortably with the relationship between monomer impurity level and the presence of tendrils.

It is of note that similar kinetic models have been reported previously; it is considered that the growth dynamics described above are superficially similar to those reported by Keith and Padden ('63). The 'Theory of Keith and Padden' describes the crystallization of polymer spherulites (see §1.5.1), and so is far from *directly* applicable to the formation of (largely amorphous) polypyrrole. However, as is discussed below, the principle of growth face impurities leading to morphological modifications is equally applicable to both (ordered spherulites and disordered polypyrrole) systems. The Theory of Keith and Padden was originally formed to account for the development of radial crystalline units, which fill space during the formation of spherulitic crystallinity. The theory considers the growth of crystalline polymers during 'melt crystallisation' and is based on the theory that 'less easily crystallised' species will tend to amass at the 'growing interface'. Such a build up of impurities is thought to be eased by the diffusion of impurities away from the growing interface to areas of lower impurity concentration.

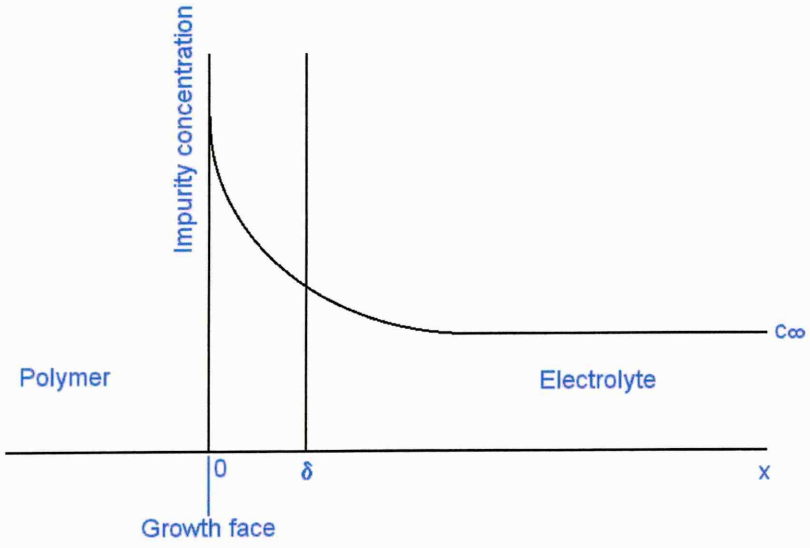

Figure 4.19: *Schematic representation of the relationship between impurity concentration and distance (x) from the growth interface. (Adapted from Keith and Padden, '63, and Bassett, '81)*

This model (which was, in turn, based on the Rutter and Chalmers model of growth of metals from impure melts) (see Bassett, '81) essentially concerned the build up of atactic, branched or entangled molecules (i.e. species less likely to crystallise) at the growth interface (the growth face) during the formation of highly crystalline material

(fundamentally dissimilar to the materials considered here). Crystal growth was then assumed to be dependent on the 'out-diffusion' of these species from the growth face area to areas of lesser 'impurity' concentration. The Keith and Padden model assumes that if an equilibrium concentration (c_∞) of 'impurities' (i.e. atactic, branched or entangled molecules) existed at all points forward of a growing crystal, then the distribution of impurities will vary as shown by Fig. 4.19 during crystal growth. The distance from the growth interface within which the concentration of impurities is increased is given as δ, where:

$$\delta = D / G$$

where D = the impurity diffusion coefficient

and G = the rate of advance of the surface (i.e. the growth rate)

The theory predicts that any protrusions on the growth face would be surrounded by media of lower impurity concentration than that at the growth face; as such, any protrusions would grow at a greater rate than the growth face. In such conditions (in a polymer melt during spherulite formation) a planar growth face would be inherently prone to break up into an array of protrusions. Again, it should be stressed that the Keith and Padden model directly concerns the formation of highly crystalline material from a polymer melt, and need not, therefore be wholly representative of the growth conditions described in this thesis. However, as stated previously, the principles of tendrillar growth are thought to be common.

In the Rutters and Chalmers model, it is assumed that breakdown into protuberant morphology will be short-lived, as impurity material will rapidly cool from the melt and therefore solidify. In the Keith and Padden model, the impurity material is far less able to solidify, resulting in the formation of far more advanced protrusions. During the formation of polypyrrole from a supporting electrolyte however, (which is considered by neither model), impurity material is unlikely to polymerise (as has been postulated in §4.2.1). Although empirical *proof* of the tendrillar polypyrrole growth theory presented in this section is inherently difficult, evidence which strongly supports the model is now presented.

4.2.6 *Verification of Tendrillar Morphology Formation Model*

Several studies were undertaken in order to verify the theory postulated in §4.2.5 (known hereafter as 'Tendrillar Morphology Theory'). These are as follows:

[a] MkIII Bass-Warwick Electrodes – Impure Monomer Growth Parameter Variation

Nine sets of type-283 polypyrrole devices (PPy/BSA(Na)/H_2O) were grown on MkIII Bass-Warwick electrodes using impure monomer (i.e. used as supplied without purification). A range of deposition parameters were used in order to investigate the formation of tendrillar morphology in varying conditions. The Tendrillar Morphology Theory predicts that an increase in polymer growth rate will increase tendrillarity level (assuming that the diffusion rates of pyrrole monomer and impurities remain constant). Devices were therefore deposited using a range of monomer concentrations and deposition potentials, the variation of both of which is known to affect growth rate. Deposition time was also varied in order to allow observation of the temporal effects of impurity layer formation.

Devices were formed using the conditions outlined in Table 4.3.

FILM I.D.	MONOMER CONC. (M)	DEPOSITION POTENTIAL (V)	DEPOSITION TIME (m)
KP1	0.25	1.0	5.0
KP2	0.25	1.0	2.0
KP3	0.25	3.0	5.0
KP4	0.50	1.0	5.0
KP5	0.50	1.0	2.0
KP6	0.50	2.0	5.0
KP7	0.50	2.0	2.0
KP8	0.25	2.0	5.0
KP9	0.25	2.0	2.0

Table 4.3: *Deposition parameters used during attempted verification of tendrillar morphology formation model.*

The morphological characteristics of the devices formed were studied by SEM and VANOX; it was noted that SEM analysis resulted in the production of micrographs of far higher resolution (this is due to the highly conductive nature of both film and substrate, which allowed SEM operation at 20kV accelerating voltage, so taking full advantage of the inherently high resolution of the instrument).

SEM examination of films grown for 120s (Fig. 4.21) and for 300s (Fig. 4.20) clearly show that [a] doubling deposition potential, or [b] doubling monomer concentration, both result in increases in film tendrillarity. This strongly supports the Tendrillar Morphology Theory, suggesting that an increase in the film growth rate consistently results in an increase in tendrillarity.

It should be considered that the conditions described above (i.e. increases in deposition potential or monomer concentration) may simply have resulted in the formation of thicker films, the morphologies of which may have been inherently more tendrillar than those of 'standard' thickness. However, the production of device sets 'KP1' and 'KP2' (Table 4.3), both of which were deposited at 'non-elevated' deposition potentials and monomer concentrations, but were grown for 2 mins and 5 mins respectively, showed morphologies of KP1 and KP2 films which were very similar to each other; both film types showing very similar tendrillarity levels. Further, KP1 films were significantly more nodular than KP2 films, thus supporting a film thickness increase. As stated, this increase in film thickness is noted not to result in an increase in tendrillarity level, so supporting the Tendrillar Morphology Theory.

KP6 (double KP1 deposition potential)

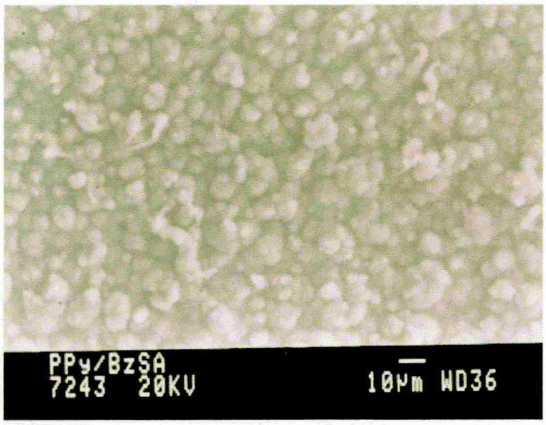

KP1

KP4 (double KP1 monomer concentration)

Figure 4.20: *Scanning electron micrographs of type-283 polypyrrole films grown for 300s under conditions described in Table 4.3. Increasing deposition potential and monomer concentration both result in the production of films with more (and more developed) tendrils.*

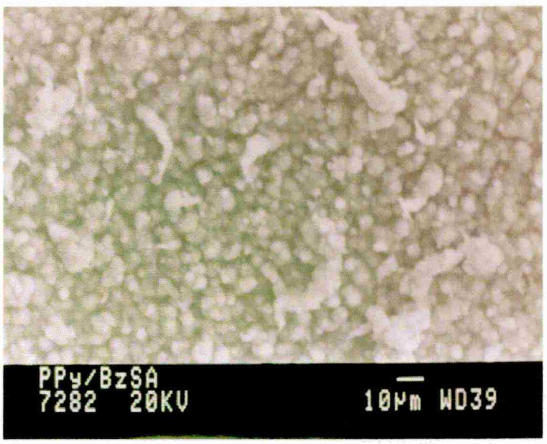

KP7 (double KP2 deposition potential)

KP2

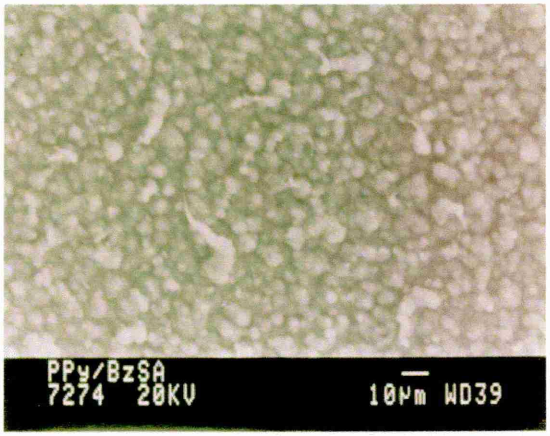

KP5 (double KP2 monomer concentration)

Figure 4.21: *Scanning electron micrographs of type-283 polypyrrole films grown for 120s under conditions described in Table 4.3. Increasing deposition potential and monomer concentration both result in the production of films with more (and more developed) tendrils.*

[b] 'Yoshi' Interdigital Electrodes – The Effects of Substrate Conductivity on Film Tendrillarity.

The effects of substrate conductivity on polypyrrole morphology were studied in order to support (or otherwise) the Tendrillar Morphology Theory. Two plates of Yoshi electrodes (see §A1.6) were identified, one having inherently high electrical conductivity, and one having inherently low conductivity (this was ascertained by 'dagging' one electrode per plate in order to short circuit the electrode, as described in §A1.7 (Fig. A1.16).

Two sets of five type-283 polypyrrole devices (PPy/BSA(Na)/H_2O) were prepared; dopant and (non-purified) monomer were used at 0.25M. Depositions were carried out for 15 mins (+30s @ 0V vs SCE) at +0.85V vs SCE.

Device set 'TIG' were deposited on Yoshi electrodes, previously shown to have standard (i.e. high) electrical conductivities when 'dagged' (i.e. shorted). Device set 'TIB' were deposited on low conductivity Yoshi electrodes. It was thought that the inherent high resistance of TIB electrodes relative to the low resistance nature of TIG electrodes would result in slower film formation due to an effective reduction in deposition potential.

The Tendrillar Morphology Theory predicts that devices from set TIB (which were postulated to grow more slowly than devices from set TIG) would result in the formation of a thinner δ layer (the region of increased impurity concentration and decreased pyrrole monomer concentration, as described in §4.2.5). This is predicted by consideration of the reduced growth face advancement rate (G), with a non-varying impurity diffusion coefficient (D).

Conversely, devices from set TIG were predicted to grow with a higher growth face advancement rate (G) than TIB devices, with a non-varying impurity diffusion coefficient (D), so resulting in a thicker δ layer. According to the theory presented,

therefore, TIB devices should be inherently less tendrillar than TIG devices (under suitable deposition conditions).

A selection of devices from set TIG and set TIB were examined by VANOX microscopy; results are shown in Fig. 4.22. It is immediately apparent that TIG devices (high growth face advancement rate, resulting in a thick δ layer) were far more tendrillar than TIB devices (reduced growth face advancement rate, resulting in a thinner δ layer). TIB devices were observed to be largely nodular; tendrillar texture was occasionally observed in localized areas. The study presented therefore strongly supports the Tendrillar Morphology Model, and provides a basis for morphological control of production electrodes.

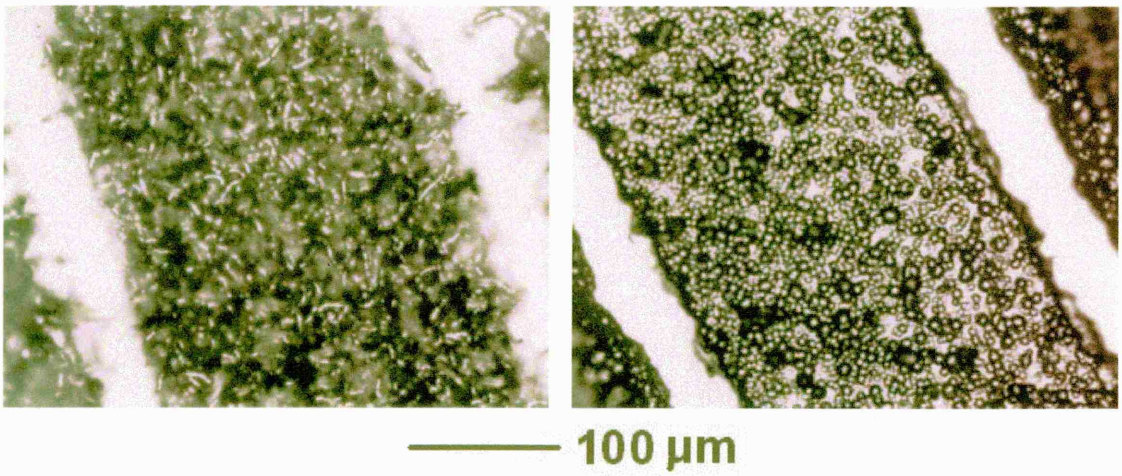

[a] [b]

Figure 4.22: *VANOX micrographs of type-283 polypyrrole films grown under [a] high, and [b] reduced growth face advancement rate.*

[c] The Effects of 'Non-Monomer' Electrolyte Solution Impurities Formed 'In-Situ'.

The deposition of type-283 polypyrrole films onto pristine Yoshi interdigitated microelectrodes has been discussed in §A1.7. It was found by the author that solder used to attach Yoshi electrodes to [a] bespoke 'Bass-Warwick' type, and [b] transistor header substrates (see Fig. A1.15) dissolved into the electrolyte solution during polymer deposition. This dissolution (which was studied by EDAX in Appendix 1) was observed by the electrolyte solution adopting a milky hue during deposition. EDAX analysis showed that films deposited from such milky electrolyte solutions were host to

detectable levels of tin, the primary constituent of the electrician's solder used. Given that the model presented previously is based around the build-up of contaminants at the growth face as opposed to the incorporation of contaminants into the film, the presence of tin *within* the films was not as intuitively expected. However, consideration of the macrostructural model reported by Ren and Pickup ('95), which describes polypyrrole aggregate enclosing discrete pockets of trapped electrolyte, justifies the presence of tin *within* the films.

Films deposited under standard conditions (produced and described in §A1.7, using Al_2O_3 filtered monomer) from lead/tin contaminated (milky) electrolyte were studied by SEM in order to ascertain the presence of a tendrillar morphology, as is predicted by the Tendrillar Morphology Theory. SEM micrographs are reproduced in Fig. 4.23. The high electrical conductivity of the materials under study, and the presence of very little insulating material on the transistor header substrates used allowed the use of a high SEM accelerating voltage with very little sample charging. The micrograph shown in Fig. 4.23 is therefore of a resolution rarely obtainable during the analysis of type-283 polypyrrole films.

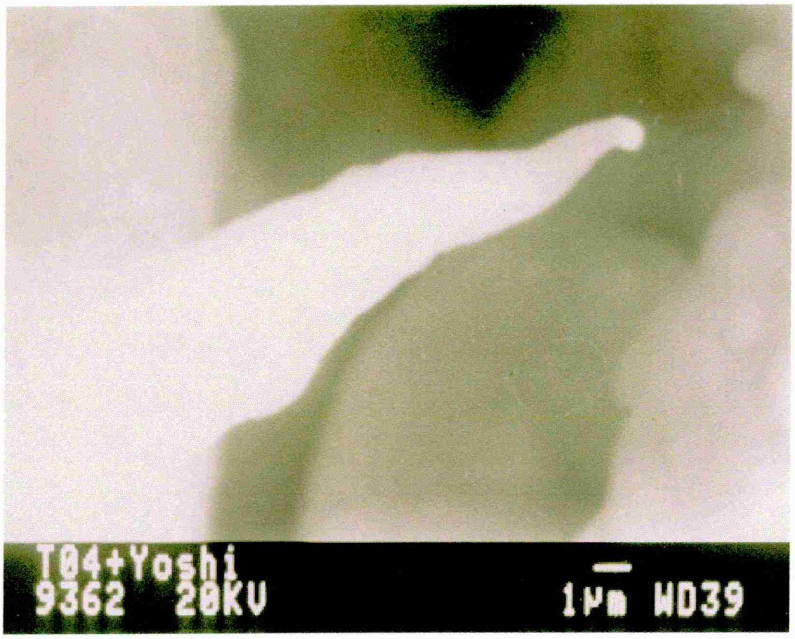

Figure 4.23: *Scanning Electron Micrograph of tendrillar type-283 polypyrrole formed during deposition from an electrolyte heavily contaminated with tin and lead.*

The presence of a finite concentration of tin in the electrolyte solution during electrochemical deposition of type-283 polypyrrole has therefore been shown to result in the production of tendrillar morphology. Devices formed under identical conditions, but soldered to transistor header substrates post-deposition (i.e. with all potential sources of lead and tin removed) were shown to be non-tendrillar (i.e. nodular). This gives further support to the Tendrillar Morphology Theory.

4.3 Nodular Morphology – the Influence of Electrolytic Gas Discharge

The work presented in this section concerns the relationship between the characteristic nodular morphology of electrochemically deposited polypyrrole and the production of gas at the interface between polymer and substrate during electrochemical deposition. Much of the work outlined has been published in the peer-reviewed press (see Lemon and Haigh, '99(a), "The Evolution of Nodular Polypyrrole Morphology During Aqueous Electrolytic Deposition: Influence of Electrolyte Gas Discharge").

The characteristic nodular morphology of electrochemically deposited polypyrrole (if deposited under suitable conditions using an appropriate dopant and supporting electrolyte) is often reported in the literature (see, for example, Stankovic et.al., '94; Herrasti and Ocón, '01), but few attempts have been made to explain the origins of this, or other, polypyrrole morphologies.

On first impression, it is tempting to assume that nodular morphology is the result of spherulitic polymer crystallinity (see §1.5.1 and Bassett, '81). This assumption is strengthened on examination of the immature stages of polypyrrole film formation; several seconds of type-283 polypyrrole deposition under standard conditions results in the formation of polymer 'sheaf' structures, as shown in Fig. 4.24 (reproduced from Lemon and Haigh, '99 (a)). These structures are highly reminiscent of those observed during the early stages of polymer spherulitic crystal growth (as shown in Fig. 1.25, §1.5.1).

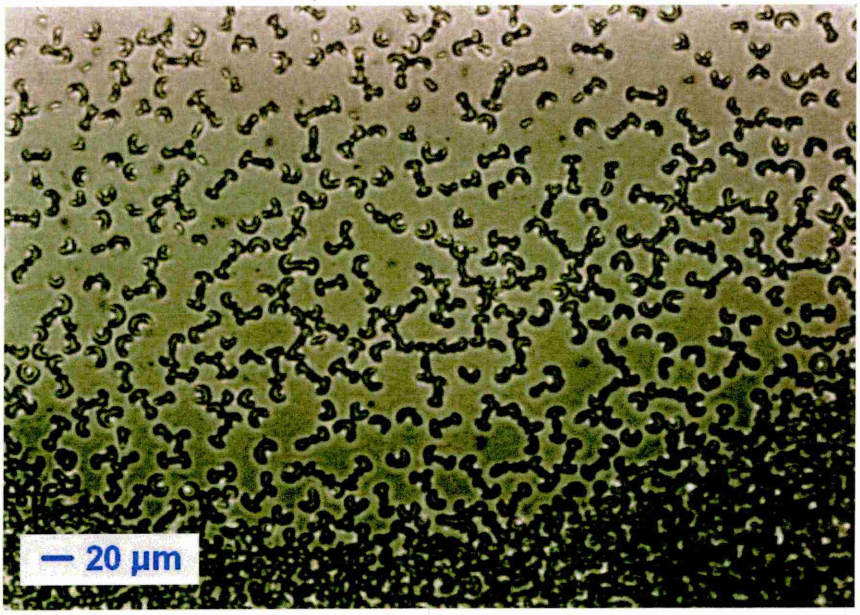

Figure 4.24: *VANOX micrograph of the early stages of immature polypyrrole film formation, showing the presence of 'sheaf' structures, characteristic of immature spherulitic crystal formation.*

4.3.1 Crossed-Polar Optical Microscopy

Examination of thin, but mature polypyrrole films under standard conditions (type-283 polypyrrole (PPy/BSA(Na)/H_2O); dopant and monomer at 0.25M concentration; deposition potential of +0.85V vs SCE for 120s (+30s @ 0V vs SCE)) by crossed-polar optical microscopy (using a Vickers Metallurgical Microscope in crossed-polar transmission mode) strongly suggested against the presence of spherulitic crystallinity. The well-accepted 'Maltese Cross', which is routinely displayed by spherulitic crystalline arrays (Keith and Paden, '63; Keller, '59) when viewed in crossed-polar mode was not observed at any time. This strongly suggests against the presence of spherulitic crystallinity.

4.3.2 θ–2θ X-Ray Diffraction

Examination of polypyrrole films formed under standard conditions (see §4.3.1) by θ–2θ X-Ray Diffractometry (see §2.2.2) deposited onto ITO glass electrodes consistently suggests the presence of very low levels of order within the (typically tens of microns thick) polypyrrole films.

(Note: low levels of order were observed despite the routine presence of sharp peaks on diffractograms. The origins of these peaks are discussed in §4.4. It is thought that the large 'amorphous' peak / plateau shown in Fig. 4.25 may be formed from a range of discrete peaks, the origins of which may stem from longer-range order than the $2\theta \approx 24°$ peak routinely observed (see §5.2). The observation of such order may represent the regular positioning of 'pockets' within the polymer matrix, as discussed in §4.3.5.).

A typical θ–2θ XRD trace is shown in Fig. 4.25 [a]; the trace from the same film is presented in Fig. 4.25 [b] after the subtraction of substrate information (see §5.1.1).

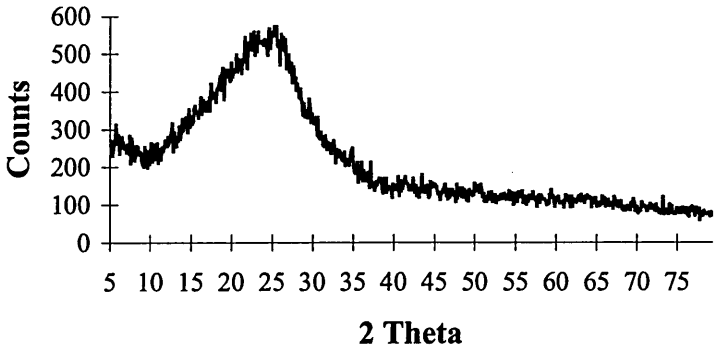

[a]

[b]

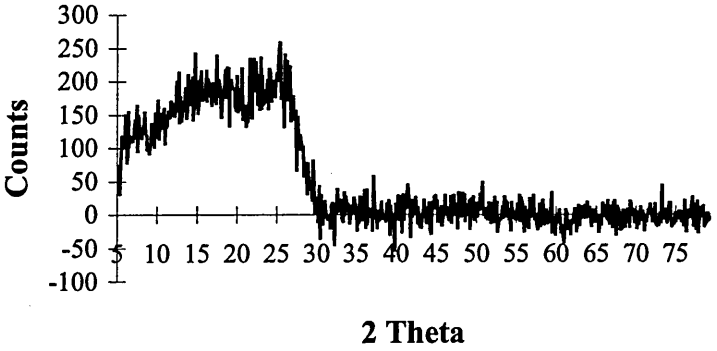

Figure 4.25: *X-Ray diffraction traces of type-283 polypyrrole films deposited under standard conditions on to ITO glass electrodes (note: films soaked and dried as described in §5.1 to remove recrystallised dopant material).*

The traces shown in Fig. 4.25 clearly show the presence of very low levels of crystallinity (similar low order levels have been reported previously in the literature, see Warren *et.al.*, '89; Mitchell, '86; Kiani and Mitchell, '92; Rikukawa and Rubner, '94). The low order level suggested by the traces shown in Fig. 4.25 is *not* considered to be at all consistent with the presence of extensive spherulitic crystallinity. The lack of sharp features (which would be expected from spherulitic material) on the traces collected from type-283 material deposited under a range of conditions (see Ch.5) suggest widespread disorder; the origins of the features observed are discussed in 5.2. XRD information therefore strongly suggests against the presence of spherulitic crystallinity.

Empirical evidence reported in §4.3.1 and §4.3.2 strongly suggests that electrochemically deposited type-283 polypyrrole is not only non-spherulitic, but also non-crystalline. Evidence is now presented which supports the hypothesis that the oft-reported nodular polypyrrole morphology is the result of the generation of gas at the working electrode (i.e. the interface between polymer and substrate) during electrochemical deposition.

4.3.3 Working Electrode Gas Generation

From an electrolyte solution containing water, sodium benzene sulfonate (benzene sulfonic acid, sodium salt) and pyrrole, the application of a deposition potential to the working electrode should result in the generation of gaseous oxygen. The process by which this might occur is;

$$2C_6H_5SO_3^- \rightarrow 2C_6H_5SO_3^{\bullet} + 2e^-$$

$$2C_6H_5SO_3^{\bullet} + 2H_2O \rightarrow 2C_6H_5SO_3H + 2OH^{\bullet}$$

$$2OH^{\bullet} \rightarrow H_2O + [O]$$

$$2[O] \rightarrow O_2$$

A simplified version of the above (Lemon and Haigh, '99(a)) is the simple H_2O electrolysis anode reaction:

$$4OH^- \rightarrow 2H_2O + O_2 + 4e^-$$

Note that dopant is not used up in the reaction and so acts as a catalyst by allowing current to flow. The potential required for this process is, at the pH used, similar to that used for polypyrrole deposition under standard conditions, so supporting the validity of the process presented.

4.3.4 *High Potential Gas Generation Verification*

The system of gas generation presented in §4.3.3 suggests the existence of several pre-requisites for the production of gas at the working electrode under the application of a deposition potential. A systematic study of the effects of the removal of key constituents of the electrolyte solution used for type 283-polypyrrole deposition is presented in §4.3.6; in this section the effects of deposition potential on gas generation are investigated. The primary aim of the work presented was not to study these effects in depth. Rather, it was intended to investigate the possibility that, under suitable conditions, the level of gas production would be directly related to deposition potential. Although it was not necessarily considered that deposition potential was the limiting factor in gas production during deposition under 'standard' conditions, logic suggested that deposition potential increase over an unknown threshold would allow confirmation (or otherwise) of the hypothesis of working electrode gas production. Films were therefore deposited using an increased deposition potential in order to increase the generation of gas at the working electrode.

A set of type-283 polypyrrole films (PPy/BSA(Na)/H_2O/Au) were deposited under standard conditions (monomer and dopant at 0.25M). However, a deposition potential of +5.00V vs SCE was used (standard deposition potential = +0.85V); this raised potential was applied for 300s (+30s @0V vs SCE).

Visual monitoring of the dynamics of film formation showed the following (in chronological order):

1 instant blackening of the working electrode due to polypyrrole formation,
2 film maturation,
3 visual observation of film 'swelling', originating at the outer edges of the working electrode, but slowly moving to include more central positions,
4 'rupture' of the main 'swell-points', along with the regular release of small gas bubbles.

SEM studies of the morphologies produced during the film swelling (stage 3, above) are presented in Fig. 4.26 [a] and [b] (please note, deposition of the films shown was halted

before film rupture). Swelling of gas pockets within the polymer films under study is considered by the authors to categorically support the hypothesis of gas generation at the working electrode during the high potential electrochemical deposition of polypyrrole. The formation of pockets within the film is thought to be the result of gas production at a higher rate than the rate of gas diffusion through the polymer film.

Further, a typical 'rupture site' (as described in stage 4, above) is presented in Fig. 4.27. It is considered that the presence of rupture sites throughout the films produced, and the visual observation of the regular and frequent release of gas bubbles from such sites during high-potential deposition, gives further firm support to the hypothesis of working electrode gas production. It is of particular interest to note that, since the publication of the above information by the author in Lemon and Haigh '99 (a), the observation of similar structures to those shown in Fig. 4.27 has been reported by Herrasti and Ocón ('01). However, the work presented (concerned with the use of polypyrrole as a corrosion inhibitor) made no attempt to explain the origins of the observed structure.

The morphologies shown in Fig. 4.26 [a] and [b] may suggest the formation of gas at several preferred sites on the working electrode. However, consideration of the sheer volume of gas produced under high deposition potential (in comparison to the volume of polymer deposited) suggests that gas may be produced at a large number of working electrode sites. Small gas pockets formed in areas of local polymer/substrate delamination are then thought to coalesce, forming large areas of film detachment. The level of detachment of the films shown in Fig. 4.26 was supported by the extremely high (kΩ) and temporally unstable electrical resistance of these devices.

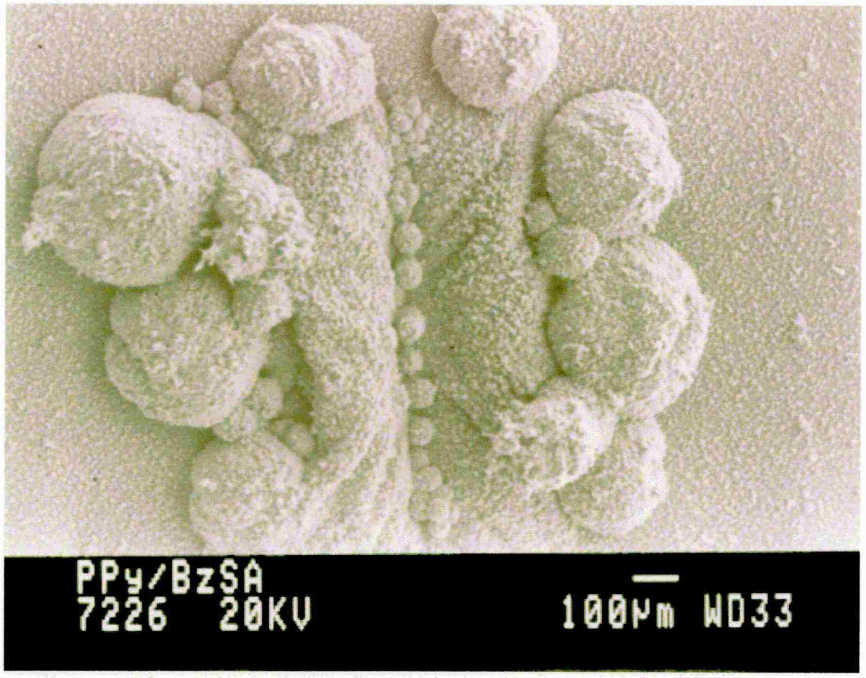

[a]

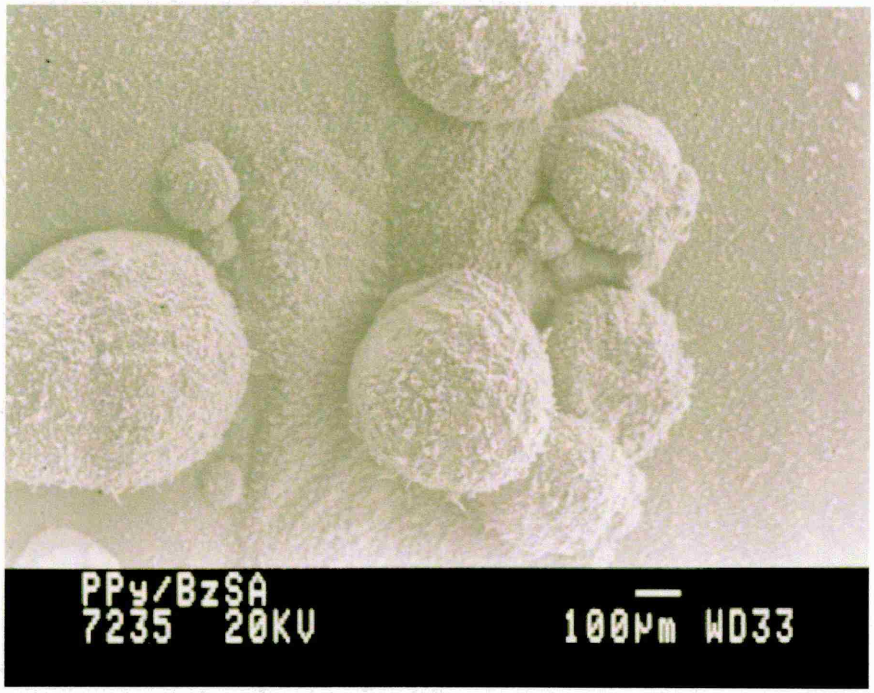

[b]

Figure 4.26: *SEM micrographs of the film morphology produced during film 'swelling' during deposition at +5.00V vs SCE. Subsequent 'rupture' shows film swelling to be due to internal gas production.*

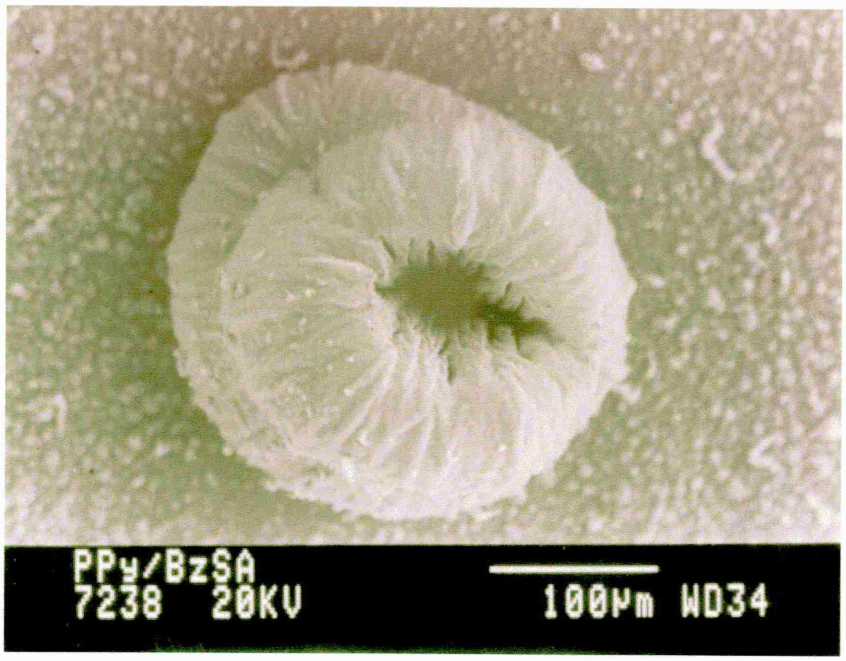

Figure 4.27: *SEM micrograph of a polypyrrole 'rupture site'. Such sites are observed to be host to regular and frequent release of small gas bubbles during deposition at +5.00V vs SCE.*

4.3.5 Standard Potential Gas Generation Verification

The study presented in §4.3.4 was engineered to over-emphasize the effects of working electrode gas production under high potential, forced deposition. It is postulated, however, that working electrode gas production also occurs at the potentials used for deposition under 'normal' conditions. Further, it is thought that gas production is responsible for the formation of nodular polypyrrole morphology.

In order to investigate this, a range of polypyrrole films were deposited onto ITO glass electrodes under standard conditions. Films were carefully detached from substrates using water / nitrogen jets whilst applying a shear force via tweezers (note areas of tweezer contact were marked with ink so as not to be included in any subsequent microscopic examination). The undersides of the films produced were examined at a glancing angle by SEM, as illustrated in Fig. 4.28.

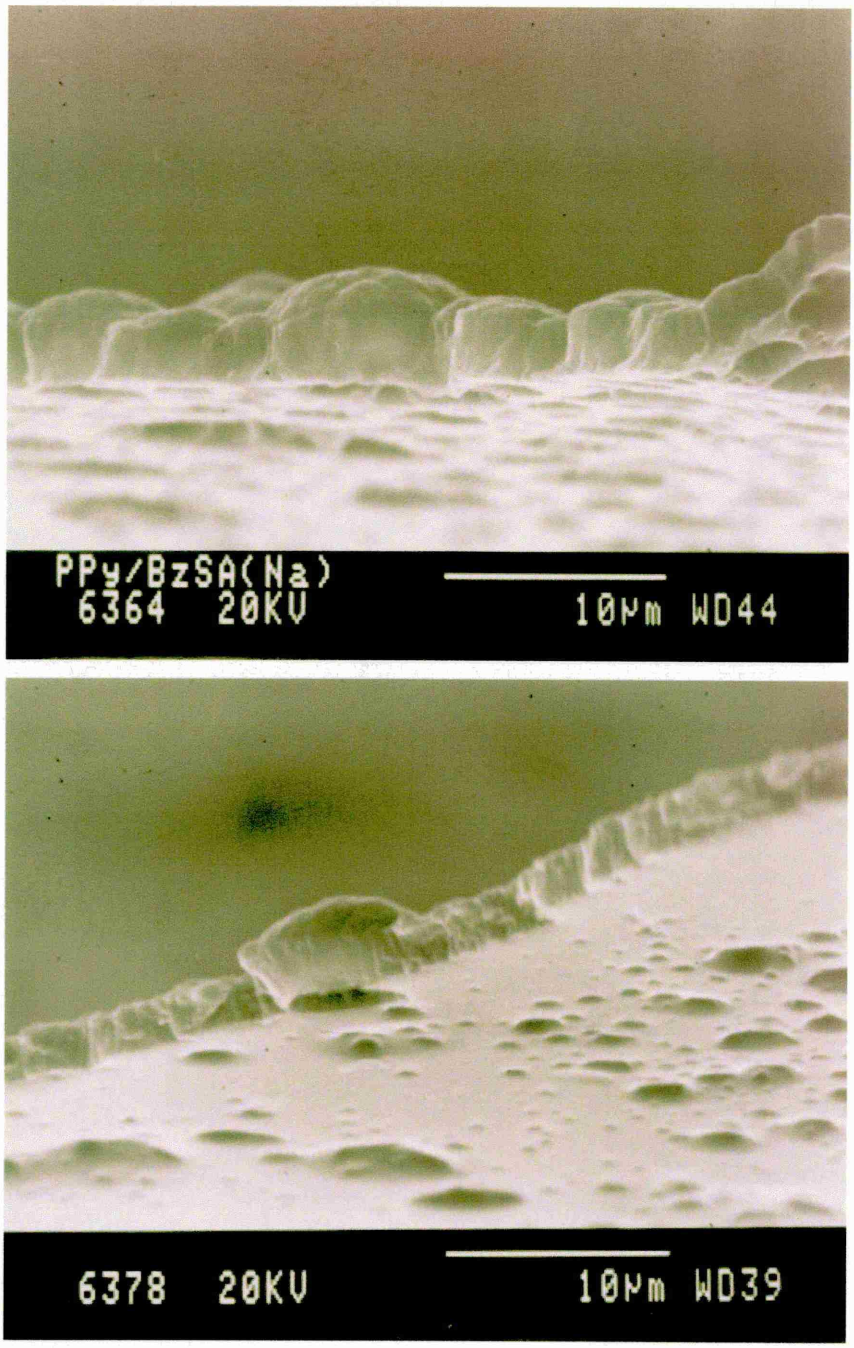

Figure 4.28: *Glancing angle SEM micrographs of the undersides of type-283 polypyrrole films after detachment from ITO glass substrates.*

Study of the films shown in Fig. 4.28 clearly demonstrates the presence of small voids on the underside of the films; these voids are routinely found to be positioned directly under individual nodules on the upper surface of the films. It is concluded that voids are formed as the result of the production of gas at the working electrode (i.e. the interface between ITO and polymer) during electrochemical deposition. However, it was also considered possible that the voids observed may have been the result of either a

characteristic morphology of the substrate used, or the adhesion of sections of polymer to the substrate during detachment. Examination of 'post-detachment' substrates showed that neither of these were the case.

As stated in §4.3.4, film detachment resulting from working electrode gas production (under high potential deposition) was thought to have been responsible for the unusually high electrical resistance of these devices. Similarly, it is considered by the author that the production of small volumes of gas at the working electrode during deposition under standard conditions (used for the production of commercial devices) may result in significant detachment of the polymer/substrate interface, so resulting in modifications to the electrical characteristics of commercial (and research grade) devices. This is demonstrated by the appearance of the underside of the films shown in Fig. 4.28, both of which suggest significantly reduced polymer/substrate (i.e. polymer/electrode) contact as a result of gas production. It is assumed that the position and severity of the detachment due to gas production may affect the reproducibility and temporal stability of commercial and research grade devices.

In order to investigate any potential improvement in the electrical characteristics (and modifications to film morphology) produced by the reduction or elimination of working electrode gas production, it would be necessary to fundamentally modify the deposition media or deposition parameters used. Such a study was not attempted, as it is accepted that even subtle modifications to deposition media or parameters can drastically affect film morphology and electrical characteristics (see Ch. 3).

4.3.6 The Effects of Electrolyte Solution Modification on Gas Production

The formula presented in §4.3.3 suggests that the presence of (ionic) benzene sulfonic acid (sodium salt) results in the catalysis of gas production. A systematic study of the effects of the removal of key constituents of the electrolyte solution used for type 283-polypyrrole deposition has been carried out; particular attention has been paid to the effects of constituent removal on gas production.

A selection of type-283 polypyrrole electrolyte solutions were produced, all based on the standard PPy/BSA(Na)/H_2O configuration. Sets of five devices were grown under standard conditions (0.25M monomer, 0.25M dopant) at +5.00V vs SCE for 300s (+30s @ 0V vs SCE); device sets were grown from solutions deprived from dopant and/or monomer as described in Table 4.4. Observations were made regarding [a] the discolouration of the device active area (i.e. polypyrrole layer production), and [b] the visual production of gas at the working electrode (i.e. the device active area) during device deposition.

SENSOR I.D.	PYRROLE	BSA(Na)	5.00V	FILM PRODUCED?	WORKING ELECTRODE GAS PRODUCTION?
GAS1	✓	✓	✓	✓	✓
GAS2	✓	✗	✓	✓	✗[3]
GAS3	✗	✗	✓	✗	✗[1]
GAS4	✗	✓	✓	✓*	✓[2]

Table 4.4: *Film production and working electrode gas production during deposition from incomplete electrolyte solutions. (* some discolouration of the working electrode on the application of deposition potential;* **not** *a polypyrrole film).*

As shown in Table 4.4, deprivation of the electrolyte solution of key constituents has a profound effect on both the production of polymer films (although active area discolouration does not necessarily denote polymer layer production), and the production of gas at the working electrode upon the application of a deposition potential. The salient point arising from this study is that the presence of BSA(Na) in the electrolyte solution appears to be fundamental for working electrode gas production. This supports the suggestion that the presence of BSA(Na) leads to the catalysis of gas production, *ergo* supporting the formula presented in §4.3.3.

Several other interesting points were noted during the study presented, these were as follows (as marked on Table 4.4):

[1] The failure to produce visually detectable volumes of gas at the working electrode in the absence of both pyrrole and BSA(Na) supports the hypothesis that gas generation is *not* the result of either the release of dissolved gas, or of (uncatalysed) water disassociation.

[2] The production of visually detectable volumes of gas during deposition in the absence of pyrrole but in the presence of BSA(Na) supports the model presented in §4.3.3 by suggesting that water disassociation is possible at the potential used *in the presence of a suitable ionic catalyst.*

[3] The production of a poor polymer film during deposition in the absence of BSA(Na) but the presence of pyrrole was as expected. Further, the nodule-free morphology of the film produced (see Fig. 4.29) supports the hypothesis of gas production being responsible for nodular morphology.

Further support for the theory presented has been given by Stankovic *et.al.* ('94), who reported that polypyrrole deposition from non-aqueous solutions (acetonitrile and propylene carbonate) led to the production of films with flat, nodule-free, wrinkled morphologies, which the authors termed 'brain-skin'. Although not considered in depth by Stankovic *et.al.*, it is considered by the authors that the absence of water in the electrolyte solution was responsible for the lack of nodular morphology; this was supported by the production of nodular morphology (termed a 'cauliflower' morphology by the authors) during deposition under similar conditions after the addition of water into the electrolyte solution.

The studies presented above show that the removal of the (strongly ionic) sodium benzene sulfonate from the electrolyte solution (or indeed the substitution of the supporting electrolyte with non-aqueous media) results in a loss of film nodularity. It is strongly suggested that this is the result of a lack of gas production at the interface between the polymer film and the substrate. The effects of the substitution of the ionic dopant used for type-283 films on film morphology have also been studied; results are presented below.

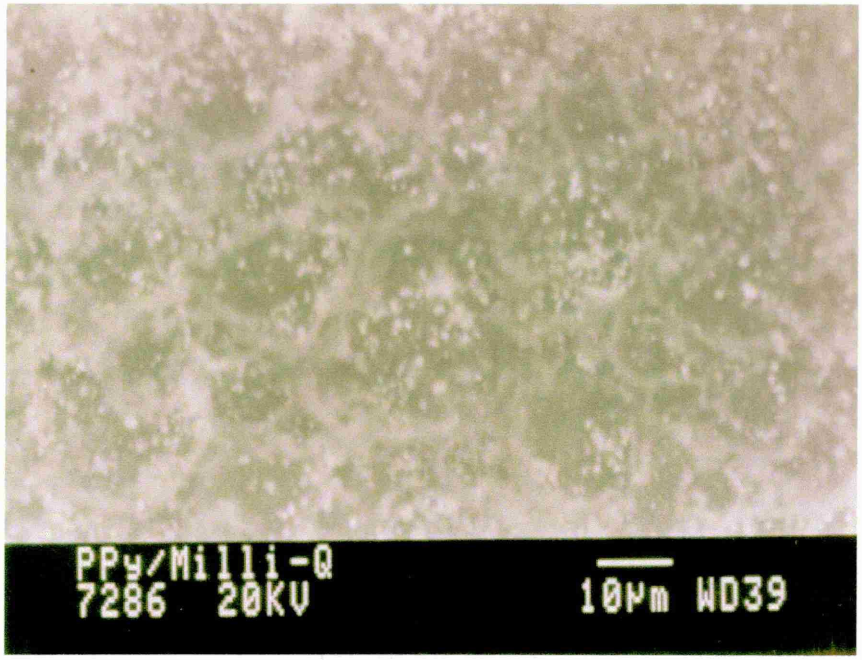

Figure 4.29: *Nodule-free polypyrrole morphology produced during deposition from dopant-free electrolyte solution.*

A selection of pyrrole-based electrolyte solutions were produced as described previously (PPy/BSA(Na)/H_2O/Au). However, benzenesulfonic acid, sodium salt dopant was replaced with:

[a] 1-butanesulfonic acid, sodium salt,

[b] benzenesulfonic acid, potassium salt,

[c] 1-hexanesulfonic acid, sodium salt, and

[d] sodium hexafluorophosphate.

Sets of five devices were grown using each of the above dopants under standard conditions (0.25M monomer, 0.25M dopant) at +3.00V vs SCE for 300s (+30s @ 0V vs SCE). Observations were made regarding the evolution of visually detectable levels of gas (as would be expected for type-283 films at the potential used).

It was noted during deposition that substitution of benzenesulfonic acid, sodium salt dopant with other sulfonic acid dopants (all strongly ionic, [a], [b] and [c]) resulted in the production of detectable volumes of gas at the working electrode (similar levels of gas production were noted during previous studies of the use of $NaClO_4$ dopant, see §4.1.6). However, the substitution of benzenesulfonic acid, sodium salt dopant with sodium hexafluorophosphate (weakly ionic) resulted in no visible gas production.

Examination by optical microscopy showed a lack of nodular morphology on sodium hexafluorophosphate doped films. A typical sodium hexafluorophosphate doped film morphology is shown in Fig. 4.12, §4.1.6.

The observed lack of nodularity supports the hypothesis that working electrode gas generation (as described in §4.3.3) is dependent not on the presence of sodium benzene sulfonate, but on the presence of a suitable, highly ionic dopant in the electrolyte solution. It has been shown that the presence of highly ionic dopant catalyses the disassociation of the aqueous electrolyte.

4.3.7 Film Detachment Modelling

The extreme level of gas production illustrated in Fig. 4.26 (§4.3.4) is observed to result in widespread polymer / substrate detachment. Although research-grade and commercial devices would not be expected to be host to this level of gas production (and therefore this level of film detachment), the mechanism of film detachment is considered to be of great importance to device properties; evidence supporting models of film detachment have therefore been considered.

If it is assumed that gas is produced at the film / substrate interface (as is supported by the evidence presented previously), then it is considered logical to assume that the substrate sites of preferred nucleation for polypyrrole growth will act as preferred sites for gas production (provided that such sites are points of preferred electron transfer between the electrolyte solution and substrate), as illustrated in Fig. 4.30.

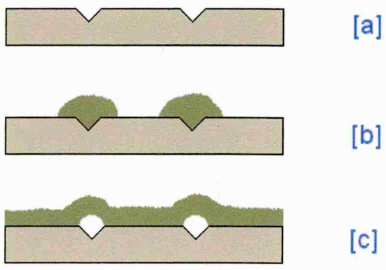

Figure 4.30: *Schematic illustration of the nucleation of polypyrrole [b] and the subsequent nucleation of disassociated gas [c] at substrate preferred nucleation sites [a].*

Examination of 'post-detachment' substrates from the ITO layers used during the study presented in §4.3.5 (as shown in Fig. 4.31) supports the model illustrated in Fig. 4.30, showing collections of lightly coloured circular areas, surrounded by darker areas. It is suggested that lightly coloured, circular areas correspond with areas of gas production (and hence with nodule position).

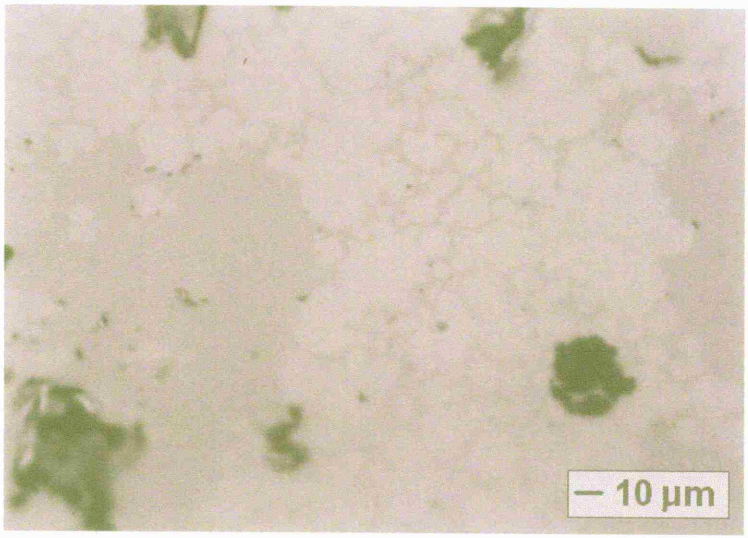

Figure 4.31: *VANOX optical micrograph of ITO substrate after detachment of polypyrrole film.*

Further evidence to support the ideas presented above (the nucleation of polymer and production of gas at common sites) has been discussed previously (see §3.6.1). It is considered that the production of gas at the interface between polymer film and substrate may occur preferentially at key substrate 'nucleation sites', such as scratches or other defects (Bassett, '81). As discussed in §3.6.1, nucleation on substrate surface features may result in nodular 'patterns'; this is strongly supported by the infrequent observation of nodular patterns, as illustrated in Fig. 3.18 (§3.6.1).

4.3.8 Nodular Growth on Insulating Substrate Areas

Very early work by the author (as reported in Lemon, '96, "Report for Transfer of Registration from M.Phil. to Ph.D.") presented evidence which suggested that the growth of nodules over insulating substrate areas was possible.

Before consideration of the possibility of working electrode gas production, it was argued that this may be the result of the ability of free-radicals to deposit on areas from which their charge may be conducted; this hypothesis was linked to the assumption that nodular morphology was the result of spherulitic crystallinity. Despite these assumptions, the possibility of a simple "bubble-growth" was considered in passing.

The models presented throughout §4.3 strongly support the hypothesis that nodular morphology results from the generation of gas at the working electrode during electrochemical deposition. The observation of such nodular growth over insulating areas may, on first impression, suggest against this hypothesis (Fig. 4.6, §4.1.4). However, consideration of the growth models presented previously (see, for example, §4.1.3) suggest the rapid formation of a planar, 'Stage 1' polymer layer on commencement of deposition; this is supported by the immediate 'blackening' of conducting areas of the working electrode on the application of a deposition potential under normal conditions (examination of the morphology of such immature layers by SEM shows them not to have resolvable surface texture, so supporting their immaturity).

Further, it has been reported by the author that polypyrrole grown under standard conditions is routinely observed to 'spread' from conducting areas of the working electrode to insulating areas, as illustrated by the 'Frame Effect' (as discussed in §3.5, see Fig. 3.14).

The rapid formation of a thin layer of electrically conductive type-283 polypyrrole on application of a deposition potential sheds light on the growth mechanisms thought to be involved during the formation of nodules over insulating substrates. The presence of a layer of polypyrrole of suitable electrical conductivity allows a conducting pathway to the 'active' areas of the working electrode. The potential applied to the working electrode may be conducted by the polypyrrole layer to areas over non-conducting substrate, such as the 10µm insulating gap (see Fig. 4.6, §4.1.4) and insulator surrounding the working electrode active area (as is the case with the 'Frame Effect').

The inherent resistivity of the polypyrrole layer will act to diminish the potential with distance from conducting substrate areas, so limiting the effective area of insulator over which deposition can take place. In conditions such as described above, if the potential at a position over an insulating substrate is sufficient to support the polymerisation process (i.e. to oxidize pyrrole monomer), then it is also sufficient to allow electrolyte disassociation in the presence of a suitable catalyst (note that the potential required for the disassociation process at the pH used is similar to that used for polypyrrole deposition).

4.4 *Electrolytic Dopant Recrystallisation*

Although the work presented in this Chapter concentrates on the elucidation of the macrostructure of polypyrrole, the XRD (X-ray diffraction) technique has been used in an attempt to increase the author's understanding of the microstructure of electrochemically deposited polypyrrole (as reported in Ch. 5). Despite the obvious merits of diffractometry techniques for the study of polypyrrole structure on the sub-micron scale, the use of such techniques has illuminated an interesting and novel feature of electrochemically deposited polypyrrole, which has not been reported elsewhere in the literature.

In this section, a series of investigations into the recrystallisation of electrolytic dopant from within the polypyrrole microstructure during the post-deposition 'ageing' process are reported. As stated, the use of the θ-2θ XRD technique is reported here; this technique is discussed in depth in Ch. 5. Much of the work presented has been published in the scientific press (see Lemon and Haigh, '99(b)).

4.4.1 *θ-2θ XRD Order Peak Observation*

The θ-2θ XRD technique was used to investigate the microstructure of a range of electrochemically deposited, type-283, polypyrrole samples (as reported in Ch. 5).

Although previous studies (see references cited in §4.3.2) have reported routinely low order levels in polypyrrole, studies undertaken by the author often resulted in the observation of strong order peaks on the X-Ray diffractograms produced. Typical peaks were observed to occur at around $2\theta = 6.1°$ and $2\theta = 6.3°$ (as shown in Fig. 4.32).

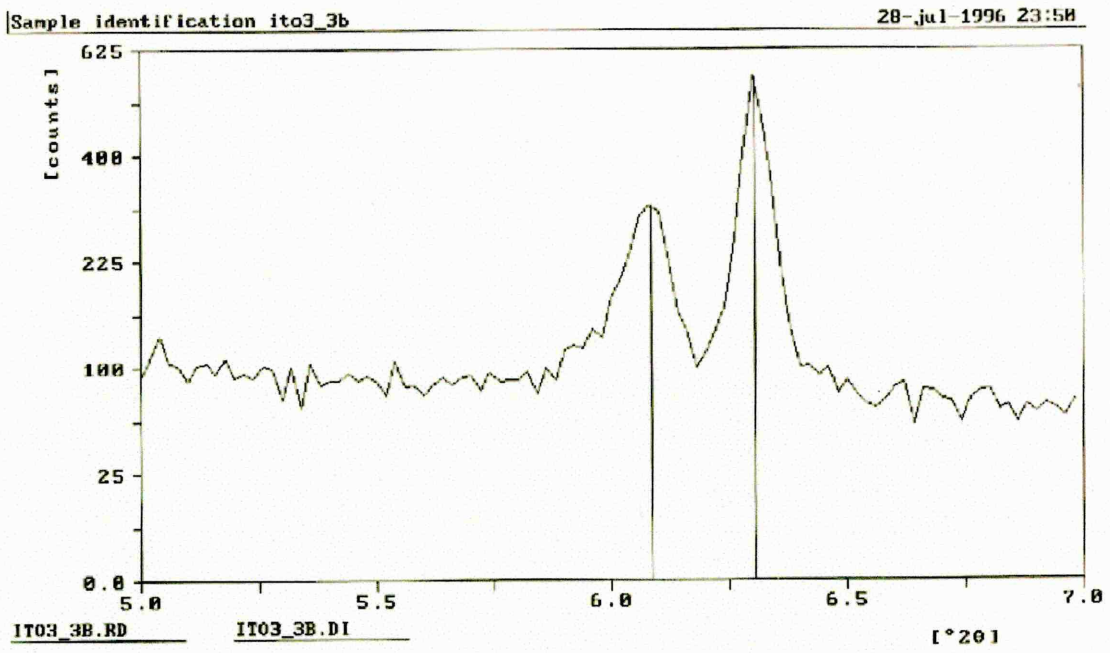

Figure 4.32: *θ-2θ X-Ray diffractogram showing typical twin order peaks observed on analysis of type-283 polypyrrole films.*

The Bragg Equation (as described in §2.2.2) was used to calculate the 'd-value' (the lattice spacing) corresponding to the observed peaks; lattice spacing values of around 14.5Å and 14.0Å were calculated. An example of the use of Bragg's Law to calculate lattice spacing is given below:

It is known that, for constructive interference to occur, the Bragg Condition must be satisfied: $n\lambda = 2d \sin\theta$

where:

n	=	the integer scattering order no.
λ	=	wavelength
d	=	interplanar spacing
θ	=	the glancing angle between the incident ray and the plane

For a 'first order' diffraction of $CuK\alpha_1$ radiation:

$$1\ (1.54060 \times 10^{-10}\text{m}) = 2d\ (\sin(6.085°/2))$$

$$2d = (1.54060 \times 10^{-10}\text{m}) / (\sin(6.085°/2))$$

$$d = 1.45130 \times 10^{-9}\text{m}$$

$$\underline{d = 14.513\text{Å}}$$

In order to study the reproducibility of the peaks observed, a set of four type-283 polypyrrole films were deposited onto ITO coated glass substrates of around 200mm^2 at +1.00V vs SCE for 120s, each using fresh electrolyte at standard solution concentrations. Each film was rinsed well in low conductivity, deionized water and dried with a high velocity jet of oxygen-free nitrogen immediately after deposition. Films were stored in separate airtight containers (without desiccation); two XRD traces were taken from each film within 24 hours.

The twin order peaks described above were observed in all cases. Although two discrete X-Ray wavelengths were used during analysis ($CuK\alpha_1$ and $CuK\alpha_2$; 1.54060Å and 1.54439Å respectively), peak positions from each wavelength were not resolvable. However, two separate 'd-values' (lattice spacings) were calculated and presented by the Philips APD 3.6 software used. As a result, all data presented here has been handled using a mean wavelength value of 1.54250Å.

Lattice spacings derived from the range of peak positions found on analysis of the films produced are shown in Table 4.5.

TRACE	LATTICE SPACING (Å)	
	PEAK #1	PEAK #2
ITO3_1A	14.366	13.827
ITO3_1B	14.354	13.838
ITO3_2A	14.591	14.035
ITO3_2B	14.567	14.035
ITO3_3A	14.531	14.035
ITO3_3B	14.531	14.024
ITO3_4A	14.531	14.002
ITO3_4B	14.556	14.047
MEAN	*14.503*	*13.980*

Table 4.5: *Lattice spacings derived from observed type-283 polypyrrole XRD peak positions.*

As shown in Table 4.5, the positions of he two observed peaks correspond to lattice spacings of around 14.5Å and 14.0Å (both ±0.3Å); the positions of the peaks were observed to be reproducible. The origins of the observed peaks will now be discussed.

4.4.2 Order Peak Origination – Homogeneous Dopant Distribution

The observation of order peaks by XRD (as described above) was not intuitively expected, since much work suggests the presence of very low levels of order in electrochemically deposited polypyrrole (see references cited in §4.3.2). However, work has been presented by Veluri *et.al.* ('95) which describes the use of Atomistic Lattice Simulation (ALS) to describe the optimum packing of polypyrrole in 'crystalline' material. The simulation predicted the formation of a unit cell of 14.48Å (as shown in Fig. 4.33), so satisfying the 14.5±0.3Å peak shown in Fig. 4.32.

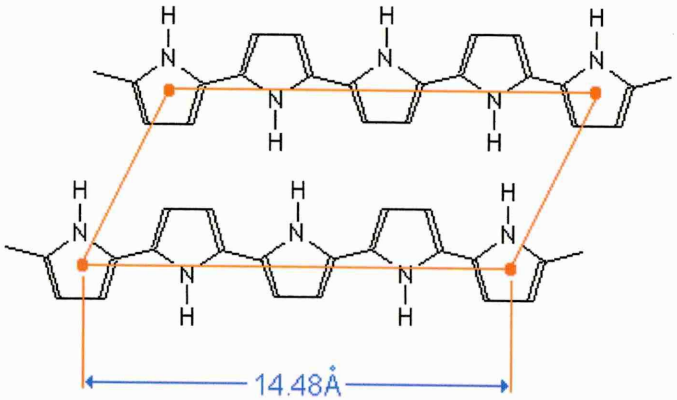

Figure 4.33: *Atomistic Lattice Simulation of crystalline polypyrrole packing (adapted from Veluri et.al., '95) showing 'ideal' 14.48Å unit cell (shown in red, with one dopant ion per unit cell).*

The logic used by Veluri leads to the conclusion that the crystal unit cell involves a centrally placed dopant ion. However, the formation of crystalline polypyrrole as described by Veluri is thought by the Author to be extremely unlikely; see Fig. 1.27 (§1.5.4), which illustrates the high probability of the widespread presence of defects throughout the polypyrrole matrix.

An alternative and far more feasible explanation for the origins of the order peaks observed may be assembled by consideration of the accepted model presented in §1.5.5

(see also Skotheim, '86). This model suggests that polypyrrole chains are distorted by the formation of pairs of polaronic charge defects during deposition, with distortion extending over four pyrrole rings, resulting in two positively charged areas. These positively charged 'bipolaronic' defects within the polymer attract and 'pin' dopant ions during deposition in order to maintain charge neutrality, as shown in Fig. 1.28 [d] (§1.5.5). It was therefore considered by the Author that the observed XRD order peaks may originate not from the ordered incorporation of dopant ions at a central position in the unit cell of crystalline polypyrrole, but rather from the ordered incorporation of dopant ion pairs throughout the disordered polymer matrix, one pair per positive bipolaronic defect.

Consideration of the ordered incorporation of dopant ions within the polymer matrix not only satisfies the observed 14.5±0.3Å peak (as does the Veluri model), but may also be adapted to satisfy the observed 14.0±0.3Å peak, as illustrated in Fig. 4.34. The upper polypyrrole chain shown in Fig. 4.34 (with an 'up-down-up' alternating chain structure, dubbed 'pseudo-syndiotactic') attracts dopant ions to both positively charged polaronic defects within each bipolaron; consideration of polypyrrole geometry suggests that incorporated dopant ions would be separated by a distance around the requisite 14.5Å. The lower polypyrrole chain shown in Fig. 4.34 (with an 'up-up-up' isotactic chain structure) also attracts dopant ions to both positively charged polaronic defects within each bipolaron. However, the chain geometry results in a reduction in the separation of the dopant ions to around 14.0Å, so mitigating the pair of peaks observed.

It was therefore considered possible by the Authors that, under suitable conditions, the presence of the observed pair of XRD order peaks may be the result of the ordered incorporation and 'pinning' of dopant ions into the polymer film by bipolaronic defects during film deposition as illustrated in Fig. 4.34.

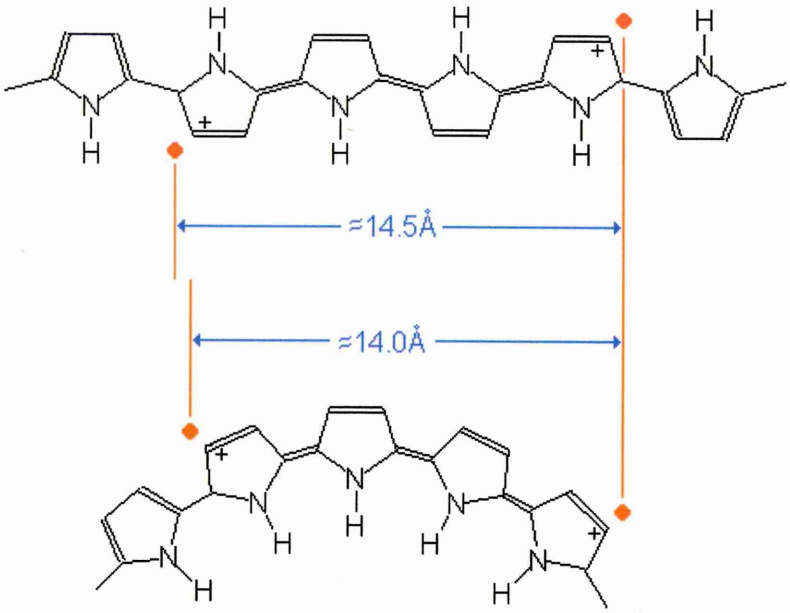

Figure 4.34: *Spacing of negatively charged dopant groups (•) attracted to positively charged bipolaronic defects in an 'up-down' polypyrrole chain (dubbed 'pseudo-syndiotactic', top) and an atactic polypyrrole chain (bottom).*

The model presented above assumes that the attraction of dopant ions to the pair of positively charged defects produced on bipolaron formation will result in a dopant ion spacing of around 14.5Å. However, this is only possible if we assume repulsion of negatively charged dopant ions from one another. Bipolaronic positive charges are localized over four pyrrole rings, as shown previously. Consideration of polypyrrole geometry tells us that pyrrole rings are typically separated by 3.62Å; polaron separation will therefore be between 10.86Å and 14.48Å. Further, pinned dopant ions will be separated similarly, with a bias towards greater separation due to the natural repulsion between ions.

An alternative, although closely related theory was considered to more accurately account for the presence of the 14.5±0.3Å peak. It was considered that, for polypyrrole films of high electrical conductivity (as is typical for type-283 material), one could assume a high density of bipolaronic defects throughout the polymer matrix. If it is assumed that a polypyrrole chain (such as shown in Fig. 4.35 [a]) is deposited under conditions conducive to the formation of bipolaronic defects (which is the case for highly conductive type-283 material), then a structure such as that illustrated in

Fig. 4.35 [b] is to be expected. If deposited under forced conditions in the presence of suitably high concentrations of dopant, then the structure illustrated in Fig. 4.35 [c] is to be expected. The structure shown will result in the separation of dopant groups by 14.5Å.

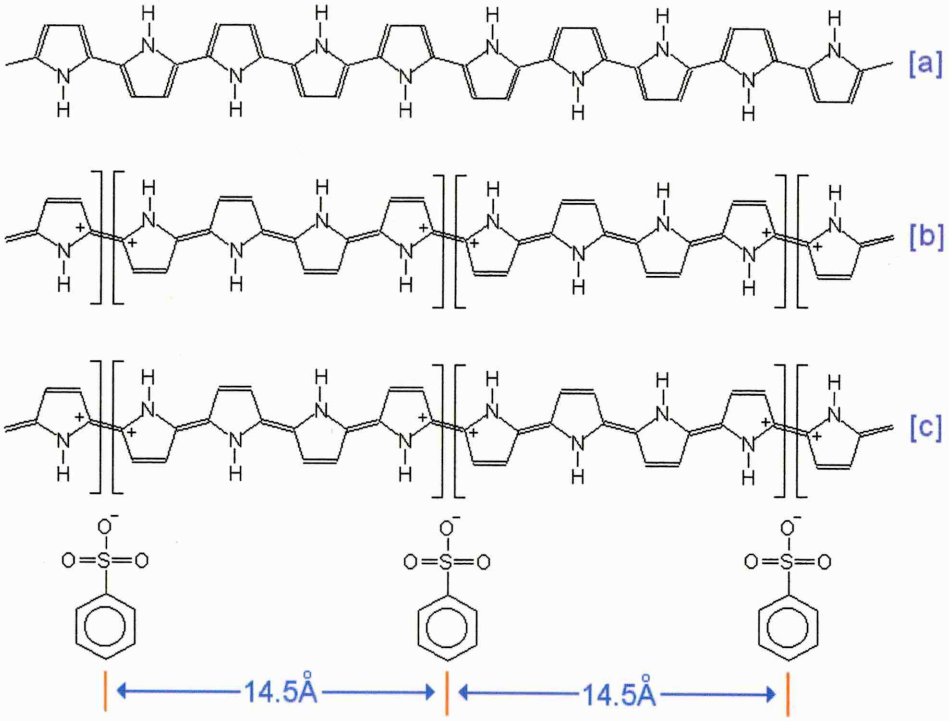

Figure 4.35: *Polypyrrole chains [a] in the pristine state, [b] under 'bipolaronic saturation', and [c] after pinning of dopant ions.*

However, despite the potential validity of the models presented in this section (§4.4.2), the formation of polypyrrole with the level of order required to result in the long range ordered incorporation of dopant was thought to be unlikely. Further, polypyrrole would be required to possess long-range 'pseudo-syndiotacticity' (see Fig. 4.34) in order to produce the 14.5Å peak commonly observed to be dominant. Also, in the unlikely event of the formation of long-range 'pseudo-syndiotactic' polypyrrole, the incorporation of dopant into the polymer would have to be at a level commensurate with *total* film doping, as represented in Fig. 4.35 [c]. This level of film doping is highly improbable under standard deposition conditions; this is supported by the significant modifications to film properties (both morphological and electrical) on modification of dopant concentration during deposition. An excess concentration of dopant would be required within the electrolyte solution to allow such *total* film doping.

Further, it is unlikely that dopant groups incorporated into the polypyrrole matrix during deposition at 'standard' concentrations (i.e. non-excess) would be incorporated in such a way as to form localized areas of high (*total*) dopant concentration, as would be required to produce the level of order illustrated by XRD. Dopant groups are incorporated and 'pinned' into polypyrrole films on an 'as-needs' basis in order to maintain charge neutrality on formation of polaronic and bipolaronic defects during deposition. This would suggest an even distribution of dopant groups throughout the polymer; such homogeneous distribution (at standard dopant concentrations) would result in crystal repeat distances far in excess of 14.5Å.

As a result, further work was undertaken to identify alternative models to explain the formation of the order peaks observed.

4.4.3 Order Peak Origination – Electrolytic Dopant Recrystallisation

Given the previous assertation that the development of extensive polymeric order within the polypyrrole matrix is most unlikely, an alternative model has been formulated to account for the detection of extensive crystallinity by XRD.

A basic model of the structure of electrochemically deposited polypyrrole has been presented by Ren and Pickup ('95) in order to account for the electrical characteristics of the material. This model assumed that bulk polypyrrole consisted of an 'aggregate' of solid polymer particles, joined in such a way as to trap a network of 'closed pores', as shown in Fig. 4.36. For electrochemically deposited material, it was assumed that these closed pores would be filled with the electrolyte solution used during deposition.

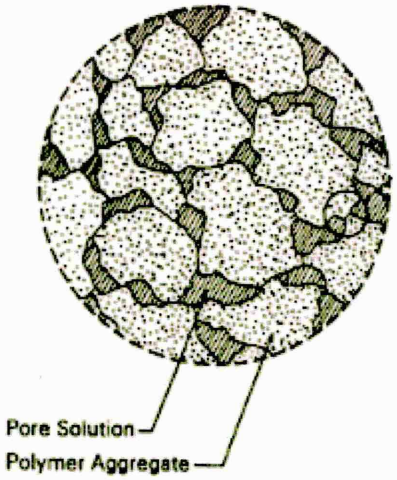

Figure 4.36: *The 'aggregate' model of polypyrrole structure, as suggested by Ren and Pickup (adapted from Ren and Pickup, '95).*

Although the presence of an aggregate of solid polypyrrole and closed pores of electrolyte solution facilitated the explanation of polypyrrole electrical characteristics, no empirical evidence was given by Ren and Pickup to support the structural model presented. However, consideration of the 'aggregate' theory, along with consideration of the theories presented by the Author in §4.3, may explain the detection of extensive order on XRD analysis of electrochemically deposited polypyrrole.

It is postulated that the development of extensive order within the polypyrrole films prepared for XRD analysis is the result not of polypyrrole order, but rather of the drying and 'recrystallisation' of dopant salts from localized pockets of electrolyte solution trapped within the polymer matrix during electrochemical deposition. This is supported by the evidence presented by the Author in §4.3 (see Lemon and Haigh, '99), which suggests that significant gas pockets may evolve within polypyrrole films during electrochemical deposition. It is considered that pockets develop as a result of the inability of evolved gas to diffuse through the film at or above the rate of gas evolution. However, the diffusion of electrolyte solution into pockets during deposition and after removal of the deposition potential (during the 30s 'settling period') is to be expected.

It is considered that the presence of localized areas of electrolyte solution within the polypyrrole films on deposition (either by diffusion into gas pockets or by entrapment

during formation) may result in the gradual formation of areas of recrystallised dopant salt within the film on drying.

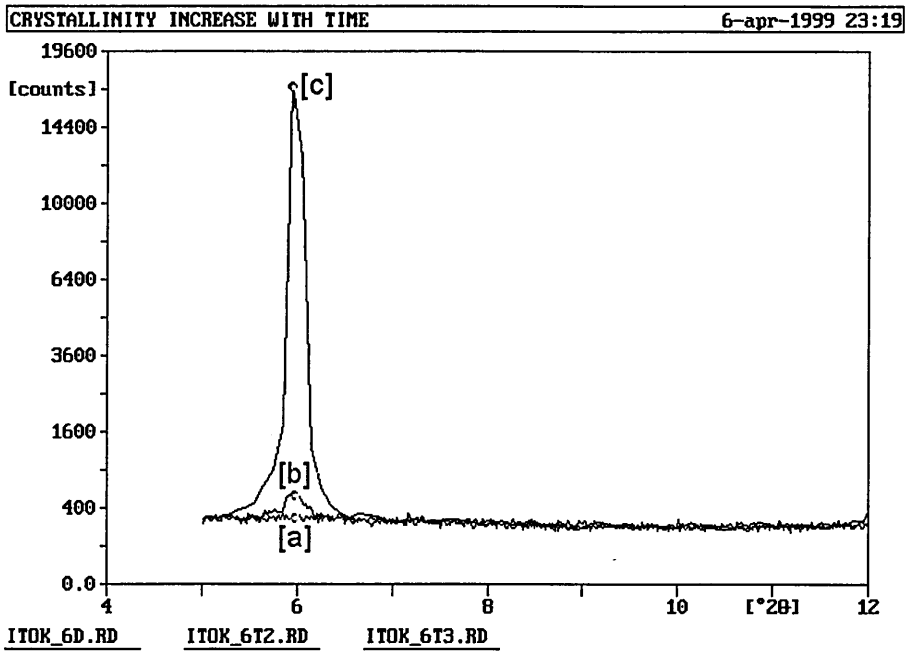

Figure 4.37: *Direct observation of the formation of order peaks from a single electrochemically deposited type-283 polypyrrole film via θ-2θ XRD; [a] immediately after deposition, [b] after two hours, and [c] after four hours.*

In order to test the hypothesis presented, a pair of type-283 polypyrrole films were deposited onto ITO coated glass slides of around 200mm^2. Fresh electrolyte solutions (25ml) were used for each, with monomer and dopant at 0.25M concentration. A deposition potential of +1.00V vs SCE was used; deposition was carried out for 30 minutes (+30s @ 0.00V vs SCE). Samples were *thoroughly* rinsed in clean water after deposition and were stored in individual, low volume, sealed sample vials containing 1ml of water to prevent film drying. Each film was studied by XRD as soon as possible after deposition, [a] immediately after removal from the humid, sealed sample vial, [b] two hours after removal, and [c] four hours after removal. Both films were observed to behave similarly; strong order peaks were formed during the first four hours of exposure to the ambient atmosphere, as shown in Fig. 4.37.

The gradual formation of order peaks during the four hours following deposition strongly supports the hypothesis of electrolyte entrapment and subsequent

recrystallisation of ionic dopant groups; Fig. 4.37 strongly suggests the systematic formation of highly ordered, non-polymeric material within the polymer matrix subsequent to deposition.

Further investigations were undertaken in order to give support (or otherwise) to the model presented above.

4.4.4 Order Peak Origination - Verification

Several mechanisms have been investigated which, in the opinion of the Author, support the hypothesis presented in this section. These are now reported.

The Effects of Electrolyte Re-use

Studies of the effects of electrolyte reuse on the morphologies and electrical characteristics of type-283 Mk-III Bass-Warwick devices are presented in §3.4. It was demonstrated that the deposition of 12 devices from a single electrolyte did not adversely affect morphology or electrical resistance. However, the volume of polymer deposited during the formation of polypyrrole films on ITO-glass electrodes is far in excess of that required for a standard Mk-III Bass Warwick electrode.

It was therefore considered that the deposition of numerous type-283 polypyrrole films from a single, 25ml electrolyte solution onto large ITO substrates would simply illustrate the effects of the reduction of available dopant on the magnitude of the peaks produced on XRD analysis. The use of a collection of electrolyte solutions of a range of dopant concentrations was considered, but was thought to be unnecessarily time consuming in relation to the 'single electrolyte' technique used.

Four type-283 polypyrrole films were deposited onto ITO coated glass slides of around $200mm^2$ using a single, 25ml electrolyte solution of standard properties. A deposition potential of +1.00V vs SCE was used; deposition was carried out for 30 minutes (+30s @ 0.00V vs SCE). Samples were thoroughly rinsed in clean water after deposition and were stored overnight in ambient conditions (without desiccation) to allow film drying. The set of films were systematically studied by XRD using short '$2\theta = 5 - 10°$' scans.

θ-2θ XRD traces from each film (carried out in the order of film deposition) illustrated very different degrees of order within the polymer films. It was noted that Film#1 (deposited from fresh electrolyte with standard dopant concentration) displayed a strong order peak at $2\theta \approx 6°$ (corresponding to an interplanar spacing of 14.5Å); the remaining films (#2, #3 & #4, deposited from pre-used electrolyte) displayed no order peaks. The above observation supports the hypothesis of electrolytic dopant recrystallisation. The formation of a strong order peak from Film#1 illustrates the successful recrystallisation of dopant groups from electrolyte solution trapped within the film; the thorough post-deposition rinse in clean water suggests against the recrystallisation of dopant present on the film surface. The formation of no order peaks from the remaining films (deposited from pre-used electrolyte) suggests depletion of the available dopant within the electrolyte solution during the first deposition. However, similarities in the morphologies of films #1 - #4 suggests the presence of sufficient dopant to allow catalysis of gas production at the working electrode in all cases.

The Effects of Film Deposition Time

The effects of the variation of polypyrrole film deposition time on the observed level of dopant recrystallisation have been studied. This study was carried out with due consideration given to the hypothesis that the recrystallisation of dopant trapped within the polymer film is responsible for the formation of the ($2\theta \approx 6°$) order peaks discussed previously.

A range of type-283 polypyrrole films were deposited onto ITO coated glass slides; a range of deposition times were used to study the relationship between order peak height and deposition time. Fresh electrolyte solutions were used for each, with monomer and dopant at 0.25M concentration. Depositions were carried out at a potential of +1.00V vs SCE for the times shown in Table 4.6; all depositions were followed by a settling period of 30s at 0.00V vs SCE. Samples were rinsed in clean water after deposition and were stored overnight in ambient conditions to assist film drying before XRD analysis.

θ-2θ XRD analysis of each film showed peak height to be closely related to film deposition time; the relationship formed is shown in Fig. 4.38, which illustrates that order peak height increases with deposition time.

FILM I.D.	DEPOSITION TIME (s)	PEAK COUNTS
ITOGT300	300	12,133
ITOGT240	240	4,033
ITOGT180	180	7,583
ITOGT120	120	1,314
ITOGT60	60	211
ITOGT50	50	275
ITOGT40	40	163
ITOGT30	30	48

Table 4.6: *The effects of deposition time variation on order peak height.*

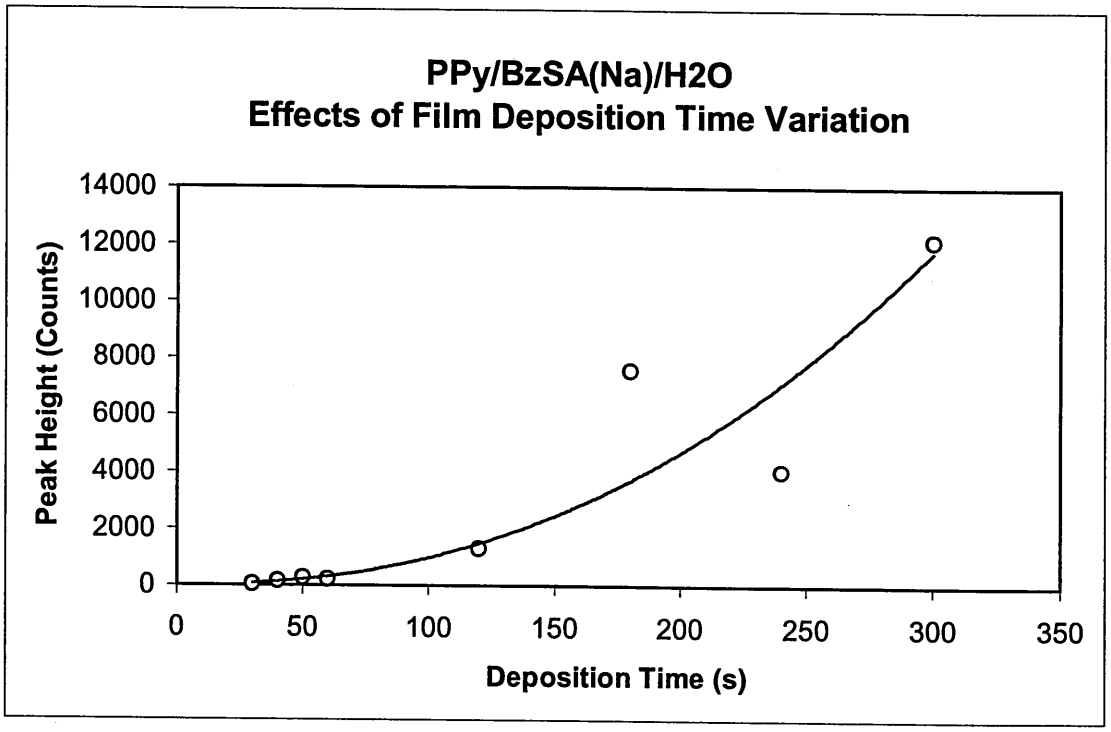

Figure 4.38: *The effects of deposition time variation on order peak height.*

Consideration of the relationship presented supports the theory presented in this section, suggesting that a greater volume of electrolyte is trapped within films of greater thickness (i.e. with increasing deposition time). Increasing the volume of trapped electrolyte would intuitively lead to an increase in the degree of dopant recrystallisation, and so to an increase in order peak height.

Investigative Techniques

A number of well-established investigative techniques (§2.2) were used in order to investigate the potential validity of the hypothesis of electrolyte recrystallisation presented in this section. Findings obtained via the use of these techniques are reported here.

Scanning Electron Microscopy

As reported in Lemon and Haigh ('99), SEM investigation of the polypyrrole films fabricated during work presented in this section has consistently led to the observation of a myriad of small crystalline clusters visible from the upper surface of the film. The observation of such clusters, (as shown in Fig. 4.39 [a] & [b]) is closely linked to XRD order peak height; clusters are observed only on films with strong XRD order peaks.

Consistent observation of such clusters within films previously shown to produce strong XRD order peaks, and failure to observe such clusters on films which produce weak (or no) order peaks strongly supports the hypothesis of dopant recrystallisation.

Energy Dispersive X-Ray Analysis

EDAX analysis was carried out during the SEM analyses reported above (both of which were undertaken on a JEOL 840A electron probe microanalyser). EDAX investigations of films previously shown to result in the formation of a strong XRD order peak were carried out in 'point analysis mode' (which allows elemental analysis of X-Rays emitted from a small, well defined area).

'Point mode' EDAX analyses on crystalline areas (as reported above) consistently resulted in the detection of roughly equivalent X-Ray emission levels from silicon (originating from the glass substrate used) and sulfur (which is assumed to originate from the benzene sulfonic acid, sodium salt dopant used)(Fig. 4.40 [a]). Conversely, point analysis on non-crystalline areas (with standard nodular polypyrrole morphologies) resulted in the detection of far greater levels of silicon X-Ray emission than sulfur (Fig.4.40 [b]). This supports the identity of the crystalline material identified

in Fig. 4.39 as recrystallised dopant, so strongly supporting the hypothesis of electrolytic dopant recrystallisation.

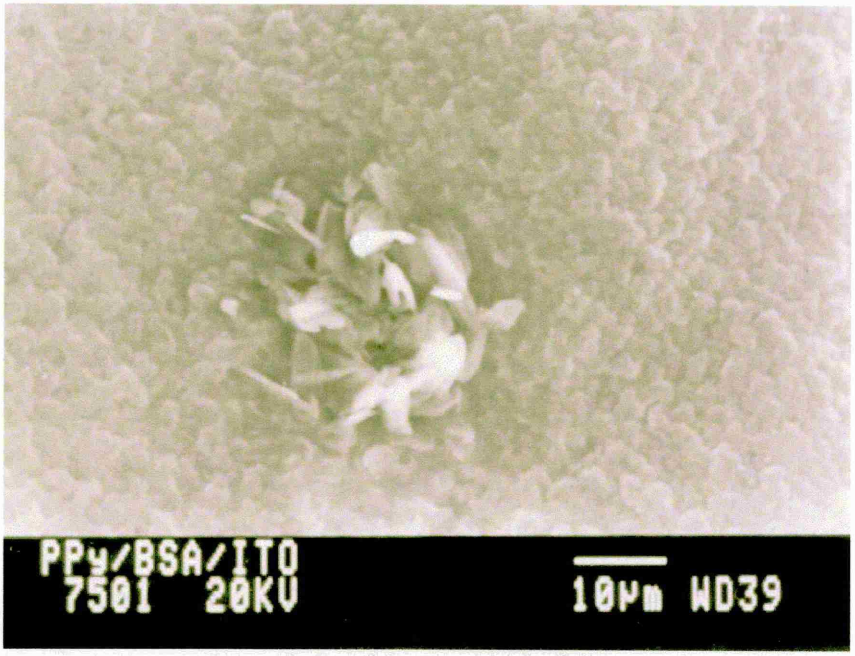

[a]

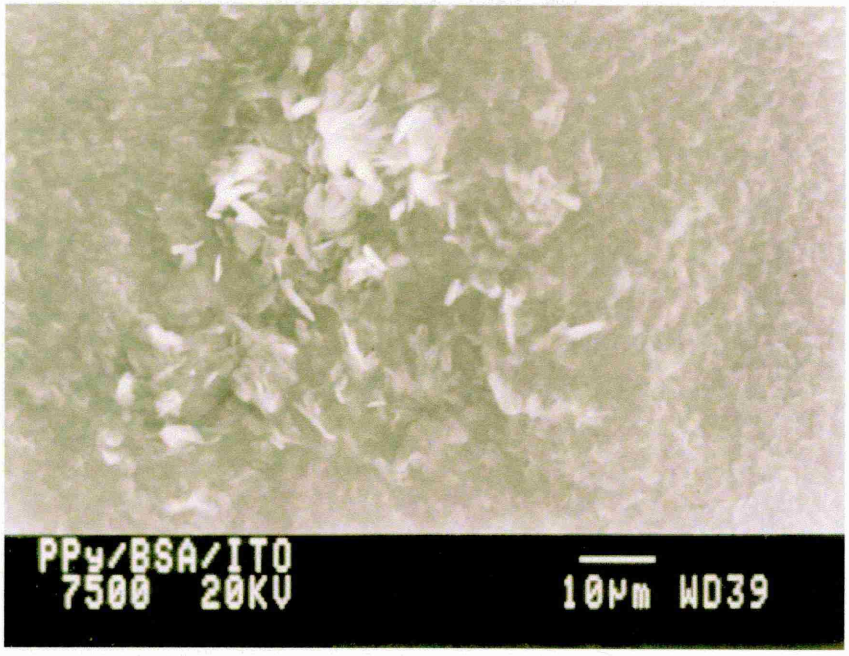

[b]

Figure 4.39: *[a] and [b], clusters of crystalline material observed during SEM analysis of polypyrrole films previously shown to exhibit strong XRD order peaks.*

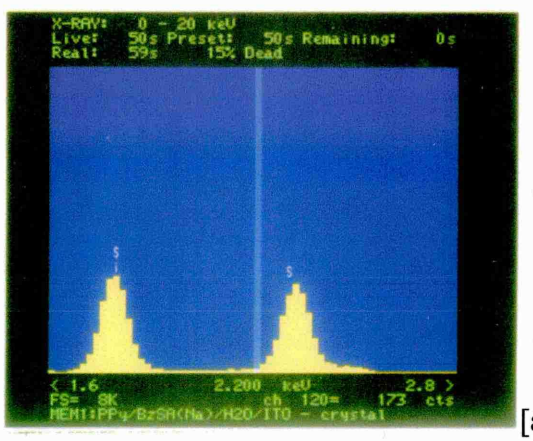

[a]
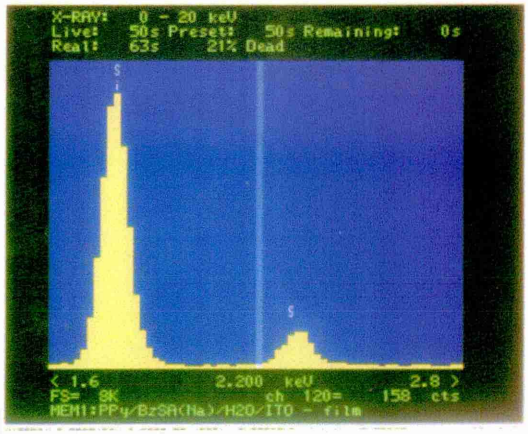

[b]

Figure 4.40: *EDAX traces of [a] crystalline clusters, and [b] standard nodular areas of polypyrrole material.*

Glow Discharge Optical Emission Spectroscopy

GDOES analyses were carried out on films previously studied by SEM (and shown to be host to sulfur-rich crystalline regions). The selection of analysis areas to specifically [a] include, and [b] exclude crystalline regions was not possible due to the significant analysis area used by the technique.

A typical GDOES trace is shown in Fig. 4.41. This, and other typical spectra, showed characteristic 'elemental profiles' of:

- Silicon (low level throughout the polymer layer, increasing at the polymer / substrate interface to a plateau throughout the substrate),
- Carbon (high level throughout the polymer layer, reducing significantly at the polymer / substrate interface), and
- Sulfur (as carbon).

The above elemental distribution is as would be expected for an organic polymer with a sulfonic acid-based dopant deposited onto a glass substrate.

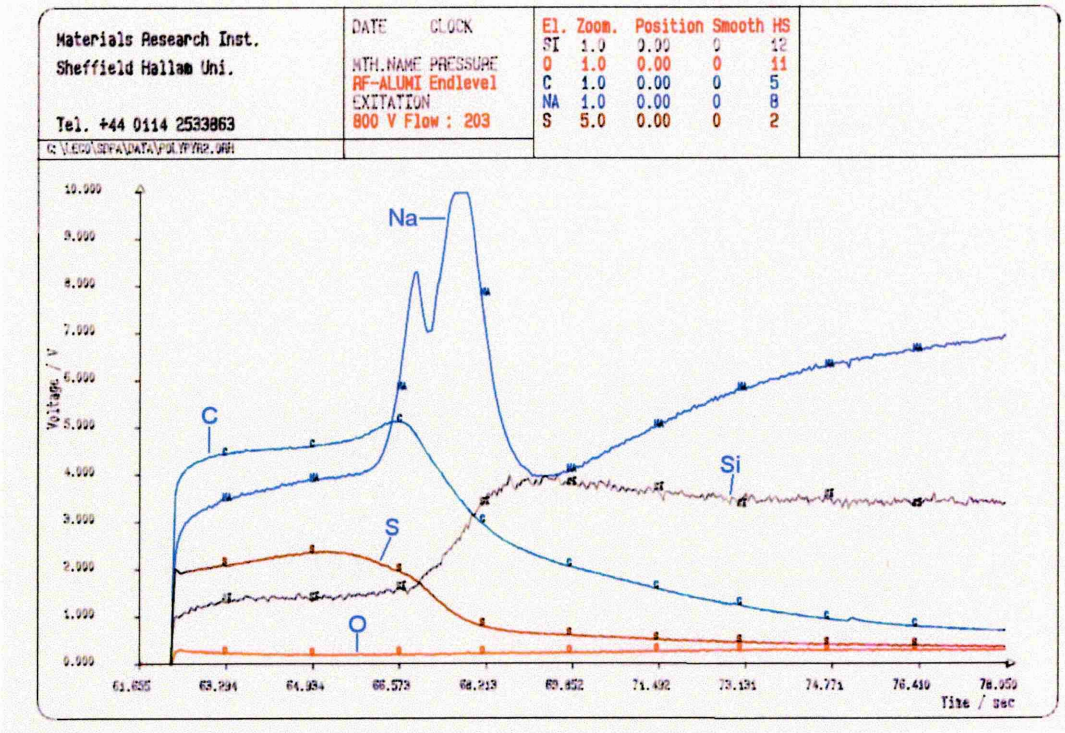

Figure 4.41: *GDOES trace showing characteristic silicon, carbon and sulfur traces, and illustrating an area of greatly increased sodium concentration at the polymer / substrate interface.*

Figure 4.41 also suggests a greatly increased concentration of sodium at the polymer / substrate interface. It was initially considered that this was evidence of a sodium-rich crystal at the interface. However, the presence of a region of crystalline dopant would almost certainly result in a concomitant sulfur peak; this has been shown not to be the case. It is therefore considered that the sodium peak observed may simply be due to the adsorption of disassociated sodium ions onto the ITO substrate material.

It is considered that the above observations in no way weaken the hypothesis of dopant recrystallisation. As material within the significant GDOES analysis area (a circle of 4mm diameter) undergoes simultaneous ablation, it is thought that small (tens of microns) clusters of recrystallised material (see Fig. 4.39) may have a negligible effect on GDOES traces. Furthermore, it is thought that the aggressive nature of the GDOES technique (which frequently resulted in the immediate destruction of polypyrrole films throughout their thickness, so allowing the collection of no representative data), leads to a severe reduction in the 'depth resolution' obtainable. The gradual increases /

decreases in elemental content shown in Fig. 4.41 (representing sharp interfaces between adjacent areas of dissimilar elemental content) are testament to this.

The Effects of Dopant Modification

In order to directly study the validity of the Electrolytic Dopant Recrystallisation model presented in §4.4.3 (which followed from the Homogeneous Dopant Distribution Model presented in §4.4.2), the effects of replacement of the benzene sulfonic acid, sodium salt dopant used in type-283 material with other commonly used dopant types have been studied.

It was anticipated that, further to the discussion presented in §4.4.3 (which cast doubt on the hypothesis of the pair of ≈14Å XRD order peaks originating from ordered, homogeneous dopant distribution), the position of order peaks observed during XRD analysis would vary with dopant choice. If observed, this would support the theory presented in §4.4.3 and undermine that presented in §4.4.2.

Polypyrrole films were deposited on ITO coated glass slides of around ≈200mm^2. Pyrrole monomer and dopant (as outlined in Table 4.7) were used at 0.25M in aqueous solution; depositions were carried out at +1.00V vs SCE for 120s (+30s @ 0.00V vs SCE). Films were thoroughly rinsed in clean water after deposition and were stored overnight in ambient conditions to assist film drying before XRD analysis.

DOPANT	FILM ID	LATTICE SPACING (Å)		
		1	2	3
Sodium Benzene Sulfonate	ITONABS	14.53	14.04	-
Sodium Hexafluorophosphate	ITONAPF6	5.32	9.71	3.97
Lithium Nitrate	ITOLINO3	-	-	-
Sodium Perchlorate	ITOCLO4	5.82	13.16	3.74

Table 4.7: *The effects of dopant choice on crystalline lattice spacing (from XRD). Spacings 1-3 quoted in order of peak intensity.*

As shown in Table 4.7, variation of dopant type has a fundamental effect on the position of order peaks observed on XRD analysis. Consideration of the theories presented in §4.4.2 (which described the homogeneous distribution of dopant attracted to

bipolaronic defects throughout the polymer matrix) suggest that order is related closely to bipolaron distribution, and less so to dopant type. It is considered by the Author that the variation of observed lattice spacing (shown in Table 4.7) with dopant type strongly supports the theory presented in §4.4.3, so undermining that presented in §4.4.2.

The above experimental methodology was repeated using films deposited under identical conditions (using the dopant types specified in Table 4.7), for a greatly increased deposition time of 30 mins (+30s @ 0.00V vs SCE). Although intended to increase the likelihood of dopant recrystallisation from lithium nitrate doped polymer (by increasing the volume of trapped electrolyte material within the film matrix), XRD analysis resulted in near identical crystalline lattice spacings, as shown in Table 4.8.

DOPANT	FILM ID	LATTICE SPACING (Å)		
		1	2	3
Sodium Benzene Sulfonate	ITONABS	14.46	14.01	15.30
Sodium Hexafluorophosphate	ITONAPF6	5.32	9.72	3.97
Lithium Nitrate	ITOLINO3	-	-	-
Sodium Perchlorate	ITOCLO4	13.38	5.82	3.73

Table 4.8: *The effects of dopant choice on crystalline lattice spacing (XRD, increased deposition time). Spacings 1-3 quoted in order of peak intensity.*

Lattice spacing values given in Table 4.8 relate closely to those in Table 4.7, so reinforcing the conclusions stated above. Increasing deposition time did not result in the detection of crystalline order within polypyrrole films doped with lithium nitrate.

Recrystallised Dopant XRD

Empirical data presented in this section has suggested that the XRD order peaks arise from the recrystallisation of dopant from electrolyte solution trapped within the polymer matrix. A short study has been carried out to confirm the origin of the order peaks observed on analysis of type-283 films (the focus of the work presented).

A saturated solution of sodium benzene sulfonate (benzene sulfonic acid, sodium salt) in milli-Q water was prepared; 5ml of solution was siphoned from the XS solution so as only to include dopant dissolved into solution. 2ml of dopant solution was pipetted onto

an ITO glass slide (of ≈200mm^2) and was stored overnight in ambient conditions to assist film drying before XRD analysis. Analysis of the dry slide by XRD resulted in the production of a range of order peaks (Table 4.9), the majority of which were found to correspond with peaks observed during the analysis of polypyrrole films doped with sodium benzene sulfonate, as reported in this chapter.

DOPANT	LATTICE SPACING (Å)		
	1	2	3
Sodium Benzene Sulfonate	14.35	14.59	14.38

Table 4.9: *The lattice spacing of recrystallised sodium benzene sulfonate (from XRD). [1] = first order peak (n=1), [2] = second order (n=2) etc.*

The Effects of Film Rinsing

In order to gather further evidence for the model presented in §4.4.3, type-283 polymer films previously analysed by XRD and shown to exhibit high levels of order suggested to originate from dopant recrystallisation were rinsed thoroughly in order to remove ionic crystalline material from the film surface. Two films (reported in Tables 4.7 and 4.8) were rinsed for around 60s under a low-velocity jet of Millipore water. Films were then allowed to dry under ambient conditions for >6 hours and were then analysed by XRD.

In both cases, XRD analysis resulted in traces characteristic of type-283 polymer (see Ch. 5), with no discernable order peaks. This is thought to represent the removal of recrystallised dopant from the film surface and dissolution of recrystallised dopant within the film matrix, so strongly supporting the hypothesis presented in §4.4.3.

The Effects of Long-Term Electrolytic Dopant Recrystallisation

Although the recrystallisation of electrolytic dopant within polypyrrole films subsequent to deposition is strongly supported throughout the work presented, some variability has been observed with respect to the level of crystalline order observed and the length of time between deposition and XRD analysis. The films used in the work presented have generally been stored overnight before XRD analysis, although instances of shorter storage have been reported. However, order peak formation has been shown to

commence within 2 hours after deposition (see §4.4.3) [Note: it is not considered that low-level, localised heating produced during a single XRD analysis is responsible for recrystallisation; this is demonstrated by the detection of no order peaks on analysis immediately after deposition (see Fig. 4.37, §4.4.3)].

A pair of type-283 polypyrrole films were prepared on standard ITO substrates, with monomer and dopant used at 0.25M at deposition potentials of +1.00V vs SCE for 5 mins (+30s @ 0.00V vs SCE). Films were thoroughly rinsed in clean water after deposition and were stored in ambient conditions (without desiccation) for two weeks to allow dopant to recrystallise to the full possible extent.

On XRD analysis, both films displayed a very high level of order; XRD traces were equivalent to those shown in Fig. 5.6, [a]) (prepared as described in §5.1.4 for a related study). It is suggested that the level of order observed represents the recrystallisation of a high level of trapped dopant throughout the film matrix, so resulting in the presence of a significant level of crystalline dopant.

It is of note that the observed order peaks originate from the 14.5Å repeat described previously in this chapter, although up to ten diffraction orders are evident in this case. Peak amplitudes are noted to describe the Laue Function and the Superlattice Structure Factor (Lewis, '97) [Note: the Laue Function arises from 'unit cell' diffraction, whilst the superlattice structure factor arises from the structure *within* unit cells].

4.4.5 The Effects of Dopant Recrystallisation on Film Resistance Characteristics

The recrystallisation of dopant within polypyrrole film structure (as demonstrated) is considered to be a possible contributor to the observed temporal instability of polypyrrole electrical conductivity.

It is possible that the crystallisation of dopant from electrolyte pockets within polypyrrole films may affect the concentration of dopant in surrounding areas of polymer. Nucleation of a dopant crystallite within the film structure subsequent to deposition may lead to depletion of the concentration of dopant in the polymer matrix in

the immediate vicinity of the nucleation site; dopant groups previously 'pinned' to polaronic / bipolaronic defects may be attracted to lower energy crystalline sites. Such dopant depletion from within the polymer film, which would be cumulative as the crystallites grow in size, could be the cause of the temporal resistance instability currently observed in polypyrrole gas-sensing devices such as those used in the e-NOSE 4000 and 5000.

Two studies are reported here, both of which were designed to investigate the effects of dopant recrystallisation on the electrical resistance of type-283 polypyrrole devices. Both involve the comparison of two sets of type-283 devices, the treatment of each set being tailored to promote or suppress dopant recrystallisation.

The Variation of Device Storage Conditions

Two sets of six type-283 devices (MkIII Bass-Warwick) were deposited from standard, aqueous solutions (dopant and monomer at 0.25M) for 5 mins at +2.00V vs SCE (+30s @ 0.00V vs SCE). Two solutions were used (A & B, see Table 4.10); individual films were rinsed well in low conductivity, deionised water and dried with a high velocity jet of oxygen-free nitrogen immediately after deposition. Films were stored in one of the following conditions:

[W] in individual, airtight vials containing 1ml of deionised water, and

[D] in individual, airtight vials containing a desiccating agent.

It was postulated that films stored in the 'W' condition would not be subject to dopant recrystallisation due to the high humidity level within the sealed sample vials. Conversely, it was postulated that films stored in the 'D' condition would undergo high levels of dopant recrystallisation. However, it was considered that differences in sensor resistance characteristics may be observed due to other effects resulting from the storage of polypyrrole films in dry and wet conditions, such as the effects of long-term exposure of polypyrrole films to water (see Charlesworth, Partridge and Garrard ('93); Barlett, Archer and Ling-Chung ('89); Janata ('89)). Measurements of electrical resistance were taken from individual devices using a calibrated DMM 2 hours, 20 hours, 7 days and 9 months after deposition.

SENSOR I.D.	ELECTRICAL RESISTANCE (Ω)			
	After 2 hours	After 20 hours	After 1 week	After 36 weeks
AD1	31	22	19	23
AD2	26	17	14	15
AD3	42	25	21	24
BD1	23	17	15	21
BD2	29	20	18	24
BD3	33	22	19	23
AW1	3	4	110	∞
AW2	250*	206*	185*	94*
AW3	45*	42*	49*	13M*
BW1	63	16	63	25
BW2	186	60	28	18
BW3	26	146	10M*	6M*

Table 4.10: *Electrical resistance of polypyrrole films after storage in moist and desiccated conditions. (*film observed by VANOX optical microscopy to delaminate, potentially leading to greatly increased resistance).*

As shown in Table 4.10, the storage of the devices produced in dry vials consistently resulted in a sharp initial resistance decrease, followed by a long-term period of stability, as reported in Appendix 2. Conversely, devices stored in moist conditions displayed unstable resistance characteristics; in many cases this was observed by optical microscopy to be the result of film delamination.

It was therefore concluded that use of the technique outlined above (storage of polypyrrole devices in moist / dry environments subsequent to deposition in order to assist / hinder the recrystallisation of dopant) to study the effects of dopant recrystallisation was not effective. Further studies were therefore undertaken in order to allow an accurate assessment of these effects to be made.

The Variation of Film Growth Rate

Two sets of five type-283 devices were deposited onto MkIII Bass-Warwick electrodes from discrete electrolyte solutions. Both device sets were deposited from aqueous solution with dopant and monomer at 0.25M. Two growth conditions were used;

conditions were optimized in order to allow the production of devices of similar film thickness, grown at a high and low deposition rate. Conditions were as follows:
[a] low growth potential (+0.80V vs SCE), high deposition time (300s + 30s @ 0.00V vs SCE), and
[b] higher growth potential (+1.20V vs SCE), lower deposition time (180s + 30s @ 0.00V vs SCE).
Both sets of deposition conditions were within the range of conditions studied previously (see Ch. 3), no unusual growth effects had been observed during previous studies.

It was postulated that the use of 'condition a' deposition would result in the slow formation of a reasonably thick polypyrrole film; slow film formation was postulated to result in a relatively ordered, more homogeneous film than produced by 'condition b' deposition. Conversely, it was considered that the use of 'condition b' deposition would result in the rapid production of a less ordered films than those produced during 'condition a' deposition. It was considered that films produced under 'condition a' would contain smaller pockets of trapped electrolyte than those formed under 'condition b', due to the ability of polypyrrole to form a less disordered matrix during formation under low growth potential. Conversely, it was considered that films formed at a high growth potential would contain larger pockets of trapped electrolyte than those formed at a lower growth potential, due to the increased propensity of polypyrrole to form a disordered matrix during high growth potential.

The two deposition conditions outlined were used after careful consideration; conditions were selected to allow the formation of two sets of films with dissimilar structures (as described above), but of roughly equivalent thickness. This was done so as not to introduce variations due to film thickness differences into the resistance data presented.

After deposition, individual films were rinsed well in low conductivity, deionised water and dried with a high velocity jet of oxygen-free nitrogen. Films were stored in individual, airtight vials containing a desiccating agent in order to [i] reduce variations in device resistance due to long-term exposure to moisture, and [ii] effectively desiccate the films produced, so leading to thorough dopant recrystallisation.

Measurements of electrical resistance were taken from individual devices using a calibrated DMM immediately after deposition, and on a number of occasions after deposition, as shown in Table 4.11. The film thickness of devices produced by 'condition a' and 'condition b' deposition were observed by optical microscopy to be roughly equivalent. It is therefore assumed that any observed differences between the resistance characteristics of 'condition a' and 'condition b' devices are not the result of differing film thickness.

SENSOR I.D.	ELECTRICAL RESISTANCE (Ω)								
	0 mins	10 mins	36 hours	50 hours	1 week	2 weeks	3 weeks	4 weeks	6 months
VS1 'A'	1.9	1.7	1.5	1.5	1.5	1.5	1.5	1.5	1.5
VS2 'B'	170*	29**	17	17	16	16	16	16	23
VS3 'A'	1.9	1.7	1.5	1.5	1.5	1.4	1.5	1.4	1.5
VS4 'B'	190*	39**	19	19	19	18	18	18	23
VS5 'A'	2.1	1.9	1.6	1.6	1.5	1.5	1.5	1.5	1.5
VS6 'B'	283*	75**	36	35	34	33	32	32	40
VS7 'A'	1.9	1.7	1.5	1.5	1.5	1.5	1.5	1.5	1.5
VS8 'B'	145*	44**	21	20	20	19	18	18	23
VS9 'A'	2.0	1.9	1.6	1.6	1.6	1.6	1.6	1.6	1.6
VS10 'B'	110*	44**	23	22	22	20	20	20	27

Table 4.11: *Electrical resistance of polypyrrole films deposited under 'Condition A' (low deposition potential, high deposition time), and 'Condition B' (high deposition potential, low deposition time).*

* resistance values observed to decrease sharply during measurement; initial value quoted.

** resistance values observed to decrease during measurement; initial value quoted.

As shown in Table 4.11 (and Fig. 4.42), deposition of type-283 polypyrrole devices using conditions A (low deposition potential, high deposition time) and B (high deposition potential, low deposition time) produces devices with significantly different resistance characteristics.

Devices deposited using 'condition A' were observed to have repeatably low resistance values, with a modest initial drop in resistance and high resistance temporal stability

over the medium term. Devices deposited using 'condition B' were, however, observed to have far higher resistance values (which often decreased sharply during measurement during the first 24 hours). Initial resistance drop was observed to be far greater than with 'condition A' devices, although resistances were equally temporally stable over the medium term, as illustrated in Fig. 4.42.

It is considered by the Author that the observed differences between the resistance characteristics of condition A&B devices suggest the following:

- The high initial resistance drop observed with 'condition B' devices supports the hypothesis that deposition at a high potential for a low deposition time results in the entrapment of a greater volume of electrolyte than deposition at a lower potential for a greater time. It is considered that the resistance drop observed is the result of dopant recrystallisation from electrolyte trapped within the polymer films grown using 'condition B'. It is postulated that 'pockets' of trapped dopant (larger than those formed using 'condition A') result in 'leaching' of dopant material from trapped electrolyte into the surrounding polymer. Such leaching results in a systematic increase in film conductivity. As the film, and therefore the pockets of trapped electrolyte within the film, dries out over time, it is logical to assume that the crystallisation of trapped dopant material will greatly reduce the level of dopant 'leaching' into surrounding polymer, so increasing the temporal resistance stability.
  Note: Further evidence was found which supported the above; comparisons between the resistance temporal stability of standard Neotronics substrates and Yoshi interdigital electrodes (§A2.1) showed Neotronics electrodes to exhibit a far greater initial resistance drop than Yoshi electrodes. It was considered that this high initial resistance drop was the result of the use of deposition parameters which led to rapid film formation. Conversely, the low initial resistance drop exhibited by Yoshi electrodes was considered to be the result of the use of deposition parameters which led to gradual film formation. As stated above it is considered that rapid film formation results in the entrapment of a greater volume of electrolyte than gradual film formation, so leading to increased dopant recrystallisation.

- The lower 'mature' resistance of 'condition A' devices than 'condition B' devices is thought to result from the entrapment of lower volumes of electrolyte during deposition at lower potential. It is not considered that film thickness differences are responsible for the observed mature resistance differences (as discussed previously). The presence of fewer 'electrolyte pockets' is considered to allow a higher degree of long-range polymer conjugation (or chain-to-chain contact) throughout the polymer film, therefore decreasing resistance.

Use of the experimental procedure outlined in this section allows the detection of significant differences between the resistance characteristics of films produced using deposition parameters tailored to allow the study of the entrapment of electrolyte during deposition and subsequent dopant recrystallisation. The resistance characteristics observed support the electrolytic dopant recrystallisation model presented in §4.4.

However, the data presented in this section does not support the hypothesis of dopant depletion in polymer surrounding areas of recrystallised dopant within the polymer film. The high degree of temporal stability exhibited by the devices studied in the work presented (which were stored in desiccated conditions between resistance measurements) suggests that dopant depletion does *not* contribute to the temporal stability common to generic polypyrrole sensing devices.

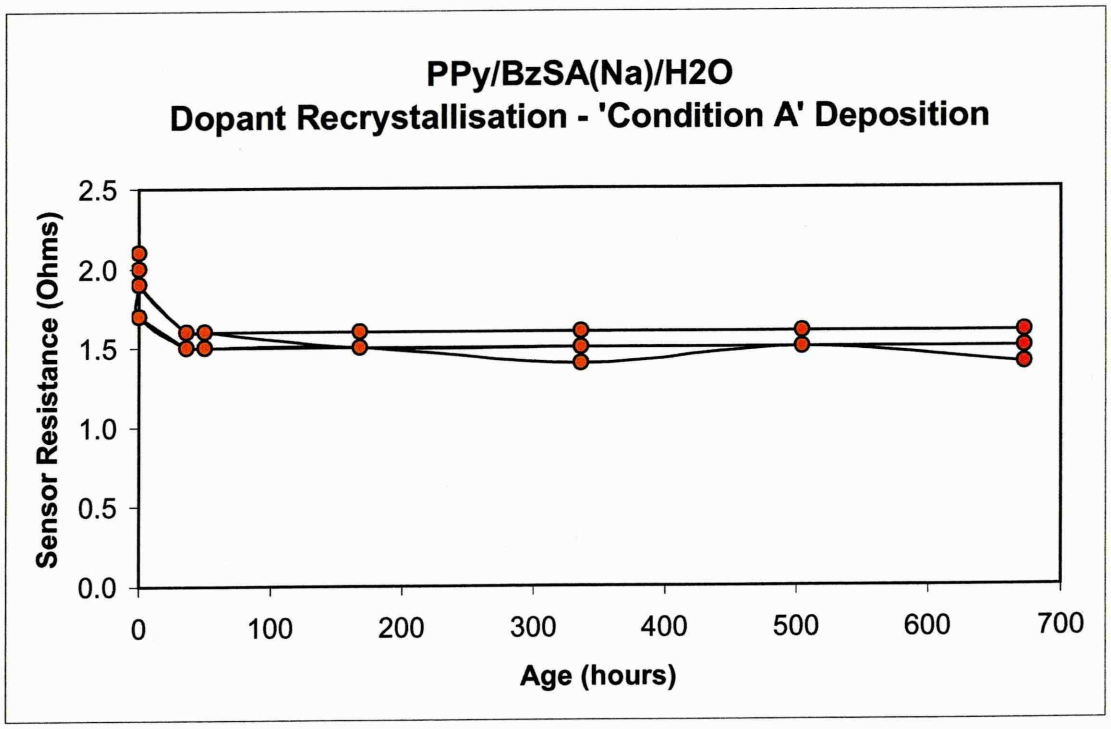

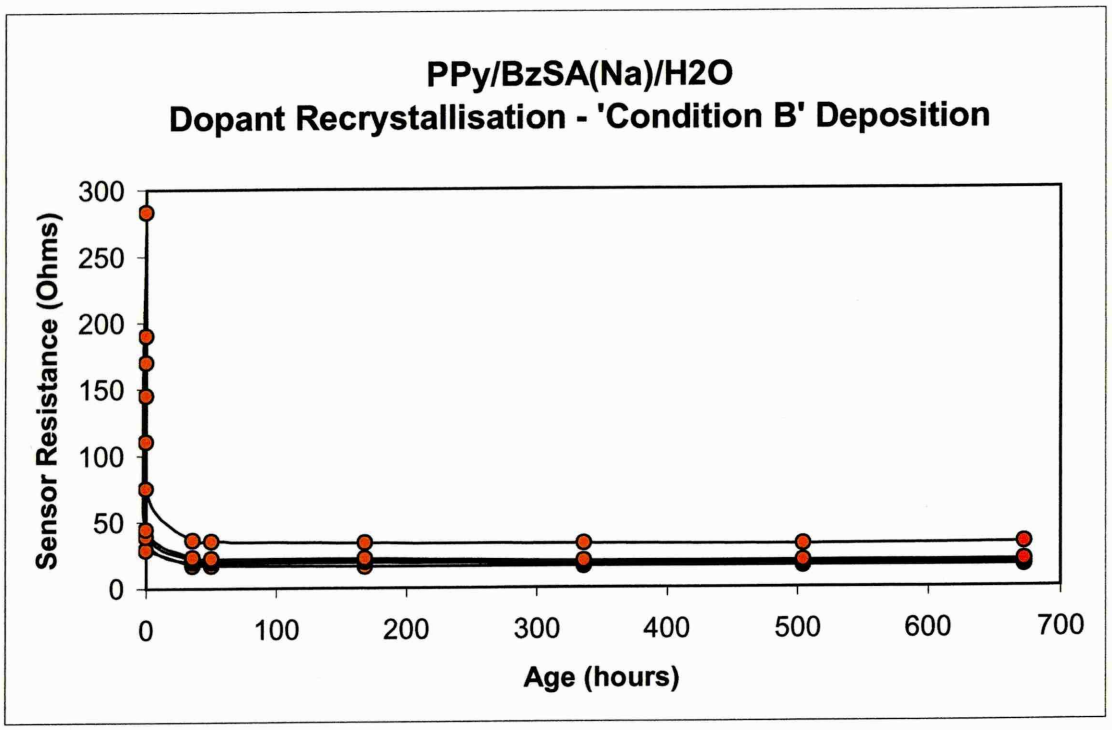

Figure 4.42: *Resistance temporal stability of type-283 polypyrrole deposited using 'Condition A' and 'Condition B' parameters (see Table 4.10).*

Summary, Chapter 4

- A series of studies have been presented regarding the macrostructure of electrochemically deposited polypyrrole.
- The growth of polypyrrole over insulating substrate regions has been discussed and related to the preferential growth of polymer in the working electrode surface plane.
- Early growth models (reported by the Author during transfer of registration from M.Phil to Ph.D.) have been discussed and superseded by models fitting subsequent empirical evidence.
- Attempts to utilise profilometric techniques to assess morphological development have not been successful (§4.1.5).
- The effects of dopant group choice on polypyrrole morphology have been reported.
- The effects of monomer purity on the morphology of polypyrrole have been studied, resulting in the publication of two papers in the scientific press. The effectiveness of monomer purification techniques were evaluated; degradation of pyrrole purified by these techniques has been monitored and reported. Attempts were made to relate resistances of devices produced from monomer of various purities; differences were not considered to be significant. Empirical evidence has shown that the use of suitably purified monomer leads to the development of nodular morphology, the use of unpurified monomer results in the development of 'tendrillar' morphology. Models have been developed and presented to account for the development of tendrillar morphology.
- The influence of electrolytic gas discharge on the development of characteristic polypyrrole nodular morphology has been discussed, resulting in peer-reviewed publication. It has been demonstrated that nodular morphology is not the result of spherulitic crystallinity, but rather of the production of gas at the substrate/film interface. Direct evidence has been presented showing the development and rupture of large gas pockets within the polymer film during high potential deposition; it has been demonstrated that gas production is the result of the catalysis of water disassociation by the presence of ionic dopant groups in the electrolyte solution.

- A structural model has been developed relating to the entrapment of pockets of electrolyte solution within the polymer film during deposition, again resulting in publication in the scientific press. Subsequent drying of polypyrrole films has been shown to result in the recrystallisation of dopant from within the trapped electrolyte solution. The model presented has been related to existing theoretical models reported previously in the literature; it is suggested that these models may be inaccurate. Dopant recrystallisation has been verified by SEM and EDAX; crystal growth has been demonstrated by XRD. It has been demonstrated that dopant recrystallisation may be responsible for the sharp drop in sensor resistance often observed after polypyrrole device formation.

5. *The Microstructure of Polypyrrole*

The research reported in this chapter focuses on studies of the microstructure of type-283, electrochemically deposited polypyrrole by θ-2θ X-Ray Diffraction (XRD) (see §2.2.2 and A3). Chapter 4, which concerns the elucidation of the macrostructure of polypyrrole, contains several sections which report the use of XRD to assist in studies of polypyrrole macrostructure; these studies are not referred to in this chapter unless directly relevant to the systematic studies presented. As per the work presented in Ch. 4, the research presented concerns only polypyrrole formed by electrochemical means.

Very little work has been reported in the literature regarding the study of the microstructure of electrochemically deposited polypyrrole; such work is reported and referenced in §1.5.2. The low volume of work in the scientific press describing polypyrrole microstructure is the result of the lack of long-range order typically displayed by this material. Work undertaken by the author utilizing XRD to study the microstructure of electrochemically deposited polypyrrole is now discussed.

5.1 *The Use of XRD to Assess Polypyrrole Microstructure – Feasibility Study*

A set of short feasibility studies were undertaken in order to assess the potential value of the use of the XRD technique to increase the current understanding of polypyrrole microstructure. A number of type-283 polypyrrole films were produced using Indium Tin Oxide (ITO) coated glass substrates of around 200mm^2 (as described in §4.4.1); ITO glass slides were used due to their high electrical conductivity and very good adhesion of the ITO layer. Large ITO coated glass plates (≈12" x 12") (Balzers) were manually cut into suitably sized rectangles before use. Large-area substrates (in comparison to standard Neotronics substrates) were used in order to maximise the surface area of X-Ray / polypyrrole interaction. Polypyrrole was deposited over the majority of the substrate in order to minimize X-Ray / substrate interaction. Depositions were carried out for several hours at either high voltage or high dopant/monomer concentration in order to attain high film thickness; this was carried out to further minimize X-Ray / substrate interaction.

Individual ITO substrates were cleaned using a thorough propan-2-ol wash (as described in §2.1.1), followed by drying under a high velocity jet of oxygen-free nitrogen. Depositions were carried out from discrete, 50ml electrolyte solutions, with monomer and dopant (BSA(Na)) at equal concentration; details of the concentrations, deposition potentials and deposition times used are given in Table. 5.1.

Films were rinsed well in fresh electrolyte (Millipore water) after deposition, soaked in clean electrolyte for at least 14 days (with electrolyte refreshed every 48 hours where possible), and dried in clean, ambient conditions (without desiccation) for at least a further 14 days. This 'soaking' and drying procedure was used in order to remove as much recrystallised dopant from the films as was reasonably practicable (see §4.4).

FILM I.D.	ELECTROLYTE CONC (M)	DEPOSITION POTENTIAL (V)	DEPOSITION TIME (H)
KW#1	XS	4.00	5
KW#2A	XS	2.00	5
KW#2	0.25	2.00	5
KW#3	XS	0.80	5

Table 5.1: *Polypyrrole thick-film deposition parameters.*

The films produced were used to both assess the potential efficacy of the XRD technique to resolve any structural differences between films deposited under differing conditions, and to assess the effects of the use of differing analysis parameters during XRD analysis. A collection of studies to rationalize the effects of XRD test procedures are presented below, followed by an assessment of the microstructural effects of the variation of film deposition parameters.

5.1.1 XRD Diffractogram Data Manipulation

The standard graphical outputs available from the Philips APD 3.6 analysis software used during the work presented (as shown in §4.4.1) are, in the opinion of the author, practical and effective. However, use of the standard graphical output does not allow any manipulation of the data under study; the ability to do so is a prerequisite of the 'Substrate Subtraction' process described in §5.1.2.

In order to overcome this limitation, all XRD diffractograms presented in this Chapter are manipulated using the following process:

1. Data collection by APD 3.6 software,
2. Export of data in ASCII format from APD 3.6 into a commercial word processing package,
3. Data treatment to allow transfer to a commercial spreadsheet,
4. Production of spreadsheet charts using processed data.

The use of the process outlined results in graphical representation of XRD diffractograms in the format shown in §5.1.2. The presentation of atypical 2-theta axis labels is an unfortunate disadvantage of the use of this technique, and results from the high number of data points generated during XRD analysis.

5.1.2 The Subtraction of Substrate Information.

Previous studies using θ-2θ XRD equipment suggested that incident X-Rays were sufficiently penetrative to result in the collection of structural information originating from the polymer film *and* the ITO glass substrate (strong variations in polymer film thickness, density and macrostructure produced by deposition parameter variation made the level of this 'over-penetration' difficult to predict).

In order to maximise the level of information available during the XRD studies presented in this chapter (by allowing the observation of structural information from the polymer film only), a process was developed to allow the physical subtraction of information generated from the substrate trace from 'combined' traces (traces containing polymer and substrate information). As the reduction of the power supplied to the X-Ray source was not practical (it causes a drastic reduction in diffractogram intensity), a manual method of subtraction of substrate information was developed and used. This technique involved the collection of an X-Ray diffractogram of a sample of substrate material (cleaned, dried and handled identically to those used for deposition),

using standard XRD parameters. Such a trace is illustrated in Fig. 5.1 (produced using the data manipulation method outlined in § 5.1.1).

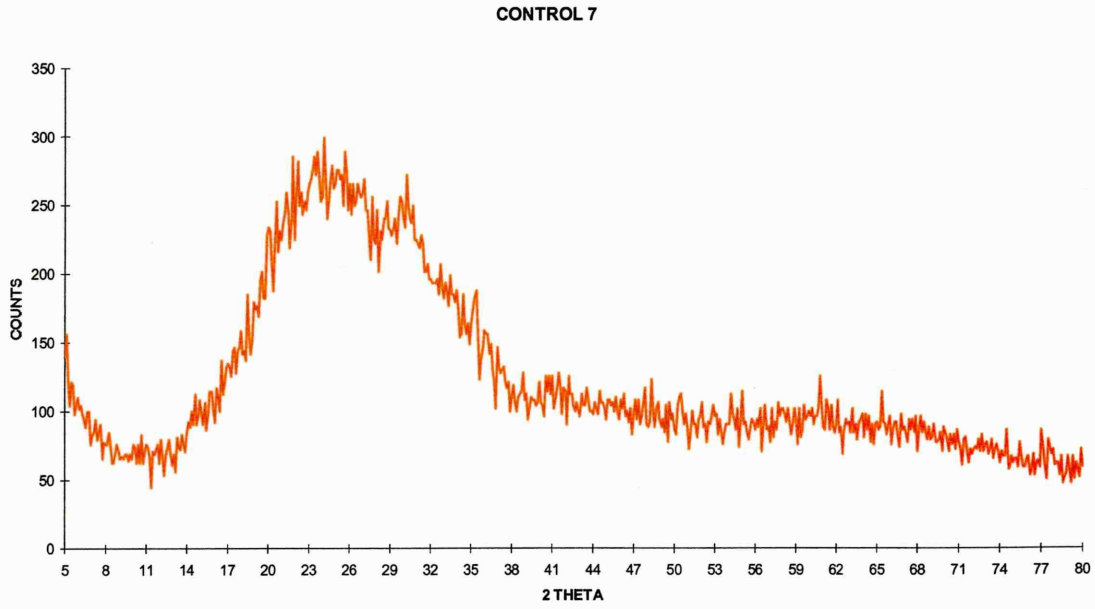

Figure 5.1: *Typical X-Ray diffractogram of ITO glass substrate material.*

The 'substrate' trace shown may be compared to a combined trace from a polypyrrole thick film, containing information originating from polymer and substrate, as shown in Fig. 5.2 (taken from KW#1). Similarities between the two traces are immediately apparent. However, combined traces were consistently observed to exhibit higher intensities below $2\theta \approx 30^{\circ}$ than substrate traces, although intensities at over $2\theta \approx 30^{\circ}$ were very similar to those taken from substrate material.

The two traces shown were manually manipulated using the spreadsheet-based ASCII files produced during the data manipulation method described in §5.1.1. Information was imported from both the substrate trace and the combined trace into a single spreadsheet (as a standard set of 2θ datum points are recorded by the APD 3.6 software unless the user specifies otherwise).

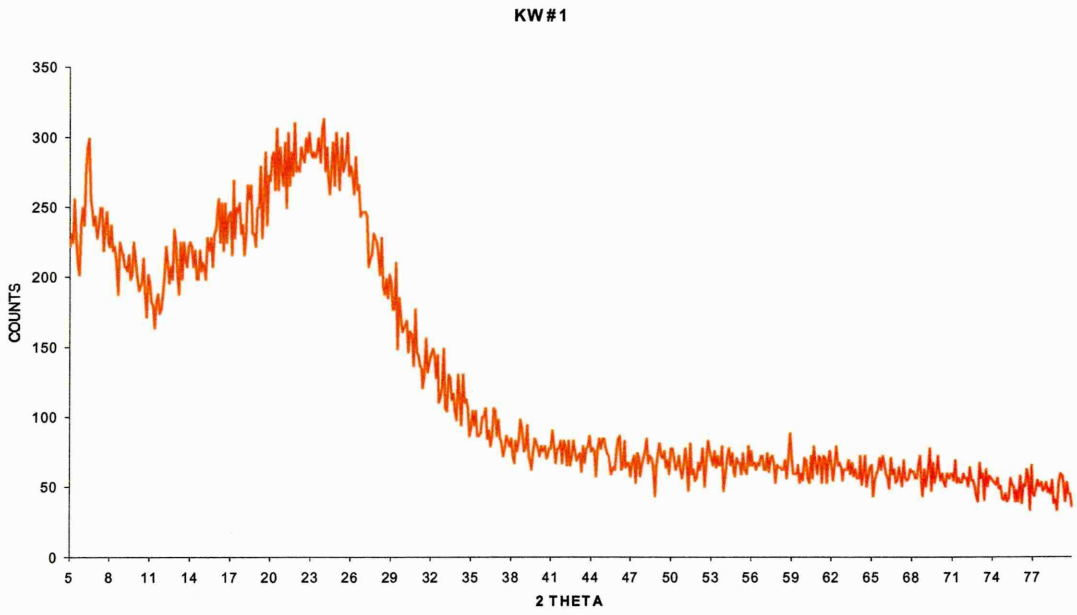

Figure 5.2: *Typical 'combined' X-Ray diffractogram of polypyrrole thick-film, containing information originating from polymer and substrate.*

Simple subtraction of substrate data from combined data typically resulted in the production of traces as shown in Fig. 5.3. As stated above, negligible differences were routinely observed between combined traces and substrate traces at over $2\theta \approx 30°$. This strongly suggests that this section of a typical combined diffractogram contains no polypyrrole structural information.

The diffractogram shown in Fig. 5.3 therefore represents structural information from polypyrrole alone. However, it is of note that the trace dips below the 'zero-counts' level at above $2\theta \approx 26°$. This is thought to be the result of X-Ray attenuation by the polypyrrole layer; attenuation results in fewer X-Rays reaching the substrate, fewer X-Rays being diffracted by the substrate, and still fewer diffracted X-Rays reaching the detector. This results in the level of substrate structural information present in combined traces being significantly less than the level of information present in a dedicated substrate trace.

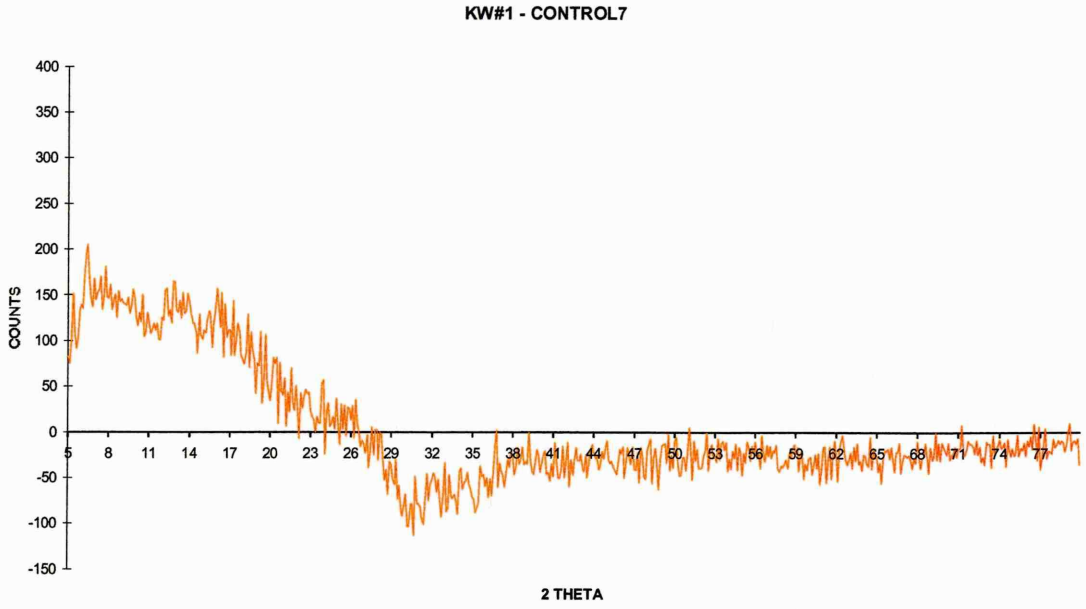

Figure 5.3: *Typical 'combined' X-Ray diffractogram of polypyrrole after manual subtraction of substrate trace.*

In order to account for the attenuation of substrate information by polypyrrole films, a method has been developed whereby decreasing percentages of the substrate trace are subtracted from the 'combined' trace until a level of subtraction is reached which results in a reasonably level trace centered around the zero intensity level at over $2\theta \approx 30^{\circ}$. It is considered that the use of this procedure results in the accurate removal of substrate information from combined diffractograms, so leaving residual structural information pertaining only to the structure of the polypyrrole film. Such a trace is illustrated in Fig. 5.4 (Note: the production of the trace shown involved the subtraction of 65% of the substrate information (hence reproducing a situation where 35% of substrate information is attenuated by the presence of the polymer film)). The presence and characteristics of the remaining 'amorphous hump' below the $2\theta \approx 30^{\circ}$ level will be used during subsequent studies to allow conclusions to be drawn regarding the effects of deposition parameters on polypyrrole microstructure.

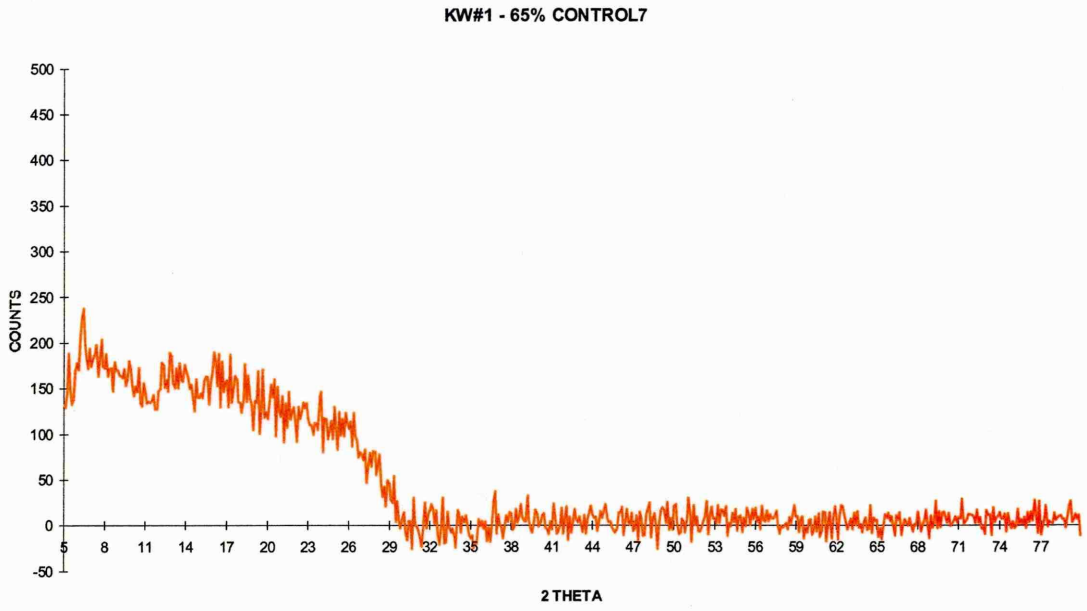

Figure 5.4: *Typical X-Ray diffractogram of polypyrrole after manual subtraction of a suitable proportion of substrate information.*

5.1.3 The Effects of Film Water Content

In order to improve the repeatability of, and to reduce the level of inconsistency between XRD analyses, the effects of the water content of polypyrrole films during analysis has been studied.

Two type-283 polypyrrole films were deposited as described in §5.1; film 'a' was analysed by XRD (using the PW1130/60 diffractometer) whilst wet, immediately after the 'soaking' procedure described in §5.1. Film 'b' was analysed after soaking & drying (again, as described in §5.1). Traces were manipulated as described previously, including the subtraction of substrate information where necessary.

Resultant traces (reproduced in Fig. 5.5 [a] and [b]) illustrate that the water content of polypyrrole films *does* affect the structural information available, although only at angles below $2\theta \approx 10°$. It is not thought that the presence of water within films results in an actual structural variation, but that the presence of water within polypyrrole films results in modifications to the level of X-Ray penetration. Although this effect is not

fully understood, it illustrates the need to ensure that all XRD samples are stabilized in ambient conditions before analysis. The observed differences between the XRD spectra from 'wet' and 'dry' films may be related to the comments made in §4.3.2; differences in the level of 'low angle' scattering may be the result of the presence of water (electrolyte) in 'pockets' throughout the polymer matrix, as discussed in §4.3.5.

It is of note that film 'a' was subsequently reanalysed after drying (maturation) in ambient conditions (see §5.1); film 'b' was reanalyzed whilst wet, immediately after a second 'soaking' process. This was undertaken in order to investigate the repeatability of the tests described above. The traces produced were found to agree well with those shown in Fig. 5.5.

5.1.4 The Effects of 'Non-Polypyrrole' Crystalline Peaks on Disordered Polypyrrole Structural Information

The standard soaking and drying regime introduced in §5.1 was carried out in order to remove as much recrystallised dopant from polypyrrole films as practicable before XRD analysis. This was done in order to remove strong dopant peaks from X-Ray diffractograms, the presence of which may obscure other information pertaining to the microstructure of polypyrrole.

Despite the introduction of this regime, several X-Ray diffractograms were collected during the work presented which displayed order peaks of significant intensity. A study was therefore carried out to assess the effects of the presence of highly crystalline material on (generally disordered) polypyrrole structural information.

Although the presence of ordered clusters of recrystallised dopant material should not adversely affect polypyrrole microstructural information, modifications to film density (through the presence of clusters of crystalline dopant) might result in modifications to the XRD traces obtained.

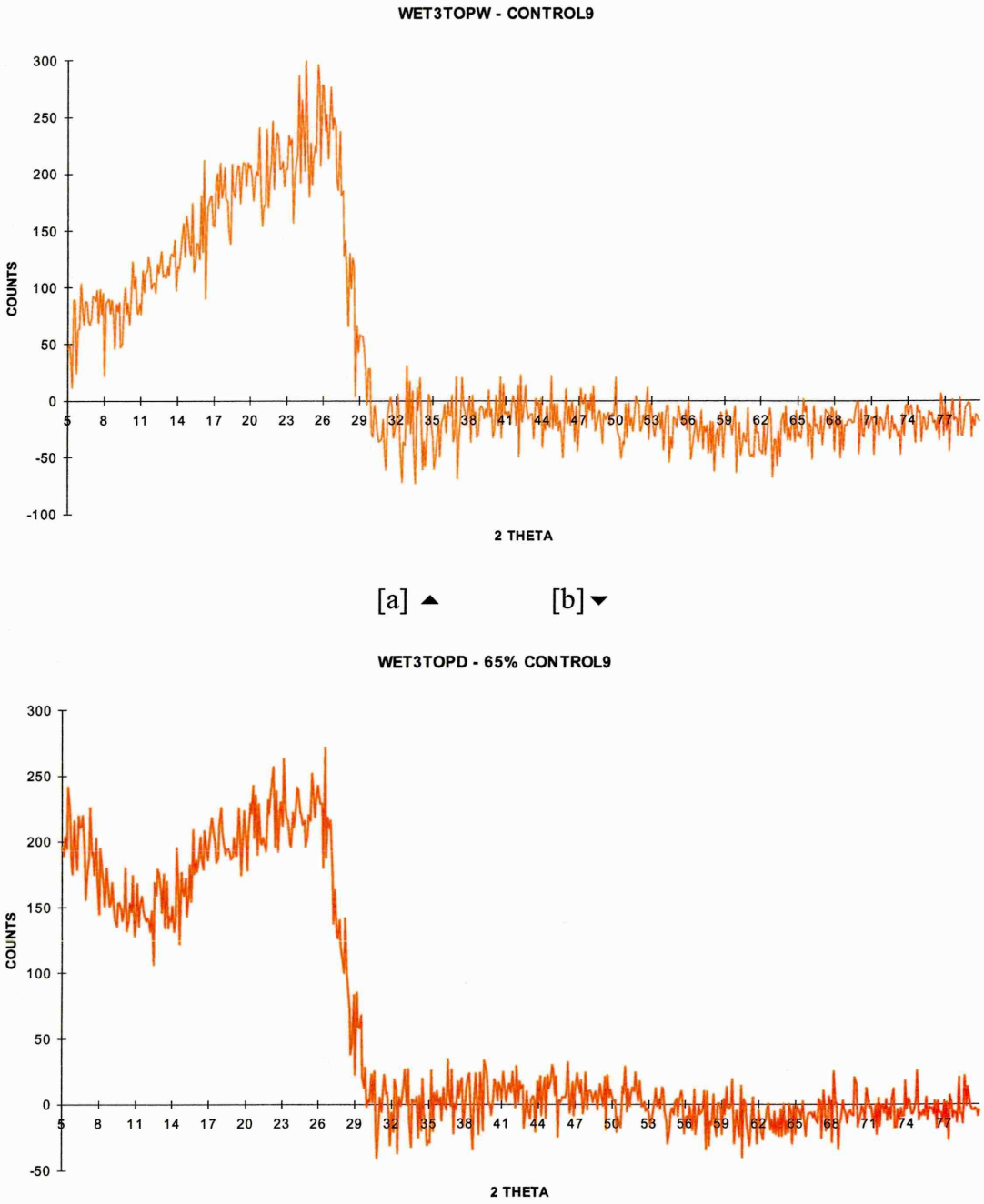

Figure 5.5: *Typical X-Ray diffractograms of polypyrrole in [a] 'as deposited' wet conditions, and [b] after film drying in ambient conditions.*

Two type-283 polypyrrole films were deposited as described in §5.1 using parameters as for film KW#2A. Films were dried as described in §5.1; soaking was *not* carried out in order to allow the recrystallisation of dopant material. Films were analysed by XRD on completion of the drying period. Traces were found to be very similar; a typical trace is shown in Fig. 5.6 [a].

Films were then soaked and dried as described in §5.1 to remove recrystallised dopant material and analysed again by XRD. Resultant traces were found to contain no sharp order peaks, as shown previously. Manipulation of ASCII data allowed the direct subtraction of the traces produced from soaked films from those produced from dried films (as shown in Fig. 5.6 [a]). A resultant trace, which contains no information originating from disordered polypyrrole, but contains all information originating from the presence of recrystallised dopant, is shown in Fig. 5.6 [b]. This may be compared to the trace shown in Fig. 5.6 [c], taken directly from the crystalline dopant.

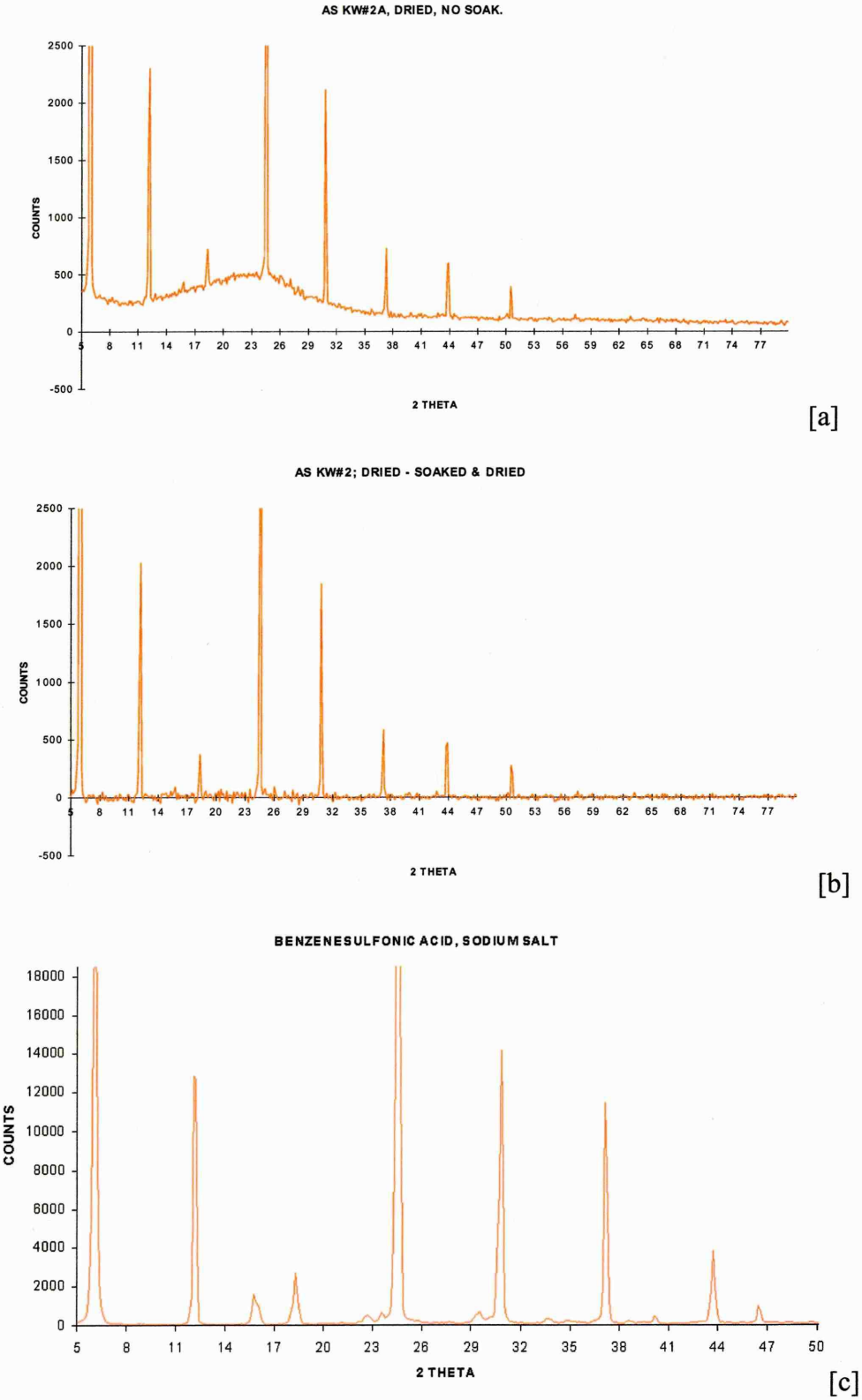

Figure 5.6: *Typical X-Ray diffractograms of polypyrrole [a] from 'non-soaked' films, and [b] from 'non-soaked' films after subtraction of all polypyrrole information, and [c] from benzene sulfonic acid, sodium salt.*

Diffractograms obtained by the subtraction of the polypyrrole 'disordered hump' from traces produced from 'non-soaked' polypyrrole (which show the presence of much order resulting from the recrystallisation of dopant from trapped electrolyte) show strong order peaks on a level 'background'. It is therefore concluded that the juxtaposition of strong order peaks onto polypyrrole disordered diffractograms does not result in any modification to the shape of the disordered hump (the characteristics of which are to be used subsequently in this chapter to assess polypyrrole film order). It is also considered that the above conclusion suggests that the microstructure of polypyrrole is not affected by the localized heating produced on XRD analysis.

5.2 *The Use of XRD to Probe Polypyrrole Microstructure*

After consideration of the conclusions drawn from work presented previously in this chapter, a study has been undertaken to elucidate the effects of type-283 polypyrrole deposition parameters on the microstructural information uncovered by the XRD analysis of the films produced.

FILM I.D.	DEPOSITION POTENTIAL (V)	ELECTROLYTE CONC (M)	DEPOSITION TIME (H)
TF#1 (4)	0.80	0.05	5
TF#2 (3)	0.80	0.10	5
TF#3 (22)	0.80	0.25	5
TF#4 (12)	0.80	0.40	5
TF#5 (11)	0.80	0.50	5
TF#8 (10)	2.00	0.25	5
TF#9 (9)	3.00	0.25	5
TF#10 (16)	3.00	0.50	5
TF#11 (14)	4.00	0.25	5

Table 5.2: *Polypyrrole thick-film deposition parameters.*

A range of films were deposited as described in §5.1 using [a] a variety of deposition potentials, and [b] a range of monomer concentrations; details of the films produced are given in Table 5.2.

(Note: repeat specimens of all film types shown in Table 5.2. were prepared in order to establish the validity of both the diffractograms produced and the structural relationships formed. Short studies are reported towards the end of this chapter which illustrate the high repeatability of both the film deposition process and the extraction of structural information by XRD).

Films were then individually analysed by XRD, with consideration given to work presented previously in this section (and to be presented in Appendix 3);

- films were soaked and dried as described in §5.1,
- XRD ASCII data was manipulated as described in § 5.1.1,
- substrate information was subtracted as described in §5.1.2,
- films were all dried under laboratory conditions before analysis, as described in §5.1.3,
- samples were not 'spun' during analysis, as described in §A3.1,
- the PW1130/60 X-Ray Diffractometer was used (§A3.2),
- low power operation was not used, as discussed in §A3.3 (the X-Ray tube was operated at 30kV and 30mA),
- no smoothing of the diffractograms produced was carried out, as described in §A3.4,
- diffractograms were collected using a standard step size (0.020°), as discussed in §A3.5.

A selection of the salient X-Ray Diffractograms produced during the analysis of the films described in Table 5.2 are systematically illustrated through Fig. 5.7 and Fig. 5.8.

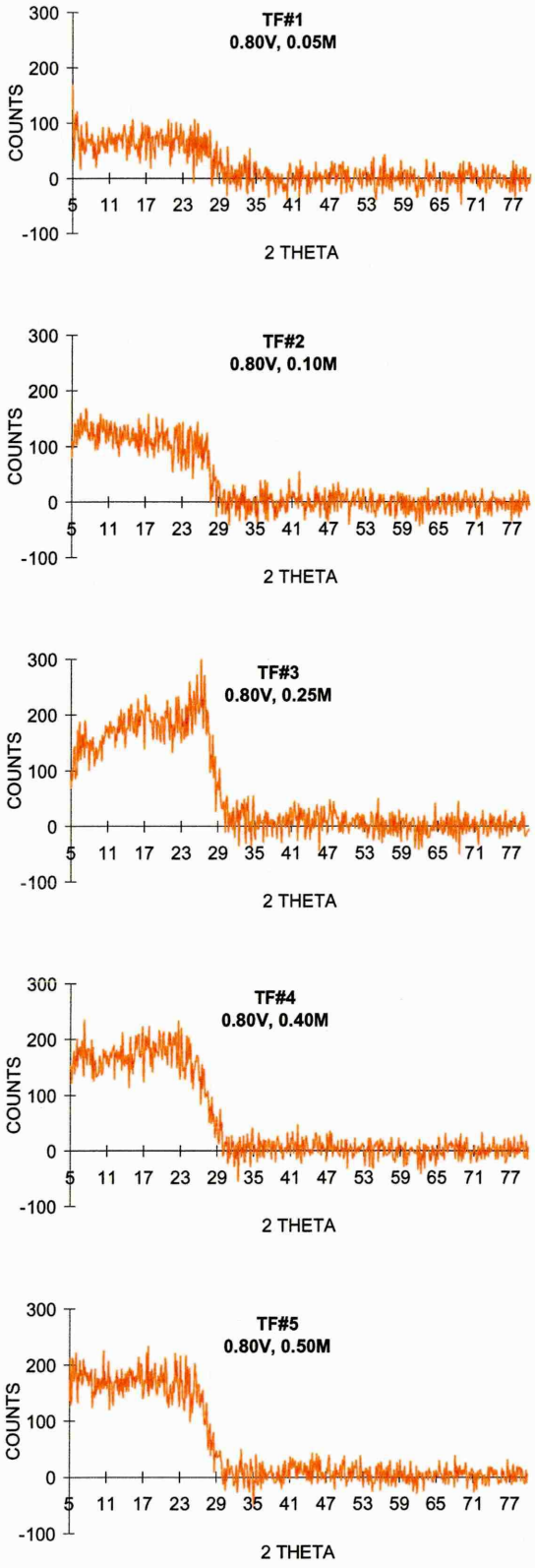

Figure 5.7: *XRD evidence of polypyrrole microstructural modifications resulting from the variation of electrolyte solution concentration.*

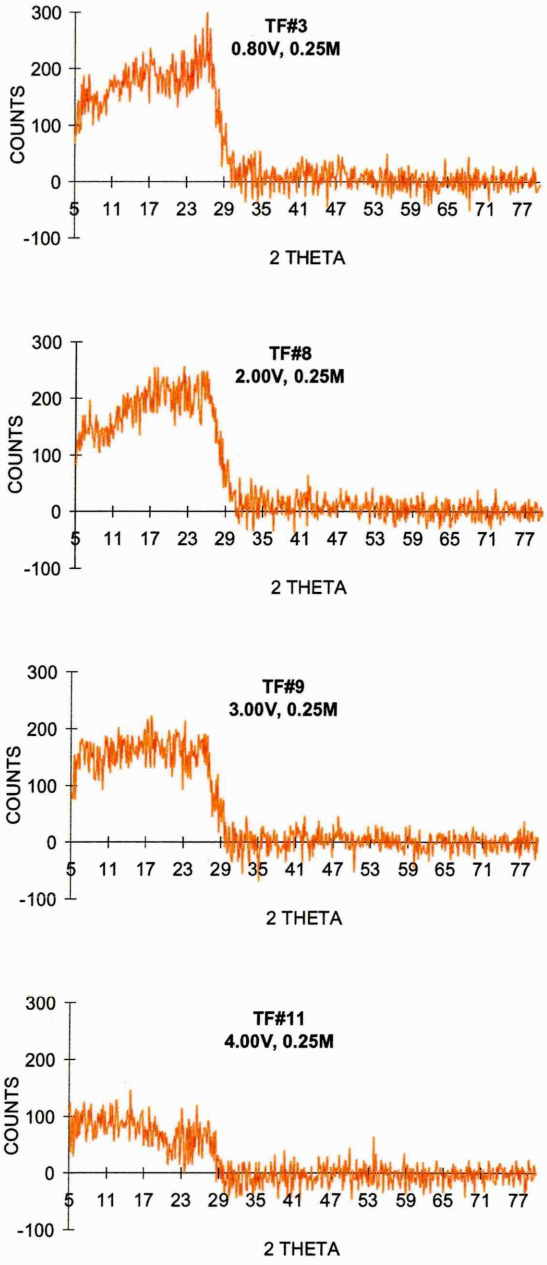

Figure 5.8: *XRD evidence of polypyrrole microstructural modifications resulting from the variation of deposition potential.*

The general appearance of all X-Ray diffractograms presented here strongly suggests the presence of very low levels of order within type-283 electrochemically deposited polypyrrole. However, several notable features of diffractograms collected from polypyrrole deposited under differing conditions redeem type-283 material from full 'amorphous' status; these features are now discussed.

The relationships between the XRD traces shown in Figs. 5.7 and 5.8 and the film deposition parameters used may be summarised as follows.

- Decreasing deposition potential (in the range +4.00V to +0.80V vs SCE, all at 0.25M solution concentration) appears to result in greater 'plateau height' at $2\theta \leq 29°$.

- Increasing solution concentration within the range 0.05M to 0.25M appears to result in:
  [a] greatly increased 'plateau height' at $2\theta \leq 29°$, and
  [b] the formation of a broad 'order peak' centered at $2\theta \approx 24°$; (present on all analyses taken from films deposited at 0.25M solution concentration).

- Increasing solution concentration further from 0.25M to 0.4M and 0.5M results in loss of the broad $2\theta \approx 24°$ order peak, but no reduction in plateau height.

The broad order peak observed at $2\theta \approx 24°$ (see Fig. 5.9) has been shown to correspond with repeat distances of between 3.42Å and 4.04Å (using the methods of calculation reported in §4.4.1).

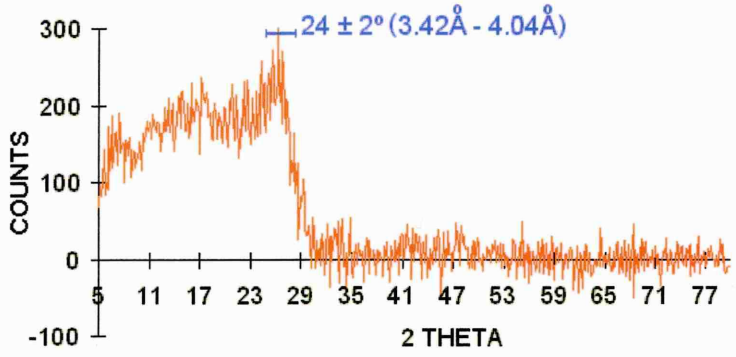

Figure 5.9: *Typical X-Ray diffractogram showing broad $2\theta \approx 24°$ order peak.*

It is logical to consider that the position of the $2\theta \approx 29°$ shoulder observed, in conjunction with the observation of the plateau at lower 2θ levels, suggests that no significant diffraction occurs within the polymer from 'scattering centres' spaced at less than

around 3.09 (between 2.88Å and 3.30Å). Furthermore, significant diffraction occurs from scattering centres spaced at or greater than 3.09Å.

Furthermore, it is considered that the development of the broad $2\theta \approx 24°$ order peak following [a] optimisation of electrolyte solution concentration to 0.25M (shown in Fig. 5.7), or [b] reduction of deposition potential to +0.80V vs SCE (shown in Fig. 5.8) relates to the development of a degree of order within the polymer film, although by no means indicates the development of low-level crystallinity *per se*. This order, centred at between 3.42Å and 4.04Å, has been related by the author to the typical spacing between adjacent pyrrole rings within an aromatic polypyrrole chain, as shown in Fig. 5.10. It is believed that this observation is novel; no such reports of this observation have been found in the literature. As reported in §1.5.2, Saunders *et.al.* ('93) reported the presence of a shoulder on X-Ray diffractograms of polypyrrole; however, the features identified were attributed to the presence of 'face-to-face' pyrrole ring alignment. It is the opinion of the author that the low level of order suggested by the XRD analyses presented (and of similar studies referenced previously, including Saunders *et.al.*, ('93)) strongly suggests against the development of significant face-to-face pyrrole ring alignment. (Note: the work presented here was carried out subsequent to the publication of Lemon and Haigh, ('99a), which suggests that that the shoulder observed during early XRD work may support the hypothesis presented by Saunders *et.al.* ('93)).

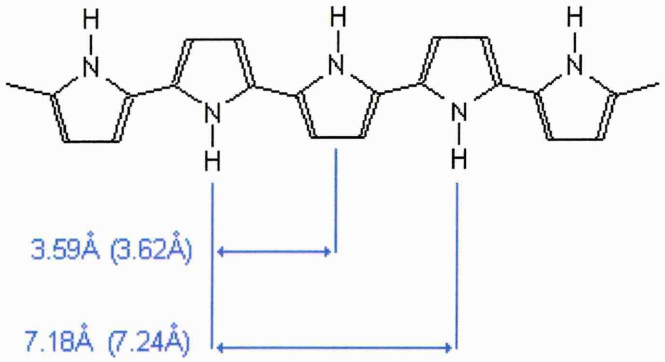

Figure 5.10: *The separation of pyrrole rings in an aromatic (as opposed to quinoid) polypyrrole chain (spacing values reproduced from Street, '86; values in parentheses calculated by the author after Brédas, '86 and Veluri et.al., '95).*

As shown in Fig. 5.10, previous reports from the literature confirm that the spacing of adjacent pyrrole rings within an aromatic polypyrrole chain is between 3.59Å and 3.62Å; this corresponds well with the order peak reproduced in Fig.5.9, centred at between 3.42Å and 4.04Å.

The development of the broad $2\theta \approx 24°$ order peak via either the optimisation of electrolyte solution concentration or reduction of deposition potential (within the ranges discussed previously) is thought to reflect a general increase in the order between adjacent pyrrole rings, and a concomitant increase in polypyrrole chain length. This increase in order (which is assumed to reflect a reduction in the level of common polypyrrole defects, as shown in Fig. 1.27, §1.5.4) agrees well with the results of device resistance studies, which showed increases in device conductivity on increasing dopant concentration from 0.01M to 0.25M (§3.1), although the effects of higher dopant concentration were not investigated. Furthermore, the increase in order observed on the reduction of deposition potential also agrees well with device resistance studies, which suggested increasing device conductivity on the reduction of deposition potential; optimum device conductivity was found on deposition at +0.80V vs SCE (§3.2).

5.2.1 X-Ray Diffractogram Repeatability

The X-Ray diffractograms presented in §5.2, and the conclusions derived, have relied upon two discrete sets of polypyrrole films. The XRD traces produced from the primary film set (as outlined in Table 5.2) have been verified via the production of a secondary film set, prepared using identical materials under identical conditions, and analysed by XRD as reported in §5.2.

XRD traces produced by each primary film have been critically compared to those produced by individual equivalent films from the secondary film set. Trace comparisons were carried out *before* the subtraction of substrate information, as substrate subtraction is known to increase the level of 'noise' present.

An example of the comparisons made is given in Fig. 5.11 [a]. It is note that traces produced using primary and secondary films (shown in red and green respectively) are subjectively identical; this is confirmed by the subtraction of the secondary trace from the primary trace, leaving a featureless plot (as shown in Fig. 5.11 [b]) save for some inherent noise.

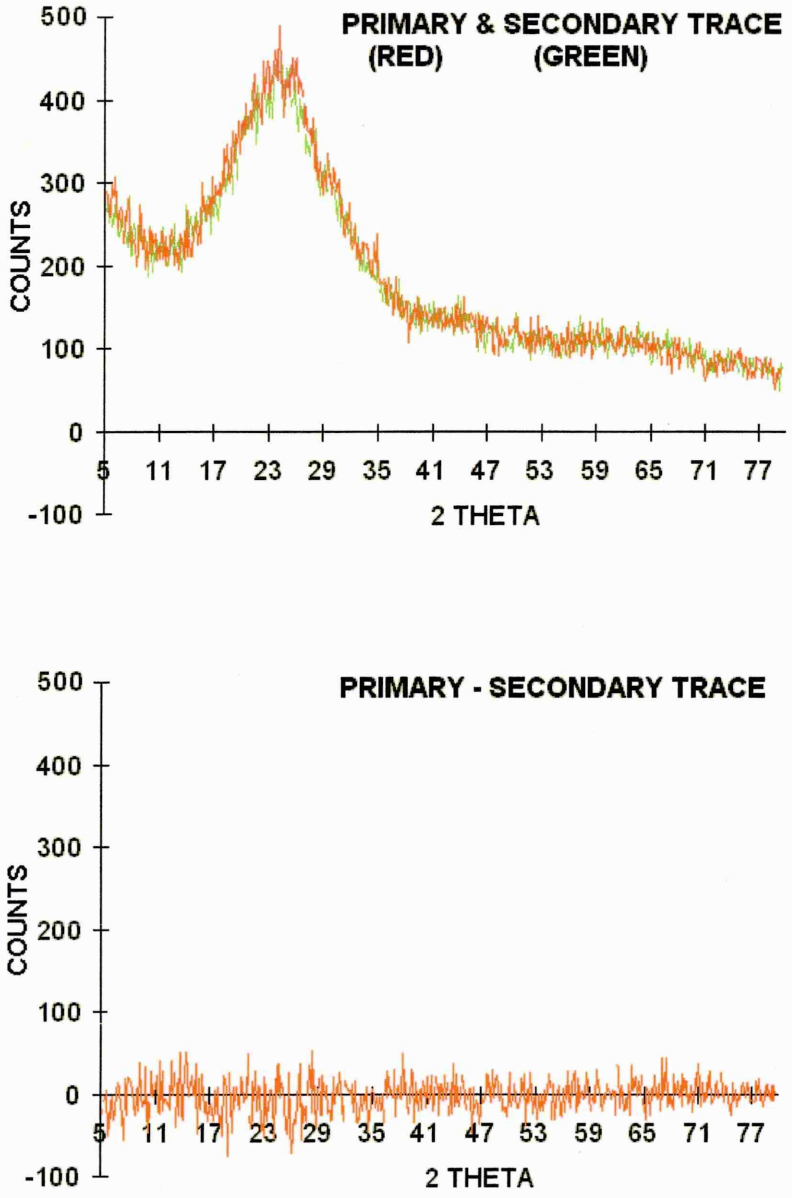

Figure 5.11: *Typical X-Ray diffractogram illustrating [a] repeated analysis of films formed under identical conditions, and [b] subtraction of information from 'primary' and 'secondary' X-Ray traces.*

Summary, Chapter 5

- Little work has been published in the literature regarding the analysis of polypyrrole microstructure by XRD. What little work exists shows polypyrrole to be highly disordered.
- A number of studies are presented which assess the effects of the use of differing XRD analysis parameters during the analysis of polypyrrole thin-films (see also Appendix 3). These studies involved:
    - The development of a technique to allow export of XRD data from the standard (basic) XRD software used into more advanced software.
    - The development of a technique to allow the subtraction of substrate structural information from the XRD traces produced.
    - An assessment of the effects of film water content; significant differences were found, all films were therefore tested in the dry state wherever possible.
    - An evaluation of the effects of large crystalline peaks on 'amorphous' traces was carried out; no adverse effects were observed.
- Using the conclusions drawn from the work presented in §5.1 (and those presented in A3), a study of the effects of polypyrrole deposition parameters on polypyrrole microstructure has been carried out by XRD. Repeatable relationships were observed between deposition potential and structure and between electrolyte solution concentration and structure. The relationships formed were noted to strongly agree with earlier resistometry studies reported previously by the author. Characteristic features of X-Ray diffractograms have been related to the typical spacing between adjacent pyrrole rings within an aromatic polypyrrole chain, it is believed for the first time.

6. Conclusions and Further Work

6.1 Introduction

Prior to the commencement of the work presented, a thorough literature search was undertaken (as reported in Ch. 1) in order to establish a firm focus for the programme of work to be undertaken.

As reflected by the title of this thesis, the selection of relevant organic polymeric species was a fundamental foundation for the direction of the work. Clearly, the study of a representative selection of the wide range of organic polymeric species currently used as gas sensors was not practicable, nor was the study of the range of organic polymers used in the Neotronics e-NOSE 4000 at the commencement of the project. It was therefore ascertained at an early stage (via the literature) that polypyrrole, a disordered polymer, was the subject of much attention as a sensing material. The popularity of polypyrrole was substantiated by its widespread use as gas sensing material in arrays within in the Neotronics e-NOSE 4000. It was therefore decided at a relatively early stage that work within this Ph.D. research programme would concentrate wholly on the elucidation of the structure and performance of polypyrrole. Experience of the operation of the e-NOSE 4000 illustrated that 'type-283' polypyrrole (electrochemically deposited from aqueous solution using a 'benzenesulfonic acid, sodium salt' dopant) was routinely used by Neotronics as a 'cornerstone' sensing material at the heart of the polymer sensor array. Therefore, although the morphology and structure of other polypyrrole sensing materials are studied as required, the work presented concentrates on the study of 'type-283' polypyrrole.

The operation of the mammalian olfactory process relies on the subtly different responses of a number of olfactory receptors. Similarly, the operation of the Neotronics e-NOSE 4000 relies fundamentally on the subtle differences between the resistance and response characteristics of the polymers used (usually polypyrrole, but also including polyaniline, polythiophene, and poly 3-methyl-thiophene). Such subtle differences within polymer species are known to be the result of variations of dopant group and fine variations in deposition parameters (deposition potential, monomer and dopant

concentrations). If the resistance and response characteristics of commercial gas sensing devices (and therefore the collective response and performance of multi-sensor arrays) are to be controlled, then it is considered that *a fundamental understanding of the structural properties of the materials used is necessary.* As stressed throughout the work presented, the level of understanding of the morphological and structural properties of electrochemically deposited polypyrrole was poor before the commencement of the work presented.

The areas of study undertaken during the course of this Ph.D. research programme have therefore been targeted to allow the systematic collection of information relating to the structure of 'type-283' polypyrrole deposited by electrochemical means. Although areas of study have been presented which do not relate *directly* to structural investigation (such as information presented in Appendix 1), such work has been undertaken in order to extend the level of structural information available.

The work presented was carried out in liaison with Neotronics Scientific. It should be noted, however, that the direction of the research programme was not influenced by Neotronics, but was led by the author and supervisory team. However, several pieces of direct support were undertaken for Neotronics where doing so was considered to be of benefit to the Ph.D. work programme. Where work reported in this thesis has been carried out at the direct request of Neotronics, this has been made clear.

6.2 Developments

Details of the work undertaken, and discussions relating to the interpretation of the results gathered and to the potential value of the results have been presented throughout this thesis. Furthermore, summaries of salient observations and developments within each Chapter have been presented in discrete 'Summary' sections. However, a selection of the more salient observations and developments resulting from the work undertaken are presented and discussed below.

- A sizeable literature search has been carried out concentrating on the properties and characteristics of polypyrrole; an *informal* review document has been

produced in order to form a firm understanding of the state of the art in this area. This review (which was formed for the author's use and is not intended for publication) has been utilized by the author as a valuable reference during the planning of the research programme and during interpretation of the results gathered.

- It is evident from the literature that a significant deficiency exists in the level of understanding of the structure of electrochemically deposited polypyrrole.

- A comprehensive and systematic study of the structure of 'type-283' polypyrrole has been performed, utilizing SEM, θ-2θ XRD, GDOES, GC and surface profilometry.

- The effects of the variation of deposition parameters (such as dopant concentration and deposition potential) have been studied. It has been shown that variations in either parameter significantly affect the electrical resistance and morphology of the films produced. It has been demonstrated that resistance and morphological variations result from reproducible differences in film structural maturity.

- Studies of the dependence between deposition time and sensor resistance have demonstrated a logical relationship. Microscopic investigations have illustrated the growth of polypyrrole over insulating substrate areas leading to direct 'polymer bridging' within the first seconds of deposition. The level of gap bridging was shown to correlate well with sensor resistance from initial bridge contact to complete coverage.

- The effects of electrolyte re-use have been studied; it was shown that the deposition of a full set of standard devices from a single electrolyte solution does not affect polypyrrole morphology, although device resistance values were observed to be significantly affected, especially at low electrolyte solution concentration. It is therefore recommended that no more than 10 depositions be undertaken from any one (50ml) electrolyte solution.

- It was found that agitation of the electrolyte solution during film deposition may affect film morphology under some circumstances; although no *adverse* effects were observed, it is recommended that electrolyte is not agitated during deposition, although gentle agitation may reduce the effects of solution depletion (discussed further in Ch. 4).

- The effects of substrate cleaning regimes have been studied; the evaporation of solvent from working electrodes before deposition has been shown to result in the adoption of non-standard morphological traits under some circumstances. It is therefore advised that substrate cleaning / solvent rinses are followed immediately by reproducible drying under high velocity gas jets. Solvent should not be allowed to evaporate on substrates after cleaning.

- Attempts to reproduce the standard Mk-III 'boot-electrode' used in the e-NOSE 4000 within the SHU wafer fabrication facility were partly successful. Efforts to produce interdigital electrodes 'in-house' were not successful; attempts to rectify the problems encountered were not made due to the identification of a reliable supply of electrodes via a third party. The potential advantages of the use of interdigital substrates have been studied, and are discussed in Appendix 2. The hypothesis of the use of interdigital electrodes in favour of standard Mk-III 'boot' electrodes has been presented to Neotronics, although experimental evidence to support this (as presented in A2) was not available at the time of presentation. Several potential electrode designs were presented which utilised interdigitisation. A substrate design was also presented by the author which aimed to improve current homogeneity over the device active area.

- The electrical resistance and temporal stability of devices formed on Mk-III 'boot' electrodes and interdigital electrodes have been assessed and compared. Devices formed using the two electrode types were found to have significantly different resistance characteristics, including severe differences in the initial stability of device resistance. Reasons for the observed differences have been discussed in depth in Appendix 2. It is suggested that the adoption of interdigital

electrodes (in preference to standard 'boot' electrodes) will improve the temporal stability of polypyrrole sensor array devices.

- Studies of the effects of the use of a 'single-comb' or 'single-side' deposition technique for the deposition of polymer onto both interdigital and standard 'boot' electrodes have been carried out. It has been suggested that the use of this technique may lessen the effects of 'interfacial' material (see Fig. A2.3 [b]) in the volume of polymer over substrate insulating areas (sections of polymer grown over insulating areas in order to allow current transfer through the polymer device; so being of crucial importance to sensor performance). Several models are presented which describe potential polypyrrole growth dynamics over insulating areas. Use of this technique was postulated to lead to more reproducible polymer structure in the interfacial regions of devices; empirical evidence supports this, illustrating a marked improvement in sensor-to-sensor resistance repeatability. It is recommended that the use of a single-side deposition technique be adopted for commercial device production.

- In a development of the single-side deposition regime described above, the effects of 'alternate single-side' deposition have been investigated. As above, models were developed describing the potential modifications to sensor layer macrostructure; empirical data supported the models developed, illustrating further improvements to sensor-to-sensor resistance repeatability. It is recommended that the use of such a technique is considered during commercial device manufacture.

- A growth model for the development of nodular morphology of type-283 polypyrrole, based on the direct microscopic observation of morphology at discrete points during morphological development, has been presented. This model supercedes models previously presented by the author (Report for Transfer of Registration from M.Phil. to Ph.D., 1996).

- A range of alternative common polypyrrole dopants have been used (as reported in the literature and as used by Neotronics) in order to study the morphological

effects of dopant group choice. A range of morphologies were observed by SEM, primarily (but not exclusively) nodular. Device resistance was shown to vary widely with dopant group choice. Morphological observations discussed during the work presented during this study were considered to be of great value to the direction of the research programme, leading to further in-depth studies of morphology and structure, in turn leading to peer-reviewed publication, as described below.

- A model has been developed to describe the effects of monomer-based impurities within the electrolyte solution during polypyrrole electrochemical deposition. The effectiveness of monomer purification techniques have been studied by GC, both immediately after purification and subsequently (allowing dynamic accounts of degradation after purification to be discussed). Resistance measurements from devices produced using monomer of a range of purities have shown non-significant differences. Morphological examination has shown that the use of suitably purified monomer leads to the development of nodular morphology, the use of unpurified (or poorly purified) monomer results in the development of 'tendrillar' morphology. Models have been developed to account for the development of tendrillar morphology. The work reported has resulted in the publication of two papers in the scientific press.

- The development of characteristic nodular polypyrrole morphology has been studied in depth. A model has been developed which relates nodule development to electrolytic gas discharge during deposition. Microstructural studies (by XRD and crossed-polar optical microscopy) have shown that nodularity is not the result of spherulitic crystallinity. Rather, it has been demonstrated that nodular morphology is the result of the production of gas at the substrate/film interface during polypyrrole deposition. Empirical evidence has been presented which strongly supported the hypothesis of gas production, including the direct observation of the development and rupture of large gas pockets within the polymer film during high potential deposition. The work presented has resulted in publication in the scientific press.

- Studies by XRD, SEM, EDAX and GDOES have ascertained that the development of strong order peaks on XRD analysis of type-283 polypyrrole films are the result of [a] the entrapment of pockets of electrolyte solution within the polymer film during deposition, and [b] the subsequent recrystallisation of dopant from within the trapped electrolyte solution. Previous models reported in the literature (which describe the 'ideal' crystalline packing of polypyrrole) predict long-range order that corresponds with the order peaks observed by XRD. However, empirical evidence has been collected which strongly suggests that existing theoretical models are inaccurate. Further studies have demonstrated that dopant recrystallisation may be responsible for the sharp drop in sensor resistance often observed after polypyrrole device formation (see Fig. A2.1, §A2.1). It is considered that the sharp resistance drop routinely displayed by type-283 devices is the direct result of the formation of localized areas of highly conductive crystalline dopant material within the polymer matrix. The work presented has resulted in publication in the scientific press.

- XRD analysis of polypyrrole microstructure has resulted in the formation of relationships between polypyrrole structural order and deposition conditions. The relationships formed agree strongly with resistometry data. Features of X-Ray diffractograms have been related to the typical spacing between adjacent pyrrole rings within an aromatic polypyrrole chain.

6.3 Further Work

It is considered that the findings of this PhD work programme (conclusions of which are outlined above) have improved the current level of understanding of the structure of electrochemically deposited polypyrrole. It is considered that the structural repeatability of commercial and research grade devices may be improved greatly by considering the recommendations outlined above. The potential improvements outlined have, in many instances, been corroborated by measurements of electrical resistance. However, if accurate and representative assessments of the potential effectiveness of the modifications suggested are to be made, then it is recommended that devices are produced and are subjected to a rigorous assessment procedure centered around their

effectiveness as 'array member' gas sensors; to do so clearly requires further extensive research.

The following proposals highlight other areas of research which, in the opinion of the author, justify further study:

- As outlined in §4.2, the collection of impurities ahead of the advancing polypyrrole growth face has been shown to result in the production of a novel morphology. It has been shown that the presence of monomer-based impurities in the electrolyte solution results in morphological modification, as does the presence of non-monomer impurities (tin). It may be of value to substantiate the model presented in §4.2 (the Tendrillar Morphology Theory) by the addition of controlled concentrations of non-reactive impurities to electrolyte solutions prior to electrochemical deposition of polypyrrole.

- The research presented concentrates on the elucidation of the structure of 'type-283' polypyrrole (PPy/BSA(Na)/H_2O), a material of fundamental importance to the operation of the Neotronics e-NOSE 4000. Although [a] the level of understanding of the structure of type-283 material has been markedly improved, and [b] many recommendations have been made, it is considered that the repetition of aspects of the work presented concentrating on the elucidation of the structure of polypyrrole doped with alternative species would be of great value. It is recommended that other dopant groups to be studied could include:

  type-257 (butane sulfonic acid),
  type-264 (tetraethylammonium toluene sulfonate),
  type-280 (lithium perchlorate),
  type-281 (lithium hexafluorophosphate),
  type-282 (lithium nitrate), and,
  type-301 (dodecylbenzene sulfonic acid, sodium salt),

  all of which are commonly used polypyrrole dopants within the Neotronics e-NOSE 4000.

- A study of the effects of the use of a range of non-standard substrate materials (such as alumina, silicon, stainless steel, copper etc.) may be carried out. Information regarding potentially novel modifications to polypyrrole morphology and structure may be gathered. However, such information may be of limited use to the operation of the e-NOSE 4000, as currently only gold electrode substrates are used.

- The developments reported above regarding the potential improvements in polypyrrole device resistance repeatability through the use of 'Yoshi' interdigitated electrodes could be applied fully by use of complete Yoshi devices (as reported in §A1.6.1) as sensing array members within the e-NOSE 4000. Device responses to basic substances could be assessed and compared to the responses of standard devices (Mk-III Bass-Warwick). Further study could include the analysis of common odourants or odiferous substances; similar comparisons to standard devices could be made.

- The gas sensing ability of polypyrrole films is postulated to be highly dependent on the porosity and gas permeability of the films produced. It is suggested that the porosity of type-283 polypyrrole (and variations in porosity on variation of deposition parameters) is assessed in order to maximise the gas permeability of the films produced. Work presented to Neotronoics by the author (not reported in this thesis) concerning the diffusion of analytes through polypyrrole films described the free movement of analyte gases throughout the polymer pore network and the diffusion of analyte through solid polymer. The movement of gas throughout the polymer bulk may be assessed by the use of a substrate containing a collection of equidistant electrodes in a single plane, as described previously by Parr *et.al.* ('93) during assessments of the gas diffusivity of phthalocyanine layers. Fick's diffusion laws may be used to model the diffusion of gas throughout the polymer bulk.

- Work presented in this thesis suggests that the position of gas generation at the substrate/film interface may be reliant upon surface defects on the working electrode. It is therefore considered that a study could be undertaken to assess

the effects on polypyrrole morphology of 'patterning' substrate (working electrode) surfaces. The application of regular, fine scratches to the substrate could result in the ordered production of gas, and therefore the ordered development of nodular morphology. It is considered that the development of ordered nodular morphology could increase sensor resistance repeatability.

- The use of interdigital substrates within the e-NOSE 4000 has been postulated to be of potential value; the use of Yoshi substrates has demonstrated the potential advantages of doing so. However, if problems encountered by the author within the SHU wafer production facility were overcome, it would be of great value to assess the results of varying the working electrode 'gap width' used on device resistance and response. It is postulated that minimization of the gap width may reduce response / recovery times, so potentially allowing real-time odour analysis.

- The modification of standard MkIII Bass-Warwick electrodes as outlined in §A1.4 in order to improve the homogeneity of current flow both during device deposition and gas sensing may be studied in more depth. As discussed previously, rationalization of the positions of the electrical contacts used may allow this; electrodes could be produced in the SHU wafer fabrication facility following resolution of the problems encountered (as described in §A1.5).

7. References

Advanced Biosensor Technology (AAI-ABTECH), 1273 Quarry Commons Drive, Suite 200B, Yardley, Pennsylvania, U.S.A.

Aishima T., *J. Agric. Food Chem.*, 39 (1991) 752 (a).

Aishima T., *Anal. Chim. Acta.*, 243 (1991) 293 (b).

Alpha M.O.S., *FOX Electronic Nose Newsletter*, Publicity Material, Alpha M.O.S. France, 20 Av. Didier Daurat 31400 Toulouse, France (1997).

Alpha M.O.S., *α-Prometheus*, Publicity Material, Alpha M.O.S. America, 102 Towne Centre Drive, Hillsborough, New Jersey, 08876, United States (1999).

Amrani M.E.H., Dowdeswell R.M., Payne P. and Persaud K.C., *Sensors and Actuators B*, 44 (1997) 512.

Bartlett P., Archer P. and Ling-Chung S., *Sensors and Actuators B*, 19 (1989) 125.

Bartlett P.N., Blair N. and Gardner J.W., *Electronic Noses, Principles, Applications and Outlook.*, ASCI, Monpellier (1993) 16.

Bartlett P.N. and Ling-Chung S.K., *Sensors and Actuators*, 19 (1989) 141 (a).

Bartlett P.N. and Ling-Chung S.K., *Sensors and Actuators*, 20 (1989) 287 (b).

Bartlett P.N. and Gardner J.W., *Odour Sensors for an Electronic Nose*, in Gardner J.W. and Bartlett P.N. (eds) *Sensors and Sensory Systems for an Electronic Nose*, Kluwer Academic Pub. (1992) 31.

Bassett D.C., *Principles of Polymer Morphology*, Cambridge University Press (1981).

Becerik I., *Annali di Chimi*, 88 (1998) 697.

Billmeyer F.W. Jr., *Textbook of Polymer Science*, John Wiley and Sons (1984).

Biswas M. and Roy A., *Journal of Applied Polymer Science*, 51/9 (1994) 1575.

Blake K., *Private Communication* (1996).

Bodor G., *Structural Investigation of Polymers*, Ellis Horwood (1991).

Bourrounet B., Talou T. and Gaset A., *Sensors and Actuators B*, 26-27 (1995) 250.

Bowen D.K. and Hall C.R., *Microscopy of Materials*, Macmillan Press, London (1975).

Brédas J.-L., Themans B., Andre J.M., Chance R.R. and Sibley R., *Synthetic Metals*, 9 (1984) 265.

Brédas J.-L., in Skotheim T.A. (ed.), *Handbook of Conducting Polymers*, Marcel Dekker, New York (1986).

Brown S.J., *Private Communication* (1995).

Brudzewski K. and Osowski S., *Sensors and Actuators B*, 55 (1999) 38.

Buck T.M., Allen F.G. and Dalton M., *Detection of Chemical Species by Surface Effects on Metals and Semiconductors*, in T. Bregman and A. Dravinicks (eds.), *Surface Effects in Detection*, Spartan Books Inc., USA (1965).

Buckley L.J., Roylance D.K. and Wnek G.E., *J. Polym. Sci., Polym. Phys. Ed.*, 25 (1987) 2179.

Bunn C.W. (Hill R. ed.), *Fibres from Synthetic Polymers*, Elsevier, Amsterdam (1953).

Byun H.G., Persaud K.C., Khaffef S.M., Hobbs P.J. and Misselbrook T.H., *Comput. Electron. Agrig.*, 17 (1997) 233.

Cai Z.H. and Martin C.R., *J. Electroanalytical Chem.*, 300/1-2 (1991) 35.

Chandler G.K. and Pletcher D., *The Electochemistry of Conducting Polymers, 'Electrochemistry', (Specialist periodical Reports),* Royal Society of Chemistry, 10 (1985) 117.

Charlesworth J.M., Partridge A.C. and Garrard N., *J. Phys. Chem.*, 97 (1993) 5418.

Chen S.J., Wang D.Y., Yuan C.W., Wang X.D., Zhang P.Y. and Gu S., *J. Mater. Sci. Lett.*, 19 (2000) 2157.

Chiang C.K., *Phys. Rev. Lett.*, 39 (1977) 1098.

Cho G., Glatzhofer D.T., Fung B.M., Yuan W.L. and O'Rear E., *Langmuir*, 16 (2000) 4424.

Coglan A., *New Scientist*, 23 (6 Dec 1997).

Cole A., McIlroy R.J., Thorpe S.C., Cook M.J., McMurdo J and Ray A.K., *Sensors and Actuators B*, 13-14 (1993) 416.

Commissioning Services Limited, *Flammable Gas Sensors*, CSL, 3 Ballymount Cross Business Park, Dublin 22, Ireland (2001).

Cullity B.D., *Elements of X-Ray Diffraction*, Addison-Wesley, Massachusetts (1978).

Dall'Olio A., Dascola Y., Varacca V. and Bocchi V., *Comptes Rendus C*, 267 (1968) 433.

Davis S., *PhD Thesis*, University of Kent at Canterbury (1997).

Davy H., *On the Fire-damp of Coalmines, and on Methods of Lighting the Mines so as to Prevent its Explosion, Phil. Trans.*, 1 (1815).

De Marcos S. and Wolfbeis O.S., *Analytica Chimica Acta*, 334 (1996) 149.

Deng Z., Stone D.C. and Thompson M., *Analyst*, 121 (1996) 671.

Diaz A.F. and Bargon J., in Skotheim T.A. (ed.), *Handbook of Conducting Polymers*, Marcel Dekker, New York (1986).

Diaz A.F. and Castillo J.I., *J. Chem. Soc, Chem. Commun.* (1980) 397.

Diaz A.F., Crowley J., Bargon J., Gardini G.P. and Torrance J.B., *J. Electroanal. Chem.*, 121 (1981) 355.

Di Natale C., Macagnano A., Paolesse R., Tarizzo E., Mantini A. and D'Amico A., *Sensors and Actuators B*, 65 (2000) 216.

Di Natale C., Macagnano A., Paolesse R., Mantini A., Tarizzo E., D'Amico A., Sinesio F., Bucarelli F.M., Moneta E. and Quaglia G.B., *Sensors and Actuators B*, 50 (1998) 246.

Di Natale C., Macagnano A., Davide F., D'Amico A., Paolesse R., Boschi T., Faccio M. and Ferri G., *Sensors and Actuators B*, 44 (1997) 521.

Dodd G.H., Bartlett P.N. and Gardner J.W., *Odours - The Stimulus for an Electronic Nose*, in Gardner J.W. and Bartlett P.N. (eds.), *Sensors and Sensory Systems for an Electronic Nose*, Kluwer Academic Pub. (1992).

Donohue L.A., *Ph.D. Thesis*, Sheffield Hallam University (1995).

Dravinicks A. and Trotter P.J., *J. Sci. Instrum.*, 42 (1965) 624.

EEV, *EEV eNOSE 5000*, Publicity Material, EEV Limited, Waterhouse Lane, Chelmsford, Essex, CM1 2QU, England (1999).

Ehrmann S., Jüngst J., Goschnick J. and Everhard D., *Sensors and Actuators B*, 65 (2000) 247.

Gabriel A.R., *SEM: A User's Manual for Materials Science*, ASM, Ohio (1985).

Gardner J.W., *Sensors and Actuators B*, 4 (1991) 109.

Gardner J.W. and Bartlett P.N., *Nanotechnology*, 2 (1991) 19.

Gardner J.W. and Bartlett P.N., *Pattern Recognition in Odour Sensing* in Gardner J.W. and Bartlett P.N. (eds.), *Sensors and Sensory Systems for an Electronic Nose*, Kluwer (1992).

Gardner J.W. and Bartlett P.N., *Device for Sensing Volatile Materials*, Int. Patent WO93/03355 (1993).

Gardner J.W. and Bartlett P.N., *Sensors and Actuators B*, 18-19 (1994) 211.

Gardner J.W. and Bartlett P.N., *Electronic Noses – Principles and Applications*, Oxford (1999).

Gardner J.W., Bartlett P.N., Dodd G.H. and Shurmer H.V., *The Design of an Artifical Olafactory System* in D. Schilid (ed), *Chemosensory information Processing*, NATO ASI Series H: Cell Biology, Springer, Berlin (1990).

Gardner J.W., Pearce T.C., Friel S., Bartlett P.N. and Blair N., *Sensors and Actuators B*, 18-19 (1994) 240.

Gardner J.W., Shurmer H.V. and Corcoran P., *Sensors and Actuators B*, 4 (1991) 117.

Garnier F., Korri-Youssoufi H., Srivastava P., Mandrand B. and Delair T., *Synthetic Metals*, 100 (1999) 89.

Gilchrist T.L., *Heterocyclic Chemistry*, Pitman Publishing Ltd. (1985).

Glazier C., *Private Communication* (1999) (Sales Manager, Alpha M.O.S. UK).

Gray H., *Anatomy; Descriptive and Surgical*, Paragon (1998).

Griffin A.R., *Coalmining*, Longman Industrial Archaeology Series (1971).

Griffin A.R., *The British Coalmining Industry - Retrospect and Prospect*, Moorland (1977).

Gustafsson G. and Lundström I., *Synt. Met.*, 21 (1987) 203.

HMSO, *EH40/99, Occupational Exposure Limits 1999*, Health and Safety Executive (1999) (a) ISBN 0 7176 1660 6.

HMSO, *Control of Substances Hazardous to Health (COSHH) Regulations (Approved Codes of Practices) 1999*, Health and Safety Executive (1999) (b) ISBN 0 11082 0878.

Haigh J., *Private Communication* (2001).

Hanawa T. and Yoneyama H., *Bull. Chem. Soc. Jpn.*, 62 (1989) 1710.

Hanawa T., Kuwabata S. and Yoneyama H., *J. Chem. Soc., Faraday Trans. 1*, 84 (1988) 1587.

Hashimoto R. and Yamada Y., *Advanced Robotics*, 8/3 (1994) 243.

Hatfield J.V., Neaves P., Hicks P.J., Persaud K. and Travers P., *Sensors and Actuators B*, 18-19 (1994) 221.

Health & Safety Court Report: Concise Summaries of Recent Health and Safey Offences Including Details of Penalties Imposed, Informa (Medico Legal) Publishing Group (2001).

Health and Safety Executive (HSE), *Preventing Slips and Trips in the Food and Drink Industries – Technical Update on Floor Specification*, FIS22, HSE Books, (1999).

Herrasti P. and Ocón P., *Applied Surface Science*, 172 (2001) 276.

Hibbert D.B., *Introduction to Electrochemistry*, Macmillan Physical Science (1993).

Hinton A., *Ph.D. Thesis*, Sheffield Hallam University (1996).

Hinton A., *Private Communication* (1995).

Hivert B., Hoummady M., Henriod J.M. and Hauden D., *Sensors and Actuators B*, 18-19 (1994) 645.

Hodgins D., *Sensor Review*, 14/1 (1995) 29.

Hodgins D., *Private Communication* (1995).

Holmberg M., Winquist F., Lundström I., Gardner J.W. and Hines E.L., *Sensors and Actuators B*, 26-27 (1995) 246.

Hong H-K., Shin H.W., Yun D.H., Kim S.R., Kwon C.H., Lee K. and Moriizumi T., *Sensors and Actuators B*, 35-36 (1996) 338.

Hong H-K., Kwon C.H, Kim S.R., Yun D.H., Lee K. and Sung Y.K, *Sensors and Actuators B*, 66 (2000) 49.

Hulkaniki A., Michalska A. and Lewenstam A., *Talanta*, 41/2 (1994) 323.

Ikegami A. and Kaneyasu M., *Olafactory Detection Using Intergrated Sensors,* Proc. 3rd Int Conf. Solid-State *Sensors and Actuators (Transducers '85),* Philiadelphia, PA, USA, June 7-11 (1985), 136.

Iredale J., *Private Communication* (1995).

Ives M., *PhD Thesis*, Sheffield Hallam University (1994).

Janata J., *Principles of Chemical Sensors*, Plenum, London (1989).

Jones T.A., Bott B. and Thorpe S.C., *Sensors and Actuators B*, 17 (1989) 467.

Josowicz M. and Janata J., *Anal. Chem.*, 58 (1986) 514.

Kanazawa K., Diaz A.F., Geiss R.H., Gill, W.D., Grant P.M., Kwak J.F. and Logan J.A., *J. Chem. Soc., Chem. Commun.* (1979) 854.

Kanesaka I. and Oda K., *Polymer Journal*, 27/3 (1995) 280.

Kaneto K., Maxfield M., Nairns D.P., MacDiarmid A.G. and Heeger A.J., *J. Chem. Soc., Faraday Trans 1*, 78 (1982) 3417.

Kaneyasu M., Ilekgami A., Arima H. and Iwanga S., *IEEE Trans. Components, Hybrids Manufact. Technol.,* CHMT-10 (1987) 267.

Katsuhiko N., Lien M. and Smyrl W.H., *J. Electrochem. Soc.*, 138 (1991) 440.

Keith H.D. and Padden F.J., *J. Appl. Phys.*, 34 (1963) 2409.

Keith H.D. and Padden F.J., *J. Appl. Phys.*, 35 (1964) 1270 (a).

Keith H.D. and Padden F.J., *J. Appl. Phys.*, 35 (1964) 1286 (b).

Keith H.D. and Padden F.J., *Ford Prize Address* (1973).

Keller A., *J. Polym. Sci.*, 39 (1959) 151.

Keller A., *Kolloid Z. Z. Polym.*, 231 (1969) 386.

Kiani M.S., Bhat N.V., Davis F.J. and Mitchell G.R., *Polymer*, 33/19 (1992) 4113.

Kiani M.S. and Mitchell G.R., *Synth. Met.*, 48 (1992) 203.

Kissinger P.T. and Heineman W.R., Eds., *Laboratory Techniques in Electroanalytical Chemistry*, Second Edition, Marcel Dekker, New York (1996).

Kornic S., *Lecture Notes*, Department of Chemistry and Biochemistry, Uniersity of Guelph, Ontario, N1G 2W1, Canada.
(www.chembio.uoguelph.ca/educmat/chm729/band/concept.htm)

Kuwabata S., Yoneyama H. and Tamura H., *Bul. Chem. Soc. Jpn.*, 57 (1984) 2247.

Lamb A.B. and Hoover C.R., *U.S. Patent* 1321062 (1919).

Lacroix J.C., Maurel F and Lacaze P.C., *J. Am. Chem. Soc.*, 123 (2001) 1989.

Lawes G., *Scanning Electron Microscopy and X-Ray Microanalysis*, John Wiley and Sons (1987).

Legin A., Rudnitskaya A., Vlasov Y., Di Natale C., Mazzone E. and D'Amico A., *Sensors and Actuators B*, 65 (2000) 232.

Lei J.T. and Martin C.R., *Chemistry of Materials*, 7/3 (1995) 578.

Leichnitz K., *Dräger Detector Tube Handbook - Air Investigations and Technical Gas Analysis with Dräger Tubes*, 7th ed., Lübeck (1989).

Lemon P.W. and Haigh J., *A Critical Bibliography of the Fundamental Considerations of Conducting Polypyrrole Thin-Film Gas-Sensing Ability*, copies available from the author (paul.lemon@hsl.gov.uk) and the School of Science and Mathematics, Sheffield Hallam University (1996).

Lemon P.W., *The Structure of Sensor Organic/Polymeric Solids Deposited on Surfaces of Interest for Sensing Devices*, Report for Transfer of Registration from M.Phil. to Ph.D., Sheffield Hallam University (1996).

Lemon P.W., Szczur N. and Haigh J., in *Sensors and their Applications VIII*, ed. A.T. Augousti and N.M. White, I.O.P. Publishing, Philadelphia (1997).

Lemon P.W., *The Effects of Surface Waviness and Pickup Orientation on Surtronic 3+ Performance*, HSL Research Report, IR/L/PE/97/05 (1997).

Lemon P.W., Griffiths R.S. and Thorpe S.C., *The Effects of Cleaning and Surface Treatment on Pedestrian Slipping*, HSL Research Report, IR/L/PE/99/05 (1999).

Lemon P.W., Szczur N. and Haigh J., *Materials Research Bulletin*, 33/6 (1998) 909.

Lemon P.W. and Haigh J., *Materials Research Bulletin*, 34/5 (1999) 665 (a).

Lemon P.W. and Haigh J., in *Sensors and their Applications X*, ed. N.M. White and A.T. Augousti, I.O.P. Publishing, Philadelphia, (1999) (b).

Lewis B., *Private Communication* (1997).

Liang W.B., Lei J. and Martin C.R., *Synth. Met.*, 52 (1992) 227.

Littlefield J.B., Yant W.B. and Berger L.B., *U.S. Bureau of Mines: Rept. Invest. 3276* (1935).

Liveing E.H., *Phil. Mag.*, 9 (1880) 126.

Madden J.D., Cush R.A., Kanigan T.S., Brenan C.J. and Hunter I.W., *Synthetic Metals*, 105 (1999) 61.

Maddison D.S., *Synthetic Metals*, 57/1 (1993) 3544.

Miasic J.J., Hooper A., and Tofield B.C., *J. Chem. Soc., Faraday Trans. 1*, 82 (1986) 1117.

McGeehin P., *Control and Instrumentation*, 25/12 (1993) 23.

McNeill R., Siudak R., Wardlaw J.H. and Weiss D.E., *Aust. J. Chem.*, 16 (1963) 1056.

Michalska A., Lewenstam A., Ivaska A. and Hulkanicki A., *Electroanalysis*, 5/3 (1993) 261.

Mitchell G.R., *Polym.Commun.*, 27 (1986) 346.

Moncrieff R.W., *J. Applied Physiol.*, 16 (742) 1961.

Morea G., *PhD Thesis*, University of Manchester Institute of Science and Technology (1993).

Moy E., *LC-GC Int.*, 8/4 (1995) 221.

Musio F., Amrani M.E.H. and Persaud K.C., *Sensors and Actuators B*, 23 (1995) 223.

Myers R.E., *J. Electron. Mater.*, 15 (1986) 61.

Nagase H., Hirono T., Okamoto Y. and Imanaka T., *Kagaku Kogaku Ronbunshu*, 19/5 (1993) 856 (a).

Nagase H., Wakabayashi K. and Imanaka T., *Sensors and Actuators B*, 13-14 (1993) 596 (b).

Nakamoto T., Fukuda A., Moriizumi T. and Asakura Y., *Sensors and Actuators B*, 3 (1991) 221.

Nakamoto T., Fukuda A. and Moriizumi T., *Sensors and Actuators B*, 10 (1993) 85.

Neotronics, *Neotronics N.O.S.E.*, Publicity Material, Neotronics Scientific Ltd., Western House, 2 Cambridge Road, Stanstead Mountfitchet, Essex, CM24 8BZ, England (1994) (a).

Neotronics, *The Electronic NOSE* (1994) (b), (http://www.neotronics.com/Scientific/nosecopy.htm)

Neotronics, *e-NOSE 4000 Sensor Specifications Listing*, Internal Communication (1994) (c).

Neotronics, *e-NOSE 4000: Neotronics Olfactory Sensing Equipment: User Manual*, Publication Number 059-0298-00, Issue C (1995).

Nishizawa M., Shibuya M., Sawaguchi T., Matsue T. and Uchida I., *J. Phys. Chem.*, 95 (1991) 9042.

Nogami Y., Pouget J.-P. and Ishiguro T., *Synthetic Metals*, 62/3 (1994) 257.

Nylander C., Armgarth M. and Lundström I., *Proc. Intl. Meeting on Chemical Sensors, Fukuoka*, ed. Seiyama T., Fueki K., Shiokawa J. and Suzuki S., Elsevier (1983) 203.

O'Rourke J.K., *PhD Thesis*, Sheffield Hallam University (1994).

Okamoto T., Tada K and Onoda M., *Jpn. J. Appl. Phys.*, 39 (2000) 2854.

Paasch G., Schmeißer D., Bartl A., Naarmann H., Dunsch L. and Göpel W., *Synthetic Metals*, 66/2 (1994) 135.

Parr A.T.J., Krier A. and Collins R.A., *Thin Solid Films*, 230/2 (1993) 225.

Patrash S.J. and Zellers E.T., *Analytical Chemistry*, 65/15 (1993) 2055.

Paul R.B., Kelley J.M., Pepper D.C. and Long C., *Polymer – London*, 38/8 (1997) 2011.

Payne P., *Private Communication* (1997).

Pearce T.C., Gardner J.W., Freil C., Bartlett P.N. and Blair N., *Analyst*, 118 (1993) 371.

Pearce T.C., Gardner J.W., Freil C., Bartlett P.N. and Blair N., *Sensors and Actuators B*, 18-19 (1994) 240.

Persaud K.C., Bartlett J.G. and Pelosi P.A., *Design Strategies for Gas and Odour Sensors which Mimic the Olfactory System*, in Dario P., Sandini G. and Aebisher P. (eds.), *Robots and Biological Systems: Towards a New Bionics?*, NATO ASI Series, Springer, Berlin (1993) 579.

Persaud K.C and Dodd G.H., *Nature*, 299 (1982) 352.

Persaud K.C., Khaffaf S.M., Payne J.S., Pisanelli A.M., Lee D.-H., and Byun H.-G., *Sens. Act. B.* 35-36 (1996) 267.

Petrillo C., Borra S., Cagnolati R. and Ruggeri G., *Journal of Chemical Physics*, 101/12 (1994) 11004.

Pfluger P., Weiser G., Scott J.C. and Street G.B., in Skotheim T.A. (ed.), *Handbook of Conducting Polymers*, Marcel Dekker, New York (1986).

Pliskin W.A. and Conrad E.E., *Nondestructive Determination of Thickness and Refractive Index of Transparent Films*, IBM Journal of Research and Development, 8 (1964) 43.

Rees D.V. and Bassett D.C., *J.Mat.Sci.*, 6 (1971) 1021.

Ren X.M. and Pickup P.G., *Journal of Electroanalytical Chemistry*, 396 (1995) 359.

Rikukawa M. and Rubner M.F., *Journal of Macromolecular Science - Pure and Applied Chemistry*, A31(7) (1994) 793.

Rumelhart D.E. and McClelland J.L., *Parallel Distributed Processing*, MIT Press, Cambridge, Mass. (1986) 318.

Sadaoka *Yoshi*hiko, Department of Applied Chemistry, Faculty of Engineering, Ehime University, Bunkyo-cho, Matsuyama, Ehime, 790, JAPAN. (www.ehime-u.ac.jp/English)

Sak-Bosnar M., Budimir M.V., Kovac S., Kukuli D. and Duic L., *J. Polym. Sci. Part A Polym. Chem.*, 30 (1992) 1609.

Sansiñena J.M., Olazábal V., Otero T.F., Polo de Fonseca C.N. and De Paoli Marco-A., *Chem. Commun.* (1997) 2217

Saoudi B., Despas C., Chehimi M.M., Jammul N., Delamar M., Bessière J. and Walcarius A., *Sensors and Actuators B*, 62 (2000) 35.

Saunders B.R., Murray K.S., Fleming R.J. and Korbatieh Y., *Chemistry of Materials*, 5/6 (1993) 809.

Saunders B. R., Fleming R.J. and Murray K.S., *Chem. Mater.*, 7/6 (1995) 1082.

Schultens H.A. and Schild D., *Biophysical Properties of Olfactory Receptor Neurones*, in Gardner J.W. and Barlett P.N. (eds.), *Sensors and Sensory Systems for an Electronic Nose*, Kluwer Academic Pub. (1992).

Schweizer-Berberich P.-M., Vaihinger S., Göpel W., *Sensors and Actutors B*, 18-19 (1994) 282.

Scrosati B., *Prog. Solid St. Chem.*, 18 (1988) 1.

Semancik S. and Cavicci R.E., *Applied Surface Science*, 70-1 (1993) 337.

Senior J., *Last of the Day-Hole Miners*, Walking International Ltd. (1997).

Senior J., *Private Communication* (1998).

Sherwood, L., *Human Physiology: From Cells to Systems*, 3rd Ed., Wadsworth (1997).

Shurmer H.V., *Identifying or Measuring Components of a Mixture*, U.K. Patent Application, GB 2 203 249 A (1988).

Shurmer H.V., Corcoran P. and Gardner J.W., *Sensors and Actuators B*, 4 (1991) 29.

Shurmer H.V. and Gardner J.W., *Sensors and Actuators B*, 8 (1992) 1.

Shurmer H.V., Gardner J.W. and Corcoran P., *Sensors and Actuators*, B1 (1990) 256.

Skotheim T.A. (ed.), *Handbook of Conducting Polymers*, Marcel Dekker, New York (1986).

Softkey, *Compton's Interactive Encyclopedia (CIE)*, Learning Company Properties Inc. (1998).

Stankovic R., Pavlovic O., Vojnovic M. and Jovanovic S., *European Polymer Journal*, 30/3 (1994) 385.

Statham I.C.F., *Coal Mining Practice*, Caxton (1958).

Stella R., Barisci J.N., Serra G., Wallace G.G. and De Rossi D., *Sensors and Actuators B*, 63 (2000) 1.

Street G.B. in Skotheim T.A. (ed.), *Handbook of Conducting Polymers*, Marcel Dekker, New York (1986).

Street G.B., Clarke T.C., Krounbi M., Kanazawa K.K., Lee V., Pfluger P., Scott J.C. and Weisser G., *Molec. Cryst. Liq. Cryst.*, 83/1-4 (1982) 1235.

Strobel H.A., *Chemical Instrumentation*, Addison-Wesley (1977).

Stubb H., Punkka E. and Paloheimo J., *Materials Science & Engineering R-Reports*, 10/3 (1993) 85.

Su W. and Iroh J.O., *J. Adhesion*, 73 (2000) 215.

Sun A., Yang Y., Jiang Y., Fan Z., Liu Q. and Zhou Q., *Sensors and Actuators B*, 66 (2000) 88.

Sukeerthi S. and Contractor A.Q., *Indian Journal of Chemistry Section A - Inorganic Bio-Inorganic Physical Theoretical & Analytical Chemistry*, 33/6 (1994) 565.

Szczur N., *Private Communication* (1997).

Taguchi N., *UK Patent Specification* 4314996 (1970).

Tamura H., Watanabe M. and Sugisawa H., *Nippon Shokuhin Kogyo Gakkaishi*, 44/5 (1994) 341.

Thorpe S.C., *Private Communication* (1997).

Threlkeld J., *Pits 2 - A Pictorial Record of Mining*, Wharncliffe (1989).

Torrez-Gómez G., Skaarup S., West K. and Gómez-Romero P., *J. Electrochem. Soc.*, 147/7 (2000) 2513.

Truong V.T., Ennis B.C. and Forsyth M., *Synthetic Metals*, 69 (1995) 479.

Truong V.T., Riddell S.Z. and Muscat R.F., *J. Mater. Sci.*, 33 (1998) 4971.

Ulmer H., Mitrovics J. Weimar U. and Göpel W., *Sensors and Actuators B*, 65 (2000) 79.

Veluri K., Corish J., Morton-Blake D. and Beniere F., *Theochem – Journal of Molecular Structure*, 334 (1995) 109.

Vlasov Y.G., Legin A.V., Rudnitskaya A.M., D'Amico A. and Di Natale C., *Sensors and Actuators B*, 65 (2000) 235.

Walsh P., *Private Communication* (2001).

Wang L.X., Li X.G. and Yang Y.L., *Reactive and Functional Polymers*, 47 (2001) 125.

Warburton J., *Private Communication* (1998).

Warren L.F., Walker J.A., Anderson D.P., Rhodes C.G. and Buckley L.J., *J. Electrochem. Soc.*, 136 (1989) 2286.

Watanabe A.,Tanaka M. and Tanaka A., *J. Bull. Chem. Soc., Jpn.*, 54 (1981) 2278.

Webster C., *Private Communication* (1995), (Neotronics Sensor Group Meeting, 26.4.95).

Whiston C., *X-Ray Methods*, John Wiley and Sons, Chichester (1987).

Wilson A., Rigby G.P., Wright J.D., Thorpe S.C., Terui T. and Maruyama Y., *J. Mater. Chem.*, 2/3 (1992) 303.

Windle A.H., *A First Course in Crystallography*, G.Bell and Sons, London (1977).

Wynne K.J. and Street G.B., *Macromolecules*, 18 (1985) 2361.

Yadong J., Tao W., Zhiming W., Dan L., Xiangdong C. and Dan X., *Sensors and Actuators B*, 66 (2000) 280.

A1. Sensor Substrate Evolution

The sensing electrode substrates ('chips') used in the latest version of the Neotronics N.O.S.E., the *'E-Nose 4000'*, (i.e. the sensor substrates used throughout this study) have been the subject of much development since their conception during early research at The University of Warwick (see § 1.4). The development and production of these substrates will be discussed in this chapter, along with the work undertaken by the author involving the use of interdigital ('comb') electrodes as substrates for electrochemically deposited polypyrrole gas sensing elements.

A1.1 Evolution of N.O.S.E. Sensing Electrodes

The early evolution of the electrode designs used in the Neotronics N.O.S.E. (and its predecessors) is discussed in §1.4.1. Several sensor types have been used to date; the original Warwick N.O.S.E. used Taguchi sensing elements (Persaud and Dodd, '82). A novel sensing electrode design (Bartlett *et.al.*, '89) was subsequently adopted shortly before the transition to the use of conducting polymer chemoresistors. These electrodes were formed by the sputter coating of gold thin-films onto *both* sides of thin (12μm) insulating mylar film. The resultant structures were encapsulated in an araldite matrix between two sheets of perspex. The edge of the 'perspex-araldite-gold-mylar-gold-araldite-perspex' laminate was then polished to reveal two thin gold electrodes. The ease by which these 'sandwiches' could be recycled (by abrasion) to leave a pristine electrode made them ideal for research applications. However, the need for a reliable supply of 'industrial grade' electrodes led to the replacement of the 'sandwich' devices by planar electrodes, based on SiO_2 substrates (Gardner *et.al.*, '91; Gardner and Bartlett, '91; Shurmer and Gardner, '92).

Note: Although technically superior to the research 'gold-mylar-gold' electrodes, recycling of the SiO_2-based electrodes was not simple. Investigative work has been carried out by the author into the efficacy of SiO_2 electrode recycling techniques. This work was at the request of Neotronics, and is summarised in §3.4.

After a period of development, Neotronics finalised the design of a suitable chip (which consisted of a substrate and an electrode, as shown in Fig. A1.1) for use in the N.O.S.E. This design, known as the "MkII Bass-Warwick Sensor " (shown in Fig. 1.12 [a], §1.4.2), was used in all Neotronics artificial olfactory equipment until early 1995, when the MKII electrode was replaced with the "MKIII" electrode. The structure of the MKII electrode will not be discussed here, as this electrode type was not utilised significantly during the work presented.

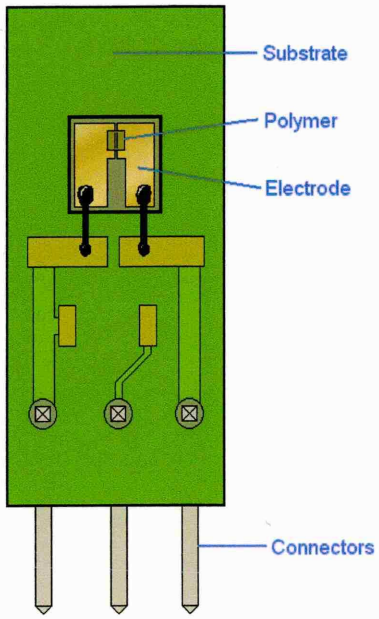

Figure A1.1: *The 'MK III' Bass-Warwick Sensor (adapted from Neotronics, '95).*

Although the structure of the MKII chip was nearly identical to that of the MKIII, the physical dimensions of the MKIII *electrode* were substantially reduced in order to both reduce the current path and cut material costs; electrode area was reduced from 7mm x 7mm to 3mm x 3mm. *Substrate* dimensions were unchanged to allow back-compatibility between MKII and MKIII chips.

A1.2 Industrial Formation of Sensing Elements

Both the MKII and MKIII sensor chips consist of a resin-based substrate, with a triple PCB header connection to allow for simple installation and rapid 'like for like' sensor replacement. The 3mm x 3mm sensing *electrodes* (see Fig. A1.1) are formed *en masse* from 4 inch <100> oriented n-type silicon wafers in a class-100 clean room.

A silicon dioxide layer is grown on the surface of the silicon wafer in order to provide an insulating barrier. This is achieved by a wet-oxide method (where the wafer is baked at 1000°C, and Nitrogen is blown over the wafer after being passed through water at 95°C). The thickness of the layers produced are measured by ellipsometry as being between 0.8 – 1.0µm (Hinton, '96).

The oxidised silicon wafers are then coated with a ≈100Å titanium bonding (or "glue") layer, followed by a ≈4000Å layer of high purity gold. The bonding layer is used to increase the adhesional characteristics of the conducting gold layer.

Photolithographic techniques are then used to define the gold/titanium "boot" electrode formation, as shown in Fig. A1.2:

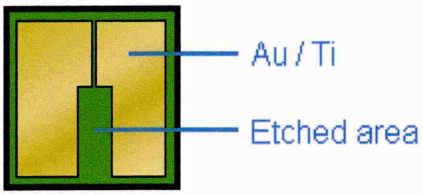

Figure A1.2: *The "MKIII Bass-Warwick Sensor" gold / titanium "boot-electrode" formation, (adapted from original photolithographic mask, courtesy of Neotronics Scientific Ltd., 1996).*

The photolithographic techniques used to define the gold "boot-electrode" formation involve the use of 'photoresist', a photosensitive material which is spin-coated onto the processed silicon wafer. [N.B. Exposure of the photoresist to ultraviolet light modifies its solubility, so allowing the removal of unexposed areas (or exposed areas) after exposure. The type of solubility change on exposure is governed by the type of photoresist used; negative resists harden on exposure to u.v. radiation, whilst positive resists become more soluble on exposure (non-exposed areas harden on heating)].

The silicon / silicon dioxide / titanium / gold wafer is spin-coated with resist, heated to 'semi-cure', and exposed to ultraviolet radiation using the mask (photolithographic plate) similar to the illustration shown in Fig. A1.2. Ultraviolet light is used due to the micron-scale of the features to be produced. Visible light, or electromagnetic radiation

of longer wavelength, cannot be used as the size of the desired features is of micron scale (i.e. is of comparable dimension to the wavelength of visible light).

Subsequent treatment of the wafer involves etching of the gold / titanium areas of the 'boot' design represented as green in Fig. A1.2, leaving two electrodes, separated by a 10µm insulating gap, and surrounded by insulating silicon dioxide. This is achieved by etching the wafer with potassium iodide and hydrofluoric acid, so removing the desired areas of soft resist, gold and titanium. A plasma asher is then used to remove the hardened resist over the gold electrodes.

A CVD-Nitride layer is then applied to the entire surface of the silicon wafer, which is similarly etched via the mask shown in Fig. A1.3. Three areas of the nitride layer are removed (shown in white on Fig. A1.3), leaving two contact points (to which electrodes are attached) and a conducting area over which the conducting polymer is deposited.

Figure A1.3: *The "MKIII Bass-Warwick Sensor" photolithographic mask for formation of insulating resist (adapted from original photolithographic mask, courtesy of Neotronics Scientific Ltd., 1996).*

A1.2.1 Sensing Element Microtopographical Analysis

The microtopographies of a range of as-supplied MkIII Bass-Warwick Sensors were studied in order to collect information regarding the depth of the insulating gap, the thickness of the insulating material surrounding the gold electrode, and the surface texture of the electrode.

The microtopographies of a selection of ten new, freshly cleaned (propan-2-ol) MkIII electrodes were analysed using a Taylor Hobson Surtronic 3+ surface microroughness transducer (see §2.2.5), calibrated to a NAMAS standard roughness specimen. Talyprofile software was used during analysis; a typical trace is shown in Fig. A1.4.

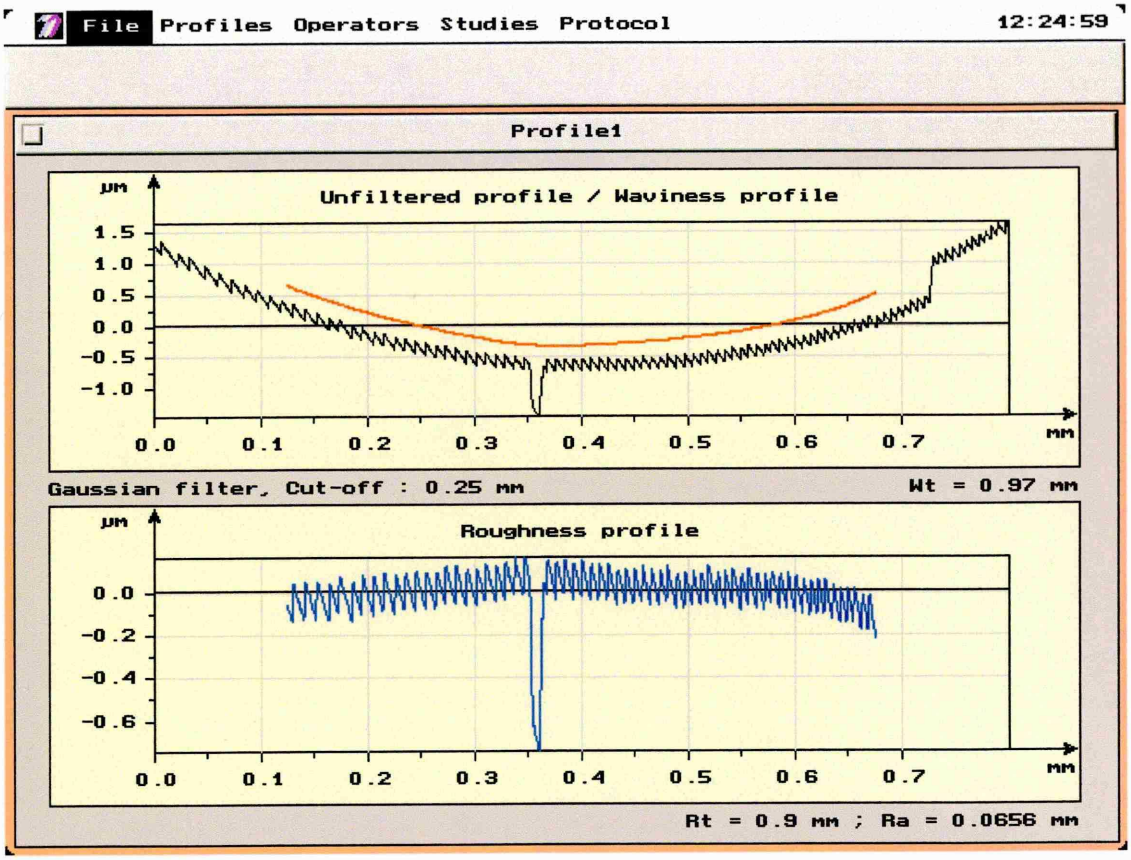

Figure A1.4: *Surtronic 3+ analysis of the microtopography of a MkIII Bass-Warwick Sensing Electrode. Note [a] the differing scale of x- and y-axes; the departure from flatness shown on the upper (black) trace represents a very slight curvature of around 1.2µm* over around 360µm*, and [b] the artificial microroughness represented on the surface of the microelectrode on the lower (blue) trace; this is known to be the result of approaching the resolution limit of the equipment used and so does not represent true texture. (*Figures quoted as means calculated directly via Surtronic output).*

Five measurements of gap depth and five measurements of insulator depth were taken; a single measurement was taken from each electrode due to damage caused by the Surtronic 'skid' during testing. Mean values were calculated as follows:

Mean Insulator Depth = 0.56±0.08µm*

Mean Gap Depth = 0.94±0.04µm*

*(*error margins presented as ± 2 standard deviants).*

Gap width measurements were not taken due to the high accuracy of figures quoted by Neotronics Scientific.

A1.2.2 Sensing Element Recycling

The electrode production techniques described in this chapter are sufficiently complex to result in production costs being of concern to Neotronics. The cost of MkIII Bass-Warwick electrode production has been estimated to be in excess of £8 per electrode (Iredale, '95). As a result, electrode recycling techniques were developed by Neotronics (the details of which were not released to SHU for commercial reasons) in order to allow the re-use of both [a] electrodes used during research and development, and [b] electrodes returned to Neotronics due to sensor failure.

It was noted that sensors produced using recycled electrodes performed poorly, with irreproducible baseline resistance and analyte responses. The author was therefore requested to assess the efficacy of the electrode recycling techniques used by Neotronics Scientific.

The morphologies of a set of 50 electrodes were studied by optical microscopy (using an Olympus VANOX model AHM-T binocular optical microscope with thermal print facility). Several features were noted to be common to many of the supplied electrodes, all of which could contribute to the reported lack of resistance and response consistency displayed by recycled electrodes. These were; [a] the failure of the recycling techniques used to remove polymer from the substrate active area (Fig. A1.5 [a]), [b] failure to remove polymer from areas of cracked insulator surrounding the active area (Fig. A1.5[b]), and [c] damage to the insulating area surrounding the gold active area (Fig. A1.5[c]). It is understood that the use of electrode recycling techniques was halted by Neotronics on presentation of the above information.

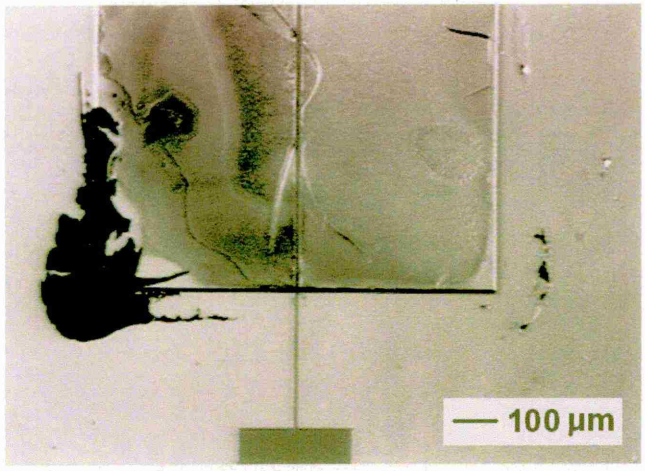

[a]

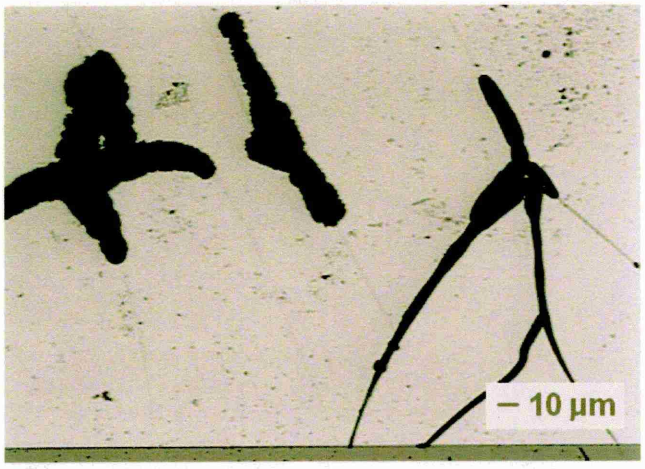

[b]

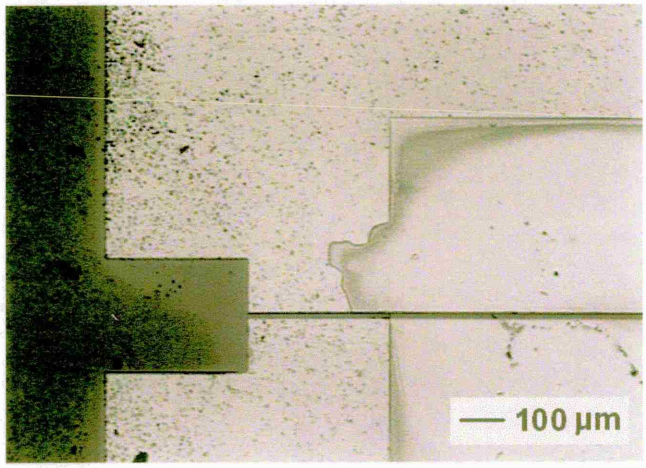

[c]

Figure A1.5: *Optical micrographs of MkIII Bass-Warwick electrodes following a standard Neotronics recycling procedure, showing [a] remaining polymer on the substrate active area, [b] remaining polymer on insulator cracks, and [c] insulator damage.*

A1.2.3 Pre-Deposition Sensing Element Treatment

In an attempt to improve the reproducibility of sensor baseline resistance and analyte response, Neotronics Scientific considered the adoption of an aggressive substrate cleaning procedure involving the application of an a.c. electrical current to MkIII electrodes during submersion in dilute H_2SO_4 (H_2SO_4 electrolysis).

The lack of effectiveness of this technique for the removal of grease and/or dust was discussed with Neotronics during a meeting between Neotronics management and an SHU delegation in July '95; it was stressed that H_2SO_4 electrolysis would not be an effective technique for the removal of dust and/or grease from substrates (J. Haigh). It was also noted that SHU had adopted an effective cleaning regime involving gentle agitation in propan-2-ol (IPA) and removal with a high velocity jet of oxygen-free nitrogen (as described previously), which removed grease and also dust, provided that the substrate was 'blown' with N_2 before evaporation occurred (see §3.7).

SHU were requested to examine a set of 'pre-' and 'post-H_2SO_4 treatment' electrodes to assess the physical effects of pre-treatment, particularly any modifications to the gold active area.

A set of four MkIII Bass-Warwick electrodes were supplied by Neotronics for analysis, and were tested by the author in the as-found state. Each electrode was examined by Optical Microscopy, Scanning Electron Microscopy and Energy Dispersive X-Ray Analysis (see §2.2.1).

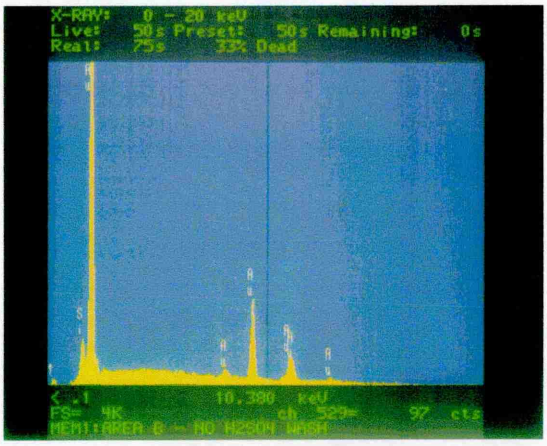

[a]▲

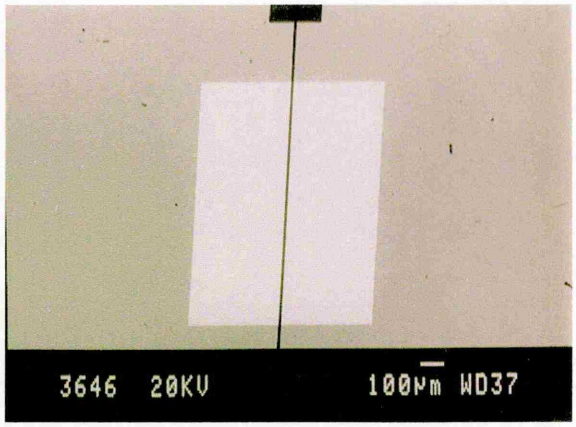

[b]▲

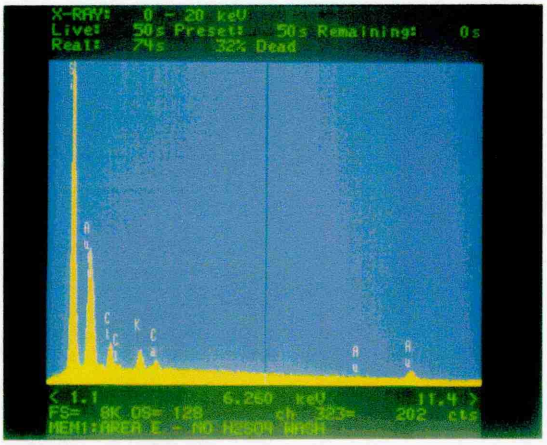

[c]▲

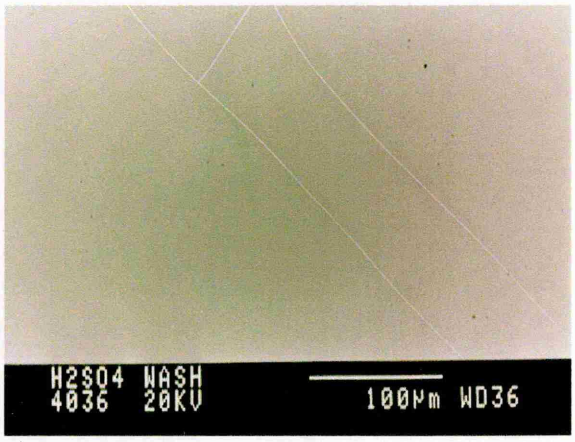

[d]▲

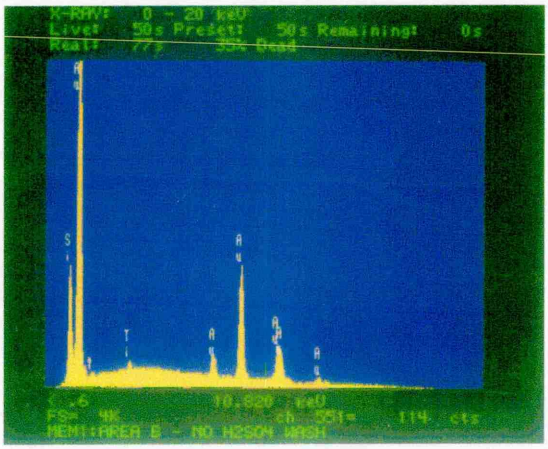

[e]▲

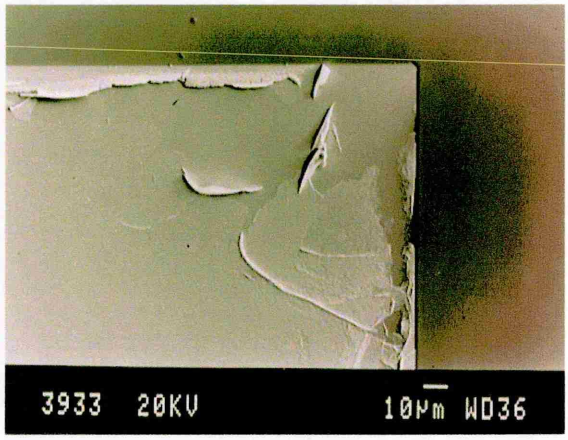

[f]▲

Figure A1.6: *SEM and EDAX studies of the effects of H_2SO_4 sensing element pre-treatment.*

All samples were found to exhibit characteristic EDAX spectra, showing strong silicon and gold peaks, as shown in Fig. A1.6 [a]. Pre- and post- electrodes were found to include particulate contamination (Fig. A1.6 [b]), shown by EDAX to contain Cl, K and Ca (Fig. A1.6 [c]). Gold morphology was found to be very fine in all cases, and did not appear to be affected by H_2SO_4 electrolysis. A degree of insulator cracking was found on many of the substrates tested (Fig. A1.6 [d]), but this was noted as being a common occurrence on MkIII electrodes, regardless of pretreatment.

Of greater concern was the poor adhesion of the gold active layer observed on a number of 'pre- and post-treatment' substrates (Fig. A1.6 [f]). EDAX analysis suggested that this was the result of a titanium bonding layer failure; Ti traces were obtained from the underside of detached metallic layers (Fig. A1.6 [e]), but no Ti could be detected from the exposed underlying areas.

As a result of the above information, H_2SO_4 electrolysis was abandoned by Neotronics in favour of a simple propan-2-ol rinse.

A1.3 Use of Interdigital Electrodes

It was found in the literature that workers in the field of conducting polymer gas-sensing occasionally reported the use of interdigitated electrodes (Nagase *et.al.*, '93(b), Nishizawa *et.al.*, '91; Yadong *et.al.*, '00), although reports of attempted comparisons between the responses of interdigital devices and traditional devices were not found. Interdigitated electrodes may be formed by photolithographic techniques similar to those described in §1.2, but unlike the conventional 'boot' electrodes (whose conducting areas are separated by a linear insulating gap between two straight elements, interdigitated electrodes are formed from a pair of 'comb' elements, the digits ('teeth') of which are interlocked, as shown in Fig. A1.7.

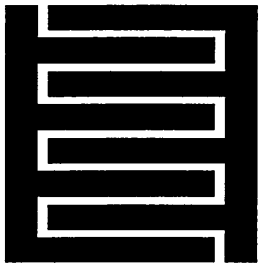

Figure A1.7: *An interdigitated 'comb' electrode.*

The initial work carried out by the author at the Materials Research Institute (involving SEM and EDAX analysis of polypyrrole sensing elements, along with optical investigations using an Olympus Vanox model AHM-T optical microscope) suggested that many of the standard MKIII Bass-Warwick sensor electrodes were failing prematurely due to delamination at the polypyrrole/gold interface. An example of failure of the polypyrrole/gold interface resulting in a complete delamination of the polypyrrole sensing layer is given in Fig. A1.8 [b] (this may be compared to a similar optical micrograph of a pristine substrate shown in Fig. A1.8 [a]). It is of note that over 90% of the polymer surface area had delaminated, with virtually no polypyrrole-gold adhesion remaining. The small areas of remaining polymer were observed to be adhering to [i] the surrounding CVD nitride insulating areas, and [ii] the silicon dioxide within the 10μm insulating gap.

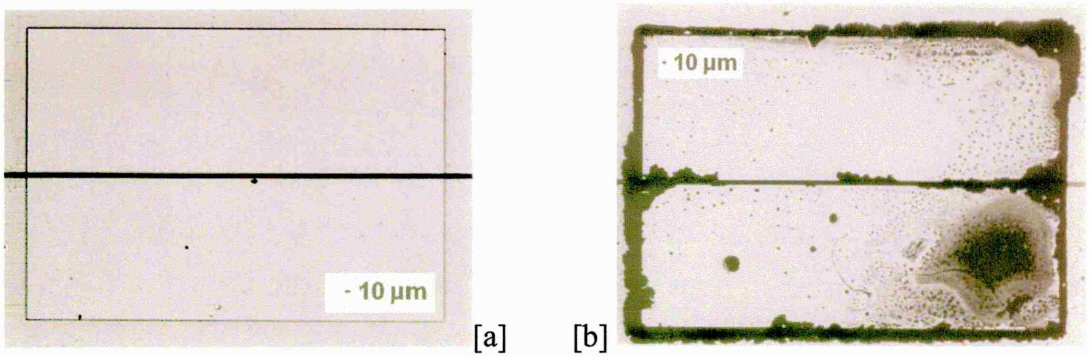

Figure A1.8: *[a] A pristine (i.e. no polypyrrole) MkIII Bass-Warwick sensor electrode, and [b] a similar electrode after delamination of an electrochemically deposited polypyrrole film, showing polypyrrole adhering to the 10µm insulating gap.*

The observation of preferential adhesion to the insulating areas of the sensing electrode was the basis of a suggestion by the author that Neotronics adopted an interdigital electrode design in an attempt to increase sensor lifetime and sensor stability during a typical service life. Consideration of the structure of MKIII Bass-Warwick devices suggests that the polymer deposited over the 10µm insulating gap between the gold boot electrodes obviously plays a fundamental role in the response of the sensing device. If the amount of polymer over the insulating gap could be maximised per unit area of electrode, then the adhesion of the polymer to the substrate might be enhanced, so increasing stability on polymer shrinkage or cracking (increasing the 'coating gap length to defect ratio'). This would be accompanied by a concomitant increase in sensitivity, owing to the increase in the area of polymer responsible for charge transfer between electrodes.

The logical method to increase gap length per unit polymer area was to introduce an interdigitated electrode structure to the standard MKIII Bass-Warwick electrode. The use of interdigital electrodes in order to enhance adhesion, sensitivity and sensor longevity was formally suggested to Neotronics by an SHU delegation consisting of the author, Dr. J. Haigh and Dr. A Hinton on 12th June 1995. The prospect of patenting the use of interdigital electrodes for olfactory sensing was considered, but was not thought to be viable due to the popularity of Interdigitated Microsensor Electrodes (IME's) in areas such as Langmuir-Blodgett sensors and biological sensing.

Two potential modifications to the standard MKIII Bass-Warwick electrode were presented to Neotronics, as shown on Fig. A1.9. Modifications to the standard sensor [a], involved [b] the adoption of an interdigital design which greatly increased the length of the insulating gap, whilst maintaining a similar analyte absorption area, and [c] the use of a second interdigital design which offered a greatly increased insulating gap length, along with an increased polymer deposition area, so providing increased analyte absorption/adsorption area.

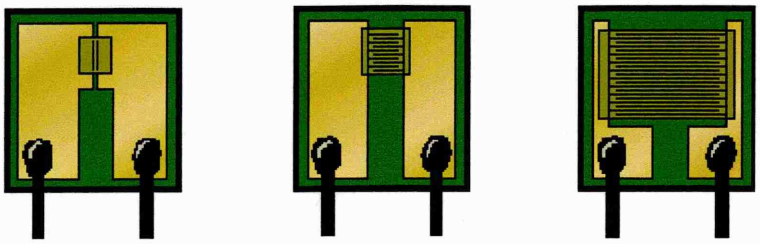

[a] [b] [c]

Figure A1.9: *[a] A MKIII Bass-Warwick electrode, [b] proposed interdigital electrode with similar polymer deposition area, and [c] proposed interdigital electrode with increased polymer deposition area.*

The commercial availability of suitable interdigital electrodes suitable for use in the N.O.S.E. was investigated by Neotronics (North America Inc.) in liaison with the author. Several sources of interdigited micro-electrodes (IME's) were found, including Advanced Biosensor Technology, who marketed a range of IME types featuring gold or platinum electrodes. IME's with various gap dimensions (including 10 μm) were available, but at a price which prohibited their use for high volume research and developmental work (around US$100 each, compared to under £8 Sterling each for MKIII Bass-Warwick sensors). It was therefore decided that attempts would be made to produce interdigital electrodes within the SHU wafer production facility, pending the identification of a viable commercial source of IME's. This is reported in §A1.5.

A1.4 Proposed Electrode Development – Current Homogeneity Model

It was observed that, on deposition of type-283 polymer onto standard MKIII Bass-Warwick electrodes under certain conditions, the polymer films produced would occasionally be thicker towards the lower portion of the active element (i.e. the exposed area of gold onto which deposition occurs) (as shown in Fig. A1.10). Although the

deposition parameters under which this phenomenon occurred could not be attained reproducibly, it was thought possible that such uneven growth may be due to either [a] localized differences in monomer / dopant concentration during growth, [b] differences in the cleanliness of substrates between adjacent areas, or [c] inhomogeneity of the current path through the active element during deposition. The latter was considered possible, especially under conditions where deposition was carried out at low potential, given the finite electrical resistance of the gold/titanium films used to form the active element.

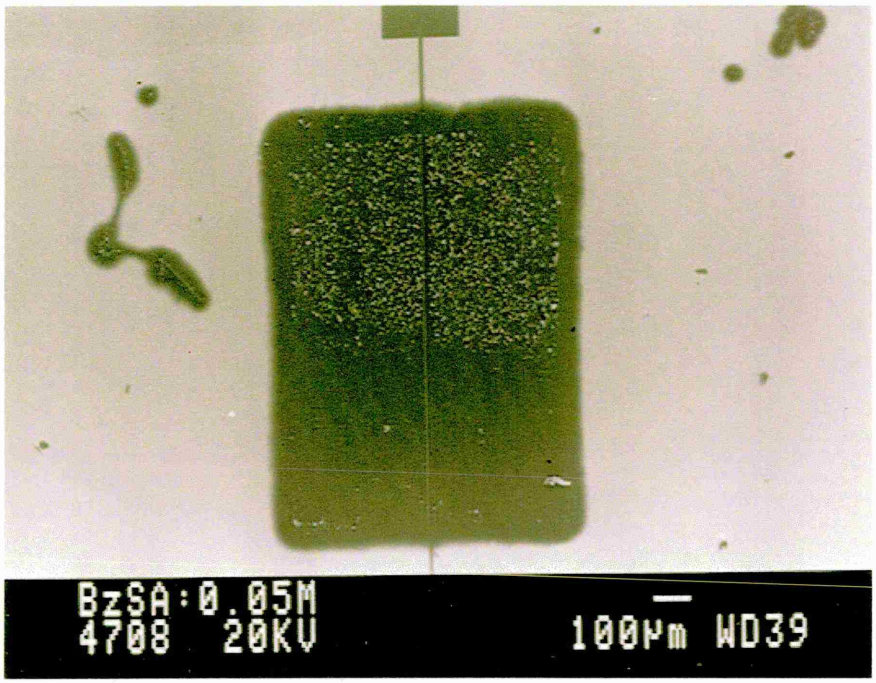

Figure A1.10: *SEM micrograph illustrating the preferential growth of type 283 polymer towards the lower portion of the active element (i.e. top of frame, showing increased nodularity due to increased film thickness).*

It was considered that the design of existing MKIII Bass-Warwick electrodes could be improved by potential 'evolution' of the placement of electrode contacts relative to the sensing material. A modification was suggested to Neotronics by the SHU delegation mentioned in §A1.3, as shown in Fig. A1.11. As shown, the rationalization of the positions of the electrical contacts used may serve to lessen the problems associated with inhomogeneous current flow during deposition; it was considered that the use of the proposed electrode might also improve current homogeneity during sensor use.

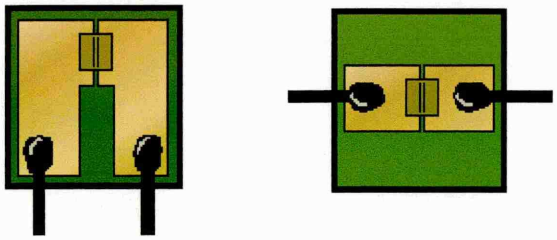

[a] [b]

Figure A1.11: *[a] Original MKIII Bass-Warwick electrode, [b] proposed electrode modification to allow greater current homogeneity during deposition and analysis.*

The prospect of patenting the use of the proposed electrode type was considered by Neotronics. However, firm empirical evidence to support the theories developed is required before this could be taken further.

A1.5 Fabrication of Sensing Electrodes within the SHU Wafer Fabrication Facility

It was agreed by the author, supervisory team and Neotronics that the feasibility of IME production within the SHU Wafer Fabrication Facility would be investigated.

Initial work involved the use of a set of photolithographic masks produced by Dr. Simon Brown and Dr. Andrew Hinton, SHU (Hinton, '96) based on original MKIII Bass-Warwick designs supplied by Neotronics, as represented in Figs. A1.2 and A1.3. Two photographic plates were formed (one negative and one positive) using an AutoCAD package; designs were converted to Electromask format and exposed repeatedly onto photographic plates. The plates formed were used to govern the exposure of resist-covered wafers, so allowing the formation of the gold boot-electrodes used in the MKIII Bass-Warwick electrodes.

The successful manufacture of MKIII Bass-Warwick electrodes at SHU was to be attempted in order to verify the suitability of the techniques and equipment available within SHU for the manufacture of electrodes with a silicon/silicon dioxide/glue-layer/gold structure. If attempts to manufacture such boot electrode structures were successful, then interdigital electrode formation would be attempted.

A1.5.1 Experimental

Wafer fabrication was carried out at SHU in a class 100 clean-room facility. Protective clothing was worn during fabrication, including a secured overcoat, hat and overboots, which prevented unnecessary contamination of the facility by skin particles etc. The level of cleanliness in the clean room facility was maintained by five high efficiency particulate air filters above a suspended ceiling, after removal of particles of diameters greater than 0.5μm by course filters. Air quality and humidity in the facility were controlled, and a positive pressure of 15Pa above ambient was maintained in order to minimise ingress of particulates on entry & exit.

Four inch <100> oriented n-type silicon wafers were used throughout. Silicon dioxide layers were grown on the surface of the wafers by a standard wet-oxide method (as

described in §A1.2). Metallic layers were deposited onto the oxide wafer by vacuum deposition; this was carried out in an Edwards evaporator. The oxide wafers to be 'metallised' were placed in the evaporation chamber, and a high purity (99.99%) sample of the metal to be deposited was placed in a tungsten wire basket beneath the wafer (wafers were oriented so as to 'face' the tungsten basket). The sample chamber was evacuated to $<10^{-4}$ Torr, and the metallic sample and the wire basket were heated to a temperature high enough to vapourize the metallic sample. This was achieved by passing an electrical current through the basket. The rate of evaporation of the metallic sample (which is proportional to the rate of deposition onto the device wafer) was monitored, and an integrated film thickness monitor gave an indication of the film thickness achieved.

A1.5.2 Boot-Electrode Production

[a] Au-SiO_2-Si

Initial attempts were made to verify the requirement for a bonding (or 'glue') layer by deposition of 'four-nine' purity gold directly onto two freshly prepared silicon dioxide wafers. Although of obvious importance for commercial devices (due to improved adhesion allowing increased sensor lifetime etc.), it was not known whether a glue-layer would be necessary during the deposition and assessment of research-grade devices.

Gold deposition (metallisation) of two four inch <100> oriented n-type silicon wafers was carried out in an Edwards evaporator under nitrogen at a vacuum of $\geq 10^{-5}$ Torr. Metallised wafers were then spin-coated at 4000rpm with negative resist (HNR120) and soft-baked at 90°C for 60s. Patterning was then carried out using the existing photolithographic mask (see Fig. A1.2) which allowed exposure of the areas of soft-baked resist covering the boot electrode design. Exposure resulted in hardening of the negative resist. Unexposed resist was removed by a series of washes, and the remaining soft-baked, exposed resist was hard-baked at 135°C for 60s. The wafers were then etched with a potassium iodide/iodine solution to remove unwanted areas of the gold layer (i.e. areas surrounding the 'boot' electrodes). Hard-baked resist was then removed by plasma-asher (this was carried out on the author's behalf by Mr. Geoff France, SHU).

The devices produced were observed to have excellent edge definition, but the Au:SiO_2 adhesion was extremely poor; much worse than had been expected. Devices were observed to be very fragile, to the extent that several gold boot electrodes were damaged when attempts were made to dry the devices with a high velocity jet of nitrogen. Electrical resistance between electrode pairs (i.e. across the 10µm gap) was shown to be infinite for all devices on both wafers, indicating that satisfactory electrode separation had been achieved and no shorts were present.

The poor adhesional characteristics of the gold microelectrodes formed confirmed that the use of a bonding (glue) layer was necessary for the production of research-grade electrodes.

[b] Au-Ti-SiO_2-Si (Nitrogen Atmosphere)

Two four inch <100> oriented n-type silicon wafers were oxidized as described above. Bonding layer deposition was carried out in an Edwards evaporator. Before deposition of titanium was attempted, the inside of the Edwards glass bell-jar was 'flashed' with a thin coating of aluminium by evaporating aluminium (as described) into the chamber at low pressure. Flashing ensured that the titanium deposition would not result in a strongly adhering layer of titanium contaminating the bell jar; such a layer would potentially threaten the purity of the aluminium layers deposited during future semiconductor manufacture within the SHU facility.

Around 5±1mm x 5±1mm of high purity titanium sheet was cleaned in isopropyl alcohol and acetone, dried (by heating to ~300°C for >600s) and placed in the tungsten wire basket directly beneath the freshly oxidized wafers. The sample chamber was evacuated to $<10^{-4}$ Torr, purged to ambient pressure with oxygen-free nitrogen, evacuated to $<10^{-4}$ Torr and the nitrogen purge repeated. The vacuum chamber was then evacuated to over $<10^{-4}$ Torr and the tungsten basket was heated slowly until the thickness indicator read >100Å (n.b. as expected, a far greater current was required than for aluminium deposition).

The metallised wafers produced were then gold coated, spin coated with negative resist, baked and patterned as described previously. Etching of the patterned wafer was carried out with potassium iodide/iodine solution to remove unwanted gold areas, and with hydrofluoric acid (HF) to remove corresponding titanium areas. Plasma ashing was then used to remove the hard-baked resist used to form the gold boot structures. The devices produced were noted to have very poor edge definition, with relatively poor adhesional characteristics. Electrical resistance between electrode pairs was, as for the Au/SiO2 devices, shown to be infinite for all devices, suggesting satisfactory electrode separation with no shorts present.

Analysis of the wafers produced by optical microscopy (Olympus Vanox model AHM-T) showed that the royal blue/violet colouration of the SiO_2 layers before metallisation had been modified during processing, and was observed to be 'off-milky-white' on both wafers. Wafer No.3 was noted to have deep blue patches around boot electrode edges; it was thought that this colouration may be the result of either [a] a modification to the thickness of the SiO_2 layers (see Pliskin and Conrad, '64) or [b] the formation of titanium oxides or titanium nitrides (Brown, '95).

The 'ideal' substrate cross-section is represented by Fig. A1.12. Theory predicts that the use of a titanium glue layer between the SiO_2 and gold film acts to increase their adhesion via an alloying process. The formation of titanium oxides or titanium nitrides during deposition as opposed to metallic titanium will, therefore, significantly reduce adhesion, as the refractory (ceramic) nature of these materials prohibits alloying (Haigh, '95).

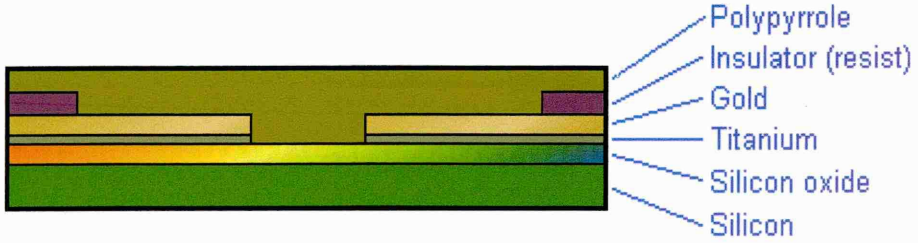

Figure A1.12: *Cross-sectional representation of sensor structure.*

The compositions of the wafers produced were studied by GDOES (see §2.2.3). A typical trace obtained during GDOES analysis is shown in Fig. A1.13. The trace shown

illustrates the elemental composition from the surface of the processed wafer (left hand side, burn time (t) = 0.0s) into the unoxidised silicon bulk material (right hand side, burn time (t) = 20.0s). Working from right to left, the trace shows unoxidised bulk silicon, followed by a combination of silicon and oxygen. This almost certainly represents the SiO_2 layer as prepared, but the nature of the technique 'as used' does not allow us to state this with absolute confidence without a full, dedicated, traceable calibration of the GDOES system. Working further from right to left, the sharp reduction in the silicon trace intensity at around t = 4.0s represents the interface between the SiO_2 substrate and the Ti bonding layer.

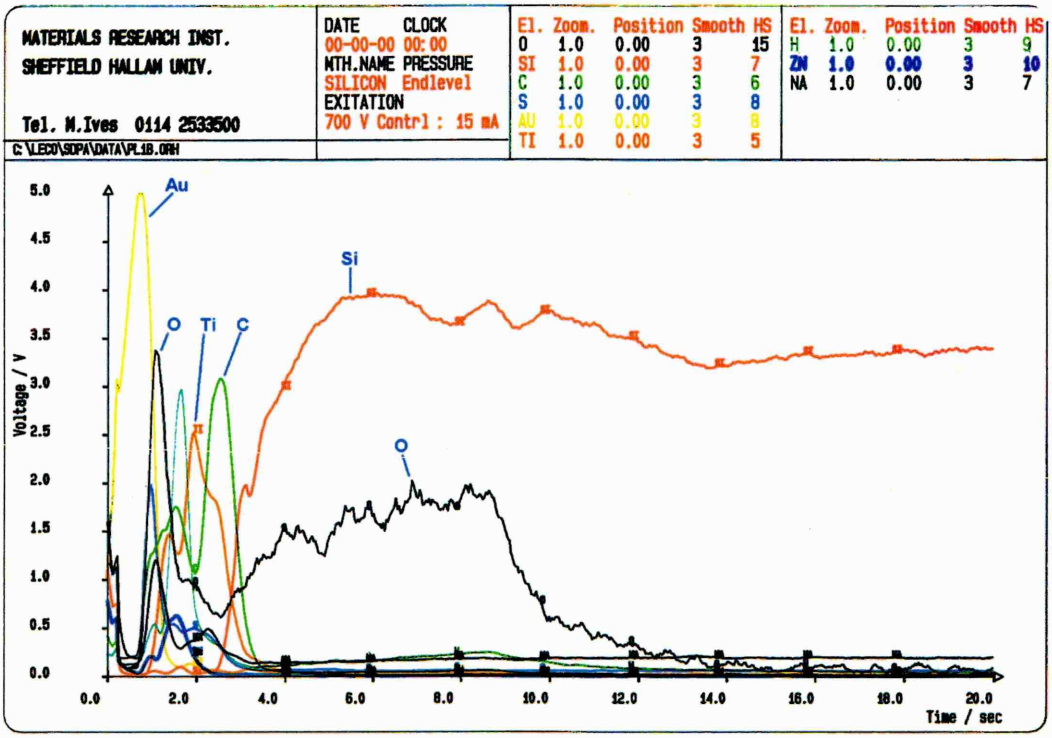

Figure A1.13: *GDOES analysis of Gold – Titanium – SiO_2 – Si wafer.*

Although a strong titanium maximum is present in this area, the bonding layer is far from pure, with carbon, oxygen, hydrogen, sulfur, sodium and zinc present in high concentration. Although not shown in Fig. A1.13 (detection was not attempted), an abundance of aluminium was also detected in this region during other analyses; this is thought to be due to the presence of the aluminium coating applied to the innards of the bell jar during 'flashing'.

Aluminium (and other metallic elements) incorporation is thought to be due to the re-evaporation of the aluminium flashing layer, along with other metals previously evaporated within the Edwards unit during semiconductor fabrication. The temperature required in the tungsten evaporation basket to evaporate the titanium foil used was significantly higher than those used during normal 'day-to-day' use of the facility. Evaporation of contaminant elements from within the chamber may therefore be reasonably expected. It was also considered possible that tungsten may migrate into the molten titanium before evaporation, so contaminating the deposited material.

Several methods were considered in order to reduce the amount of aluminium incorporated into the titanium bonding layer during deposition. These included the use of a (high Bp) metallic foil to line the bell jar before deposition of titanium, so negating the need for a flashed aluminium layer.

Methods of reducing the consistently high concentration of organics in the bonding layer region were also considered. A more stringent cleaning regime was planned for the titanium foil used, along with all implements used to handle the foil before evaporation. The use of a shutter mechanism within the bell jar was also considered, which would allow initial evaporation of a portion of the titanium foil used (along with the majority of the organics present) before opening the shutter. Opening the shutter after this period would allow the deposition of organic-free titanium onto the SiO_2 substrate.

Deposition in a less reactive atmosphere was also considered. Deposition at $<10^{-4}$ Torr (a relatively poor vacuum) without a nitrogen purge (i.e. in a low concentration of air) was assumed to result in the formation of titanium oxides and (to a lesser extent) nitrides. Purging with nitrogen was therefore carried out in order to reduce the level of oxide contamination, but it is reasonable to assume that titanium nitrides may be formed. Wafers were therefore prepared under $<10^{-4}$ Torr vacuum repeatedly purged with argon in order to reduce the formation of titanium oxides and nitrides; this is now reported.

[c] Au-Ti-SiO_2-Si (Argon Atmosphere)

Freshly oxidized <100> orientated n-type silicon wafers and high purity titanium were prepared as described in [b]. Titanium was placed in the tungsten basket beneath the wafers. The sample chamber was evacuated to $<10^{-5}$ Torr, purged to ambient pressure with high purity argon, evacuated a second time with a view to a second argon purge. However, a fault with the vacuum pumping system was identified, leading to vacuum loss. A second attempt at deposition in an argon atmosphere was made; an argon 'double purge' was successfully carried out followed by deposition of a titanium bonding layer of greater than 100Å thickness. The ball jar was vented and high purity gold placed in the tungsten blanket with a view to deposition. The bell jar was evacuated and double-purged with argon. Final evacuation was attempted overnight in order to achieve a good vacuum before deposition was attempted, but the vacuum was again lost. The continued unreliability of the SHU vacuum system led to the decision that, at this stage in the research, time would be spent more productively by investigating other routes to interdigitated microelectrode formation.

A1.6 'Yoshi' Electrodes

Extensive and detailed discussions with staff of the Health and Safety Laboratory (HSL) and the Health and Safety Executive (HSE) led to a potential source of research-grade interdigitated microelectrodes. Interdigital microelectrodes were used within HSL during the formation of Langmuir-Blodgett gas sensors and were originally sourced from Ehime University, Japan. A limited supply of interdigital electrodes was acquired from Dr. S. Thorpe, HSL for use during the work presented. Electrodes were originally sourced from Prof. Sadaoka Yoshihiko, Ehime University. This led to them being dubbed 'Yoshi' electrodes.

Yoshi electrodes were supplied on 3" circular glass plates, pre-scored with a 6mm x 6mm matrix. Individual electrodes were obtained by carefully fracturing the circular plates into strips along score lines, then fracturing strips into individual devices. The glass plates used were low alkali-metal content (i.e. low Na^+, Li^+), and were sputter coated with an unknown thickness of platinum before photolithographic formation of the interdigital electrode structure (Thorpe, '97). Although the formation techniques

involved during the manufacture of Yoshi electrodes were known, information regarding the physical dimensions of the devices used was not available.

The microtopography of a selection of Yoshi electrodes was therefore analysed by a Taylor Hobson Surtronic 3+ surface microroughness transducer using Talyprofile software, as described in §2.2.5. A typical trace is shown in Fig. A1.14.

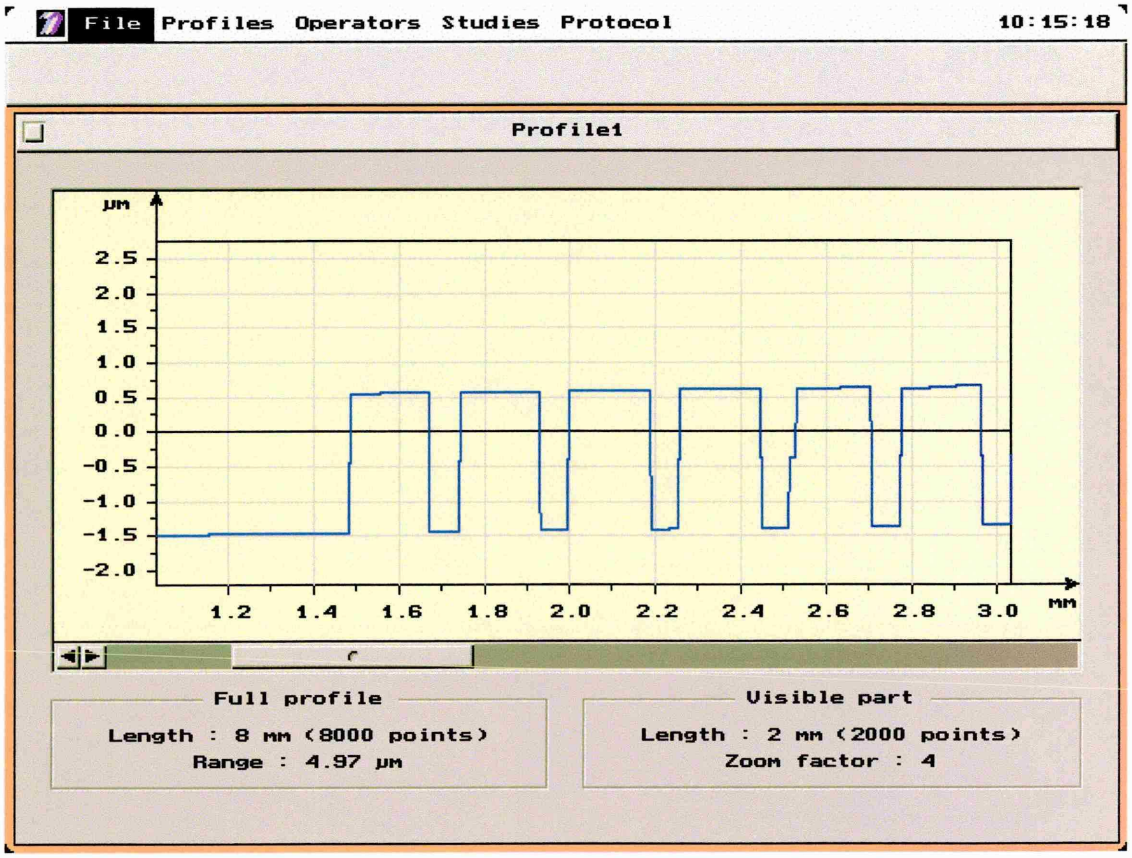

Figure A1.14: *Surtronic 3+ analysis of the microtopography of a Yoshi interdigital microelectrode.*

A set of ten measurements were made in order to ascertain both the typical dimensions of the devices and their dimensional reproducibility. The platinum layer thickness was found to be 2.0±0.1µm, electrode width 0.20±0.005mm, and gap width 0.075±0.005mm.

The 75µm gap width (electrode separation) between platinum comb electrodes was appreciably greater than the 10µm gap width found on MkIII Bass Warwick electrodes. Although it was considered that the electrical properties of complete devices would be

affected (as would the microstructure of the polymer grown *over* the gap) increased gap width was not expected to produce detrimental effects.

A1.6.1 'Yoshi' Device Production

In order to allow [a] polymer to be electrochemically deposited onto, and [b] electrical measurements to be taken from Yoshi electrodes, individual electrodes were attached to suitable contacts by one of two discrete methods.

[a] Bespoke "Bass-Warwick Type"

Yoshi electrodes were attached to custom-made stripboard substrates (R.S.) with cyanoacrylate glue; electrical connections were made via solder 'bridges' between Yoshi contacts and the relevant copper tracks. Copper strips were broken as required so as not to allow growth of polypyrrole onto strips during deposition, as shown in Fig. A1.15 [a]. Tin right angle PCB Pin Headers (R.S.) were used to allow electrical measurements to be taken; these were tailored to match the dimensions of standard MkIII Bass-Warwick substrates. This not only allowed use of standard deposition and resistance monitoring equipment, but also allowed use of these substrates in the e-NOSE if required.

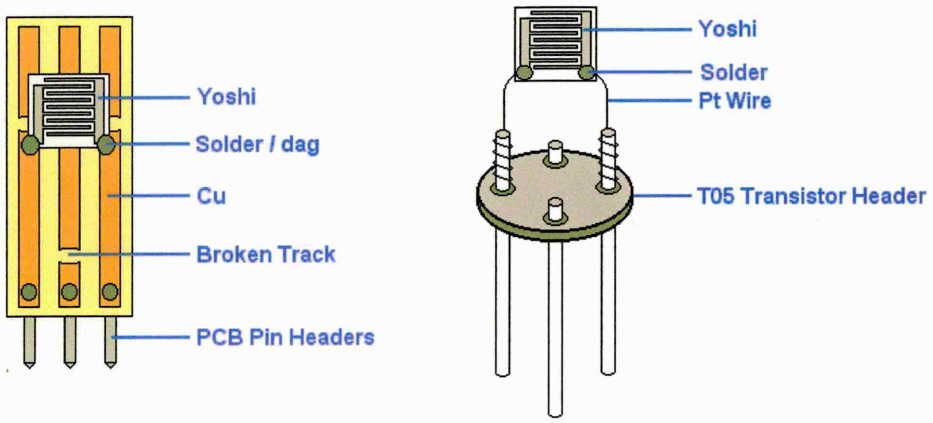

Figure A1.15: *Mounting of Yoshi interdigital electrodes on [a] bespoke "Bass-Warwick type", and [b] transistor header substrates. Both types allow use in standard Neotronics electrochemical cell.*

[b] T/05 Transistor Header:

Fine platinum wires were soldered to either side of the Yoshi electrode, taking care not to contaminate the surface of the element with solder or flux. Wires were wrapped around two contacts of a T/05 transistor header; the remaining header contacts were trimmed, as shown in Fig. A1.15 [b]. The use of this technique was popularised during early phthalocyanine research within HSE (Cole *et.al.*, '93). Electrical measurements were taken from the lower header contacts using standard equipment used for MkIII Bass-Warwick electrode measurement.

A1.7 Polypyrrole - Yoshi Sensor Production

Early 'pilot' polypyrrole depositions were carried out with both 'bespoke SHU' and 'T/05' Yoshi electrodes in order to ascertain the benefits, if any, of the use of each electrode type.

Deposition of material type-283 (PPy/BSA(Na)/H_2O) was carried out under standard conditions using a three-electrode electrochemical cell as described in §2.1. Deposition onto T/05 substrates showed that a +5.00V vs SCE growth potential was required to produce a substantial polypyrrole film; trials showed that deposition of type-283 material at the standard level of +0.85V vs SCE resulted in the very inhibited growth of poor polymer. The requirement for such a high deposition potential was uncommon, both for standard Neotronics gold electrodes and for I.T.O. glass electrode material. The electrical resistance of the T/05 devices produced were therefore studied.

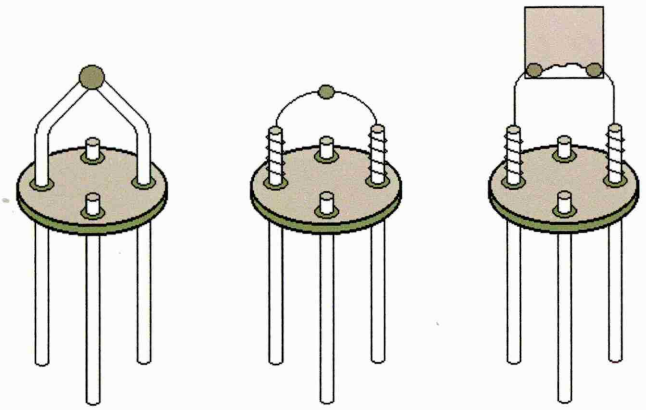

Figure A1.16: *Investigation of resistance sources in T/05 substrates, [a] through connector posts, [b] through connecting wires, and [c] through 'dagged' Yoshi electrode.*

As shown in Fig. A1.16, T/05 devices were shorted in several ways; [a] by direct contact between connector posts (soldered joint), [b] by direct contact between connector wires (wires soldered together, attached to connector posts as described previously), and [c] by the application of silver dag (a highly electrically conductive adhesive material) over the surface of the Yoshi electrode.

Repeat tests were carried out on two sets of T/05 electrodes (from the same batch of devices); it was found that type [a] 'shorting' resulted in mean resistances of 0.3Ω; type [b] in mean resistances of 0.5Ω; and type [c] in mean resistances of 1.6Ω. Taking into account the small resistance resulting from the connections between the electrodes and the DMM used, the great majority of the measured impedance was found to be due to either the solder joint between the Yoshi electrode and the connecting wires, or the presence of an electrically resistive contaminant layer on the surface of the platinum Yoshi electrodes.

The above 'shorting' exercise was repeated with devices formed from a more recent batch of Yoshi electrodes. The 'Type [c]' devices formed were found to have impedances of around 0.8Ω, therefore suggesting that the batch of Yoshi devices used previously had been contaminated by an unidentified material of sufficient tenacity to

resist the standard IPA, water, acetone substrate cleaning regime used. Deposition of type-283 material was therefore repeated.

Type-283 material (PPy/BSA(Na)/H_2O) was deposited onto bespoke-SHU and T/05 Yoshi electrodes, having first demonstrated that the batch of Yoshi electrodes used were pristine. This was done by shorting a single electrode per glass sheet with silver dag (as shown in Fig. A1.16 [c]) and measuring the resulting resistance. Deposition was carried out under standard conditions as described above, but a lower growth potential of +2.00V vs SCE was used.

Deposition was carried out using both bespoke-SHU substrates and T/05 transistor header substrates in turn. The use of a +2.00V vs SCE deposition potential resulted in the rapid growth of polypyrrole films over the surface of the Yoshi interdigital electrodes. However, it was noted that the electrolyte solution rapidly adopted a milky colour throughout the deposition; this was true of both electrode types.

The likelihood of cyanoacrylate dissolution was considered (which polymerises during its 'curing' process (see Paul *et.al.*, '97)), but no cyanoacrylate adhesive was used during the formation of T/04 substrates.

It was therefore considered likely that the presence of solder in or around the electrolyte solution during polymerisation was responsible for the visible solution contamination. It is known that electrochemically deposited polypyrrole 'traps' pockets of electrolyte solution during growth (see Lemon and Haigh, '99, as discussed in §4.4). Electron probe microanalysis was therefore used to qualitatively investigate the elemental content of the polypyrrole films produced; the presence of tin and/or lead in the polypyrrole would strongly support the hypothesis that solution milkiness during deposition onto bespoke-SHU and T/04 electrodes was the result of solder dissolution.

Energy dispersive X-ray analysis was used to qualitatively investigate the elemental composition of polypyrrole films produced from contaminated (milky), and from pristine solutions. It is shown in Fig. A1.17 that polypyrrole films produced from contaminated electrolyte contain a relatively large amount of tin; films produced under

'non-contaminated' conditions do not. This supports the hypothesis that solution contamination results from the dissolution of solder during electrochemical deposition of polypyrrole onto Yoshi electrodes.

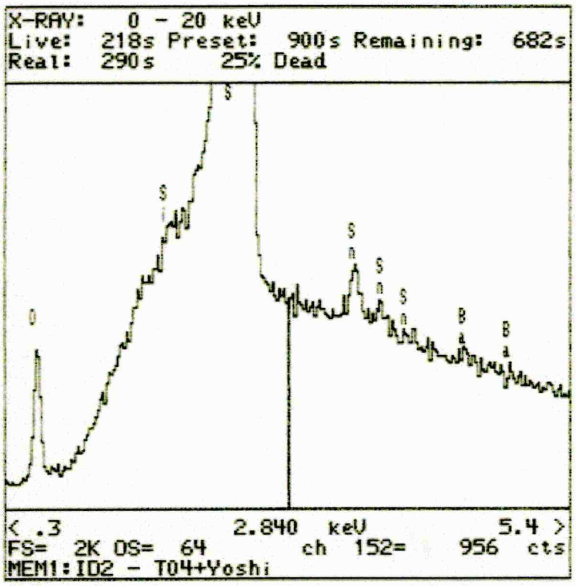

Figure A1.17: *Energy Dispersive X-ray Analysis of polypyrrole deposited from 'contaminated' solution. Strong tin peaks support hypothesis that solder is responsible for electrolyte solution contamination.*

The absence of trace amounts of lead in the 'contaminated' films may contradict the above theory. However, it is known that electricians' solder (as used) has an increased concentration of tin, with a concomitant reduction in lead concentration (Lewis B., private communication, 1997), so reducing the possible lead peak height.

Observation of the post-deposition morphology of the surface of the solder applied to Yoshi electrodes was carried out by scanning electron microscope. It was noted that the surface of the solder studied was heavily pitted; an example of this is shown in Fig. A1.18.

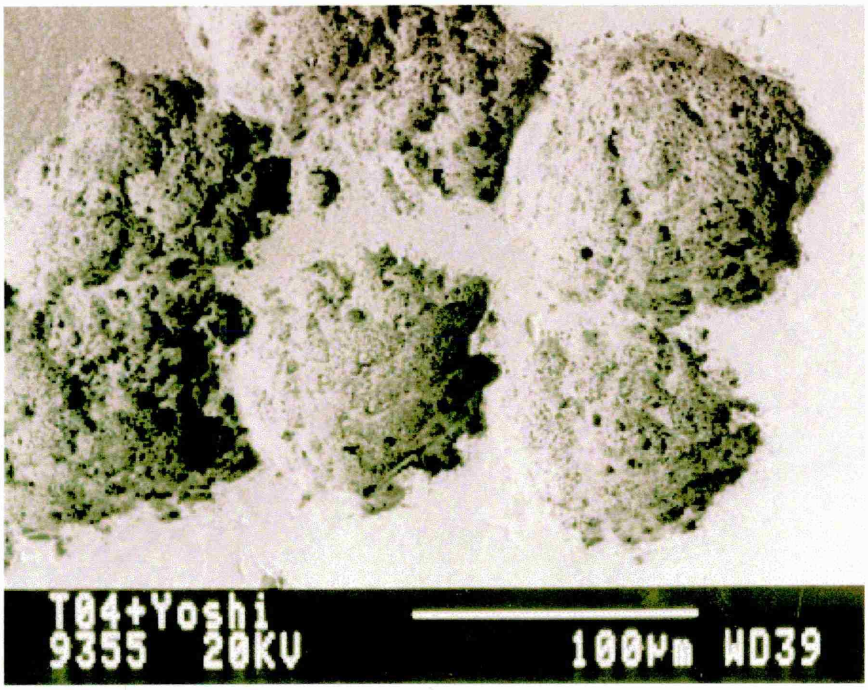

Figure A1.18: *Scanning Electron Micrograph of solder employed to bond and electrically connect Yoshi electrode to T/05 substrate (see Fig. A1.15 [b]).*

It is postulated that the heavy pitting observed is the direct result of dissolution of solder during submersion in electrolyte solution during polypyrrole deposition; pristine solder (after application to a Yoshi electrode) was observed by SEM to have a far smoother morphology. This further supports the hypothesis of electrolyte contamination via solder dissolution.

As a result of the observed potential for electrolyte solution contamination, subsequent formation of polypyrrole films on 'Yoshi' electrodes were carried out prior to attachment to either T/04 or bespoke-SHU electrodes. Deposition was carried out by the direct attachment of individual Yoshi electrodes to a custom-made contact, the design of which will now be discussed.

A1.7.1 Yoshi Deposition – Direct Attachment

The use of several techniques to allow the direct electrical integration of Yoshi electrodes during electrochemical deposition were considered. Direct contact between the working electrode (Yoshi) and the current source was obviously required; the use of

solder had previously been rejected. The use of silver-dag had not been studied in depth, but it was known that the bond produced by 'dag' is often rather weak. The use of direct, mechanical contact was therefore required.

The use of a simple crocodile-clip was considered, and attempted. However, inaccuracies in the manufacture of the clips used (R.S.) were observed to result in irregular contact with Yoshi platinum contacts, as shown in Fig. A1.19.

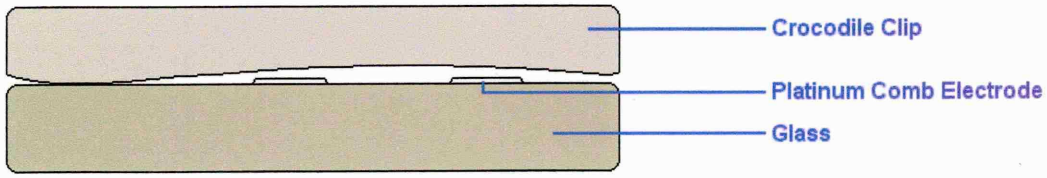

Figure A1.19: *Crocodile clip inaccuracy resulting in lack of electrical contact with platinum Yoshi working electrode.*

Similar clips were modified in order to allow a more consistent and reliable electrical contact between Yoshi electrode and the working electrode circuit during electrochemical deposition. An illustration of a modified clip is shown in Fig. A1.20. A similar clip was used throughout the deposition of polypyrrole onto Yoshi electrodes presented here.

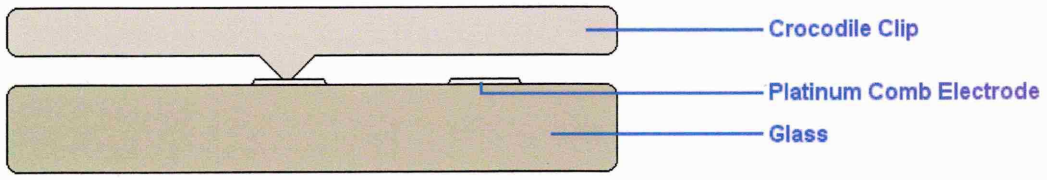

Fig. A1.20: *Modified crocodile clip used during the electrochemical deposition of polypyrrole directly onto platinum Yoshi electrodes.*

A1.7.2 Single-Comb Yoshi Deposition

The practicability of the simultaneous deposition of polypyrrole onto *both* sides of Yoshi electrodes (i.e. onto both of the individual, interlocking electrode 'combs') was considered. Although successful attempts were made to allow 'dual-comb' deposition

(using modified crocodile clips, similar to that shown in Fig. A1.20, but using dual contacts), it was considered that the study of the macro-scale growth mechanisms of polypyrrole would be facilitated by the use of single-comb deposition.

A pilot study (involving the 'single-comb' deposition of several polypyrrole Yoshi electrodes) showed that this resulted in the rapid deposition of conducting polypyrrole onto the 'live' comb (i.e. the comb subjected to growth potential via connection to the clip) (as illustrated in Fig. A1.21). After a period of growth, the colouration of the inert comb was observed to change rapidly from silver-grey to matt black (characteristic of electrochemically deposited polypyrrole), suggesting the early stages of polymer growth on the 'inert' comb. The mechanisms responsible for this observed 'crossover' between live and inert electrodes were considered. It was thought likely that crossover was the result of the formation of a direct electrical/mechanical 'bridge' between live and inert electrodes through polymer growth, as suggested by the sudden and rapid colouration change observed. A study of the morphological development of the polypyrrole films produced before, during and after crossover by optical and scanning electron microscopy is presented later in the thesis.

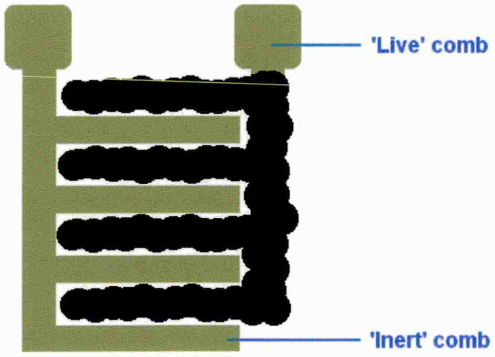

Fig. A1.21: *Growth of polypyrrole on 'live' comb of Yoshi electrode during 'single-comb' deposition.*

A1.7.3 Yoshi Coverage Maximization

In order to maximise the level of deposition over Yoshi electrodes during 'single-electrode' deposition, substrates were placed into the electrolyte solution at an angle of around 45° to the horizontal. Deposition was attempted with *no* contact between the clip and the meniscus of the electrolyte solution, but the resultant polypyrrole films were

observed to grow unevenly, with film maturity per unit deposition time decreasing in the vicinity of the meniscus. As a result, deposition was routinely carried out with Yoshi electrodes well submerged in the electrolyte solution; a degree of clip submergence was tolerated, along with commensurate polymer deposition onto the clip. Failure to submerge the working electrode and clip into the electrolyte solution sufficiently was observed to result in the formation of uneven polymer films, with film maturity per unit time increasing with depth into the solution. All traces of polymer were removed from the clip between depositions, followed by a thorough solvent-based clean equivalent to that used during electrode preparation.

Summary, Appendix 1

- Early work during the programme of work presented concentrated on the development of interdigital electrodes. Development was attempted in house, due to the oppressive cost of commercial devices.
- The dimensional characteristics of Mk-III Bass-Warwick electrodes have been assessed by profilometry in order to facilitate the development of polypyrrole growth models.
- The effects of sensing element 'recycling' have been assessed at the direct request of Neotronics Scientific. It was found that sensors produced using recycled electrodes performed very poorly; this was found to be due to [a] failure of the recycling technique to effectively remove existing polymer from electrodes, and [b] damage to the substrate insulator layer.
- The efficacy of a novel substrate cleaning regime was assessed at the direct request of Neotronics Scientific. The morphologies of Mk-III gold electrodes were not found to be affected by the use of this regime (H_2SO_4 electrolysis), although some evidence was found which suggested damage to the titanium bonding layer.
- The use of interdigital electrodes as opposed to standard Mk-III 'boot' electrodes has been investigated; improved sensor performance was predicted due to observed preferential polypyrrole adhesion to insulating areas of Mk-III electrodes. Several potential electrode designs were presented utilizing interdigitisation. A substrate model was also presented which aimed to improve current homogeneity during sensor use.
- The possibility of manufacturing electrode substrates in the SHU wafer fabrication facility was explored in depth. Attempts were made to replicate the Mk-III Bass-Warwick 'boot electrode' with some success. However, a source of proprietary interdigital electrodes was identified before successful production of an 'SHU' Mk-III boot electrode.
- A range of custom-built mounts have been produced to allow polymer deposition on Interdigital electrodes and, potentially, use of interdigital devices in the e-NOSE 4000.

- The adoption of a 'single electrode' deposition technique has been described. This technique has been adopted to facilitate the study of polypyrrole growth mechanisms.

A2. Device Resistance Temporal Stability

The establishment of 'Yoshi' interdigital electrodes as viable substrates for the production of olfactory sensing devices led to a requirement for the investigation of the properties of such devices. In this chapter, the electrical resistance temporal stability of Yoshi devices is investigated and compared to that of standard Bass-Warwick devices. The growth mechanisms resulting from the use of a novel 'single electrode' Yoshi deposition regime are also discussed; the effects of this deposition regime are also investigated by its application to standard Bass-Warwick devices.

A2.1 Resistance Temporal Stability – a Comparison between 'Yoshi' and 'Bass-Warwick' Devices.

Two sets of polypyrrole gas sensors, one set using Neotronics electrodes & substrates (MkIII Bass-Warwick sensors, as described in §A1.1), and one using Yoshi electrodes subsequently fixed to T/05 transistor headers (as described in §A1.6.1) were prepared in order to study the potential improvements to sensor resistance stability resulting from the introduction of an interdigital electrode design, as discussed in §A1.3.

Neotronics electrodes were prepared as described in Ch.2, and thoroughly cleaned (with a dichloromethane/water/acetone/IPA/water/acetone/dry N_2 cleaning regime). Deposition of type-283 polypyrrole [PPy/BSA(Na)/H_2O : 0.25M/0.25M/50ml] was carried out under standard conditions at a potential of +0.85V vs SCE for 120s + 30s @ 0V vs SCE.

Yoshi electrodes were prepared similarly, thoroughly cleaned with a dichloromethane regime as outlined above and attached to the working electrode as described in §A1.7.1 to §A1.7.3. Type 283 polypyrrole [PPy/BSA(Na)/H_2O : 0.25M/0.25M/50ml] was deposited at a potential of +5.00V vs SCE for 30mins + 30s @ 0V vs SCE.

After polymer deposition, individual devices were rinsed in clean electrolyte (Millipore water), dried under a high velocity jet of oxygen-free nitrogen (as described previously) and stored individually.

A calibrated DMM was used to measure the electrical resistance of individual devices [a] immediately after drying, before initial storage, and [b] at weekly intervals for a period of ten weeks after deposition. Results are presented in Fig. A2.1 (n.b. all resistance data are after subtraction of external circuit resistance).

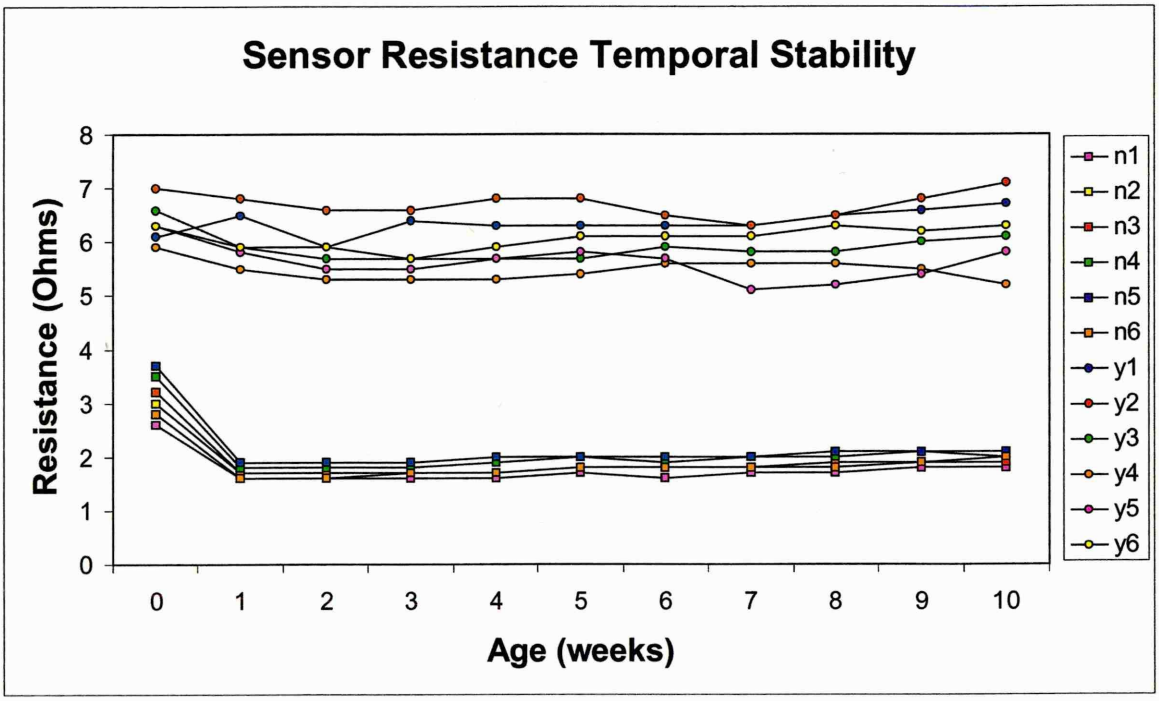

Figure A2.1: *Resistance temporal stability for Type-283 polypyrrole material deposited on [a] standard Neotronics "Mk III Bass-Warwick" substrates ('n' series), and [b] T/05 Yoshi substrates ('y' series).*

The resistance data presented suggests that:

[a] the resistance variability displayed by Yoshi devices is somewhat greater than that displayed by Neotronics devices,

[b] the long-term resistance stability displayed by Yoshi devices is inferior to that of Neotronics devices, but

[c] Yoshi devices do not appear to be susceptible to the considerable resistance drop found during weeks 0 to 1 with Neotronics devices.

It is considered that point [a] may be due to the quality of the Yoshi electrodes used during the study; both the separation and the physical thickness of the electrodes were

routinely found to vary slightly. This variability necessitated the individual inspection of each device before use, and may account for inter-device resistance variations.

Point [b] may be addressed in part by the technique used to collect resistance information. Yoshi devices were formed by single-electrode deposition, and were *subsequently* attached to T/05 headers. Electrical measurements were taken directly from Yoshi contact pads using probes in order to minimize the effects of variations in the electrical contact between Yoshi and T/05 and variations in individual T/05 devices. Variations in probe position during measurement may account for a degree of measurement-to-measurement inconsistency, along with the effects of contact pad wear, which was noted after several weekly measurements. The effects of contact pad wear / damage through repeated measurements were exacerbated by the necessity to remove polypyrrole from the contact pad submerged during single-electrode deposition, onto which polymer was deposited. It was noted that polypyrrole / electrode adhesion was very strong.

It is postulated that point [c] may reflect the potential advantages of the use of IMEs (interdigitated micro-electrodes) predicted earlier in this thesis. The reduction in the initial resistance drop observed with Yoshi devices may result from a reduction in the effects of partial layer delamination (due to an increase in the 'coating gap length to defect ratio') as the polymer film dries.

However it is thought to be highly probable that the greater initial drop (during week 1) in device resistance displayed by Neotronics devices than by Yoshi devices is evidence of the structural model presented in §4.4, which concerns the recrystallisation of dopant from pockets of electrolyte solution trapped within the polymer film during deposition (see §4.4.5 for a discussion of the effects of dopant recrystallisation on the electrical resistance of polypyrrole devices; see also "Electrolytic Dopant Recrystallisation in Polypyrrole Gas-Sensing Thin-Films.", Lemon and Haigh, '99).

A2.2 Yoshi Electrode 'Live-to-Inert' Crossover

The use of a 'single-comb' deposition technique was adopted during growth of type 283 [PPy/BSA(Na)/H_2O] polymer onto Yoshi interdigital electrodes, as described in §A1.7.2. Initial pilot studies showed that, on the application of a growth potential to the working electrode, vigorous polymer deposition began immediately on the live comb whilst no (visible) polymer deposition occurred on the inert comb, as would be expected. After a period of deposition, a rapid colouration change of the inert comb was observed (see §A1.7.2), followed by characteristic polymer growth.

A study was undertaken by optical microscopy (using an Olympus VANOX model AHM-T binocular optical microscope with thermal print facility) and scanning electron microscopy in order to investigate the growth mechanisms involved during single-comb deposition. The hypothesis that the 'crossover' observed between live and inert electrodes was the result of a direct, physical/electrical contact between polymer deposited onto the live electrode and the inert electrode was plausible, but was challenged by suggestions that electrolyte conductivity may, under certain circumstances, result in charge transfer from the live to the inert comb, so resulting in polymer deposition onto the inert comb (see §A2.2.1).

Individual Yoshi electrodes were prepared with a Millipore water rinse and a propan-2-ol (IPA) wash, as described in §2.1.1. Electrodes formed the electrochemical working electrode, using the techniques described in §A1.7.1 to §A1.7.3. Standard type 283 electrolyte solutions were freshly prepared before each deposition. A deposition potential of +5.00V vs SCE was used throughout. After application of the deposition potential, a polymer film was allowed to form on the live comb. The colouration of the inert comb was monitored visually during deposition; deposition potential was stepped down to +0.00V vs SCE either shortly after the inert comb was observed to discolour, or as soon before discolouration as possible. It was of note that the time taken for discolouration to occur during deposition was not constant for the set of Yoshi electrodes used (ranging from 15 to 70s). This was assumed to be the result of inconsistencies in the physical characteristics of individual devices.

Figure A2.2 shows the electrochemical deposition of a polypyrrole film onto the live electrodes of Yoshi elements, [a] showing the results of removing the deposition potential (i.e. stepping the deposition potential down to +0.00V vs SCE) well before the postulated live-to-inert crossover, and [b] showing the effects of the removal of deposition potential shortly before crossover.

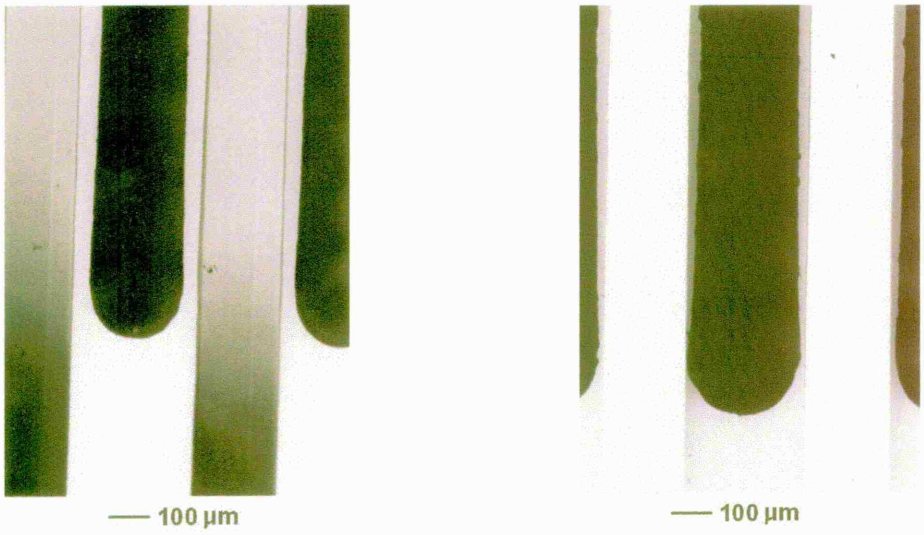

[a] [b]

Figure A2.2: *Optical micrographs of polymer deposition onto the 'live' comb of an interdigital Yoshi electrode (top of frame), [a] after the deposition of a mature polypyrrole film, and [b] after further deposition, shortly before contact between the live and inert combs.*

It is of note that the morphologies observed on the inert electrodes shown in Fig. A2.2 [a] and [b] are representative not of electrochemically deposited polypyrrole (at any stage of immature *or* mature growth) but rather are visually similar to those of 'pre-deposition' platinum Yoshi electrodes. This strongly supports the theory that polypyrrole deposition onto the inert comb results from direct physical contact, and suggests against arguments that solution conductivity may result in charge transfer and therefore polymer deposition onto the inert electrode. A short study of the possibility of solution charge transfer is now presented.

A2.2.1 Live to Inert Crossover - Influence of Solution Electrical Conductivity

The electrical conductivity of a typical electrolyte solution (PPy/BSA(Na)/H_2O : 0.25M/0.25M/50ml) was studied to allow the possibility of polymer deposition onto the inert electrode to be assessed. A pair of platinum electrodes were lowered into the electrolyte solution, separated by 10.0±0.5mm and linked to a calibrated DMM to allow measurement of electrical resistance (Note: measurements were made in a.c. mode, in order to reduce the effects of [a] electrochemical reactions at the electrode surfaces and [b] electrolyte diffusion)(see Hibbert, '93). After subtraction of the circuit resistance, the resistance of the electrolyte solution between the two platinum electrodes, (R) was found to be 27±0.1 kΩ. As 20mm lengths of 1mm diameter platinum wire were used as electrodes, solution resistivity (ρ) was calculated using:

$$R=\rho.(L/A)$$

where L = the electrode separation, and A the electrode area. The solution resistivity (ρ) was found to be ≈84.8±4.0 Ω.m. Knowledge of the resistivity of a typical electrolyte solution allowed calculation of the resistance between 'live' and 'inert' Yoshi electrodes whilst immersed in electrolyte. Typical dimensions of the Yoshi electrodes used were substituted into the above formula (75±5μm electrode separation, 2.0±0.1μm electrode thickness and 3.0±0.5mm electrode overlap) to calculate 'live' to 'inert' resistance; a value of 1.0±0.5 MΩ was calculated.

During potentiostatic electrochemical deposition onto Yoshi electrodes, a deposition potential of +5.00V vs SCE was used. As depositions were carried out in d.c. mode, Ohm's Law may be used to calculate a current flow between live and inert electrodes of around 5μA, around one thousandth of that measured during typical polymer depositions.

It is therefore considered that the deposition of polymer onto the inert electrode *before direct physical contact between the live and inert electrodes via a polymer bridge* is extremely unlikely.

A2.2.2 Live to Inert Crossover – Direct Physical/Electrical Contact

The study described in §A2.2 strongly suggested that the observed crossover of polypyrrole deposition from the live comb to the inert comb was due to direct physical (electrically conductive) contact between the live and inert electrodes.

Optical and electron micrographs of the sensors produced during the study presented in §A2.2 (see Figs. A2.2 and A2.3) show beyond reasonable doubt that polymer growth on the inert electrode was the result of direct contact.

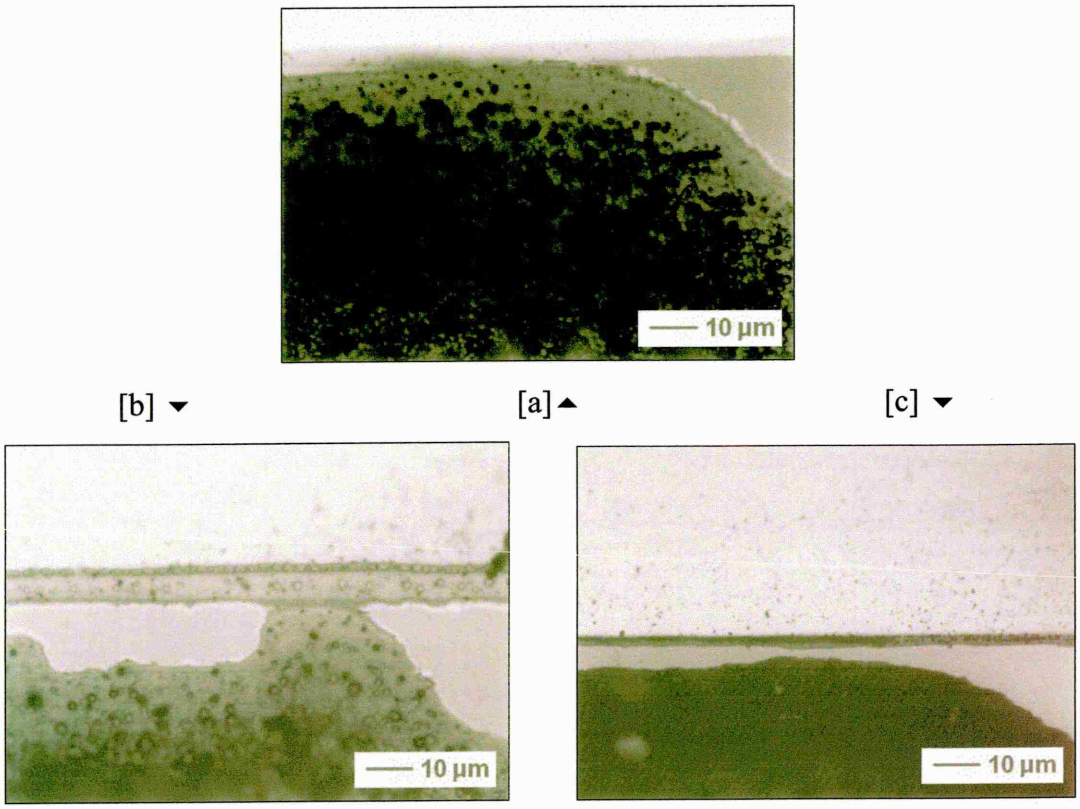

Figure A2.3: *Optical micrographs of polymer deposition between the 'live' and 'inert' combs of interdigital Yoshi electrodes, [a] immediately on crossover between the mature polypyrrole film on the live electrode and the inert electrode, [b&c] shortly after crossover elsewhere on the electrode.*

Fig. A2.3 [a] shows initial contact between type-283 polypyrrole growing on the live comb (lower dark area, nodular morphology) and the inert comb (top of frame, white area of pristine platinum). It is suggested that this 'primary' contact between the live and inert combs results in the application of a growth potential to the formerly inert comb (resulting from the presence of a highly conducting polypyrrole 'short', or bridge)

so resulting in immediate deposition of polymer onto it. The potential applied to the formerly inert comb will certainly be lower than that present on the live comb, due to the slight electrical resistance of the polypyrrole bridge; the magnitude of the potential drop will depend on the thickness of the polypyrrole layer, the resistance of the specific polymer used, comb separation and the degree of bridging contact. Darkening of the lower area of the inert platinum comb shown by Fig. A2.3 [a] shows the early stages of polypyrrole growth on the formerly inert comb. Figure A2.4 shows a similar electrode during SEM analysis; direct contact between the live and inert electrodes is clearly visible, although micrograph quality is reduced due to the requirement to use a 2.0kV accelerating voltage. The 'standard' 20kV accelerating voltage could not be used due to rapid charging of the insulating glass Yoshi substrate. Darkening of the formerly inert electrode suggests the initial stages of polypyrrole growth, although no polypyrrole texture is evident.

Fig. A2.3 [b] shows 'secondary' contact between the two combs. Unlike Fig. A2.3 [a], it is of note that a significant amount of polymer has deposited onto the formerly inert (upper) comb before contact with the live (lower) comb, suggesting that primary contact had occurred previously at a different site. Fig. A2.3 [c] shows a similar situation to that shown in [b]; the early stages of polymer growth are present on the formerly inert comb (top), suggesting that primary contact had previously occurred elsewhere. However, it is of great interest to note that the strip of early polymer growth visible at the lower edge of the formerly inert comb is of variable width in [c]. It appears that proximity of this early growth to the mature polymer present on the live comb may have affected its growth rate. It is postulated that the higher growth potential on the live comb results in an increased concentration of monomer / oligomer radical cations in the vicinity of the polymer growth face, monomer / oligomer radicals which may deposit on the (lower potential) formerly inert comb after oxidation. The increased availability of monomer radical cations results in an increased deposition rate onto the formerly inert comb.

Figure A2.4: *Scanning electron micrograph showing the direct physical contact between 'live' and 'inert' Yoshi electrodes during electrochemical deposition. Note the use of an unusually low accelerating voltage.*

A2.3 Neotronics 'Bass-Warwick' Electrodes – the Effects of Single Electrode Deposition.

The effects of 'live to inert crossover' as discussed in §A2.2 on the resistance characteristics and resistance temporal stability of Mk-III Bass-Warwick polypyrrole devices have been investigated. Three discrete studies were carried out in order to investigate; [a] the effects of 3-electrode vs 1-electrode deposition on sensor resistance (full deposition period) [§A2.3.1], [b] as [a] but for a much reduced deposition period in order to allow the 'interfacial' region (hypothesized in [a]) to be studied [§A2.3.2], and [c] the effects of reduced period 3-electrode deposition vs reduced period single electrode deposition on alternate sides (left and right) of the gold electrode [§A2.3.3].

A2.3.1 The Effects of Three-Electrode Deposition vs Single-Electrode Deposition

Three-Electrode Deposition

It is considered that standard 'three-electrode' polymer deposition (during which a deposition potential is applied to both sides of the Bass-Warwick electrode) will result in the immediate growth of polypyrrole onto both sides of the electrode active area (with each area of polymer growth segregated by the presence of the 10μm insulating gap). The two growth faces will coalesce after a finite level of polymer growth; it is postulated that this coalescence will lead to the presence of an interfacial area between the two growth fronts, positioned over/in the 10μm insulating gap. It is reasonable to expect that the presence of such an interface may result in reduced levels of polymer conjugation and hence decreased device conductance; it is also considered that build up of impurities at the polymer growth faces (as described in Ch. 4) may lead to the presence of many impurities within interfacial material. Such a growth mechanism is illustrated in Fig. A2.5 through steps [a] (initial polymer growth on both live electrodes); [b] (further growth on both live electrodes resulting in direct contact and therefore initial interfacial formation; [c] further growth and concomitant maturation of the polymer interface between electrodes.

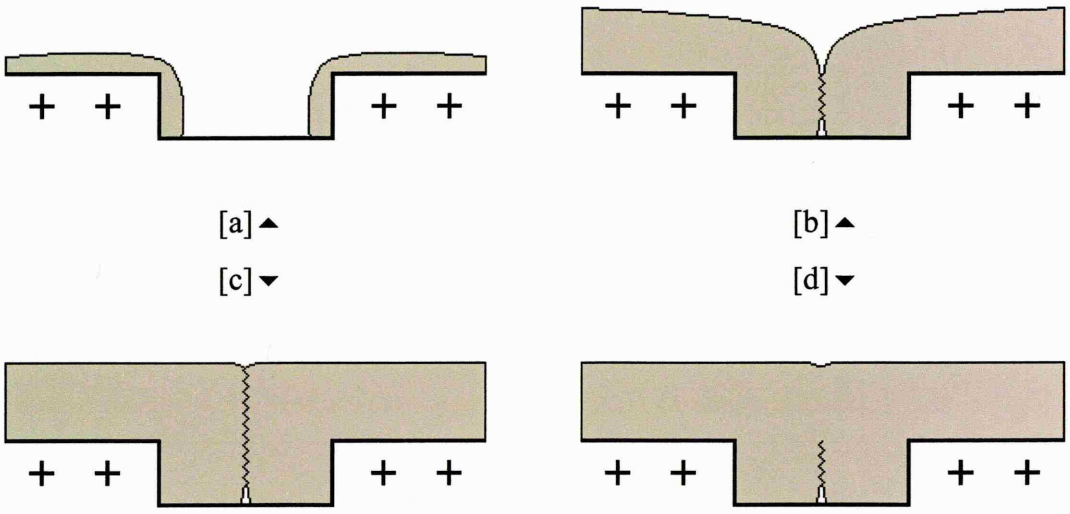

Figure A2.5: *Postulated polypyrrole growth mechanisms on Bass-Warwick electrodes (10μm insulating gap shown as trough) during 'three electrode' deposition.*

Alternatively, it was considered that polymer growth under the conditions specified may continue from step [b] directly to step [d] (see Fig. A2.5), which illustrates the effects of continued deposition of polymer onto both sides of the electrode active area resulting in the formation of a *connected*, conducting mass of polymer over the interfacial region (note that this is dissimilar to the polymer deposited over the conducting region in (c), which is postulated to be separated by an interfacial region).

Single-Electrode Deposition

Similarly, it was considered that 'single electrode' polymer growth (during which a deposition potential is applied to a single side of the Bass-Warwick electrode) will result in the immediate growth of polypyrrole onto the live side with no polymer growth on the inert side. It is postulated that continued polymer growth on the live electrode will result in direct contact between live and inert electrodes via a conducting polymer 'bridge', as observed during polymer deposition onto Yoshi electrodes. Such direct contact may reduce the extent of any interfacial regions as predicted during three-electrode growth above, and so possibly increase both device conductance and reproducibility.

Such a growth mechanism is illustrated in Fig. A2.6 through steps [a] (initial polymer growth on LHS live electrode); [b] (further growth on live electrode resulting in direct contact between live and inert electrodes and therefore application of reduced growth potential on formerly inert electrode; [c] immediate polymer growth on the formerly inert electrode (provided that polymer conductivity is sufficient) and; [d] further growth and film maturation without interface formation.

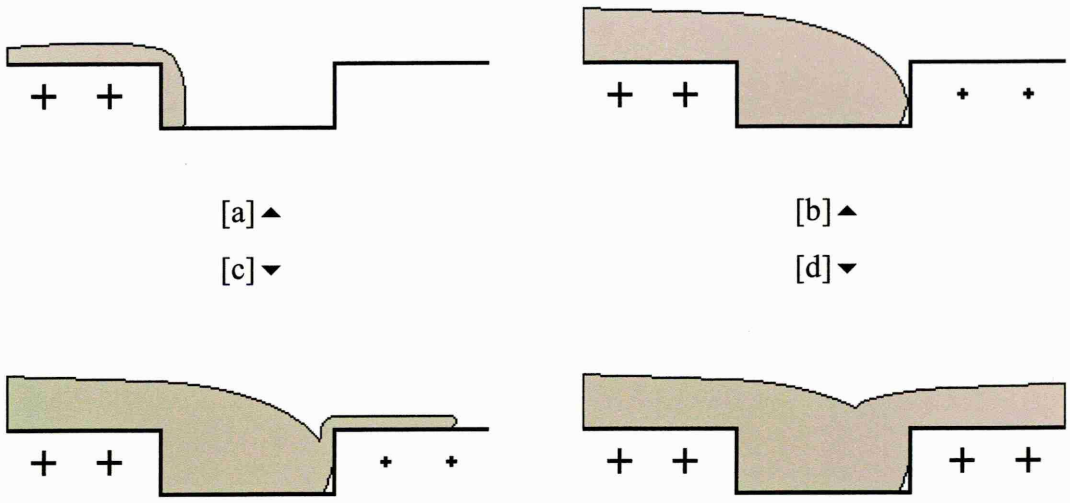

Figure A2.6: *Postulated polypyrrole growth mechanisms on Bass-Warwick electrodes during 'single electrode' deposition.*

Two sets of polypyrrole gas sensors were prepared, both using Bass-Warwick electrodes & substrates (MkIII Bass-Warwick sensors, as described in §A1.1, see Fig. A2.7) in order to investigate the effects of single electrode deposition (see §A2.3) on the electrical resistance and resistance temporal stability of type 283 polypyrrole material.

Bass-Warwick electrodes were used as supplied, but were cleaned immediately before use with IPA & acetone and dried with a high velocity jet of oxygen-free nitrogen. Type-283 polypyrrole [PPy/BSA(Na)/H_2O : 0.25M/0.25M/50ml] was deposited under standard conditions at a potential of +0.85V vs SCE for 120s + 30s @ 0V vs SCE. Ten devices were formed from a single electrolyte solution (as discussed in §3.1) due to the low volume of material used during each deposition.

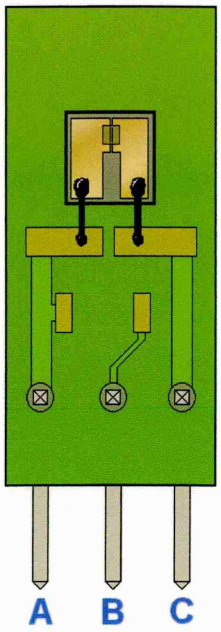

Fig. A2.7: *The MKIII Bass-Warwick electrode. Polymer deposited by standard 'three-electrode' Neotronics procedure by use of contacts A, B & C; 'single-electrode' deposition carried out by use of contact A.*

Two sets of devices were produced:

[a] 'Three-Electrode' devices, grown by the application of deposition potential to all three electrodes (A, B & C, see Fig. A2.7) as per the standard Neotronics procedure. Connection of all electrodes allows both sides of the device active area (which are separated by the requisite 10μm insulating gap) to be deposited immediately, as described previously. Devices were labelled as the '3X' series.

[b] 'One-Electrode' devices, grown by the application of deposition potential to electrode A (see Fig. A2.7), resulting in the deposition of polymer onto a single side of the device active area. Devices were labelled as the '1X' series.

Individual device depositions were staggered between the '3X' and '1X' series to reduce the unlikely effects of electrolyte solution depletion (i.e. first deposition = 1A, second deposition = 3B, third = 1C, fourth = 3D and so on).

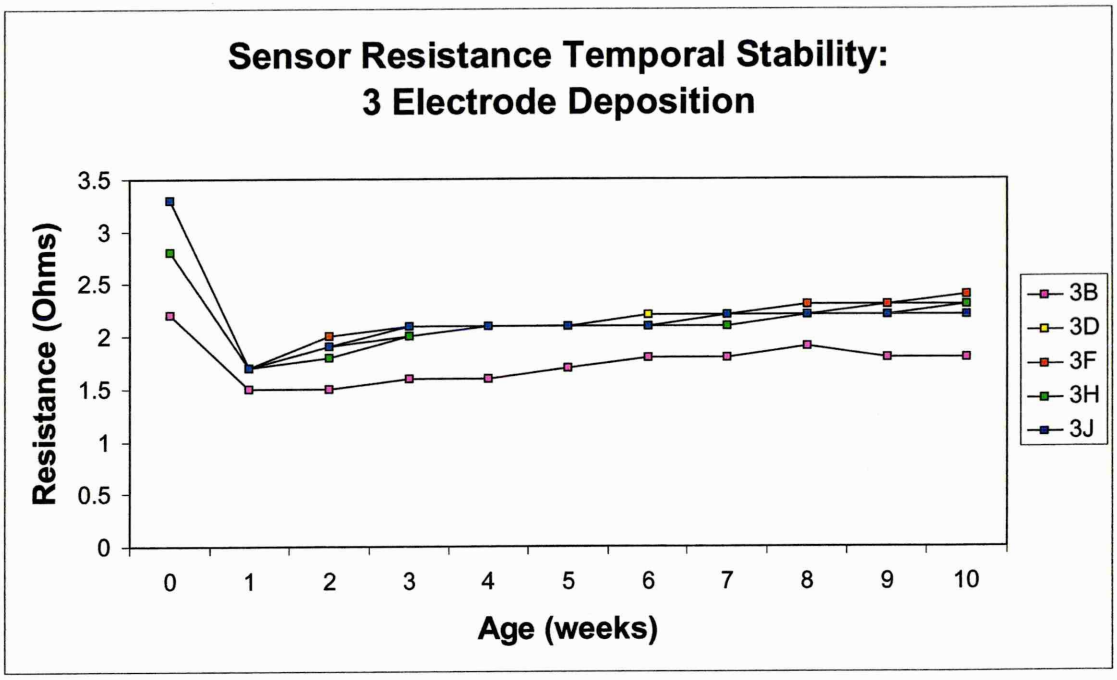

[a] ▲ [b] ▼

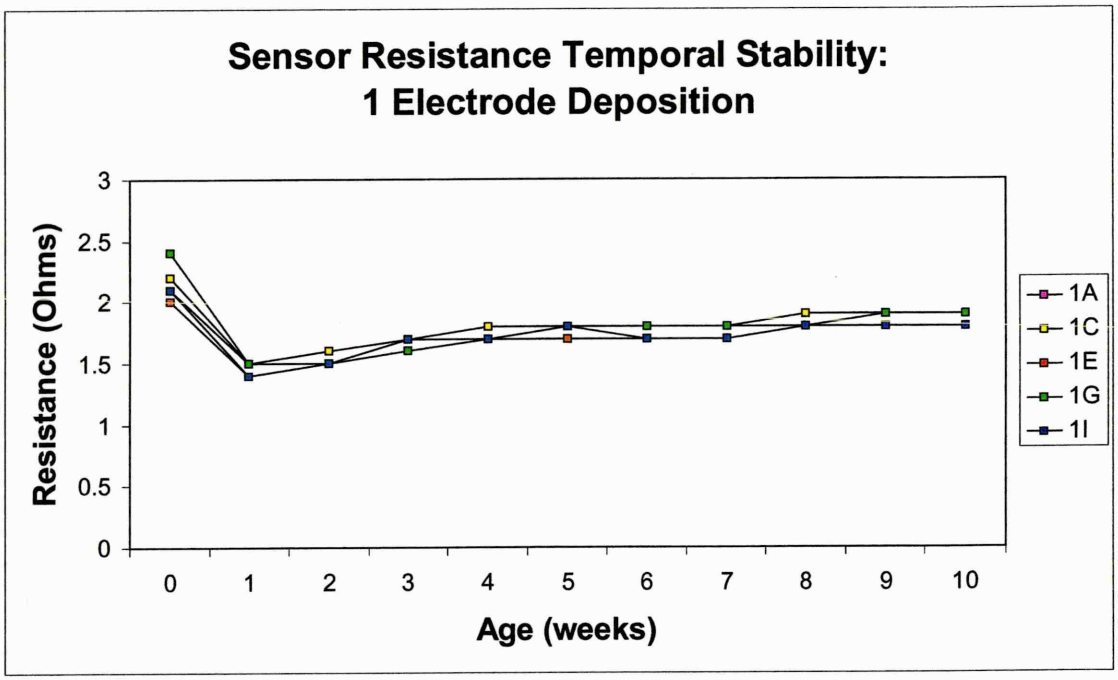

Figure A2.8: *Resistance temporal stability for Type-283 polypyrrole devices (standard Neotronics "Mk III Bass-Warwick" electrodes) using [a] '3-electrode' deposition ('3X' series), and [b] '1-eletrode' deposition ('1X' series).*

After deposition, individual devices were rinsed in clean electrolyte, dried under a high velocity jet of oxygen-free nitrogen and stored individually. A calibrated DMM was used to measure the electrical resistance of individual devices [a] immediately after drying, before initial storage, and [b] at weekly intervals for a period of ten weeks after

deposition. Resistance stability traces for the '3X' series (deposited with both sides of the device active area 'live') are presented in Fig. A2.8 [a]; traces for the '1X' series (deposited with only one side of the device active area 'live') are shown in Fig. A2.8 [b]. All resistance data are presented after subtraction of external circuit resistance.

The data presented in Fig. A2.8 suggests that the use of 'single electrode' deposition in preference to 'three electrode' deposition results in:
[a] no discernable change in sensor resistance temporal stability,
[b] a slight reduction in the initial resistance drop inherent to standard Neotronics type 283 devices (i.e. those deposited by a 'three electrode' method),
[c] improved sensor-to-sensor resistance repeatability (i.e. greatly reduced resistance standard deviation).

If the above observations are related to the growth mechanisms postulated in this section (see Fig. A2.5 and Fig. A2.6), it is reasonable to assume that the observed improvement in sensor-to-sensor resistance repeatability is the result of the reduction of the postulated interfacial region produced during 3-electrode polymer growth; inconsistency of the extent and position of the interfacial region may explain the resistance irreproducibility observed with 3-electrode devices.

The above observations support the hypothesis presented in this section; it is therefore suggested that the use of a 'single electrode' deposition regime may improve the reproducibility of industrial type-283 devices.

A2.3.2 The Effects of Three-Electrode Deposition vs Single-Electrode Deposition (Reduced Deposition Time)

The growth models formed in §A2.3.1 suggest that the effects of interface formation during 3-electrode polymer growth on sensor resistance properties *may* be reduced as deposition time increases (see Fig. A2.5 [d]). Therefore, although the empirical evidence presented above supports the presence of an interfacial region as postulated, the effects may be masked to a degree by the lengthy (but standard) deposition time used. A similar study to that presented in §A2.3.1 was therefore carried out, but using

much reduced deposition times. It was intended that deposition time reduction (and therefore reduction of the *amount* of polymer deposited) would focus the effects of the interfacial region on sensor resistance properties.

Three-Electrode Deposition

As was the case during study [a] (§A2.3.1), 'three electrode' deposition allows the immediate growth of polymer onto both sides of the Bass-Warwick electrode active area (with regions segregated by the 10μm insulating gap). It is postulated that the two polymer growth fronts will coalesce after a short growth period, so forming the interfacial region suggested (and supported by empirical evidence) above.

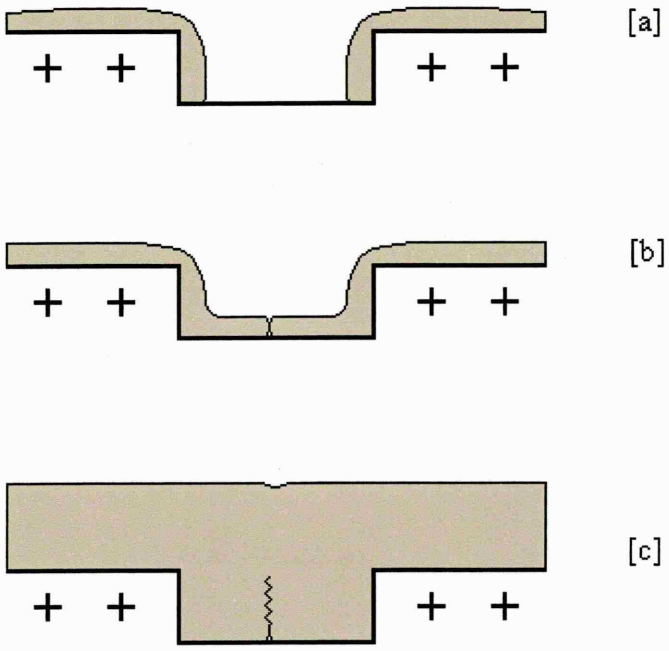

Figure A2.9: *Postulated polypyrrole growth mechanisms on Bass-Warwick electrodes during 'reduced deposition time, three electrode' device formation.*

The growth mechanism involved is thought to follow the steps shown in Fig. A2.9, via; [a] initial polymer growth on both live electrodes, and [b] further growth on both live electrodes resulting in direct contact and therefore *initial* interfacial formation. Deposition was halted significantly before film maturity (represented in white, step [c]) in order to intensify the effects of the interfacial region.

Single-Electrode Deposition

As for study [a] (§A2.3.1), 'single-electrode' depositions allows the immediate growth of polymer onto the 'live' side of the Bass-Warwick electrode active area, with no polymer growth on the 'inert' side until such a time as direct, physical contact between the live and inert electrodes occurs via a polymer bridge. Direct bridging may reduce the extent of any interfacial region formed during three-electrode growth, and so improve device conductance and reproducibility.

The bridging mechanism postulated is thought to follow the steps shown in Fig. A2.6, although it is considered that film thickness may be less than is shown (Fig. A2.6 was exaggerated to illustrate the mechanism involved during study [a]). The growth mechanism shown in Fig. A2.10 is thought to be more representative, and may proceed via: [a] initial polymer growth on single live electrode (LHS), [b] further growth on the live electrode resulting in polymer bridging over the insulating gap and therefore application of a reduced deposition potential to the inert electrode, and [c] continued deposition onto both electrodes (although to a lesser extent on the formerly 'inert' electrode due to the reduced deposition potential); it is postulated that no significant interfacial regions are formed.

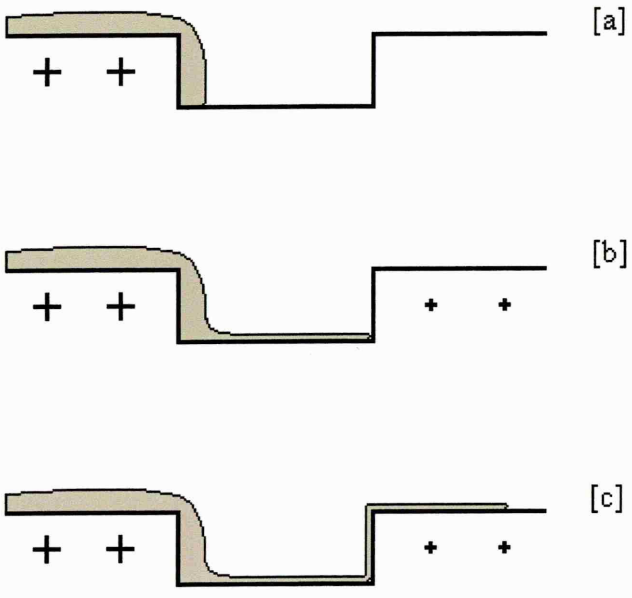

Figure A2.10: *Postulated polypyrrole growth mechanisms on Bass-Warwick electrodes during 'reduced deposition time, single electrode' device formation.*

Two sets of polypyrrole devices were prepared, both using MkIII Bass-Warwick electrodes in order to investigate the effects of reduced period, single electrode deposition on electrical resistance and resistance temporal stability.

Bass-Warwick electrodes were cleaned immediately before use with IPA & acetone and dried with a high velocity jet of oxygen-free nitrogen. Type-283 polypyrrole [PPy/BSA(Na)/H_2O : 0.25M/0.25M/50ml] was deposited under standard conditions at a potential of +0.85V vs SCE. Trial depositions under identical conditions were carried out; it was noted that electrode 'inert' sides blackened (i.e. became live, leading to polypyrrole deposition) around 5±1s after application of deposition potential. Depositions were therefore carried out for 10s + 30s @ 0V vs SCE. Ten devices were formed from a single electrolyte solution.

Two sets of devices were produced:
[a] 'Three-Electrode' devices, grown by the application of deposition potential to all three electrodes (A, B & C, see Fig. A2.7), labelled as the '3RX' series (***3***-electrode deposition, ***R***educed deposition time, ***X***).
[b] 'One-Electrode' devices, grown by the application of deposition potential to electrode A (see Fig. A2.7), labelled as the '1RX' series (1-electrode deposition, ***R***educed deposition time, ***X***).

Individual device depositions were staggered between the '3RX' and '1RX' series to reduce the unlikely effects of electrolyte solution depletion (i.e. first deposition = 1RA, second deposition = 3RB, third = 1RC, fourth = 3RD and so on).

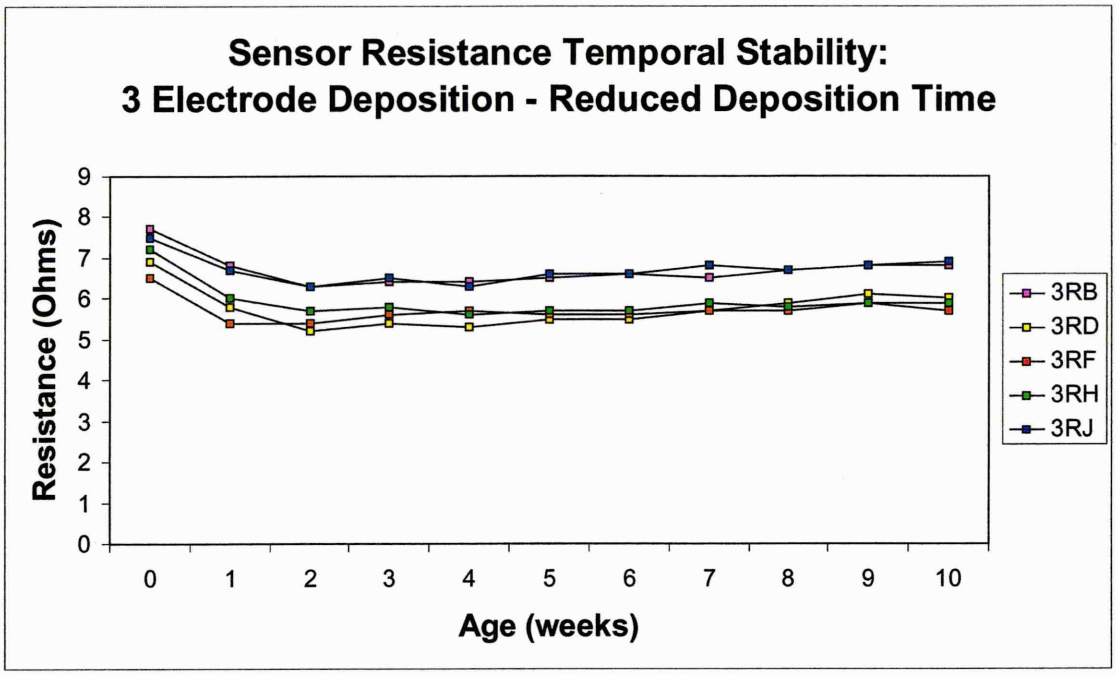

[a] ▲ [b] ▼

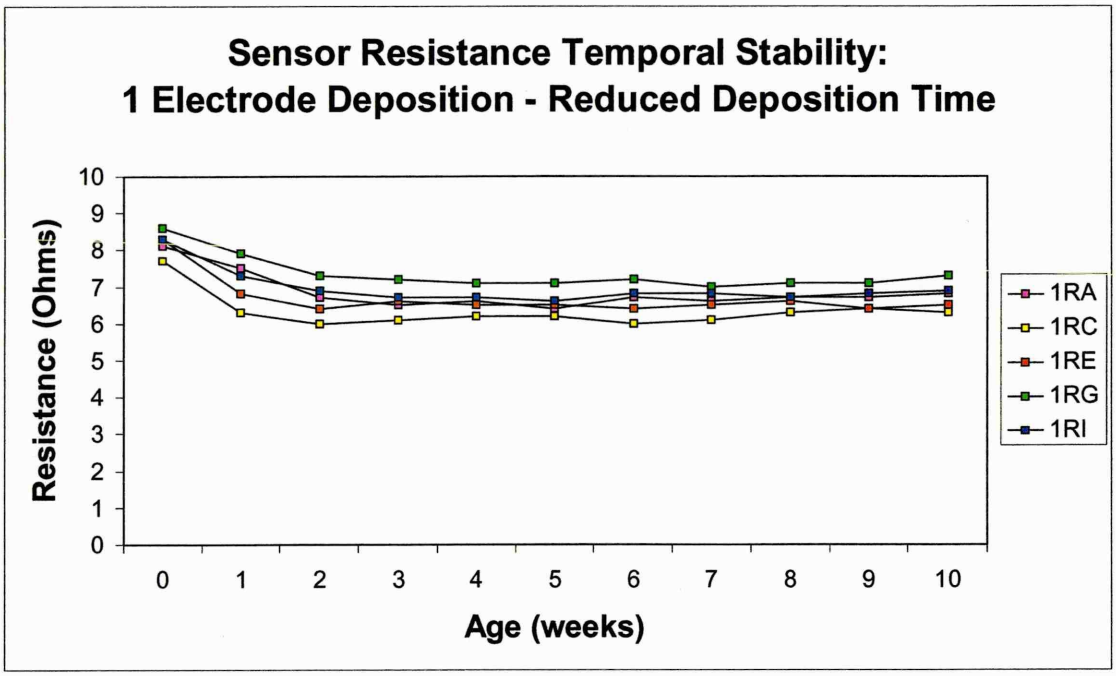

Figure A2.11: *Resistance temporal stability for Type-283 polypyrrole devices (standard Neotronics "Mk III Bass-Warwick" electrodes) using [a] 'reduced deposition time, 3-electrode' deposition ('3RX' series), and [b] 'reduced deposition time, 1-eletrode' deposition ('1RX series).*

After deposition, individual devices were rinsed in clean electrolyte, dried under a high velocity jet of oxygen-free nitrogen and stored individually. The resistance of individual

devices were measured immediately after drying, and were monitored at weekly intervals for a period of ten weeks after deposition. Resistance stability traces for the '3RX' series are presented in Fig. A2.11 [a]; traces for the '1RX' series are shown in Fig. A2.11 [b]. All resistance data are presented after subtraction of external circuit resistance.

The data presented in Fig. A2.11 suggests that the use of 'single electrode' deposition in preference to 'three electrode' deposition results in:
[a] a subjective improvement in sensor resistance temporal stability,
[b] no discernable change in the initial resistance drop,
[c] a subjective improvement in sensor-to-sensor resistance repeatability (i.e. reduced resistance standard deviation).

The marked increase in the resistance of 'reduced deposition time' devices over those deposited for standard times (§A2.3.1) is thought to be the result of reduced polypyrrole layer thickness, as would be intuitively expected. The effects of interfacial areas on device resistance characteristics are less pronounced than in study [a] (§A2.3.1), contrary to plan. However, the improvements resulting from the removal of the postulated interfacial areas (through 1-electrode as opposed to 3-electrode deposition) are, nonetheless, subjectively evident.

A2.3.3 The Effects of 'Alternate-Side, Single-Electrode' Deposition (Reduced Deposition Time)

In order to investigate the effects of interface formation during 3-electrode polymer growth on sensor resistance properties, a study was undertaken involving the comparison of the resistance properties of [a] devices grown by three-electrode deposition (reduced deposition time) and [b] devices grown by the application of a deposition potential to each side of the active area in turn (reduced deposition time).

As per previous studies presented here, 3-electrode devices were studied as a control; it has been suggested that 3-electrode growth results in the formation of an interfacial

region. It is thought that the growth mechanisms involved during deposition of type [b] devices (above) may greatly reduce the extent of interface production.

Three-Electrode Deposition

Devices were deposited as described in §A2.3.2.

Alternate-Side, Single-Electrode Deposition

It has been shown previously that single-electrode deposition results in deposition onto the live side of the electrode active area, with no deposition on the inert side until direct physical contact occurs via a polymer bridge. Evidence presented previously suggests that the use of this method reduces the extent of interface formation, so improving device resistance characteristics. The production of 'alternate-side, single electrode' devices aims to further reduce the effects of interface formation by the application of a deposition potential to each side of the electrode active area in turn, with the total deposition time used equal to that of standard three-electrode devices.

The growth mechanism during 'phase 1' (the application of a growth potential to the LHS of the electrode) is thought to follow the steps shown in Fig A2.10, leading to a structure as shown in Fig. A2.12 [a]. Further growth (during 'phase 2', the removal of growth potential from the LHS, and application of growth potential to the RHS) is postulated to occur as shown in Fig. A2.12 [b]. It is thought that polymer deposition will occur on both sides of the electrode during this stage (regardless of the removal of applied potential to the LHS) as a result of the electrical bridge between the electrodes.

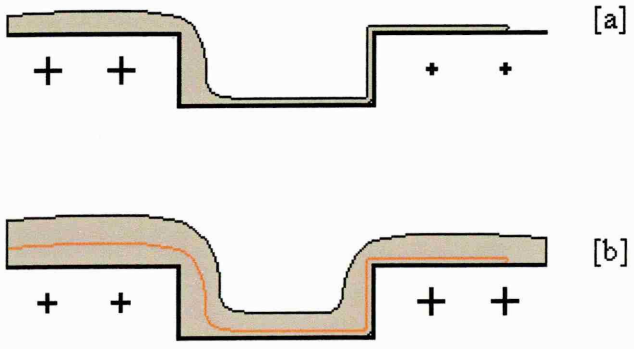

Figure A2.12: *Postulated polypyrrole growth mechanisms on Bass-Warwick electrodes during 'alternate-side, single electrode' device formation.*

MkIII Bass-Warwick electrodes were used throughout, prepared as described in §A2.3.2. Type-283 polypyrrole [PPy/BSA(Na)/H_2O : 0.25M/0.25M/50ml] was deposited at a potential of +0.85V vs SCE. Pilot depositions suggested that six seconds of deposition were required to ensure polymer bridging (see §A2.3.2). Alternate-side, single-electrode depositions were therefore carried out for 6s per side (i.e. for a total of 12s) + 30s @ 0V vs SCE. Three-electrode depositions were therefore carried out for 12s (+ 30s @ 0V vs SCE) in an attempt to equilibrate the amount of polymer deposited to that of alternate-side, single-electrode devices.

The two sets of devices produced were as follows:
[a] 'Three-Electrode' devices, grown by the application of deposition potential to all three electrodes (A, B & C, see Fig. A2.7), labelled as the '12X' series (***12*** seconds overall deposition, ***X***).
[b] 'Alternate-side, single-electrode' devices, grown by the application of deposition potential to electrode A (see Fig. A2.7) for 6s, followed by the application of deposition potential to electrode C (see Fig. A2.7) for 6s, labelled as the '6X' series (***6*** seconds deposition per side, ***X***).

Individual device depositions were staggered between the '12X' and '6X' series as previously reported (i.e. first deposition = 6A, second deposition = 12B, third = 6C, fourth = 12D and so on).

After deposition, individual devices were prepared and stored as described in §A2.3.2. Device resistances were monitored for a period of ten weeks at weekly intervals. Resistance stability traces for the '12X' series are presented in Fig. A2.13 [a]; traces for the '6X' series are shown in Fig. A2.13 [b]. All resistance data are presented after subtraction of external circuit resistance.

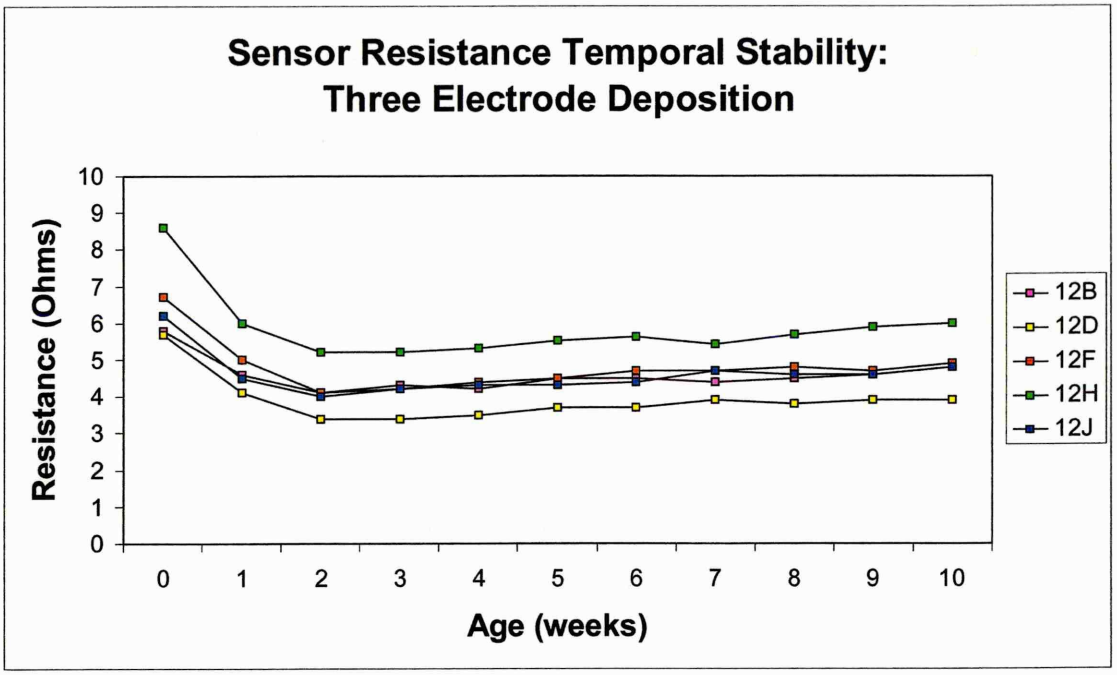

[a] ▲ [b] ▼

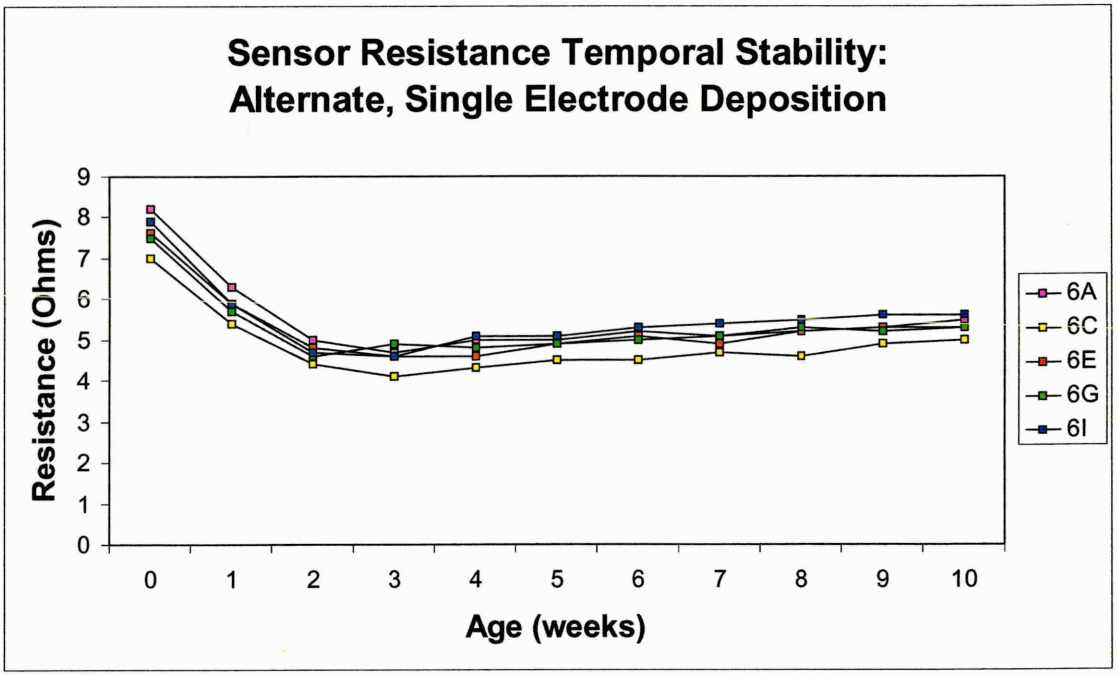

Figure A2.13: *Resistance temporal stability for Type-283 polypyrrole devices (standard Neotronics "Mk III Bass-Warwick" electrodes) using [a] 'reduced deposition time, 3-electrode' deposition ('12X' series), and [b] 'reduced deposition time, alternate-side, single-electrode' deposition ('6X' series).*

The data presented in figure A2.13 suggests that the use of 'reduced deposition time, alternate-side single-electrode' deposition in preference to 'reduced deposition time, three electrode' deposition results in:

[a] no discernable improvement in sensor resistance temporal stability,

[b] no discernable change in the initial resistance drop,

[c] an improvement in sensor-to-sensor resistance repeatability (i.e. reduced resistance standard deviation).

The above suggests that the removal of interfacial regions from Bass-Warwick sensing devices improves device resistance characteristics (and so supports and strengthens the other evidence presented in this chapter). The empirical evidence collected supports the growth models presented.

Summary, Appendix 2

- The temporal stability of the electrical resistance characteristics of Mk-III Bass Warwick electrodes and 'Yoshi' interdigital electrodes have been compared. Significant differences were observed between the resistance characteristics of devices formed using the two electrode types. Explanations were given for the observed differences, which strongly support the theory presented in §4.4.
- The use of a 'single-comb' technique for the deposition of polymer onto interdigital electrodes has been described; polymer bridging of insulating substrate areas (resulting in charge transfer to previously inert sections of electrode) has been demonstrated. Use of this technique facilitates the study of initial polypyrrole structure and was considered to lead to more reproducible polymer structure in the 'interfacial' regions of devices (sections of polymer grown over insulating areas in order to allow current transfer through the polymer).
- The use of the single-comb deposition technique has been applied to Mk-III Bass-Warwick Sensors. Use of this technique resulted in the formation of models describing the resultant macrostructures of the devices formed; it was also demonstrated that the use of a single-electrode deposition technique resulted in increased sensor resistance reproducibility.
- Devices were produced utilizing an 'alternate side, single electrode' deposition technique; the potential effects on film macrostructure were discussed. Resistance data was found to support the predictions of structural modifications.

A3. The Effects of XRD Test Protocol

The work reported in this appendix concerns the effects of variation of the test protocol used during the analysis of type-283, electrochemically deposited polypyrrole by θ-2θ X-Ray Diffraction (XRD) (see §2.2.2). The research presented supports the work presented in Ch.5 (The Microstructure of Polypyrrole), which focuses on the elucidation of the microstructure of type-283 polypyrrole by XRD.

A3.1 The Effects of Spinner Use

The effects of the use of sample 'spinning' during XRD analysis have been studied. The spinning facility is provided within the XRD facility to allow the reduction of the effects of sample inhomogeneity by rapid sample rotation during analysis.

A pair of type-283 polypyrrole films were deposited on ITO glass substrates (as described previously). Depositions were carried out as for sample KW#2 (see Table 5.1, §5.1). Films were rinsed in fresh electrolyte after deposition and subjected to the long term soaking & drying procedure described in §5.1.

XRD analyses were carried out on each film, with and without the use of the spinning facility. Traces were manipulated using the techniques described in §5.1.1 & §5.1.2; typical traces are shown in Fig. A3.1 [a] and [b], which show traces of the same film with and without sample spinning respectively.

The typical traces shown in Fig. A3.1 illustrate that the use of the spinning facility does not affect the level of polypyrrole-based structural information available. Furthermore, the characteristics of the XRD diffractogram (shoulder/peak position, intensity profile etc.) are not affected by spinner use. It was therefore thought reasonable to conclude that the use of the spinner facility during XRD analysis was not necessary.

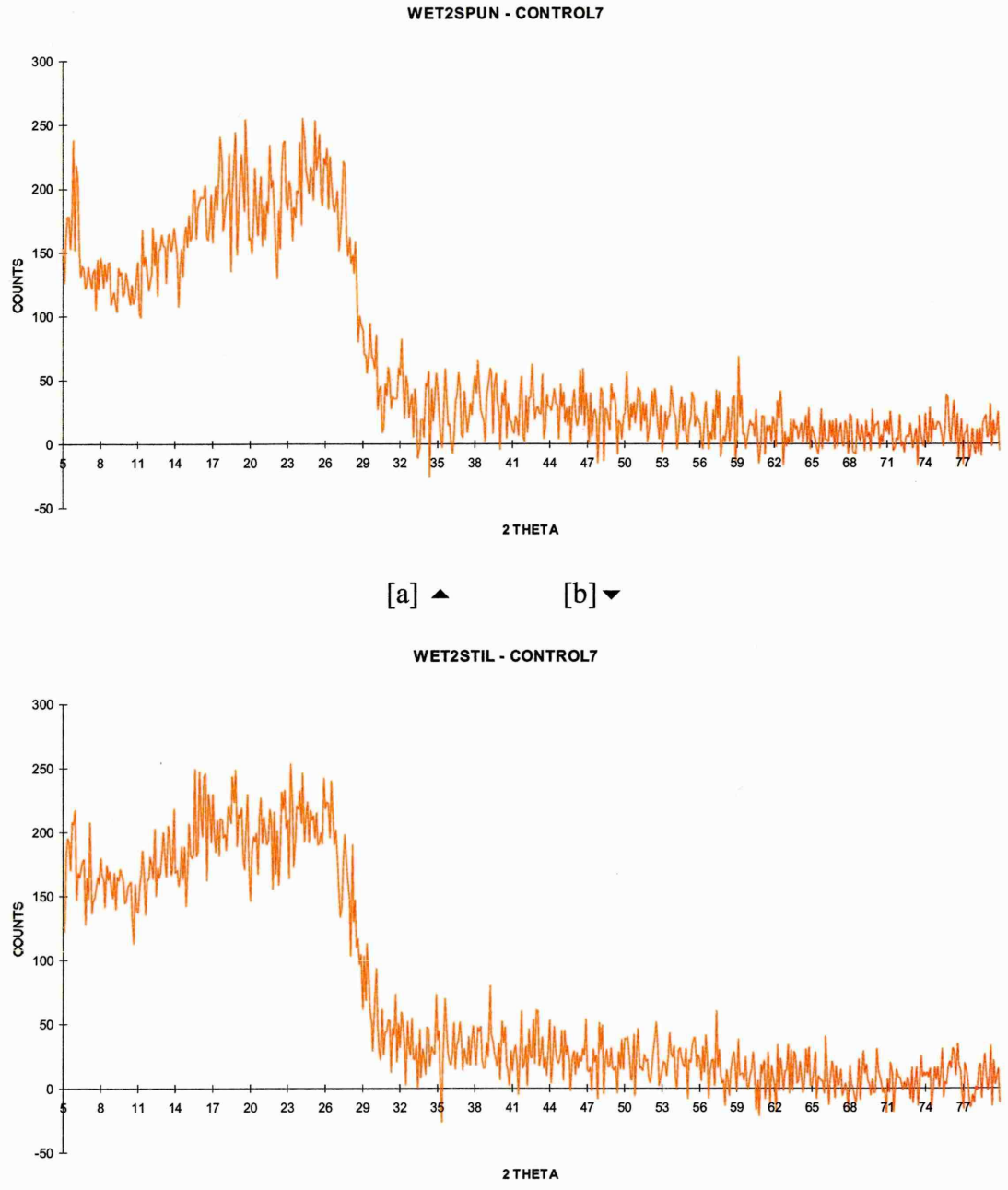

Figure A3.1: *Typical X-Ray diffractograms of a polypyrrole thick-film, [a] with, and [b] without the use of the 'spinning' facility. Diffractograms are shown after the subtraction of substrate information.*

A3.2 The Effects of Hardware Selection

The studies presented above were undertaken using a Philips PW1810 θ-2θ horizontal axis powder diffractometer. However, before completion of the work presented, technical difficulties led to the medium-term reliance on a PW1130/60 θ-2θ horizontal axis powder diffractometer, a model which shared the majority of its characteristics

with the PW1810. Despite the inherent similarities between diffractometer models, a study of the potential discrepancies between diffractograms produced by each model was undertaken.

Two pairs of type-283 polypyrrole films were deposited and matured as described in §A3.1. XRD analyses were carried out on each film using [a] the PW1810 and [b] the PW1130/60 diffractometer. Traces were manipulated as described previously.

The use of the PW1130/60 equipment consistently resulted in the production of lower intensities than did the use of the PW1810; an example of the low intensities produced is given on Fig. A3.2, after the subtraction of relevant substrate information.

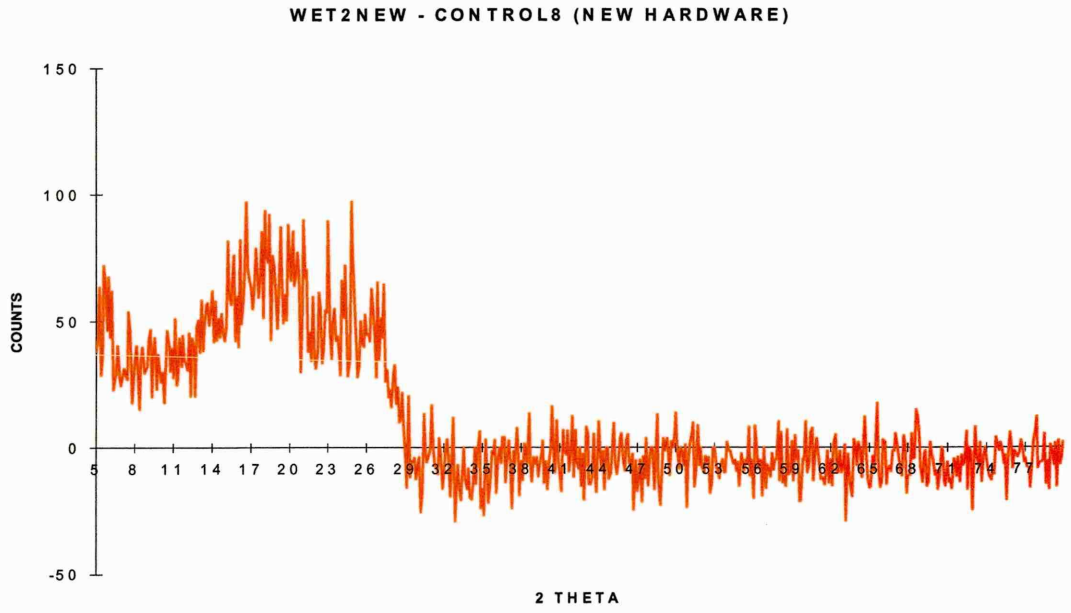

Figure A3.2: *Typical X-Ray diffractogram of polypyrrole produced using PW1130/60 diffractometer (standard 'Time per Step' value).*

The low intensity trace reproduced in Fig. A3.2, taken using the PW1130/60 diffractometer, may be compared to typical traces produced by the PW1810 diffractometer, as presented in §A3.1; note that no spinner facility was available on the PW1130/60.

In order to redress the reduced intensities of the diffractograms produced by the PW1130/60, use of the standard 'Time-per-Step' value of 1s was discarded in favour of

a longer time per step value. It was intuitively expected that doing so would result in an increase in diffractogram intensity. XRD analyses were carried out on each film prepared for this study using the PW1130/60 diffractometer with a range of time-per-step settings. As shown in Fig. A3.3, the use of a 2.5s time-per-step value resulted in the production of diffractograms of equivalent intensity to those produced by the PW1810 using the standard 1.0s time-per-step value.

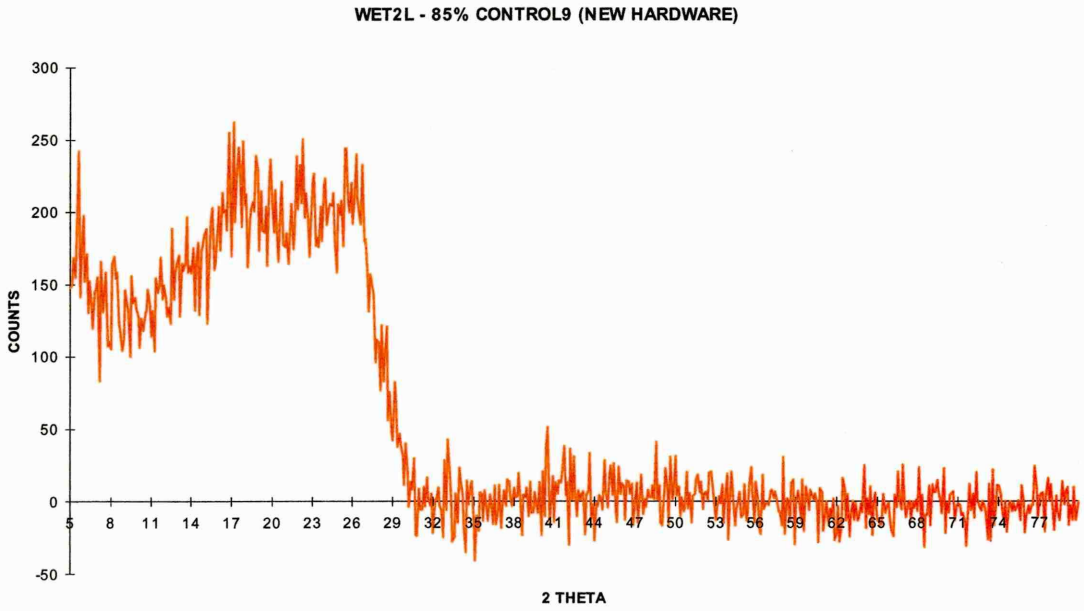

Figure A3.3: *Typical X-Ray diffractogram of polypyrrole produced using PW1130/60 diffractometer (increased 'Time per Step' value).*

It is considered that the reduced diffractogram intensity inherent to the PW1130/60 was the result of the reduced power of the XRD tube used in the instrument (the PW1810 was routinely run at 40kV & 40mA, whilst it was advised (Blake, '96) that the PW1130/60 was run at a maximum of 30kV & 30mA).

As a result of the modifications made to the analysis parameters (increased time-per-step value), diffractograms produced using the PW1810 and PW1130/60 were found to be very similar. The PW1130/60 diffractometer was therefore used for all subsequent research.

A3.3 The Effects of Low Power Operation

The use of the data manipulation methodologies reported in §5.1.2 was necessary in order to remove structural information from 'combined' traces originating from the glass substrate. Alternatively, reduction of the level of 'substrate' information may be achieved by reduction of the quality (or *penetrating power*) of the X-rays used. X-ray quality may be reduced by lowering the X-Ray tube operating voltage, so lowering the depth of X-ray penetration, therefore decreasing the level of substrate information included in 'combined' traces.

It was considered, however, that differences in film density and thickness would result in a greatly variable requirement for surface sensitivity between films in order to collect polypyrrole-specific structural information (i.e. to collect *no* information from the substrate layer). Furthermore, as discussed previously, operation of the X-Ray tubes used at lower working voltage results in the production of diffractograms of consistently low intensity (this has been shown to be the case via XRD analysis). Although this could be overcome to a degree by the use of increased time-per-step values, the variability of the polymer films produced during the studies presented would result in a high potential for inconsistency between measurements.

Therefore, attempts were not made to increase the surface sensitivity of the XRD technique by use of 'softer' X-Rays (i.e. X-Rays of lower penetrating power).

A3.4 The Effects of XRD Trace 'Smoothing'

As a result of the basic nature of the APD 3.6 software used during the work presented, much work is required to convert the ASCII output produced into a format recognized by popular spreadsheet packages; this is due to inconsistent spacing of the data produced. This problem is compounded by the large volume of text-based data produced during ASCII conversion (52kB of text).

The volume of data produced during XRD analysis may be substantially reduced by the use of a 'smoothing' technique included in the APD 3.6 package which is capable of

smoothing a typical diffractogram until ASCII conversion results in only 3kB of text, so greatly reducing the level of manual data manipulation required.

In order to assess the potential effects of diffractogram smoothing, a pair of films produced during previous studies were separately analysed by XRD using standard parameters. ASCII files were produced for each film [a] before smoothing, and [b] after smoothing (note, two films were tested in order to allow the repeatability of the smoothing process to be assessed). Subsequent manual treatment of the ASCII files produced resulted in the traces shown in Fig. A3.4 [a] and [b].

The resultant traces clearly demonstrate that trace smoothing results in the preservation of some structural information. However, order peaks within 'non-smoothed' traces (as reported previously) were not preserved through the smoothing process. Because of this, although it is not anticipated that the variation of polypyrrole deposition parameters will result in sufficient order to result in the production of appreciable order peaks (although the possibility cannot be discounted), the smoothing process will not be used during the work presented.

A3.5 The Effects of Step Size Variation

XRD information is collected by the hardware described in §2.2.2 by the detection of X-Rays in a series of 'segments' around the arc of rotation of the X-Ray detector. In order to attain high resolution, the standard 5° to 80° 2θ range used during the majority of the work presented here is split into segments of 0.020°.

As discussed in §A3.4, the basic nature of the APD 3.6 software requires much effort to convert data files into the graphical representations shown throughout this chapter. Although the data smoothing technique described in §A3.4 was not used, increasing the step size during analysis could greatly reduce the volume of data to be manipulated. Further, the use of the XRD hardware described in §2.2.2 with an increased step size could reduce the time taken for XRD analysis from several hours to several minutes per trace.

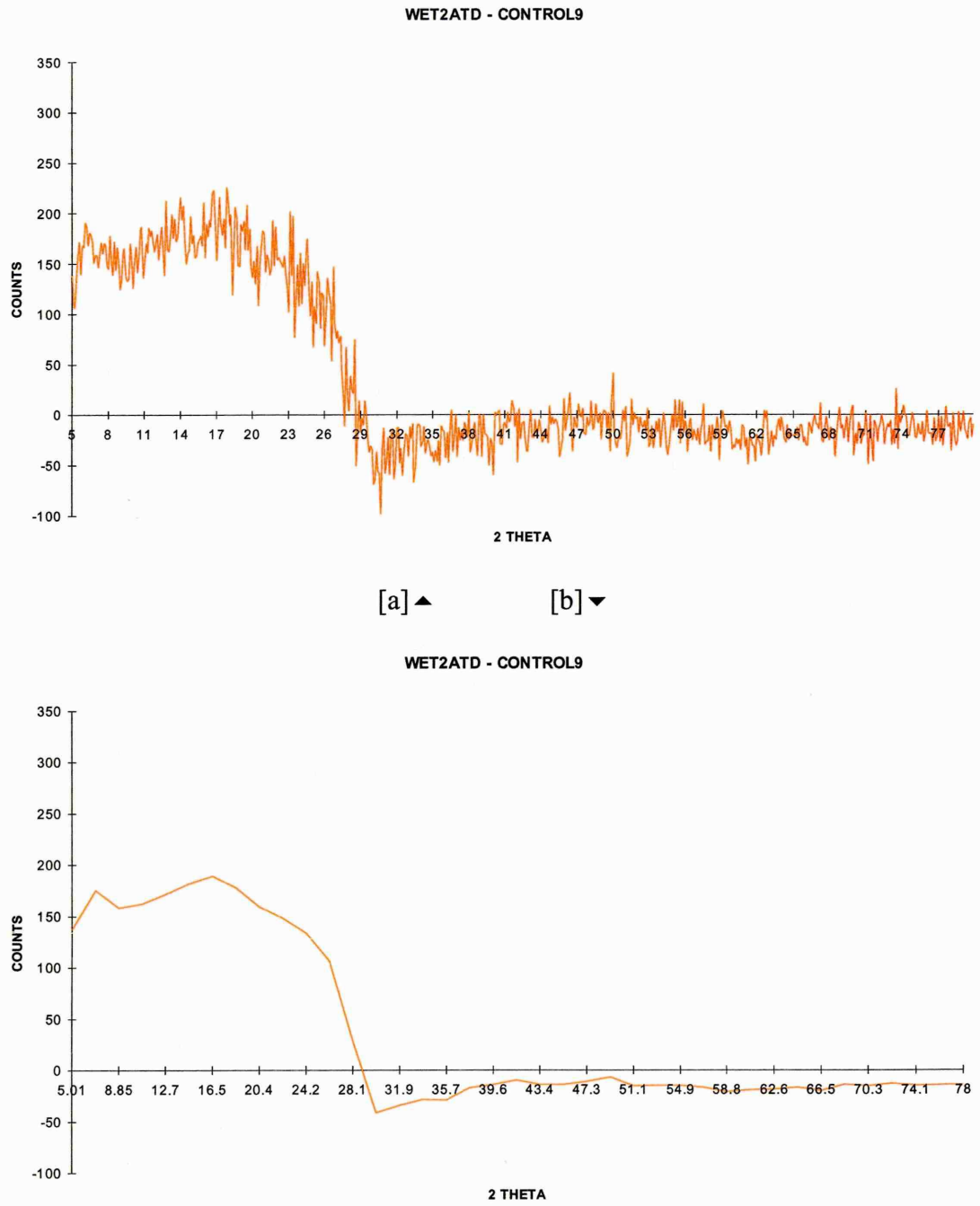

Figure A3.4: *Typical X-Ray diffractograms of polypyrrole [a] before, and [b] after trace smoothing.*

The effects of step size variation were assessed using two separate, typical type-283 polypyrrole films produced previously. A range of XRD step sizes were used, from the (standard) 0.020°, through 0.200° to 2.000°. ASCII files were produced for each film using each step size, subsequent treatment of ASCII data gave traces as shown in Fig. A3.5 [a] and [b].

The traces shown clearly illustrate that a substantial increase in step size preserves a high degree of generic structural information. However, step size increase routinely results in the loss of information from fine peaks and other fine features within the original diffractogram. Although the presence of sharp XRD order peaks originating from polypyrrole is unlikely, it was decided not to reduce step size unless strictly necessary.

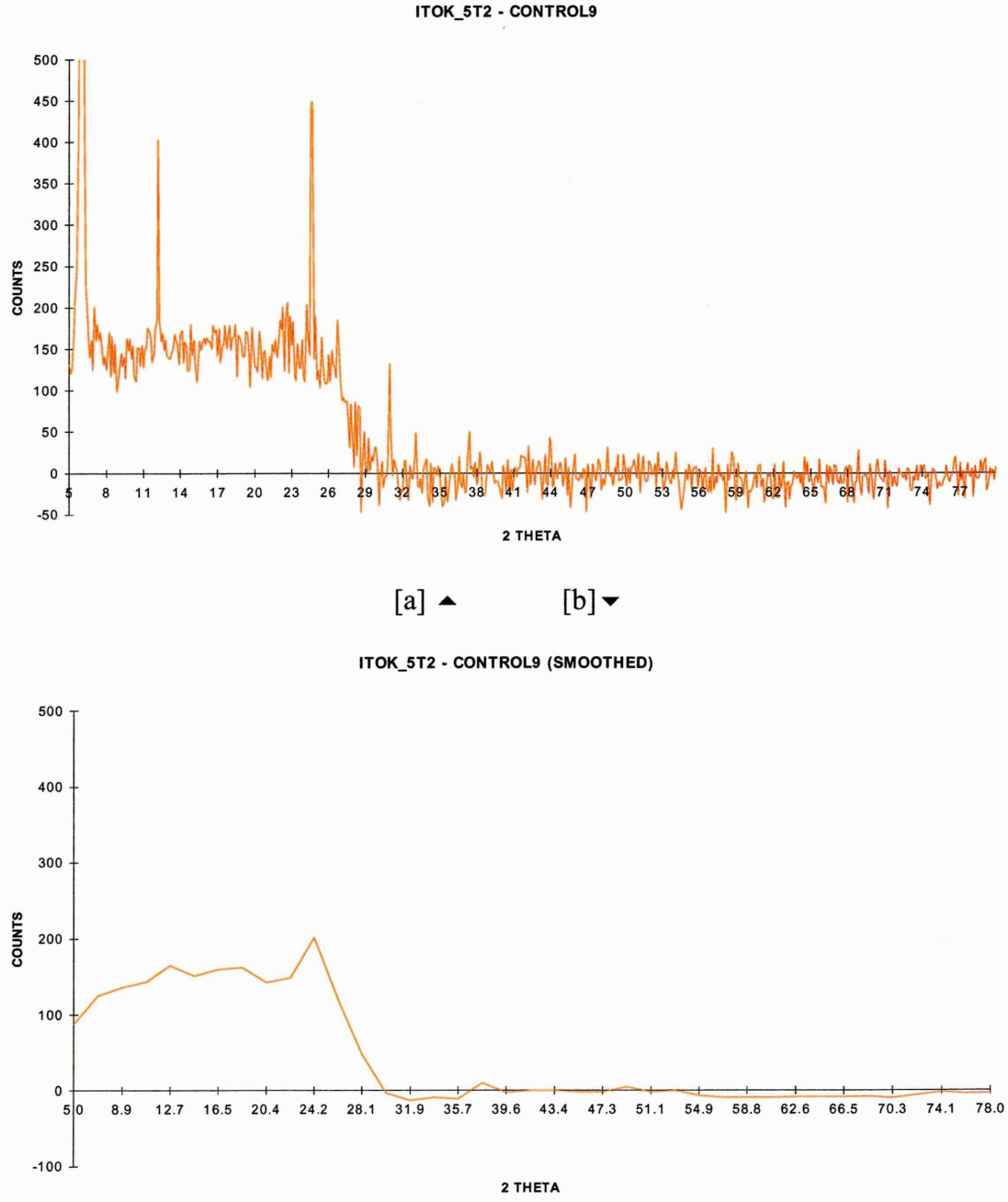

Figure A3.5: *Typical X-Ray diffractograms of polypyrrole using [a] small, and [b] large step size.*

Summary, Appendix 3

- A number of studies are presented which assess the effects of the use of differing XRD analysis parameters during the analysis of polypyrrole thin-films. These complement those described in Ch.5. These studies involved:
    - An assessment of the use of the sample 'spinning' facility during XRD analysis; no adverse effects were observed.
    - An assessment of the effects of the use of PW1810 or PW1130/60 XRD diffractometers; significant differences were observed. Differences were addressed by modification of the 'time-per-step' value used during analysis.
    - An assessment of the effects of low-power X-Ray tube operation in order to increase the surface sensitivity of the technique; low-power operation was found to produce traces with an unsuitable signal to noise ratio.
    - An assessment of the effects of the use of XRD trace 'smoothing'; the use of this facility was found to yield unsuitable information.
    - A study of the effects of the use of an increased step size during XRD analysis; increased step size was found to produce unsuitable traces.

Publication Reprints

(See "Publications" in Thesis preamble (§II) for details).

"Electrolytic Dopant Recrystallisation in Polypyrrole Gas-Sensing Thin-Films."
P.W. Lemon and J. Haigh, in "*Sensors and their Applications X*", ed. N.M. White and A.T. Augousti, I.O.P. Publishing, Philadelphia, 1999, pp.179-184.

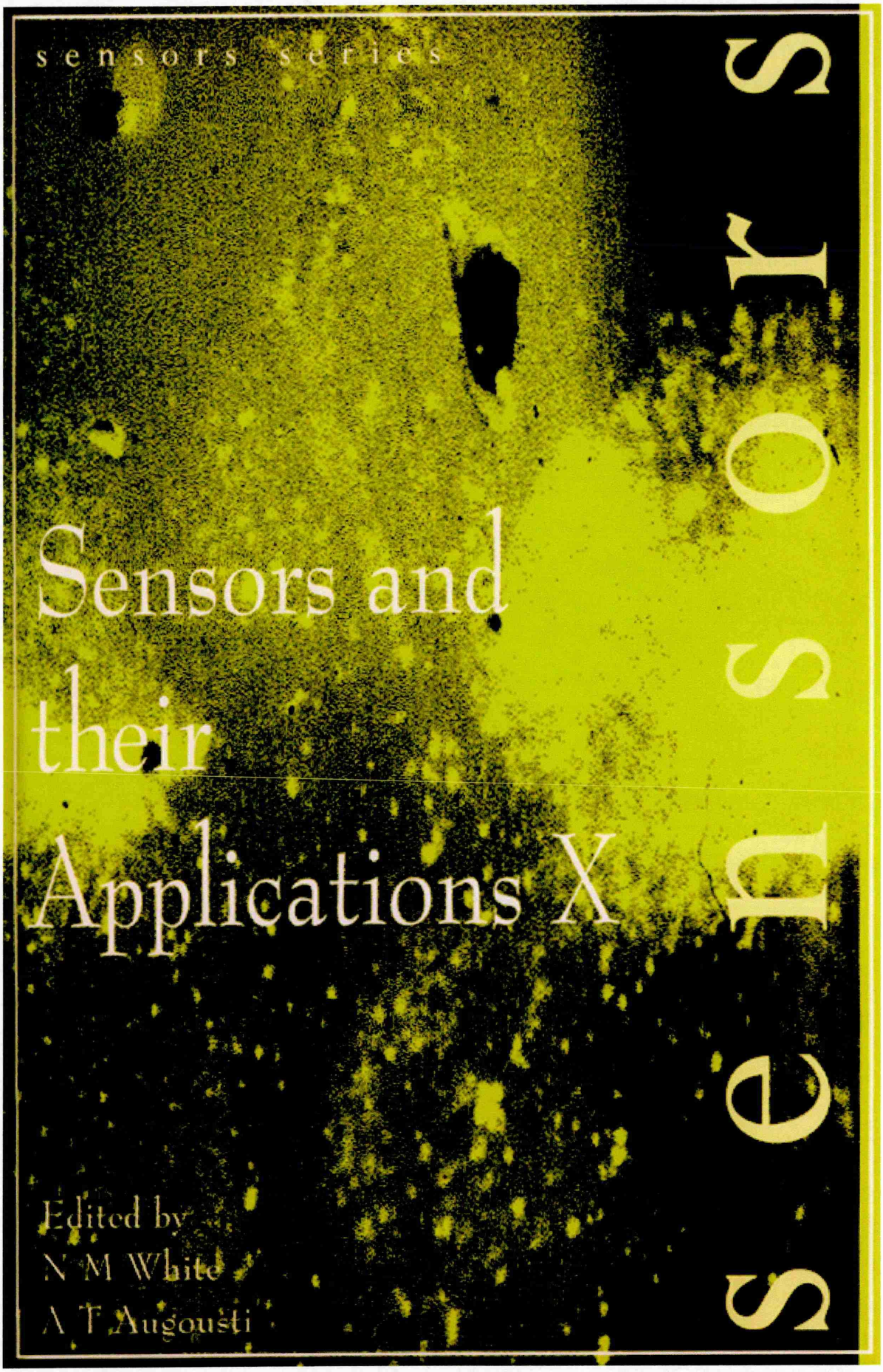
sensors series
Sensors and their Applications X
Edited by
N M White
A T Augousti
sensors

Paper presented at Sensors and their Applications X, 5-8 September, 1999

Electrolytic Dopant Recrystallisation in Polypyrrole Gas-Sensing Thin-Films

P Lemon[a] and J Haigh[b]

[a] Materials Research Institute, Sheffield Hallam University, Sheffield, South Yorkshire, S1 1WB, UK.

[b] School of Science and Mathematics, Sheffield Hallam University.

Abstract. Polypyrrole gas-sensitive thin-films have been deposited electrochemically onto gold and indium-tin-oxide glass electrodes. Structural analysis of the films produced has shown, we believe for the first time, that areas of highly crystalline material develop within the polymer matrix as an inherent part of the aging process. It is shown that the crystalline material produced results from the entrapment of pockets of (strongly ionic) electrolyte solution within the polymer matrix during deposition. We suggest that this process may be a major contributor to the temporal resistance instability inherent to many electrochemically deposited polypyrrole active layers.

1. Introduction

The ability of polypyrrole and its derivatives to conduct electricity when doped during formation by chemical or electrochemical means has long been appreciated [McNeill *et.al.* '63]. It was shown at an early stage that the conductivity of polypyrrole could be varied on exposure to many gaseous analytes [Nylander *et.al.* '83], but selectivity was not sufficient to allow use as 'stand alone' gas sensing devices. It was soon observed, however, that the broad sensitivity range of doped polypyrrole could be modified by the use of subtly different dopant groups and deposition regimes. This characteristic led to the widespread application of polypyrrole-based devices as members of gas sensing arrays; the response of each array element being carefully tailored to complement the responses of the other array members [Shurmer and Gardner '92].

Polypyrrole-based sensing elements are commonly deposited electrochemically from solution containing pyrrole monomer, dopant salt and supporting electrolyte. Electrochemical deposition requires the use of an inert, conducting substrate; devices are therefore often formed by the deposition of polymer onto two gold electrodes, separated by a thin (micron scale) insulating gap [Bartlett *et.al.* '89]. The application of a growth potential results in the deposition of polymer onto the gold electrodes. Continued deposition results in bridging of the insulating gap by the polymer, so allowing current flow between the gold electrodes via the polymer layer.

The structure and morphology of polypyrrole has been shown to strongly influence its electrical conductivity and gas sensitivity. The morphology and structural properties of polypyrrole are, in turn, known to depend sensitively on deposition parameters such as applied potential, counter-ion type, temperature, supporting electrolyte and monomer/counter-ion concentrations [Kiani *et. al.* '92]. Structure has also been shown to be heavily influenced by the presence of impurities in the electrolyte solution [Lemon *et.al.* '97] and by the production of gaseous oxygen at the working electrode during electrochemical

deposition [Lemon and Haigh '99]. The observed dependence of conductivity and gas sensitivity on structure and morphology necessitates a thorough understanding of the phenomena leading to structural variations.

A systematic study of the morphological and structural features exhibited by electrochemically deposited polypyrrole doped with benzenesulfonic acid (sodium salt) has been carried out by scanning electron microscopy (SEM), X-ray diffraction (XRD), energy dispersive X-ray analysis (EDXA) and glow discharge optical emission spectroscopy (GDOES). Morphological and structural modifications resulting from variations in deposition potential, monomer concentration, electrolyte treatment and growth time have been studied. In this paper, we report on the post-deposition recrystallisation of dopant salts within the polymer matrix, and relate this phenomenon to the temporal resistance variability displayed by these materials.

2. Experimental

2.1 Film preparation

Pyrrole monomer (Aldrich) was purified by solid-liquid chromatography. Monomer was passed through two separate alumina-filled columns (each of 3ml volume) in order to remove oxides and oligomers. Purified material was stored in low light conditions at 5°C prior to use, and was used as soon as possible after purification in order to suppress degradation (Lemon *et.al.* '98). Benzenesulfonic acid (sodium salt) (Aldrich) was used without further purification. Low-conductivity deionized water was used as solvent.

Two types of conducting substrate were used during the study, gold microelectrodes consisting of two active contacts, each of 0.5mm^2, and indium tin oxide coated glass slides (Balzers), cut to allow deposition over an area of around 200mm^2. Both substrate types were thoroughly cleaned in iso-propanol (propan-2-ol) before use, and dried under a high velocity jet of oxygen-free nitrogen.

Thin films of polypyrrole were deposited from aqueous solution containing pyrrole and benzenesulfonic acid (sodium salt), each at a range of concentrations from 0.1M to excess. Deposition was carried out in a standard three-electrode electrochemical cell (Kissinger and Heineman '96), controlled by a combination potentiostat / galvanostat (Oxford) in potentiostatic mode. A platinum coil was used as counter electrode, which was flamed prior to each experiment. A saturated calomel electrode (SCE) was used as a reference; all potentials are quoted relevant to this. Depositions were carried out at +0.85V unless stated otherwise, typically for 120s. Films were left in the electrolyte solution for 30s after deposition in order to provide a standard settling time, and were then removed, rinsed well in low-conductivity deionized water and dried under a jet of oxygen-free nitrogen. Analyses of film resistance, morphology and structure were then carried out.

2.2 Analysis

X-ray diffraction (XRD) studies were carried out using a Philips PW1810 θ-2θ diffractometer with CuKα radiation, and results analysed by a Philips PW3710 control unit via Philips APD 3.6 analysis software. Scanning electron microscopy (SEM) and Energy dispersive X-ray analysis (EDXA) was carried out with a JEOL 840A electron probe microanalyser in SEM mode at 20 kV accelerating voltage. Optical microscopy was carried out on an Olympus Vanox model AHM-T and on a Vickers metallurgical microscope in

crossed polar transmission mode. GDOES analysis was carried out on a LECO GDS-50 QDP.

3. Results and discussion

The structure of polypyrrole films deposited from concentrated electrolyte solutions were examined by XRD (see Fig. 2). The diffractograms produced consistently exhibited strong, sharp diffraction peaks at around $2\theta = 6°$, with up to 10^{th} order repeats in some cases. The intensity profile of the peaks observed were shown to describe a convolution of the Laue function and a superlattice structure factor; this is indicative of the presence of very highly ordered material.

The positions of the observed peaks suggest a lattice spacing of 14.8Å (±0.3Å). This spacing is in agreement with a recent structural model [Veluri *et.al.* '95] which used atomistic lattice simulation to describe the optimum packing of polypyrrole chains in 'crystalline' material. The simulation predicted the formation of a unit cell 14.48Å in length which comprised of five pyrrole units, therefore satisfying the lattice spacing suggested during XRD analysis. However, it is thought highly unlikely that the order peaks observed by XRD are the result of the crystalline packing of polypyrrole (as predicted by Veluri); previously reported work [Lemon and Haigh '99, Kiani and Mitchell '92] has suggested that polypyrrole deposited under similar conditions has a highly disordered structure.

The possibility of the observed peaks originating from the ordered incorporation of dopant groups within the disordered polymer matrix was also considered. It is accepted [Skotheim '86] that the distortion of polypyrrole chains by the formation of bipolaronic charge defects during deposition extends over four pyrrole rings and results in two areas of positive charge. These positive charges attract and 'pin' dopant anions in order to maintain charge neutrality, as shown in Fig. 1.

The exact positions adopted by dopant anions on incorporation will depend upon many factors, but it is logical to predict that the separation of two anions attracted to the bipolaronic positive charges will mimic the separation of the positive charges. Regular spacing of dopant groups could therefore result in the production of the order peaks observed. However, further XRD analyses have disproved this hypothesis by showing that order peaks develop over a period of several hours after deposition (Fig. 2). This observation is not consistent with the origination of order peaks as a result of dopant group spacing. Dopant groups are incorporated and 'pinned' on an 'as needs' basis during deposition, and are thought not to migrate through the polymer matrix unless an external impetus forces them to do so. Dopant groups are therefore highly unlikely to diffuse *en masse* to achieve an orderly distribution throughout the polymer matrix.

We suggest that order peaks arise as a result of the entrapment of electrolyte solution within the polymer matrix during deposition. Subsequent crystallisation of the highly ionic dopant salt used will result in the presence of highly ordered, non-polymeric material in the polymer matrix, as observed by XRD. This hypothesis is supported by previous observations (Lemon and Haigh '99) which suggested that gas formation during deposition often leads to the production of voids within the polymer matrix into which electrolyte solution may migrate. Further support is given by Ren and Pickup (1995), who showed that, in order to explain the electrical characteristics of polypyrrole formed under similar conditions, the polymer matrix must consist of a polypyrrole aggregate which encloses and traps pockets of electrolyte solution during deposition.

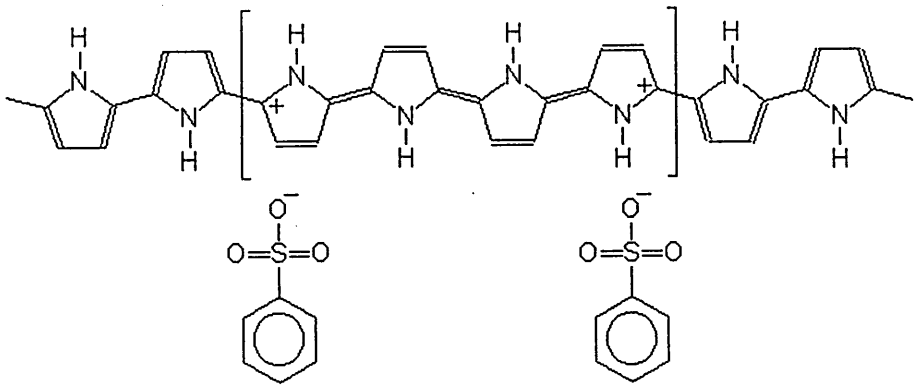

Figure 1: *Polypyrrole chain with a bipolaronic charge distortion (bracketed) attracting dopant anions*

Several investigative techniques were used to test the hypothesis of dopant recrystallisation. Analysis of the films produced by SEM, EDXA and GDOES has illustrated the presence of highly crystalline, sodium/sulfur-rich material within the polymer matrix. Electron probe microanalysis has been used to verify the presence of such material; polypyrrole films grown under the conditions specified showed the presence of many small crystalline clusters on the film surfaces (Fig. 3). EDXA was used in 'point analysis' mode to analyse the clusters found, and showed that the cluster material was extremely rich in sulfur with respect to the surrounding material. GDOES analysis (which produces elemental information akin to that available from SIMS) showed the presence of areas of unusually high sodium content throughout the polypyrrole films, although reliable information was not available for sulfur content.

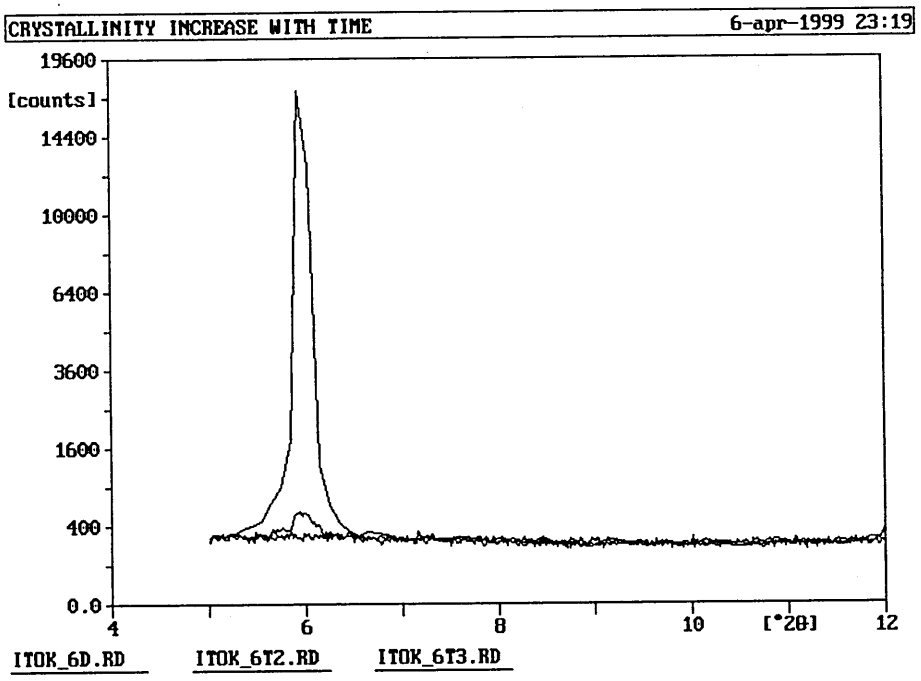

Figure 2: *XRD diffractograms of polypyrrole film showing peak intensity increase during film aging.*

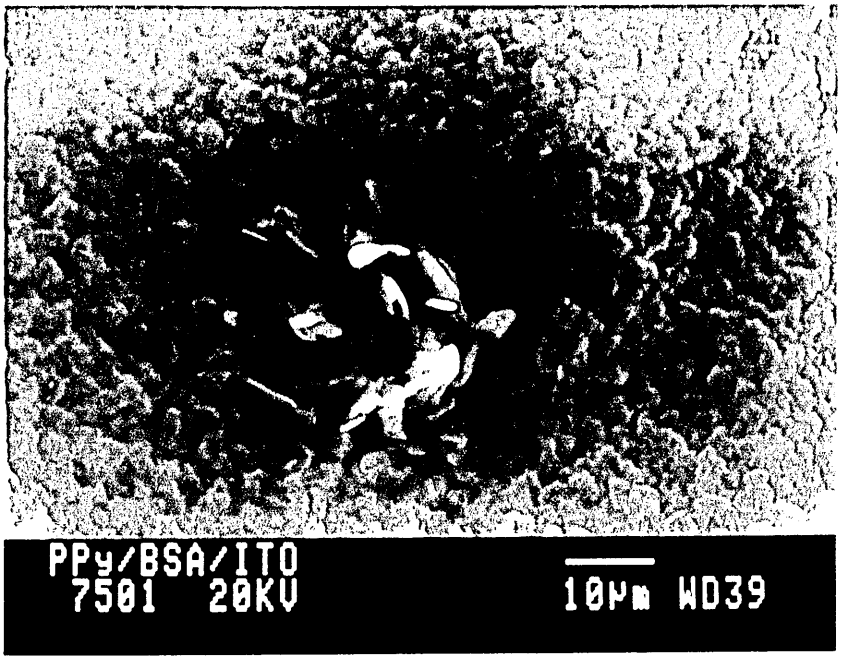

Figure 3: An Electrochemically deposited polypyrrole film displaying a cluster of crystalline dopant material.

Subsequent analysis of the electrolytic materials used during this study (benzenesulfonic acid, sodium salt and pyrrole monomer) by XRD has shown that the order peaks observed (as shown in Fig. 2) are characteristic of the dopant salt used (benzenesulfonic acid, sodium salt). Storage of the films in low conductivity, deionized water for several days has since been shown to result in the production of characteristically disordered XRD information. This is due to diffusion of the crystalline electrolytic material out of the polymer matrix into the storage solution.

Further work in this area may include an analysis of the effects of dopant recrystallisation on sensor performance. It is considered highly probable that the formation of crystalline dopant material may lead to depletion of the dopant concentration throughout the active polymer layers of sensing devices. This may be a leading cause of the temporal resistance instability currently observed in many electrochemically deposited conducting polymer gas sensing devices.

4. Conclusions

It has been shown, we believe for the first time, that the entrapment of electrolyte solution within polypyrrole films during electrochemical deposition may result in the recrystallisation of dopant material throughout the polymer matrix. It is thought that dopant crystallisation may affect the temporal stability of the electrical conductivity (and therefore gas sensitivity) of the active devices formed in this way.

Acknowledgements

The authors wish to thank Dr. Malcom Ives for his assistance with GDOES analysis and the Health and Safety Executive for their kind support.

References

Bartlett P N and Ling-Chung S K 1989 *Sensors and Actuators* **19** 141

Kiani M S and Mitchell G R, 1992 *Synthetic Metals* **48** 203

Kiani M S, Bhat N V, Davis F J and Mitchell G R 1992 *Polymer* **33** 4113

Kissinger P T and Heineman W R (Eds.) 1996 *Laboratory Techniques in Electroanalytical Chemistry 2nd Ed.* (Marcel Dekker)

Lemon P W, Szczur N and Haigh J, 1998 *Materials Research Bulletin* **33/6** 909

Lemon P W and Haigh J, 1999 *Materials Research Bulletin* **34/5** (in press)

McNeill R, Siudak R, Wardlaw J H and Weiss D E 1963 *Aust. J. Chem.* **16** 1056

Nylander C, Armgarth M and Lundström I 1983 *Proc. Intl. Meeting on Chemical Sensors, Fukuoka (1983)*, ed. Seiyama T, Fueki K, Shiokawa J and Suzuki S (Elsevier), pp.203-207

Ren X M and Pickup P G 1995 *Journal of Electroanalytical Chemistry* **396** 359

Shurmer H V and Gardner J W 1992 *Sensors and Actuators B* **8** 1

Skotheim T A 1986 *Handbook of Conducting Polymers* (Marcel Dekker) p.287

Veluri K, Corish J, Morton-Blake D and Beniere F 1995 *Theochem - Journal of Molecular Structure* **334** 109

"The Evolution of Nodular Polypyrrole Morphology During Aqueous Electrolytic Deposition: Influence of Electrolytic Gas Discharge."
P.W. Lemon and J. Haigh, *Materials Research Bulletin*,
Vol. 34, No. 5, (1999), pp. 665-672.

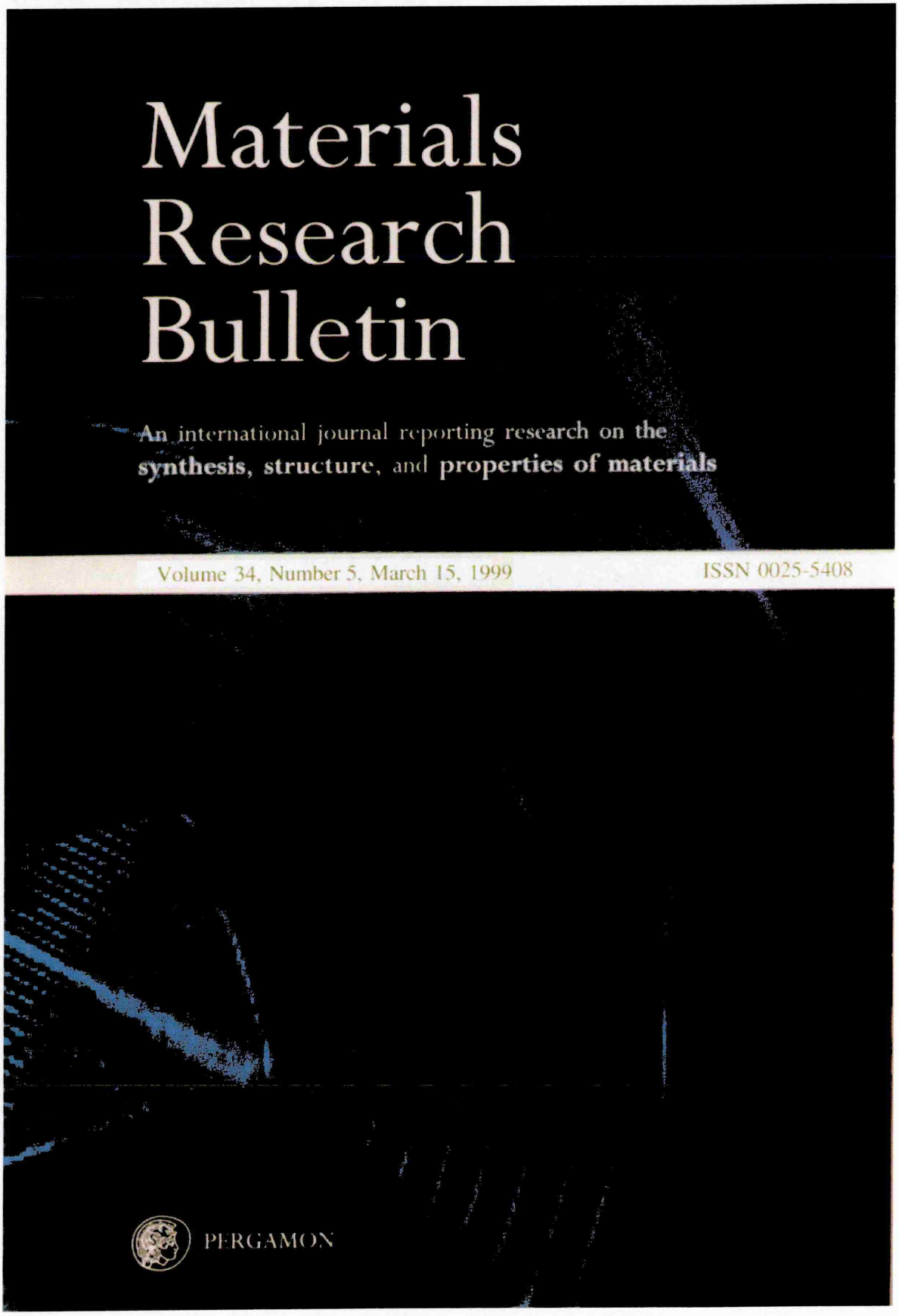
Materials
Research
Bulletin
An international journal reporting research on the synthesis, structure, and properties of materials
Volume 34, Number 5, March 15, 1999
ISSN 0025-5408
PERGAMON

Pergamon

Materials Research Bulletin, Vol. 34, No. 5, pp. 665–672, 1999

0025-5408/99/$–see front matter

PII S0025-5408(99)00069-0

THE EVOLUTION OF NODULAR POLYPYRROLE MORPHOLOGY DURING AQUEOUS ELECTROLYTIC DEPOSITION: INFLUENCE OF ELECTROLYTE GAS DISCHARGE

P. Lemon[1]* and J. Haigh[2]

[1]Materials Research Institute, Sheffield Hallam University, Sheffield, S1 1WB, UK
[2]School of Science and Mathematics, Sheffield Hallam University, Sheffield, S1 1WB, UK

(Refereed)
(Received April 9, 1998; Accepted August 3, 1998)

ABSTRACT

The surface morphology and structure of electrochemically deposited polypyrrole films have been investigated by electron probe microanalysis, crossed polar optical microscopy, and X-ray diffraction (XRD). The films have been shown to possess only low levels of crystalline order despite a mature morphology indicative of highly ordered spherulitic structure. We suggest that the morphological features observed are the result of the production of gaseous oxygen at the working electrode surface during electrochemical deposition. This has strong implications for the electrical characteristics and gas-sensing function of the films. © *1999 Elsevier Science Ltd*

KEYWORDS: A. polymers, C. chemical synthesis, C. electron microscopy, C. X-ray diffraction

INTRODUCTION

Research into the properties of conducting polymers has been widespread during the last two decades, fueled by their potential application in areas such as gas sensing, energy storage and thin-film display technology. The development of these materials has been the subject of several reviews [1,2], which show that polypyrrole is among the most heavily studied of the many conducting polymers in current use. This is partly due to the ease with which polypyrrole may be electrochemically prepared and its subsequent stability.

*To whom correspondence should be addressed.

The morphology of electrochemically deposited polypyrrole has been the subject of much recent discussion [3–6]. It is accepted that variations in the parameters used during polypyrrole deposition such as growth potential, counterion type and concentration can greatly affect the morphology of the resultant polymer. A nodular morphology is often reported [3,7] with morphological attributes characteristic of spherulitic crystalline material, but little has been presented in the literature regarding the origins of this morphology. Alternative polypyrrole morphologies have also been reported [7,8], but a similar lack of information regarding their evolution exists in the literature.

We have systematically studied the structure of polypyrrole thin films by electron probe microanalysis, crossed polar optical microscopy, and X-ray diffraction (XRD). We report on novel results of this research, which relate the formation of polypyrrole nodules to the production of gas at the working electrode during electrochemical deposition.

EXPERIMENTAL

Pyrrole (Aldrich) was purified by solid–liquid chromatography. "As supplied" monomer was passed through two separate alumina-filled columns (each of 3 ml volume) to remove pyrrole oxides and oligomers. Samples were stored at 5°C in low light conditions and were used as soon as possible after purification to suppress degradation [3]. Benzenesulfonic acid (sodium salt) (Aldrich) was used as dopant without further purification. Low-conductivity deionized water was used as electrolyte.

Two substrate types were used: gold microelectrodes consisting of two active contacts separated by a thin insulating gap, allowing deposition over a total area of 1 mm^2, and indium tin oxide (ITO)-coated glass slides (Balzers) cut to allow deposition over an area of about 50 mm^2. Both substrate types were thoroughly cleaned in isopropanol (propan-2-ol) and dried under a high velocity jet of oxygen-free nitrogen before use.

Polypyrrole thin films were deposited from aqueous electrolyte containing pyrrole and benzenesulfonic acid (sodium salt), each at 0.25 M concentration. Deposition was carried out in a standard three-electrode electrochemical cell [9], controlled by an Oxford combination potentiostat/galvanostat. A platinum coil was used as counter electrode and was flamed prior to each experiment. Depositions were carried out potentiostatically at 0.85 V (measured against a saturated calomel reference electrode), unless stated otherwise, typically for 120 s. Films were left in the electrolyte for 30 s after deposition, to provide a standard settling time, and then removed, rinsed well in low-conductivity deionized water, and dried under oxygen-free nitrogen.

X-ray diffraction studies were carried out using a Philips PW1810 θ-2θ diffractometer with Cu Kα radiation, and results analyzed with a Philips PW3710 control unit via Philips APD 3.6 analysis software. Scanning electron microscopy (SEM) was carried out with a JEOL 840A electron probe microanalyzer in SEM mode at 20 kV accelerating voltage. Optical microscopy was carried out on an Olympus Vanox model AHM-T and on a Vickers metallurgical microscope in crossed polar transmission mode.

RESULTS AND DISCUSSION

At both the initial stages and, under certain conditions, more well-developed stages, electrochemically deposited polypyrrole shows structures resembling spherulites [10]. After a

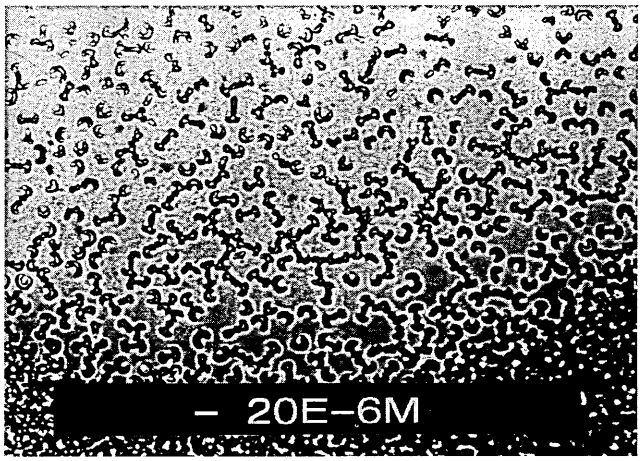

FIG. 1
Sheaf structures observed during the immature stages of polypyrrole growth.

few seconds of deposition under standard conditions on ITO glass substrates, we have frequently observed sheaf-like structures (Fig. 1), analogous to those seen in the early stages of spherulitic growth. More well-developed layers show a nodular, spherulite-like morphology (Fig. 2) under SEM examination. However, structural analysis of polypyrrole films deposited under identical conditions categorically rules out the presence of spherulites.

X-ray diffractometry of the films produced (typically tens of microns thick) consistently suggests very low levels of order within the polypyrrole film structure (Fig. 3). Past studies [11–14] of polypyrrole by XRD have invariably led to the observation of similarly low order levels. The sole feature consistently exhibited by the polypyrrole diffraction traces obtained

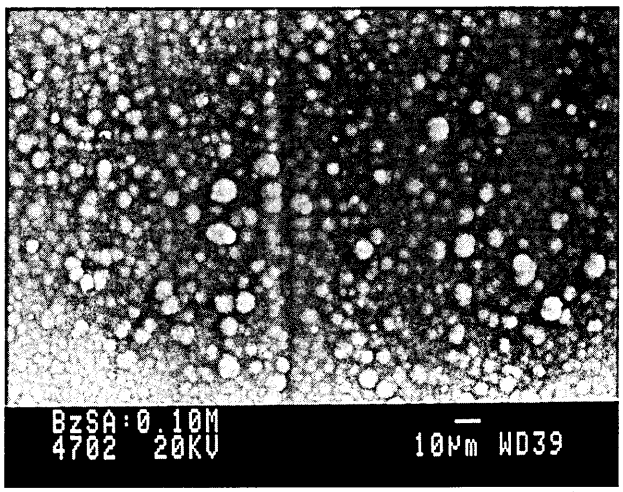

FIG. 2
Mature polypyrrole film showing well-developed nodular structure.

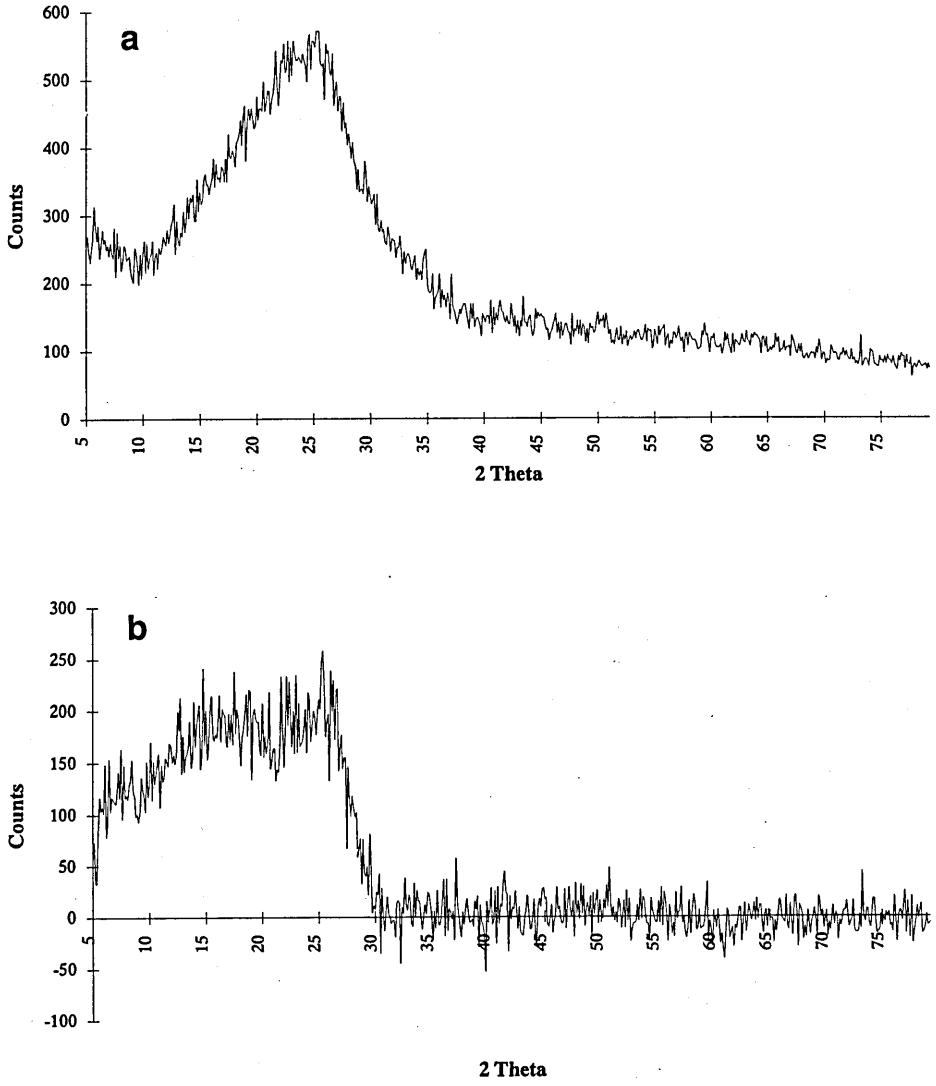

FIG. 3
θ-2θ X-ray diffraction traces of electrochemically deposited polypyrrole (a) before and (b) after subtraction of substrate information.

(after subtraction of substrate information) is a broad shoulder at about $2\theta = 25°$. We postulate that this represents the order between "face-to-face" pyrrole rings throughout the polymer matrix. This degree of ordering is not consistent with the development of extensive crystallinity such as that required by spherulitic structure. It is of note that strong order peaks are routinely observed via XRD analysis after aging of the polypyrrole films in ambient conditions for 12 h or more; we believe that this is due to the presence of small pockets of crystalline dopant salt within the polymer, formed as a result of the out-diffusion and crystallization of dopant from the polymer matrix. Said crystals can be leached out of the

polymer matrix by soaking in dopant-free electrolyte; this is observed by an accompanying reduction in the magnitude of the diffraction peaks displayed.

Crossed-polar optical microscopy supports the notion that the structures observed are nonspherulitic. Spherulitic arrays of crystals clearly display a high contrast "Maltese cross" [15,16] when viewed between crossed polars, with arms lying parallel to the extinction directions of polarizer and analyzer. No Maltese cross patterns were found during examination of polypyrrole layers in this way, supporting the hypothesis of nonspherulitic structure.

The experimental evidence presented strongly suggests that the structure of polypyrrole deposited as described is highly disordered. Nodular morphology cannot, therefore, be assumed to be evidence of extensive spherulitic crystallinity. We will now present evidence that suggests that the formation of this morphology is the result of the production of gas from the aqueous, ionic electrolyte solution at the working electrode during electrochemical deposition.

For an electrolyte solution containing water, benzenesulfonic acid (sodium salt), and pyrrole monomer, the application of a potential to the anionic working electrode is likely to result in oxygen generation:

$$4OH^- \rightarrow 2H_2O + O_2 + 4e^-$$

At the pH used the potential for this process is close to that used for the polypyrrole production and can be expected to occur under forcing polypyrrole deposition conditions.

The effects of the removal and substitution of benzenesulfonic acid (sodium salt) dopant from the electrolyte solution on gas production was studied. The removal of the sulfonic acid dopant was found to halt the production of gas at the working electrode, resulting in a nodule-free film, therefore supporting the model presented. Substitution of the sulfonic acid dopant with sodium hexafluorophosphate also halted gas production. However, substitution with other sulfonic acid dopants (1-butanesulfonic acid, sodium salt; 1-hexanesulfonic acid, sodium salt; benzenesulfonic acid, potassium salt) resulted in gas production and, hence, nodular films.

The volume of oxygen produced per unit time is governed by solution concentrations, deposition potential, and the overpotential characteristics of the working electrode (substrate) material. Stankovic et al. [7] found that polypyrrole films deposited from nonaqueous electrolytes (acetonitrile and propylene carbonate) displayed a flat but wrinkled morphology termed "brain-skin" by the authors. This is in agreement with the gas-production kinetic model presented here: Elimination of water from the electrolyte solution removed a vital component of O_2 generation, thus resulting in nodule-free films. It was noted that the subsequent introduction of water to the nonaqueous electrolyte solution resulted in the production of nodular films.

In order to gain experimental evidence for the theory presented, scanning electron microscopy was used to carry out a novel investigation into the validity of the kinetic model. Thin, nodular polypyrrole films grown on ITO glass electrodes under standard conditions were carefully detached from their ITO substrates and viewed at a glancing angle by secondary electron scanning electron microscopy. Figure 4(a) and (b) shows that the undersides of the films formed by electrochemical deposition of polypyrrole under the conditions described contain a high density of voids. These voids lie directly below individual nodules observable on the surface of the polymer films. We conclude that the formation of these voids is the direct result of gas evolution at the interface between the polymer film and the

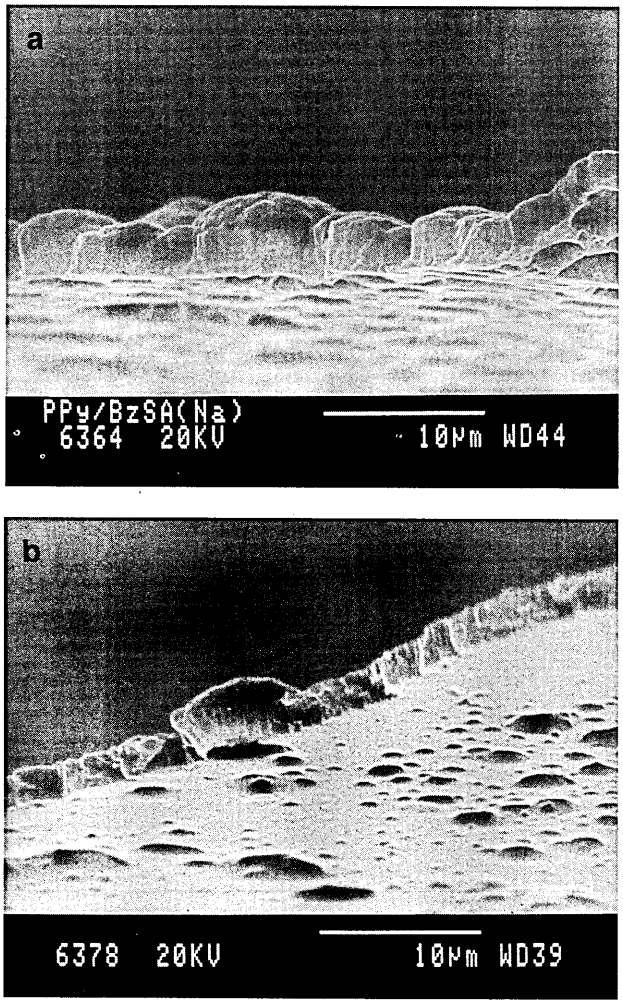

FIG. 4
Glancing-angle views of the undersides of electrochemically deposited polypyrrole films (a) illustrating voids produced by electrode gas production and (b) showing void positions directly below surface nodules.

substrate; the reaction presented predicts that the gas evolved is oxygen. It is possible, however, that the voids observed might have resulted from the adhesion of hemispheres of polymer to the substrate on detachment. The original substrates were therefore examined by SEM; no evidence of such polymer hemispheres was found.

To demonstrate the validity of the gas production model presented, polypyrrole was deposited onto gold working electrodes under the conditions specified, but with a +5.00 V vs. SCE deposition potential, far greater than the standard deposition potential of +0.85 V. The results of such a high potential deposition are shown in Figure 5(a) and (b). Gas production at several preferred sites resulted in the formation of large gas pockets visible to

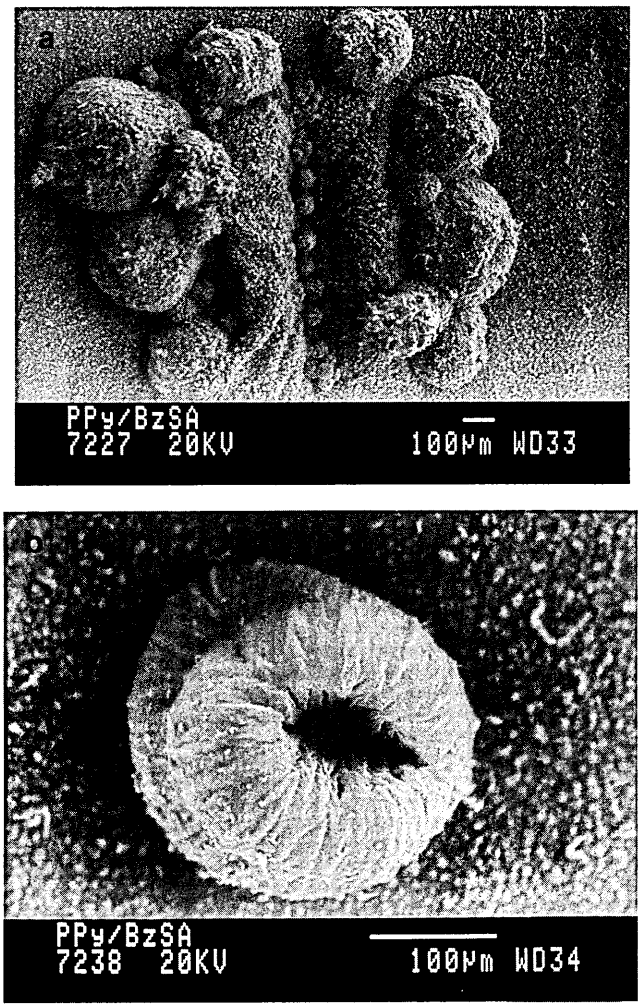

FIG. 5
Electrochemically deposited polypyrrole showing (a) the exaggerated effects of substrate gas production by deposition at high potential and (b) a gas pocket "rupture" site.

the naked eye (Fig. 5(a)). This is the result of the production of gas at the electrode/polymer interface at a rate higher than the rate of gas escape via diffusion through the polymer matrix. When continued deposition was attempted, the gas-filled "pockets" of polypyrrole were clearly observed to rupture, allowing the escape of small gas bubbles (again, visible to the naked eye). Subsequent examination by SEM clearly illustrated such a rupture site, as shown in Figure 5(b).

The kinetic model presented has significant implications in situations where electrochemically deposited polypyrrole layers are used directly in electronic devices. Gas voids at the interface between the polymer film and substrate serve as an electrical insulator, thus modifying the electrical characteristics of the interface and, hence, the devices produced. The

unpredictability of the position and severity of the gas pockets produced may also be reasonably expected to affect the reproducibility and subsequent stability of devices produced.

CONCLUSIONS

We have shown that the regularly reported "nodular" morphology of electrochemically deposited polypyrrole is not the result of spherulitic crystallinity, but rather results from the production of gas at the working electrode during three-electrode potentiostatic electrochemical deposition.

ACKNOWLEDGMENTS

The authors would like to thank the Materials Research Institute (M.R.I.) for funding this work. Many thanks are also due to Mr. K. Blake and Mr. S. Creasey of the M.R.I. for invaluable assistance with XRD equipment.

REFERENCES

1. *Handbook of Conducting Polymers*, ed. T.A. Skotheim, Vols. 1 and 2, Marcel Dekker, New York (1986).
2. J.W. Gardner and P.N. Barlett, *Sens. Actuators, B* **18**, 211 (1994).
3. P. Lemon, N. Szczur, and J. Haigh, in *Sensors and Their Applications VIII*, Proceedings of the Eighth Conference on Sensors and Their Applications, Glasgow, Scotland, 7–10 September 1997, ed. A.T. Augousti and N.M. White, IOP Publishing, Philadelphia, PA (1997).
4. D.A. Kaplin and S. Qutubuddin, *Polymer* **36**, 1275 (1995).
5. M.S. Kiani, N.V. Bhat, F.J. Davis, and G.R. Mitchell, *Polymer* **33**, 4113 (1992).
6. M. Brie, R. Turku, and C. Neamtu, *Rev. Roum. Chim.* **38**, 1317 (1993).
7. R. Stankovic, O. Pavlovic, M. Vojnovic, and S. Jovanovic, *Eur. Polym. J.* **30**, 385 (1994).
8. P. Lemon, N. Szczur, and J. Haigh, *Mater. Res. Bull.* **33**, 909 (1998).
9. *Laboratory Techniques in Electroanalytical Chemistry*, 2nd ed., ed. P.T. Kissinger and W.R. Heineman, Marcel Dekker, New York (1966).
10. D.C. Bassett, *Principles of Polymer Morphology*, Cambridge University Press, New York (1981).
11. L.F. Warren, J.A. Walker, D.P. Anderson, C.G. Rhodes, and L.J. Buckley, *J. Electrochem. Soc.* **136/8**, 2286 (1989).
12. G.R. Mitchell, *Polym. Commun.* **27**, 346 (1986).
13. M.S. Kiani and G.R. Mitchell, *Synth. Met.* **48**, 203 (1992).
14. M. Rikukawa and M.F. Rubner, *J. Macromol. Sci., Pure Appl. Chem.* **A31** (7), 793 (1994).
15. H.D. Keith and F.J. Padden, *J. Appl. Phys.* **34**, 2409 (1963).
16. A. Keller, *J. Polym. Sci.* **39**, 151 (1959).

"On a Novel Polypyrrole Morphology."
P.W. Lemon, N. Szczur and J. Haigh, *Materials Research Bulletin*, Vol. 33, No. 6, (1998), pp. 909-914.

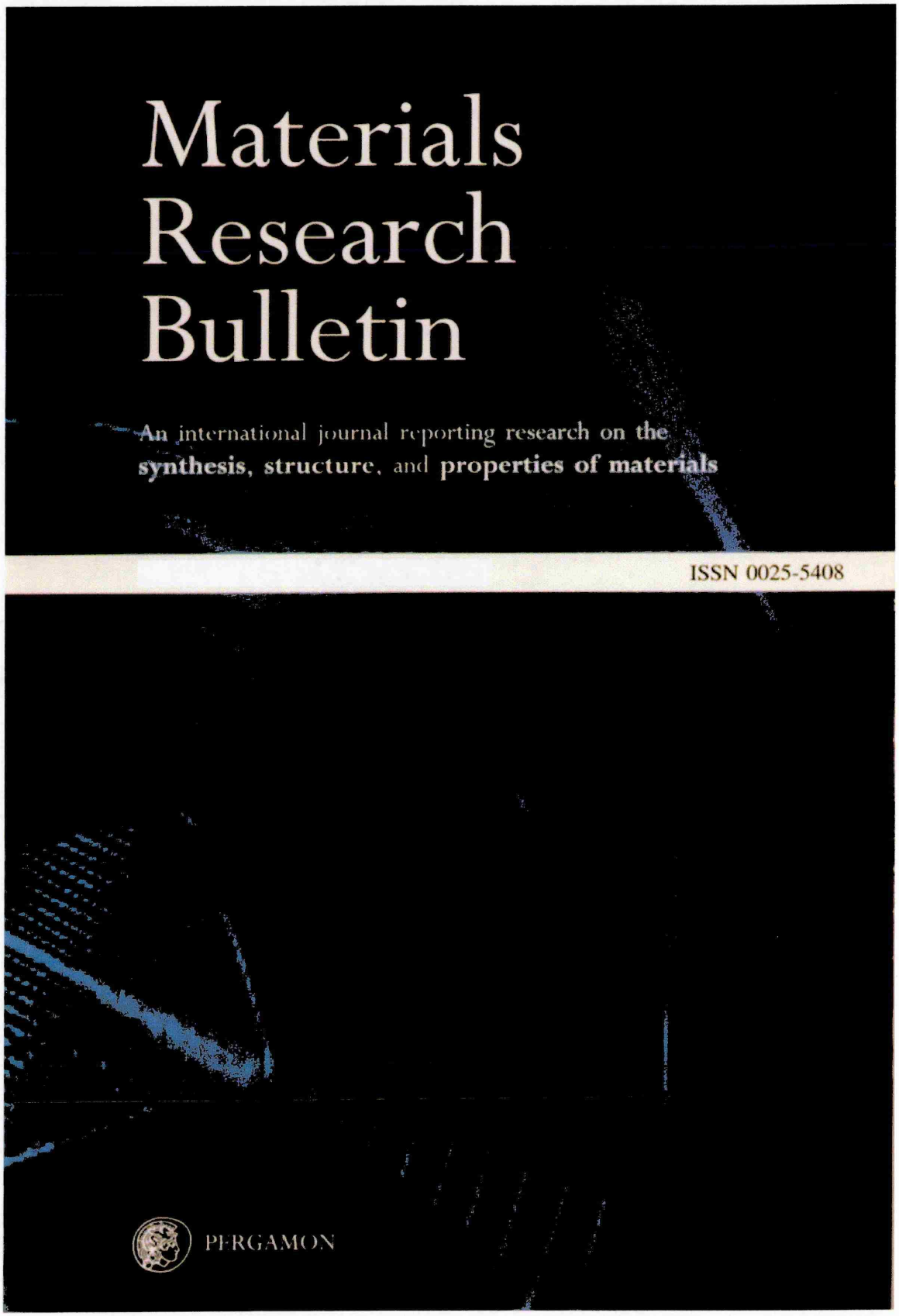
Materials
Research
Bulletin
An international journal reporting research on the synthesis, structure, and properties of materials
ISSN 0025-5408
PERGAMON

Pergamon

Materials Research Bulletin, Vol. 33, No. 6, pp. 909–914, 1998

0025-5408/98 $19.00 + .00

PII S0025-5408(98)00058-0

ON A NOVEL POLYPYRROLE MORPHOLOGY

P. Lemon[1]*, N. Szczur[2], and J. Haigh[3]
[1]Materials Research Institute, Sheffield Hallam University, Sheffield, S1 1WB, UK
[2]Environmental Research Centre, Sheffield Hallam University, Sheffield, S1 1WB, UK
[3]School of Science and Mathematics, Sheffield Hallam University, Sheffield, S1 1WB, UK

(Refereed)
(Received September 29, 1997; Accepted November 20, 1997)

ABSTRACT

Electrochemically deposited polypyrrole thin-film gas sensors have been observed to exhibit significantly different structural and morphological properties on variation of deposition conditions. The careful control of all deposition variables, therefore, is crucial if reproducibility is to be attained. This paper attempts to explain the origins of a novel morphological variant which involves the formation of a tendrillar texture on the growth face of the polymer thin film. We suggest that this morphological feature is the result of variations in electrolyte purity levels during electrochemical deposition. We show that the oxidation of pyrrole monomer is a significant source of electrolyte impurity. *© 1998 Elsevier Science Ltd*

KEYWORDS: A. polymers, A. surfaces, C. electron microscopy, D. diffusion

INTRODUCTION

The ability to render polypyrrole electronically conductive by the incorporation of anionic dopant groups into the polymer matrix has long been recognized [1]. The extent of this conductivity may be controlled simply by subtle variations in deposition conditions, but permanent modification of the material's baseline conductivity after deposition is difficult. Resistance may be temporarily modified following deposition, by exposure of the polymer to a wide variety of gases, the removal of which and the application of a clean, dry-air purge

*To whom correspondence should be addressed.

generally results in the restoration of the original (baseline) conductivity. As a result of this electrochemically deposited polypyrrole thin films are in widespread use as gas-sensin materials.

Variation of the deposition parameters used during polypyrrole growth, such as applie potential, counter-ion type, temperature, supporting electrolyte and monomer/counterio concentrations [2,3], may have a considerable influence on the morphology and structure o the resultant polymer, as well as on its conductivity. The growing commercial requiremen for increasingly reliable and versatile materials to detect low concentrations of gaseou analytes makes a thorough understanding of the effects of these individual variations essential.

A systematic study of the morphological and structural features exhibited by electrochemically deposited polypyrrole doped with benzene sulfonic acid (sodium salt) has been carried out by scanning electron microscopy (SEM), energy dispersive X-ray analysis (EDAX), and gas chromatography (GC). Morphological and structural features obtained by the variation o deposition potential, monomer concentration, electrolyte treatment, and growth time have been studied. Despite the fact that it was well known [4] that nitrogen-containing aromatic compounds (such as pyrrole) are easily contaminated with oxidation products on exposure to air, previous investigations did not consider the effects of monomer oxidation on film structure. In this paper, we report on the effects of pyrrole oxidation products on film morphology and relate this to the formation of a tendrillar texture on the growth face of the polymer during electrochemical deposition. Such texture has been described previously [5,6], but attempts to explain its formation have been ambiguous.

EXPERIMENTAL

Purification and Analysis. Pyrrole (Aldrich) was used in three purity states: (a) as supplied, (b) twice passed through separate alumina-filled columns (each of about 3 mL volume), and (c) distilled under oxygen-free nitrogen at 23–24°C at a pressure of 2 mmHg. Samples were stored at 5°C in low light conditions before and after purification. Impurity contents were estimated by GC. Benzenesulfonic acid (sodium salt) was used as dopant without further purification.

GC-mass selective detection (GC-MSD) and GC-flame ionization detection (GC-FID) were used for purity analysis. GC-MSD was carried out using a Hewlett-Packard model 5890 series II gas chromatograph with a Hewlett-Packard 5971A series mass selective detector and a Restek RTX-5 column (5% diphenyl, 24 m, 0.250 mm i.d., 0.25 m film thickness) with helium as the carrier gas (1 mL/min. flow). A solvent delay of 10 min. was used on a mass spectrometer with a m/z range of 30 to 400. The oven temperature was held at 40°C for 5 min., then ramped to 280°C at 10°C/min. and held for 10 min., giving a total run time of 39 min. All samples were injected splitless in a volume of 1 L.

A Hewlett-Packard model 5890 gas chromatograph was used for GC-FID with nitrogen as the carrier gas (1 mL/min.). An RTX-5 Restek column was fitted (5% diphenyl, 30 m, 0.250 mm i.d., 0.25 m film thickness). The oven temperature was held at 50°C for 1 min., then ramped to 170°C at 10°C/min. and then to 270°C at 30°C/min. and held for 6 min., giving a total run time of 22.3 min. All samples were injected split in a ratio of 30:1. C_{20} at 20 ppm was used as the internal standard.

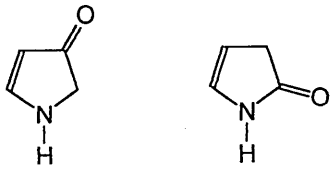

FIG. 1
Impurities in pyrrole monomer, pyrrol-2-en-4-one and pyrrol-2-en-5-one (mass 82).

ilm Preparation. Two substrate types were used: gold microelectrodes consisting of two old contacts (each 0.5 mm^2) separated by a thin insulating gap, and electrically conductive ndium tin-oxide-coated glass slides (Balzers), cut to allow deposition over an area of around 00 mm^2. Both substrate types were cleaned in propan-2-ol (isopropanol) and dried under a igh-velocity jet of oxygen-free nitrogen.

Electrolyte solutions were 0.25 M in both pyrrole and benzenesulfonic acid (sodium salt). standard three-electrode system [7] was controlled by an Oxford potentiostat. A saturated alomel electrode (SCE) was used as a reference, and all potentials are quoted relevant to his. The counter electrode used was a platinum coil, which was flamed prior to each xperiment.

Typical films were electrochemically deposited by stepping the applied potential to +1.00 for a fixed growth period of 120 s. On completion of the deposition, the potential was tepped back to 0.00 V. The electrode was kept in the electrolyte for another 30 s, to allow he current to decay until stability was reached (this stage controls the oxidation state of the olymer and, therefore, the resistance of the film). The polypyrrole films were then washed with milli-Q water and carefully dried under oxygen-free nitrogen. Analyses of film resistance, morphology, and structure were then carried out.

RESULTS AND DISCUSSION

Pyrrole Impurity Analysis. GC-MSD analysis of the three monomer grades used revealed the presence of many pyrrole oxidation products both in the as-supplied and, to a lesser extent, in the purified pyrrole. Two peaks were found to consistently dominate GC traces; their origins were determined to be a pair of isomeric oxidation products, pyrrol-2-en-4-one and pyrrol-2-en-5-one (Fig. 1).

Subsequent work by GC-FID was concentrated on these dominant oxidation products. GC analysis showed that both purification techniques remove the impurity peaks displayed by the as-supplied monomer (see Table 1). The masses associated with these peaks lead to identification of the impurities present in the monomer as a variety of oxidation products and oligomers. The peaks observed in distilled monomer were more intense when oxygen was present in the N_2 bleed. This supports the identities of the oxide groups shown in Figure 1.

Comparative analyses were performed of the monomer impurity peak areas displayed by GC traces. The internal standard used was maintained at a precise concentration (20 ppm). This allowed monitoring of any fluctuations in instrument performance. The ratios of internal standard to monomer impurity peak areas are given in Table 1.

GC-FID data from freshly purified monomer showed that alumina purification removed a high proportion of the oxidation products and oligomers from the monomer, but distillation removed these impurities to below the lower detection limit of the chromatographs used. The

TABLE 1
Impurity Levels Against Purification Technique and Post-Purification Period

Purification technique		Impurity peak area ratio (vs. monomer age) 0	30 min.	180 min.	3 days
None	Peak 1	1:9.12	-	-	-
	Peak 2	1:16.90	-	-	-
Alumina	Peak 1	1:0.11	1:0.12	1:0.18	1:5.07
	Peak 2	1:0.34	1:0.42	1:0.94	1:12.95
Distillation	Peak 1	1:0.00	1:0.00	1:0.03	-
	Peak 2	1:0.00	1:0.00	1:0.02	-

Ratios shown are between GC internal standard and impurity peak areas. Peaks 1 and 2 represent pyrrol-2-en-4-one and pyrrol-2-en-5-one, respectively.

peak area of the oxide impurities shown in Figure 1, taken from alumina-purified monome increased substantially within 30 min. of purification under standard laboratory conditions Freshly distilled pyrrole monomer was analyzed repeatedly over a period of time and lov levels of impurity mass 82 were detected after just 180 min. This indicates that monome analyzed as little as 3 h after distillation (and immediately after alumina filtration) contain measurable levels of impurities. It was also found that impurity concentrations 3 days afte alumina purification at STP are comparable with those observed in the as-supplied pyrrole

Sensor Film Structure. A Jeol 840A electron probe microanalyzer was used in secondar electron SEM mode at 20 kV. It was noted that films grown from impure pyrrole were hos to large columnar structures ("tendrils," often more than 30 μm in height), which appeare to have developed from nodules present on the polymer surface (nodular growth is a inherent feature of polypyrrole grown with the dopant species used). Systematic SE examination showed that use of unpurified pyrrole resulted in the regular formation o tendrils (see Fig. 2a), while separated and distilled pyrrole gave films with a level but nodula growth surface on which tendrillar growth could not be detected (Fig. 2b).

The influence of impurities in the solution ahead of the polymer growth face during electrochemical deposition of polypyrrole may be explained by the application of depletion theory. The nature of pyrrole's oxidative polymerization leads to the preferential incorporation of pyrrole monomer units into the polymer chain (or matrix as in the case of low-polymers such as polypyrrole) than of impurities such as pyrrole-2-en-4-one. Under certain circumstances, this preferential use of pyrrole monomer may result in decreased pyrrole concentration in the vicinity of the polymer growth face, along with an increase in relative impurity concentration, ultimately leading to the exhaustion of the available pyrrole. This may be regarded as the development of a "pyrrole depletion region." In such "monomer depletion" conditions, impurities tend to diffuse away from areas of high impurity concentration (such as the depletion region) to areas of lower impurity concentration. This increases the relative concentration of pyrrole monomer and, thus, promotes polymer growth. This is only possible, however, if the impurity diffusion rate is higher than the rate at which the polymer growth face advances (the growth rate). If not, then a potential stalemate is reached and growth rate is drastically reduced. Growth rate reduction may then result in significant

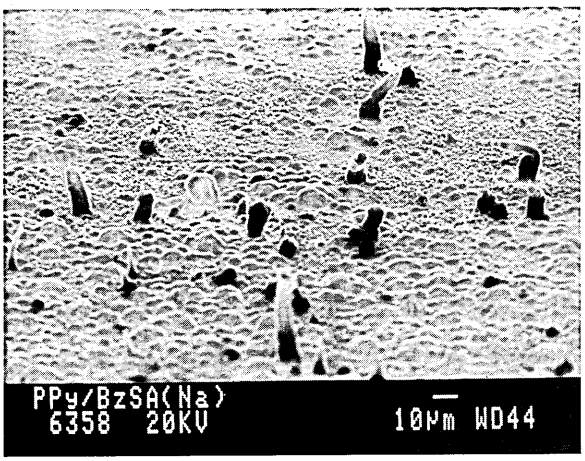

(a)

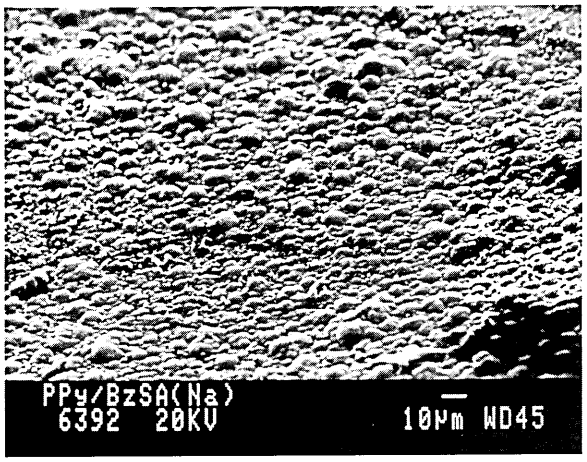

(b)

FIG. 2

Polypyrrole grown from (a) nonpurified monomer and (b) purified monomer. Close examination of films grown in purified monomer show an absence of tendrillar excrescences, while the tendrils displayed in (b) are a regular feature of films grown using impure monomer.

impurity diffusion away from the growth face, along with the diffusion of pyrrole monomer towards the growth face. In these circumstances, the recovery of polymer growth is feasible.

In the case of a flat growth face (i.e., flat with respect to the thickness of the depletion layer), diffusion of both pyrrole and of impurities towards and away from the depletion region may allow variations in growth rate throughout the polymer growth period. The basis of the theory presented here relies on the fact that the growth face of electrochemically deposited polypyrrole is, under all but the most extreme circumstances, far from flat. It is well known that electrochemically grown polypyrrole forms a nodular morphology when dopants such as benzene sulfonic acid (sodium salt) are used. These nodules have been observed to

be as much as 10 μm in height (as measured by a Taylor Hobson Surtronic 3+ talysurf), b are routinely found to be several micrometers high. In pure electrolyte with low impurit concentrations, the rough polymer growth face will advance ad infinitum until the eventu exhaustion of the electrolyte or the removal of the growth potential. In impure condition however, a depletion layer may form ahead of the growth face as described. In depletio conditions, it is reasonable to expect that sundry nodule peaks will be far enough ahead the growth face to be unaffected by the depletion, as monomer concentrations will b significantly higher than those at the growth face. Nodules in this position will experienc unrestricted growth away from the depletion layer, while the growth of the surrounding area will rapidly decline. Such nodules are said to have "broken through" the depletion zone an are free to evolve into a tendril.

To obtain further evidence for this theory, polymer films were grown at various potential and electrolyte concentrations (increases in either of which produce more rapid growth). Th results clearly illustrated that increased growth rate produces more tendrillar films, thu supporting the theory presented.

Similar kinetic models concerning comparable effects have been formed in the past. Keit and Padden [8] formed a related theory concerning the development of spherulitic crystals i high-polymers (polymers with highly developed crystal structures) grown from melt condi tions. It was postulated that ordered polymer growth was inhibited by the presence of tangle chains and atactic groups in the polymer melt.

CONCLUSIONS

It has been shown that electrolyte purity affects the morphology and structure of electro chemically grown polypyrrole gas sensors. A theory that explains the morphological mod ifications observed has been applied to polypyrrole growth.

ACKNOWLEDGMENTS

The authors thank the Materials Research Institute for funding this work. Many thanks ar also due to Mr. D. Douce of the Department of Chemistry, Sheffield Hallam University fo his assistance with GC work and Mrs. C. Shaw of the Materials Research Institute for th processing of SEM micrographs.

REFERENCES

1. R. McNeill, R. Siudak, J.H. Wardlaw, and D.E. Weiss, *Aust. J. Chem.* **16**, 1056 (1963).
2. D. Schmeisser, H. Naarmann, and W. Göpel, *Synth. Met.* **59**, 211 (1993).
3. M.S. Kiani, N.V. Bhat, F.J. Davis, and G.R. Mitchell, *Polymer* **33**, 4113 (1992).
4. T.L. Gilchrist, *Heterocyclic Chemistry*, Pitman Publishing Ltd., London (1985).
5. P. Lemon, N. Szczur, and J. Haigh, in *Sensors and Their Applications VIII: Proceedings of th Eighth Conference on Sensors and Their Applications, Glasgow, Scotland, 7–10 September 1997* ed. A.T. Augousti and N.M. White, IOP Publishing, Philadelphia (1997).
6. A. Kaynak, *Mater. Res. Bull.* **32**, 271 (1997).
7. P.T. Kissinger and W.R. Heineman (eds), *Laboratory Techniques in Electroanalytical Chemistry* 2nd ed., Marcel Dekker, New York (1966).
8. H.D. Keith and F.J. Padden, *J. Appl. Phys.* **34**, 2409 (1963).

"The Effects of Monomer Purity on the Morphology of Polypyrrole Thin-Film Gas-Sensing Layers."
P.W. Lemon, N. Szczur and J. Haigh, in "*Sensors and their Applications VIII*", ed. A.T. Augousti and N.M. White, I.O.P. Publishing, Philadelphia, 1997, pp. 189-193.

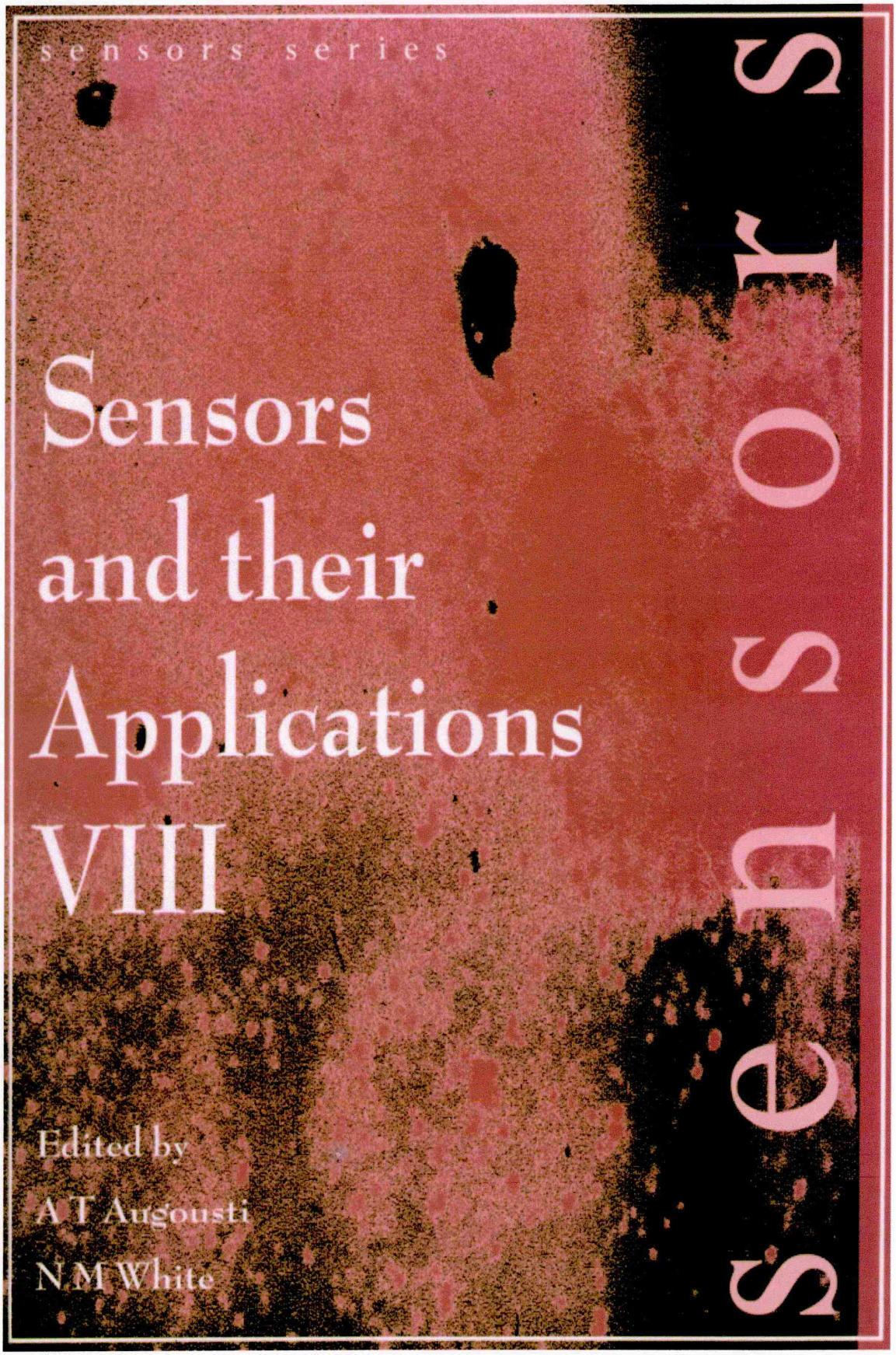
sensors series
Sensors and their Applications VIII
Edited by
A T Augousti
N M White
sensors

Section E: Gas and Chemical Sensors
Paper presented at Sensors and their Applications VIII, 7-10 September 1997

The Effects of Monomer Purity on the Morphology of Polypyrrole Thin-Film Gas-Sensing Layers

P Lemon[a], N Szczur[b] and J Haigh[c]

[a] Materials Research Institute, Sheffield Hallam University, Sheffield, South Yorkshire, S1 1WB, UK.
[b] Environmental Research Centre, Sheffield Hallam University.
[c] School of Science and Mathematics, Sheffield Hallam University.

Abstract. Electrochemically deposited polypyrrole thin-film gas-sensors have been observed to exhibit significantly different structural and morphological properties as deposition conditions are varied. In order to attain reproducibility, all process variables must therefore be carefully controlled. A morphological modification not before reported in polypyrrole is shown to be due to variations in monomer purity.

1. Introduction

It has long been known [McNeill *et.al.* '63] that polypyrrole may be made electronically conductive by the incorporation of dopant ions into the polymer matrix during or after electrochemical polymerisation. Subsequently its electrical resistance may be modified by exposure to a wide variety of gaseous analytes, thus allowing the use of electrochemically deposited thin films as gas-sensing materials.

Polypyrrole's morphology and structural properties depend sensitively on deposition parameters such as applied potential, counter-ion type, temperature, supporting electrolyte and monomer/counter-ion concentrations [Schmeisser *et.al.* '93, Kiani *et. al.* '92]. The requirement for increasingly reliable and versatile techniques to detect gaseous analytes at low concentrations, in areas such as environmental monitoring and industrial process control [Semancik and Cavicci '93], makes an understanding of these effects essential.

We have studied the morphological and structural features in electrochemically deposited polypyrrole doped with benzenesulfonic acid (sodium salt) by scanning electron microscopy (SEM) and gas chromatography (GC), under changing conditions of deposition potential, monomer concentration, electrolyte treatment and growth time. Despite the fact that it is well known (see Gilchrist '85) that nitrogen-containing aromatic compounds (such as pyrrole) are prone to become contaminated with oxidation products on exposure to air, there appears to have been no previous investigation of the effects of monomer oxidation on film structure. We report such an investigation below.

2. Experimental

2.1. Purification and analysis

Pyrrole (Aldrich) and was used in three purity states; [a] as supplied, [b] twice passed through separate, alumina filled columns (each of around 3ml volume) and [c] distilled under oxygen

free nitrogen at 23-24°C at a pressure of 2 mmHg. Samples were stored at 5°C in low light conditions before and after purification. Impurity contents were estimated by gas chromatography. Benzenesulfonic acid (sodium salt) was used as dopant without further purification.

Gas Chromatography - Mass Selective Detection (GC-MSD) and Gas Chromatography - Flame Ionisation Detection (GC-FID) were used for purity analysis. GC-MSD was carried out using a Hewlett Packard model 5890 series II gas chromatograph with a Hewlett Packard 5971A series mass selective detector and a Restek RTX-5 column (5% diphenyl, 24m, 0.250mm i.d., 0.25μm film thickness) with helium as the carrier gas (1 ml/min flow). A solvent delay of 10 mins was used on the mass spectrometer with a *m/z* range of 30 to 400. The oven temperature was held at 40°C for 5 mins, then ramped to 280°C at 10°C min^{-1} and held for 10 mins, giving a total run time of 39 mins. All samples were injected splitless in a volume of 1μl.

Hewlett Packard model 5890 gas chromatograph was used for GC-FID with nitrogen as the carrier gas (1 ml/min). An RTX-5 Restek column was fitted (5% diphenyl, 30m, 0.250mm i.d., 0.25μm film thickness). The oven temperature was held at 50°C for 1 min then ramped to 170°C at 10°C min^{-1} and then to 270°C at 30°C min^{-1} and held for 6 mins, giving a total run time of 22.3 mins. All samples were injected split in a ratio of 30:1. C_{20} at 20 ppm was used as the internal standard.

2.2. Film Preparation

Two substrate types were used; gold micro-electrodes consisting of two gold contacts (each of 0.5mm^2) separated by a thin insulating gap, and electrically conductive indium tin oxide coated glass slides (Balzers), cut to allow deposition over an area of around 200mm^2. Both substrate types were cleaned in propan-2-ol (iso-propanol) and dried under a high velocity jet of oxygen-free nitrogen.

Electrolyte solutions were 0.25M in both pyrrole and benzenesulfonic acid (sodium salt). A standard three electrode system (see, for example, Kissinger and Heineman '96) was controlled by an Oxford potentiostat. A saturated calomel electrode (SCE) was used as a reference, and all potentials are quoted relevant to this. The counter electrode used was a platinum coil, which was flamed prior to each experiment.

Typical films were electrochemically deposited by stepping the applied potential to +1.00V for a fixed growth period of 120s. On completion of the deposition, the potential was stepped back to 0.00V. The electrode remained in the electrolyte for a further 30s in order to allow the current to decay until stability was reached (this stage controls the oxidation state of the polymer and therefore the resistance of the film). The polypyrrole films were then washed with milli-Q water and carefully dried under oxygen-free nitrogen. Analyses of film resistance, morphology and structure were then carried out.

3. Structural properties

3.1. Pyrrole impurity analysis

GC-MSD analysis of the three monomer grades used revealed the presence of many pyrrole oxidation products in both 'as supplied' and (to a lesser extent) purified pyrrole. Two peaks were found to consistently dominate GC traces, the origins of which were identified as a pair of isomeric oxidation products; pyrrol-2-en-4-one and pyrrol-2-en-5-one (Fig. 1).

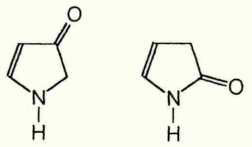

Figure 1: *Logical Impurity structures in Pyrrole Monomer, pyrrol-2-en-4-one and pyrrol-2-en-5-one (mass 82).*

Subsequent work by GC-FID concentrated on these dominant oxidation products. GC analysis has shown that both purification techniques remove the impurity peaks displayed by "as supplied" monomer (see Table 1). The masses associated with these peaks lead to identification of the impurities present in the monomer as a variety of oxidation products and oligomers. It was noted that the peaks observed in distilled monomer were more intense when an air bleed was used during distillation in place of the more conventional N_2 bleed. This supports the identities of the oxide groups shown in Fig. 1.

Qualitative analyses were performed by a technique involving the comparison of monomer impurity *peak areas* displayed by GC traces. It was considered that, due to the nature of the work undertaken, the derivation of true concentration data would not be a significant advantage over simple comparisons between monomer impurity peak areas. The internal standard used was maintained at a precise concentration (20 ppm). This allowed monitoring of any fluctuations in instrument performance. The ratios of internal standard to monomer impurity peak areas are given in Table 1.

GC-FID data from freshly purified monomer showed that alumina purification removed a high proportion of the oxidation products and oligomers from the monomer, but distillation removed these impurities to below the lower detection limit of the chromatographs used. The peak area of the oxide impurities shown in Fig. 1 taken from *alumina purified* monomer increases substantially within 30 mins of purification in standard laboratory conditions. Freshly *distilled* pyrrole monomer was analysed repeatedly with respect to time and low levels of impurity mass 82 were detected after just 180 mins. This indicates that monomer analysed as little as 3 hours after distillation (and immediately after alumina filtration) contains measurable levels of impurities. It was also found that impurity concentrations three days after alumina purification at STP are comparable with those in as-supplied pyrrole.

Table 1: *Impurity levels against purification technique and post-purification period. Ratios shown are between GC internal standard and impurity peak areas. Peaks 1 & 2 representing pyrrol-2-en-4-one and pyrrol-2-en-5-one.*

Purification Technique		**Impurity Peak Area Ratio** *(vs monomer age)*			
		0	30 mins	180 mins	3 days
None	Peak 1	1 : 9.12			
	Peak 2	1 : 16.90			
Alumina	Peak 1	1 : 0.11	1 : 0.12	1 : 0.18	1 : 5.07
	Peak 2	1 : 0.34	1 : 0.42	1 : 0.94	1 : 12.95
Distillation	Peak 1	1 : 0.00	1 : 0.00	1 : 0.03	
	Peak 2	1 : 0.00	1 : 0.00	1 : 0.02	

(a)
(b)

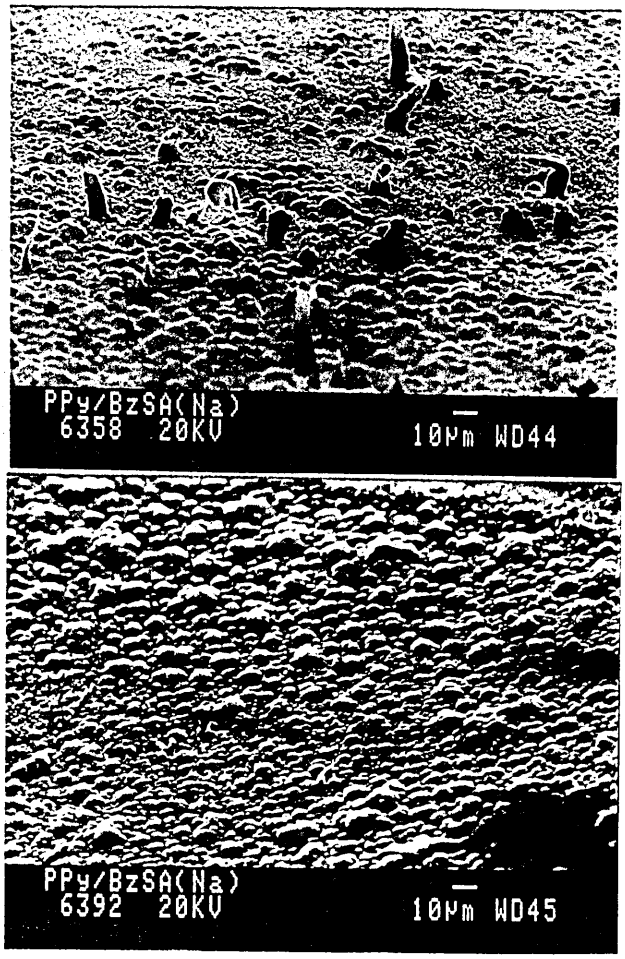

Figure 2: *Polypyrrole grown from (a) non-purified monomer, and (b) purified monomer. Close examination of films grown in purified monomer show an absence of tendrillar excrescences, whilst the tendrils displayed in (b) are a regular feature of films grown using impure monomer.*

3.2. Sensor film structure.

A JEOL 840A Electron Probe Microanalyser was used in secondary electron SEM mode at 20kV. It was noted that films grown from impure pyrrole were host to large columnar structures ('tendrils', often more than 30μm in height), which appeared to have developed from nodules present on the polymer surface (nodular growth is an inherent feature of polypyrrole grown with the dopant species used). Systematic SEM examination showed that use of unpurified pyrrole resulted in the regular formation of tendrils (see Fig. 2a), whilst separated and distilled pyrrole gave films with a level but nodular growth surface on which tendrillar growth could not be detected (Fig. 2b).

During film deposition impurity concentrations ahead of the advancing polymer growth face are likely to rise, thus resulting in a decreased polymerisation rate (the

polymerisation of pure pyrrole monomer is preferential to that of pyrrole impurities such as pyrrol-2-en-4-one). Film surface asperities are therefore likely to result in "breakthrough" of deposition through the impurity layer ahead of the moving growth face resulting in the formation of rapidly-growing tendrils. Equivalent relationships have been formed in the past concerning similar kinetic effects, see for example Keith and Padden ('63) who considered the growth of spherulitic crystals in high-polymers grown from the melt where ordered polymer growth may be inhibited by the presence of tangled chains or atactic groups. To obtain further evidence for the model, films were grown at various potentials and electrolyte concentrations (increases in either of which produce more rapid growth), from which it was clear that increases in growth rate produced more tendrillar films.

4. Conclusions

It has been shown that monomer purity affects the morphology and structure of electrochemically grown polypyrrole gas sensors. A theory has been applied to polypyrrole growth which explains the morphological modifications observed.

Acknowledgements

The authors thank Dr. Steve Collins (Neotronics Scientific Ltd.) for the supply of gold microelectrodes and Mr. D. Douce for his assistance with GC work.

References

Gilchrist T L 1985 *Heterocyclic Chemistry* (Pitman Publishing Ltd.) p.127

Keith H D and Padden F J 1963 *J. Appl. Phys.* **34** 2409

Kiani M S, Bhat N V, Davis F J and Mitchell G R 1992 *Polymer* **33** 4113

Kissinger P T and Heineman W R (Eds.) 1996 *Laboratory Techniques in Electroanalytical Chemistry 2nd Ed.* (Marcel Dekker)

McNeill R, Siudak R, Wardlaw J H and Weiss D E 1963 *Aust. J. Chem.* **16** 1056

Schmeisser D, Naarmann H and Göpel W 1993 *Synth. Met.* **59** 211

Semancik S and Cavicci R E 1993 *Appl. Sur. Sci.* **70** 337

"The Macrostructure of Polypyrrole Gas-Sensors."
P.W. Lemon and J. Haigh - Poster Presentation to the Royal Society of Chemistry (Analytical Division) Conference, "*Advances in Analytical Chemistry - Miniaturisation and Sensors*", University of Huddersfield, U.K., February 1997.

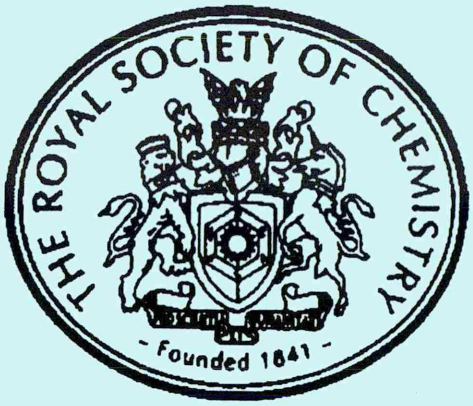

ROYAL SOCIETY OF CHEMISTRY
NORTH EAST REGION, ANALYTICAL DIVISION,

Co-sponsored by
Environment Agency and University of Huddersfield

Advances in Analytical Chemistry

Miniaturisation and Sensors

Wednesday 19 February 1997

Huddersfield, Yorkshire

The Macrostructure of Polypyrrole Gas-Sensors

Paul W. Lemon and J. Haigh

Materials Research Institute, Sheffield Hallam University, Pond St., Sheffield

The use of electrochemically deposited polypyrrole as a gas-sensing material is currently very popular. This is primarily due to the variability of its electrical conductivity on exposure to gaseous analytes.

The ability to produce gas-sensitive polypyrrole thin films with reproducible microstructure and morphology during electrochemical polymerisation is thought to be a fundamental factor when considering the reproducibility and subsequent stability of the films formed. A number of techniques have been used in order to gain morphological and structural information from polypyrrole, such as electron probe microanalysis, x-ray diffraction, SIMS and GDOES.

Models for the growth kinetics of polypyrrole on gold and ITO glass substrates have been developed. The first of these considers the production of gas (at the working electrode during electrochemical deposition in a standard three electrode cell) being responsible for the observed nodular morphology of the films produced. The mechanisms of gas production are considered, and the effects of gas bubble formation on gas-sensing ability are discussed. A second growth kinetics model has been developed which explains the growth of excrescent tendrils from the polymer growth face (not before reported in polypyrrole) under certain conditions. It was found that tendrillar polymer was formed only when monomer of suspect purity was used.

"The Structure of Polypyrrole Gas-Sensors."
P.W. Lemon and J. Haigh - Poster Presentation to the Institute of Physics Conference, "*Condensed Matter and Materials Physics*", University of York, U.K., December 1996.

Institute of Physics

CMMP 96

Condensed Matter and Materials Physics Conference 1996

17 - 19 December 1996
University of York

Programme and Abstracts

PLD thin film transistors (TFTs) deposited onto room-temperature substrates exhibit a field effect mobility, μ_{FE}, of 3 x 10^{-2} $cm^2V^{-1}s^{-1}$, a 0.25 V threshold voltage, and an on/off current ratio of more than 1400. In contrast, TE devices prepared under otherwise identical conditions exhibit a μ_{FE} of only $\sim 10^{-4}$ $cm^2V^{-1}s^{-1}$, a 0.8 V threshold voltage, and an on/off ratio of 240.

The mobility values for the PLD TFTs are already the highest reported for undoped pentacene devices, and are sufficient to make the material viable for prototype active circuits. Moreover, our most recent experiments have established that raising the substrate temperature during PLD deposition to 473 K yields a dramatic reduction in the surface roughness of films, to a value of 0.4 nm which is comparable to the dimensions of the pentacene molecule! This is accompanied by further improvements in electrical conductivity, offering exciting possibilities for even higher performance devices.

TA.1.5
Photoluminescence and Nanostructure of Si and Ge Clusters Embedded in SiO_2 Matrices

M Spurr, D Bazeley, P J Harris, S C Bayliss

Solid State Research Centre, School of Applied Sciences, De Montfort University, Leicester LE1 9BH

Silicon and germanium nanostructures embedded in SiO_2 were deposited by rf co- sputtering followed by N_2 annealing at 600 and 800°C. The target used was SiO_2 on which pieces of the element had been placed. The density of clusters of the nanostructures was varied by altering the target coverage. Stable visible photoluminescence (PL) was recorded from the samples showing individual clusters by TEM, and the emission was visible to the naked eye when excited by a low power HeCd laser. The fundamental optical bandgap has been determined from PLE and is found to shift with particle size. The size distributions of the nanoclusters obtained from TEM suggests that the PL is consistent with quantum confinement being responsible for the enlarged bandgap and recombination path. The PL and nanostructure data are compared with those from ion-implanted silicon. The implications of these results for optoelectronics based on connected silicon nanoclusters embedded in bulk matrices will be discussed.

TA.P1
Experimental Studies Of Ge-S-Ag Glasses

G Saffarini

Physics Department, An-Najah National University, Nablus, Via Israel

Glasses belonging to the Ge-S-Ag system were investigated by differential scanning calorimetry (DSC) and X-ray diffractin. The DSC results show that the glass transition temperature (T_g), the onset crystallization temperature (T_c), as well as T_c-T_g decrease with the increase of Ag content in the glass. The decrease of the interval T_c-T_g indicates that the thermal stability of the glass decreases . The X-ray structure factors obtained on the glasses with 5, 10 and 15 at %Ag have a first sharp diffraction peak, characteristic of intermediate range order, whose intensity decreases gradually with the increase of the amount of Ag content in the glass up to 15 at$\geq$ 20 at%, this first sharp diffraction peak is totally absent. These results may be taken as prima facie evidence that the decrease or the absence of intermediate range order in the glass decrease its thermal stability.

TA.P2
Intermediate Range Order in $Se_{1-x}S_x$ Glasses

G Saffarini

Physics Department, An-Najah National University, Nablus, Via Israel

$Se_{1-x}S_x$ bulk glasses, within the composition range $0.1 \geq x \geq 0.5$ (x in at %), were prepared from high purity constituent elements. The X-ray structure factors obtained from these glasses show the presence of the first sharp diffractin peak (FSDP), which is the most universal signature of intermediate range order (IRO). The position and the full-width at half-maximum(FWHM) which relate, respectively, to the intercluster distance and the cluster size, remain essentially the same. The intensity of this peak increases with the amount of S content in the glasses. We interpret these results by proposing that the IRO in this system is related to the formation of ring-like clusters.

TA.P3
The Structure of Polypyrrole Gas Sensors

P W Lemon, J Haigh

Materials Research Institute, Sheffield Hallam University

Electrochemically polymerised polypyrrole is currently in widespread use as a gas-sensing material due to the variability of its electrical conductivity on exposure to gaseous analytes.

The reproducibility and subsequent stability of the gas-sensitive polypyrrole thin-films formed during electrochemical polymerisation are thought to be reliant on the ability to produce films with reproducible microstructure and morphology. Morphological and structural information has been gathered from polypyrrole by a number of techniques, such as electron and optical microscopy, x-ray diffraction, SIMS and GDOES.

Models for the growth kinetics of polypyrrole on gold and ITO glass substrates have been developed. The first of these considers the production of gas (at the working electrode during electrochemical deposition in a standard three-electrode cell) being responsible for the observed nodular features of the films produced. The mechanisms of gas production are considered, and the effect of gas bubble formation on gas sensing ability are discussed. A second growth kinetics model has been developed which explains the growth of excrescent tendrils from the polymer growth face (not before reported in polypyrrole) under certain conditions. It was found that tendrillar polymer was formed only when monomer of suspect purity was used.

Evidence for the out-diffusion of dopant (the sodium salt of benzene sulfonic acid) from the polymer matrix to the surface of the film has also been found by use of wide angle [theta - two theta] x-ray diffraction. The implications of dopant diffusion on the gas-sensing properties of polypyrrole thin-films have been considered; (i) out diffusion and recrystallisation are thought to be related to sensor instability, and (ii) results indicate that accepted models for dopant incorporation during electrochemical synthesis may require modification.

TA.P4
Structural Transformations in Bulk Amorphous $(GaSb)_{1-x}(Ge_2)$ Under High Pressures

A V Sapelkin, S C Bayliss, *A G Lyapin, *V V Brazhkin, #J P Itie, #A Polian, S M Clark, A J Dent

De Montfort University, Leicester, LE1 9BH

**Institute of High Pressure Physics, Troitsk, Moscow Region, Russia*

"The Effects of Preparation Conditions on the Structures of Electrochemically Polymerised Polypyrrole Thin Films Doped with Benzenesulfonic Acid Sodium Salt."
P.W. Lemon and J. Haigh - Poster Presentation to the Royal Society of Chemistry (Analytical Division) Conference, "*Research & Development Topics in Analytical Chemistry*", Nottingham Trent University, U.K., July 1996.

THE ROYAL SOCIETY OF CHEMISTRY

ANALYTICAL DIVISION

RESEARCH & DEVELOPMENT TOPICS IN ANALYTICAL CHEMISTRY

Nottingham Trent University
22-23 July 1996

BOOK OF ABSTRACTS

The Effects of Preparation Conditions on the Structures of Electrochemically Polymerised Polypyrrole Thin Films Doped with Benzenesulfonic Acid Sodium Salt

P Lemon
Materials Research Institute/ Division of Chemistry
Sheffield Hallam University
City Campus
Sheffield S1 1WB

Abstract

Morphological, structural and electrical conductivity studies were made on polypyrrole thin films prepared by electrochemical polymerisation under galvanostatic conditions on to gold electrodes. A range of deposition potentials and concentrations of benzenesulfonic acid (sodium salt) used as dopant were examined. Morphologies were studied by optical and electron microscopy, and microstructures of films on ITO glass electrodes by x-ray diffraction.

The accepted growth mechanism accounts in only a limited fashion for the observed features, which may be better explained in terms of the adhesion of gas bubbles to the surface of the polymer growth face during deposition.